A Geophysical Investigation
of
Geologic Structure and Regional Tectonic Setting
at the
Savannah River Site, South Carolina

by

William Joseph Domoracki

Dissertation submitted to the Faculty of the
Virginia Polytechnic Institute and State University
in partial fulfillment of the requirements for the degree of
Doctor of Philosophy
in
Geophysics

APPROVED:

John K. Costain, Co-chairman

Cahit Çoruh, Co-chairman

Edwin S. Robinson

Lynn Glover III

Dale E. Stephenson

May 11, 1995

Blacksburg, Virginia

A Geophysical Investigation

of

Geologic Structure and Regional Tectonic Setting

at the

Savannah River Site, South Carolina

by

William Joseph Domoracki

John K. Costain, Co-chairman

Cahit Çoruh, Co-chairman

Geophysics

(ABSTRACT)

Time-structure, isochron, and reflection amplitude maps were constructed from 270 km of reprocessed seismic reflection data recorded at the Savannah River Site (SRS), South Carolina. These maps indicate the presence of three major basement blocks bounded by northeast trending faults that penetrate upward from basement into the Atlantic Coastal Plain sediments. Most of these faults are interpreted to be Paleozoic and Mesozoic structures reactivated under compression.

The northernmost fault block is bounded on the southeast by the Tinker Creek fault (TCF), a high-angle southeast dipping reverse fault, that appears to be a reactivated splay from a major decollement (Augusta fault?) at 5 km depth. The TCF can be traced with certainty for a distance of 15 km across SRS where it offsets the top of basement and shallower reflections. The throw of the fault, as does its upward penetration into the sedimentary section, increases to the northeast where the shallowest reflections ($\approx$ 20 m) appear to be disturbed. The northwest boundary of this block is unknown.

The central fault block, 9 km wide in a NW-SE direction, is bounded on the northwest by the Tinker Creek fault and on the southeast by the Pen Branch fault, the northwest border fault of the concealed Dunbarton Triassic basin, now reactivated as a southeast dipping high-angle reverse fault within the Coastal Plain sediments. The Pen Branch fault (PBF) is the main throughgoing fault in a 3 km wide, 25 km long, fault zone consisting of subparallel fault segments that are commonly down-to-the-northwest north of PBF and down-to-the-southeast south of PBF. The offset of time horizons by the PBF increases to the northeast and the shallowest resolvable horizons appear in time to be deformed across its length. The Steel Creek fault, an antithetic fault to PBF, controls the drainage of Pen Branch, a tributary stream to the Savannah River.

The third fault block is bounded by the Pen Branch fault on the northwest. The southeast boundary of this southernmost block is unknown, but could be defined by the Martin fault, a down-to-the-northwest fault located south of SRS that appears to be a major structure.

Interpretation of isochron maps and analysis of trend surfaces fitted to reflection time horizons suggest that faulting was ongoing through the Late Cretaceous and was accompanied by tilting and horizontal rotation of the fault blocks. Fault block movements in the Tertiary are uncertain as shallow time horizons cannot be correlated areally with confidence; however, isochrons and reflection horizons correlated across faults reveal deformation, but not offset, of the shallowest resolvable events. The comparison between time-structure and topography reveals areas of positive correlation that suggest either near surface velocity variations or possible Cenozoic uplift.

The reprocessed seismic data elucidate the geometry of the Dunbarton basin and the underlying crustal structure. The Dunbarton basin is essentially a half-graben bounded on the northwest by the near vertical Pen Branch fault. The maximum thickness of the basin fill, as determined by seismic modelling, is between 4 and 5 km. Minor intrabasinal faults are imaged within the basin as well as bright discontinuous reflections that probably represent sills. The crystalline crust below SRS is highly reflective and is distinguished by zones of southeast dipping reflections that are correlatable between seismic lines. Two major crustal reflections, tentatively identified as the Augusta fault and a midcrustal decollement, appear to correspond to events imaged in seismic lines collected by COCORP 60 km to the southwest where the latter event was interpreted to be the Appalachian Master decollement. The continuity of deep reflection events along geologic strike from Georgia to South Carolina supports models for evolution of the Appalachian orogen that incorporate large scale, presumably Paleozoic age, thrusts beneath the Piedmont and under the Atlantic Coastal Plain.

Acknowledgements

I would like to thank Dr. Cahit Çoruh and Dr. John K. Costain for serving as my co-advisers. Additional thanks go to Dr. Edwin S. Robinson, Dale Stephenson and Dr. Lynn Glover III for serving as members of my graduate committee. Before his retirement Dr. Gilbert A. Bollinger also served on my graduate committee.

To my fellow graduate students past and present I extend my appreciation for their support and tolerance. I especially would like to mention the names of: Dr. M. Emin Demirbag, Cpt. Michael R. Mason USACE, "Amazing" Susan W. Hubbard, Alan Hubbard, Michael Moses, "New Guy" Douglas Eppler, Laura Lampshire, George Tsoflias, Carol Howard, Ashok Kumar Sen, Dwight Holland, Sandy Setterquist, Edmundo Norabuena, Suzanne Sayer, and Sam Peavy. To these individuals and to unnamed others I express my deepest thanks.

Funding for my dissertation research was provided by a research contract to Dr. Çoruh and Dr. Costain from Westinghouse Savannah River Laboratory. During my studies financial support was received from the Department of Geological Sciences in the form of three years of teaching assistantships. Additional support was received through fellowships sponsored by Chevron, Unocal, and Amoco. Mobil Oil Corporation through the Society of Exploration Geophysicists awarded scholarship monies 1989-1993.

Table of Contents

List of Illustrations

List of Tables

Introduction

Over the past two decades it has become increasing apparent that the sediments of the Atlantic Coastal Plain have been disturbed by widespread Cretaceous and Cenozoic fault movement (York and Oliver, 1976; Mixon and Newell, 1977; Prowell, 1983; 1988; Wentworth and Mergner-Keefer, 1983). Furthermore, it appears that faulting has been ongoing since at least the Cretaceous and at fairly uniform rates of movement (Prowell, 1988). In some areas, fault movement and upwarp have shaped topography and affected stream courses (Mixon and Newell, 1977; Rhea, 1989; Marple and Talwani, 1993; 1994). Most of these post-Jurassic faults occur parallel to preexisting Paleozoic tectonic trends; however, it is not often clear that preexisting geologic structures have been reactivated. Reverse faults are ubiquitous, although strike-slip and normal faults also occur. Exposures of faults are known along the Fall Line where faulting has juxtaposed crystalline basement rock and Cretaceous sediments (Prowell and O'Connor, 1978; Reinhardt et al., 1984). Farther out in the Coastal Plain evidence for post-Jurassic faulting comes from seismic reflection profiling and borehole data (Jacobeen, 1972; Behrendt et al., 1981; Snipes et al., 1993a)

The existence of widespread post-Jurassic faulting in the Atlantic Coastal Plain is a relatively new discovery. As noted by Prowell (1988), prior to 1970 the eastern United States was thought to be devoid of young faults. The documentation of extensive faulting in the Atlantic Coastal Plain raises questions about the origin and mechanism of the faults. The question is not merely academic, as the siting of nuclear power plants and public works depends upon the assessment of seismic hazard. That many faults show recurrent movement or even uniform movement over geologic time implies a common causative mechanism. The eastern United States, however, is a passive continental margin and such a tectonic setting constrains the range of possible models. Commonly, faulting is attributed to the crustal state of stress caused by ridge push (e.g. Talwani and Rajendran, 1991). Other proposed causes and/or trigger mechanisms include lithospheric

cooling and contraction, depositional loading, mantle hotspot migration, and hydroseismicity (see reviews by Prowell, 1988; Gardner, 1989).

In this study over 270 km of seismic reflection profiles collected over the Savannah River Site on the South Carolina Atlantic Coastal Plain, an area known to have concealed post-Jurassic faults, were reprocessed and interpreted. The interpretative reprocessing effort was directed to producing improved seismic reflector images of the Coastal Plain sediments and basement faults known to penetrate the sedimentary section. Particular attention was given towards recovering images of the shallow time section and detecting previously unknown basement faults. The seismic data were also reprocessed with the intent to recover reflections from geologic structures between the Coastal Plain and the upper mantle that could aid in the interpretation of the regional tectonic framework.

Time-structure, isochron and reflection amplitude maps were prepared on reflecting horizons within the Atlantic Coastal Plain sediments and the crystalline basement. Trend surface analysis of time horizons within the Coastal Plain was performed to study possible tilt and rotation of fault blocks through geologic time. The possible correlation between time-structure and surface topography, which could indicate Cenozoic tectonic movement, was also investigated.

The reprocessed SRS seismic reflection data were integrated with potential field, borehole and regional seismic reflection data in an overall interpretation of the regional tectonic framework.

Savannah River Site

The Savannah River Site (SRS) covers approximately 800 square kilometers on the Atlantic Coastal Plain along the Savannah River in Aiken and Barnwell counties, South Carolina (Figure 1). The nearest city is Augusta, Georgia, 26 km to the northwest; Charleston, South Carolina is located 150 km east-southeast.

The Savannah River Site was established in the early 1950s as a tritium and plutonium production facility for defense purposes. Early stewardship of the site was under E.I. du Pont de Nemours & Company for the Atomic Energy Commission. Currently, Westinghouse, Incorporated manages the site for the Department of Energy. Since the end of the Cold War the production facilities have been put in "cold standby" mode and the site has become a locus of environmental research. SRS, exclusive of the production facilities, has been declared a National Environmental Research Park.

The Savannah River Site is situated on the Aiken Plateau, a subdivision of the Atlantic Coastal Plain, which extends from the Fall Line on the northwest to the Citronelle Escarpment on the southeast and between the Savannah and Congaree rivers. The topography is developed on poorly consolidated sediments of mainly Tertiary age, is highly dissected, and is characterized by narrow steep-sided stream valleys and broad interstream areas. Elevations at SRS range from 115 m above sea level in the north of the site to less than 20 m above sea level along the Savannah River. The average dip of the topographic surface is 1.5 m per kilometer southeast (Siple, 1967). The onsite stream drainage is to the southwest, subparallel to regional dip, to the Savannah River. Important tributaries include: Upper Three Runs, Pen Branch, Steel Creek, Meyers Branch and Lower Three Runs. Upper Three Runs, in the northern third of the site, occupies a 3 km broad valley with an average topographic relief of 30 m. The other streams occupy much smaller valleys.

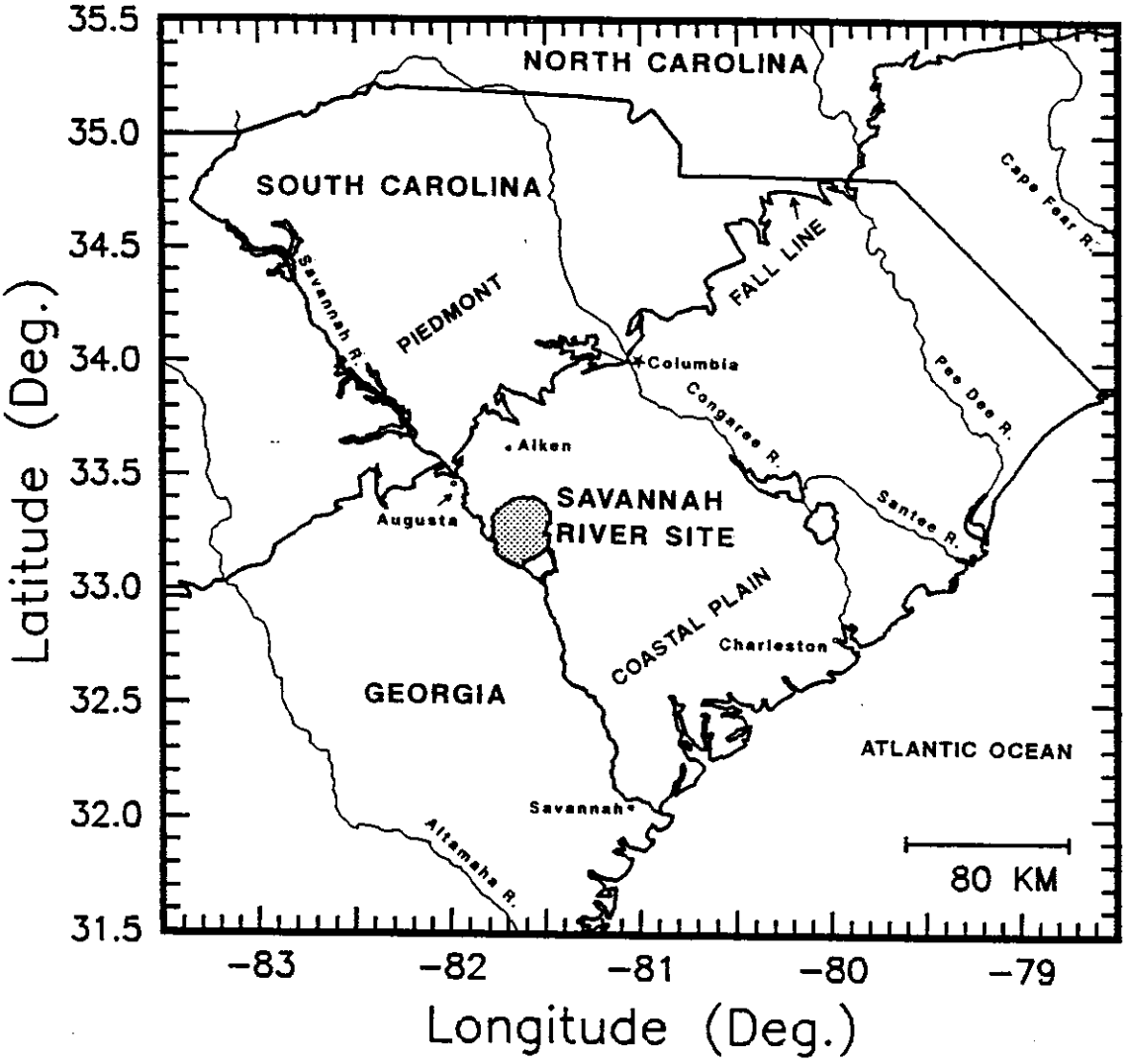

Figure 1. Location map of the Savannah River Site.

Geology

The Savannah River Site is underlain by a seaward-thickening wedge of Late Cretaceous-Tertiary nonmarine and marine strata of the Atlantic Coastal Plain. The sedimentary package thickens southeastward across the site from about 210 m to 430 m. From the base to the top of the section structural dips progressively lessen from 6.8 m/km to only 3.0 m/km (Siple, 1967; Snipes et al., 1993a). The strata unconformably overlie Paleozoic crystalline rocks in the northwestern part of the site and terrigenous Triassic siltstones and sandstones of the concealed Dunbarton basin in the southeastern part of the site.

Crystalline Basement

The nature of the crystalline basement at SRS is known from limited borehole data onsite and environs (Figure 2, Table 2). Most of the lithologies are amphibolite grade schists and gneisses and greenschist grade metavolcanic rocks similar to that found in the Kiokee and Belair Belts of the Piedmont (Diment et al., 1965; Siple, 1967; Daniels, 1974). In rock cores foliations with dips up to 55° are noted and structural fabrics typically show a combination of crystal-plastic and brittle deformational histories (Cumbest and Price, 1989b). The boundaries between the lower and higher grade metamorphic rocks at SRS have been interpreted to be fault bounded (Cumbest and Price, 1989b) similar to that observed in the Piedmont where belts of high and low grade metamorphic rocks are bounded by faults of the Eastern Piedmont fault system. From potassium-argon dating of crystalline rock from the DRB-7 and DRB-8 boreholes at SRS the last metamorphism occurred 290-258 Ma consistent with an Alleghanian age (Marine, 1976). Later Mesozoic rifting and post-Jurassic compression caused extensive reactivation of pre-existing zones of weakness, including the Eastern Piedmont fault system, and accounts for the observed brittle structural fabrics.

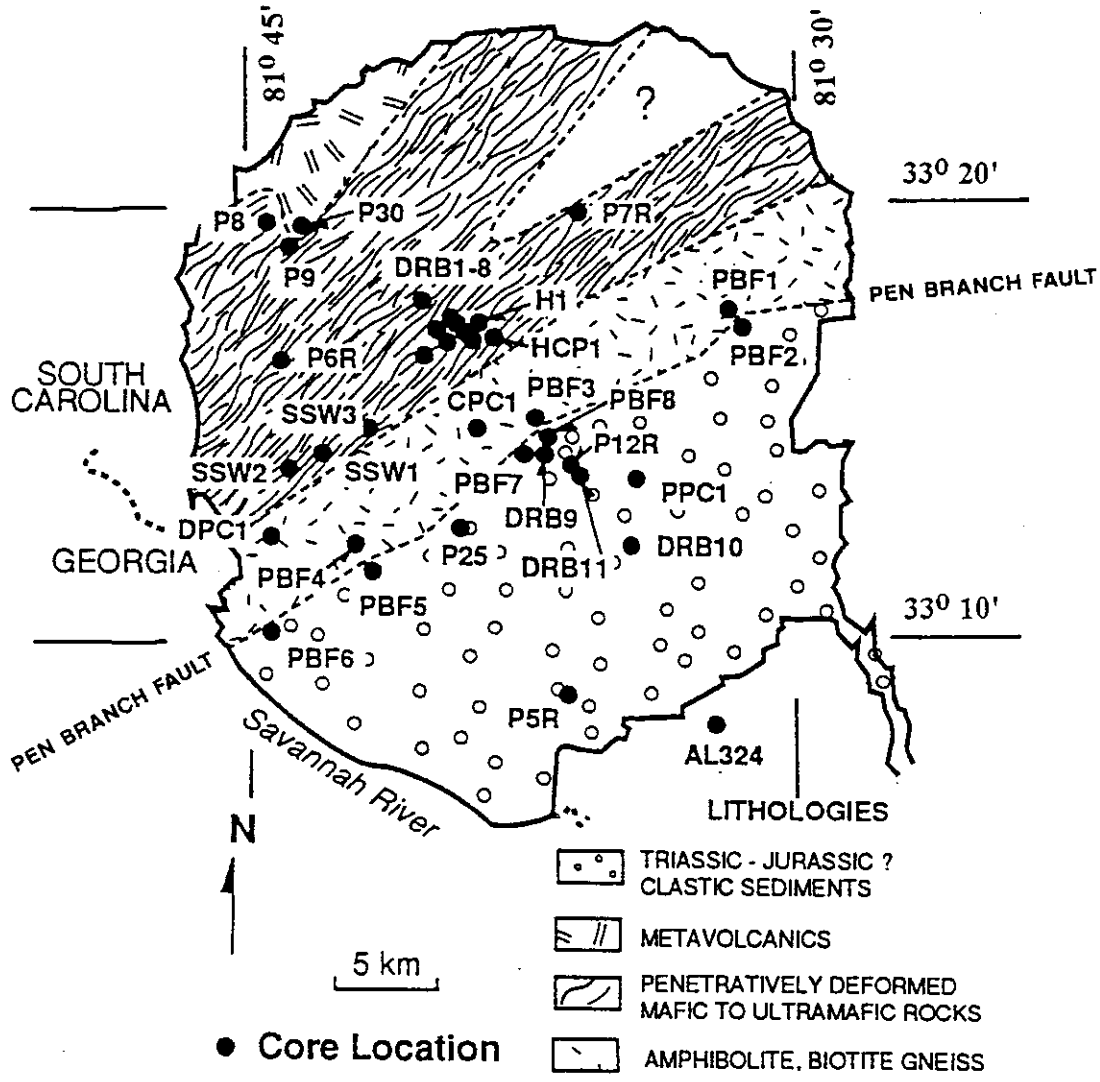

Figure 2. Basement geology map of SRS: (adapted from Cumbest and others, 1992).

The acoustic velocities of the crystalline rocks as determined from seismic refraction and borehole sonic log measurements range from 5000-7000 m/s and average approximately 5700 m/s near the top of basement (Bonini and Woollard, 1960; Chapman and DiStefano, 1989; Demirbag, 1990). The upper 2-9 meters of the crystalline basement is deeply weathered to saprolite. On sonic logs and temperature logs this interval is well defined and characterized by low acoustic velocity (≈2140 m/s) and higher thermal gradient, although in core and on other geophysical logs the top of basement can be difficult to distinguish from the basal lithologies of the Late Cretaceous Cape Fear Formation (D. Prowell, USGS, 1993 personal communication).

Eastern Piedmont Fault System

Thirty kilometers northwest of SRS crystalline basement emerges from beneath the Atlantic Coastal Plain to form the Piedmont physiographic province. The lithologic/structural divisions of eastern Piedmont are in part delineated by the Eastern Piedmont fault system (EPFS), an anastomosing network of northeast trending cataclastic zones distinguished by a common structural history and prominent linear aeromagnetic signatures (Hatcher et al., 1977). The EPFS and associated structures can be traced under the Coastal Plain using aeromagnetic data and certain major faults have been interpreted in seismic reflection data at SRS and elsewhere in the southeast (Cook et al., 1981; Chapman and DiStefano, 1989; Cumbest and Price, 1989a,b).

The faults of the EPFS typically exhibit a complex polyphase deformational history comprising early ductile deformation and mylonitization followed by one or more episodes of brittle faulting. Various parts of the EPFS are interpreted to be pre-Alleghanian in age, but major movement on the fault system occurred during the later stages of the Alleghanian orogeny (Bobyarchick, 1981). Alleghanian dextral strike-slip movement on the EPFS caused "shuffling" of lithostratigraphic units to juxtapose low and high grade metamorphic rocks. Recent work has shown that some of this movement was apparently transtensional as well as transpressional (Maher et al., 1994). Subsequent Mesozoic rifting caused extensive brittle reactivation of the EPFS and localized the development of rift basins during the Mesozoic (Bobyarchick, 1981; Petersen et al., 1984). Reactivation

of the EPFS in the current crustal stress field is a component of seismicity in the southeastern United States.

Near SRS the northwestern boundary of the EPFS is the Modoc zone, a steep northwest dipping metamorphic gradient and/or an intrusive contact (Pirkle, 1982; Snoke and Secor, 1982). The Modoc zone defines the boundary between the Carolina Slate belt (greenschist grade metamorphic rocks) on the northwest and the antiformal Kiokee belt (amphibolite grade metamorphic rocks) on the southeast (see Figure 17 on page 48). Overprinting the Modoc zone is a zone of dextral shearing up to 10 km wide (Secor et al., 1986a). Isotopic evidence indicates that movement on the Modoc zone was down to the northwest (transtensional) and occurred 315-290 Ma (Maher, 1994). The southeastern boundary of the EPFS is the Augusta fault (zone), a cataclastic zone and metamorphic gradient 250+ m wide between the Belair belt (greenschist grade metamorphic rocks) on the southeast and the Kiokee belt on the northwest. The Augusta fault dips to the southeast and is concordant with the structural fabric of both belts. Near Augusta, Georgia, part of the Augusta fault is offset by the Cretaceous-Tertiary Belair fault zone, an *en echelon* series of northeast trending brittle fault segments that penetrate into the Coastal Plain sediments (Prowell and O'Conner, 1978; Bramlett et al., 1982).

The Augusta fault has been the subject of much debate regarding its sense of movement, timing of movement, and the lateral and vertical extent of the fault. Variously, the Augusta fault has been interpreted as a dextral wrench fault (Hatcher et al., 1977; Bobyarchick, 1981), a thrust fault (Cook et al., 1981; Bramlett et al., 1982; Snoke and Secor, 1982) and a normal fault (Maher, 1987; Maher et al., 1994). Much of the controversy surrounding the Augusta fault derives from the interpretation of geophysical data collected across the structure. The Augusta fault is associated with a prominent aeromagnetic signature that can be traced from southern Virginia through Georgia, but for nearly all this distance the fault is concealed beneath the Atlantic Coastal Plain. On the basis of aeromagnetic data Hatcher and others (1977) proposed that the Augusta fault was a major Alleghanian strike-slip structure that formed the southeastern boundary of what was named the Eastern Piedmont fault system. Seismic reflection profiling in eastern Georgia by the Consortium for Continental Reflection Profiling (COCORP) imaged a prominent southeast dipping re-

flection that was interpreted to be the Augusta fault (Cook et al., 1981). The reflection in the COCORP data was traceable for over 80 km under the Atlantic Coastal Plain where it appeared to be a major decollement; however, because the Augusta fault is not actually exposed along the profile, the identification of the reflection as the Augusta fault was based on aeromagnetic data. Inconsistencies between the reflection event imaged in the COCORP data and the characteristics of the fault as exposed in outcrop led Iverson and Smithson (1983a) to dispute Cook and others' identification of the Augusta fault. Cook (1984b) dismissed Iverson and Smithson's contention that the Augusta fault is not a major reflective boundary and most interpreters have concurred with the original identification by Cook and others.

The Augusta fault has been most often called a thrust in interpretations of seismic reflection and field data, regardless of the fact that lower metamorphic grade rocks in the hanging wall are juxtaposed against higher metamorphic grade rocks in the footwall - a contradictory arrangement for a thrust fault. Recent field, petrographic and isotopic evidence indicates, however, that movement on the Augusta fault spanned ductile to brittle conditions, was late Alleghanian in age (274 Ma) and was hanging wall down, i.e., oblique-normal (Maher, 1987; Maher et al., 1994). Furthermore, the Augusta fault is now known to separate rocks of different cooling ages, 314 Ma for the Belair belt versus 278-272 Ma for the Kiokee belt (Maher et al., 1994). Importantly, movement on the Augusta fault was not contemporaneous with, but later than, movement on the Modoc zone which it resembles (Maher et al., 1994). This evidence has been interpreted to suggest that the Augusta fault represents normal faulting associated with gravitational collapse of the Alleghanian orogenic front (Maher, 1987; Maher et al., 1994).

Dunbarton Basin

The Dunbarton basin underlies the Atlantic Coastal Plain sediments in the southern half of the Savannah River Site (Figure 2 and Figure 3). The basin is named after the hamlet of Dunbarton, South Carolina, which was evacuated in the 1950s for the construction of the Savannah

River Site. The presence of the basin has been confirmed by at least 11 boreholes and the extent and gross geometry of the basin has been inferred from seismic refraction, seismic reflection, gravity, magnetic and electromagnetic surveys (Siple, 1967; Marine and Siple, 1974; Daniels, 1974; Daniels et al., 1983; Chapman and DiStefano, 1989; Price et al., 1989; Anderson, 1990; Stephenson and Stieve, 1992). Identification of the basin as Triassic in age is based on structural and sedimentologic similarities to the exposed Triassic basins in the Piedmont (Siple, 1967; Steele and Colquhoun, 1985; Manpiezer and Cousminer, 1988).

The Dunbarton basin is approximately 15 km wide, at least 40 km long and trends N 60° E. From gravity and magnetic modelling studies the floor of the basin has been interpreted to dip to the southeast (Marine and Siple, 1974; Anderson, 1990). The depth of the Triassic fill is unknown, but drilling confirms it is in excess of 900 m (Marine and Siple, 1974). Transient electromagnetic soundings indicate that the depth of the basin fill is in the excess of 1800 m (Price et al., 1989) and gravity and magnetic modelling studies have yielded similar depths (Marine, 1974; Daniels et al., 1983; Anderson, 1990; Cumbest et al., 1992). Drilling in the nearby Riddleville basin has established the minimum thickness of that basin to be 2250 m (Daniels and Leo, 1985) and this value is probably applicable to the Dunbarton basin as well. The northwestern boundary of the basin is defined by the northeast trending Pen Branch fault. The southeastern boundary of the basin occurs offsite and is uncertain. South of SRS drilling has revealed an up-to-the-southeast fault, named the Martin fault, between metamorphosed Triassic sediments and weathered schist that might define the southeastern boundary of the Dunbarton basin (Snipes et al., 1993b). North of the same general area Faye and Prowell (1982) interpreted a major southeast dipping fault that they named the Millet fault; however, geophysical surveys described by Anderson (1990) have disputed the existence of the Millet fault. The continuation of the basin to the northeast and southwest off the site area is interpreted from potential field data.

The Dunbarton basin has been interpreted to connect with the Riddleville Triassic basin to the southwest (Daniels et al., 1983; Petersen et al., 1984). Daniels and others (1983) recognized the Dunbarton basin as the southernmost Triassic basin oriented parallel to the Appalachian structural trend, whereas the Riddleville basin, as interpreted from aeromagnetic data, trends east-west. The

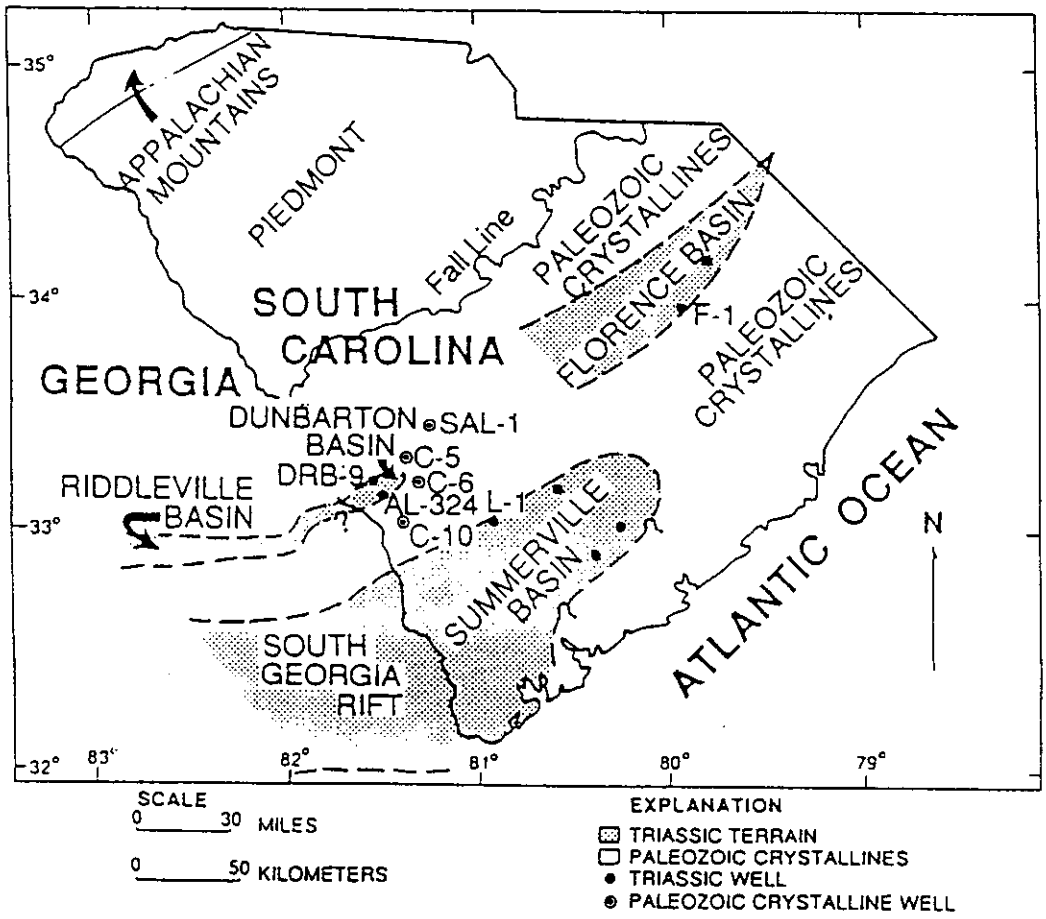

Figure 3. Location map of the Dunbarton basin: (adapted from Snipes and others, 1993a).

magnetic field anomalies associated with the basins differ and are separated by an east-west magnetic lineament that merges westward with Goat Rock fault (Daniels, 1974). This difference in potential field anomaly character led Daniels and others to suggest that the two basins, though connected, might be structurally different. There is no evidence that indicates the Dunbarton-Riddleville basin connects to the larger South Georgia Rift/ Summerville basin to the south (Figure 3). Gravity, magnetic and borehole data point to the presence of a vertically extensive mafic mass, probably related to Mesozoic rifting, that separates the basins from the South Georgia rift (Daniels, 1974; Cumbest et al., 1992; Kish, 1992).

Petersen and others (1983) on the basis of the interpretation of seismic reflection data collected across the Riddleville basin by COCORP proposed a model for the formation of the Riddleville basin involving reactivation of the Augusta fault and related structures. In their model Mesozoic rifting caused backslip on the Augusta fault and faults within its hanging wall such that at a location where the Augusta fault steepens, the Magruder fault, the northwest border fault of the Riddleville basin, was formed and ensuing block rotation of the upper plate opened the basin graben. Petersen and others found no evidence for the Magruder fault offsetting the Augusta fault and interpreted the fault to sole into the detachment. A similar scenario might apply for the Pen Branch fault and the Dunbarton basin; however, the COCORP data are not unambiguous. Nevertheless, it is clear that many of the Triassic rift basins of the eastern United States were formed as a consequence of Mesozoic reactivation of pre-existing faults (Bobyarchick and Glover, 1979; Ratcliffe and Burton, 1985; Swanson, 1986; Costain and Çoruh, 1989).

The existence of a Triassic basin beneath the Atlantic Coastal Plain sediments at the Savannah River Site was not known until the early 1960s. Early seismic refraction work by Bonini and Woollard (1960) revealed an anomalously low basement seismic refraction velocity (4830 m/s) in the southern part of SRS as opposed to the north (5945 m/s), but the variation was attributed to lower velocity Carolina Slate Belt rocks. In 1962 a program to investigate the feasibility of storing high level radioactive waste in caverns excavated in the crystalline basement led to the drilling of hole P5R near where the low basement seismic refraction velocity was measured. Hole P5R (Elev. 63.5 m, TD 400.3 m) encountered reddish brown claystones and sandstones at a depth of

374.9 m after drilling through the weathered zone at the base of the Coastal Plain (Marine and Siple, 1974). The similarity of these red beds to those in known Triassic basins led to the assignation of a Triassic age (Siple, 1967).

Aeromagnetic surveys conducted over the Savannah River Site and surrounding areas in the 1950s and 1960s revealed a well defined magnetic low over the southern half of the site trending N 57° E (Petty et al., 1965; see also Figure 24 on page 65). With the confirmation of Triassic sediments in P5R successive researchers interpreted this magnetic anomaly as defining the extent of the basin (Siple, 1967; Marine and Siple, 1974; Daniels and Leo, 1985). Marine and Siple (1974) on the basis of these aeromagnetic data interpreted the Dunbarton basin as having an asymmetric cross-section with a gentle northwestern flank and a steep southeastern flank. The steep magnetic gradient on the southeastern flank was interpreted as evidence for a large normal fault that bounded nonmagnetic Triassic basin fill from crystalline basement rock; however, they did allow for an alternative explanation that the magnetization of the crystalline rock on the southeastern side of the basin is sufficiently greater than that on the northwestern side to account for the steep observed gradient. Recent combined magnetic and gravity modelling by Cumbest and others (1992) of the Dunbarton basin and nearby potential field anomalies has indicated that this steep gradient and the magnetic low over the Dunbarton basin is simply part of the magnetic anomaly associated with a presumed mafic complex south of the basin. Indeed, the magnetic modelling indicated that the Dunbarton basin itself contributes little to the overall magnetic anomaly.

An effort to determine the northwestern boundary of the Dunbarton basin and to investigate the hydrologic nature of the crystalline/Triassic contact led to the drilling of hole DRB-9 in 1969 (Marine, 1974; Marine and Siple, 1974). Hole DRB-9 (KB 92.1 m, TD 823.3 m) was located on the basis of seismic reflection data that indicated the absence of a reflector interpreted to be top of crystalline basement. This hole passed into weathered red beds at 306-315 m at the base of the Coastal Plain and entered hard red beds at 323.4 m depth. At a depth of 800.7 m the drillbit entered crystalline rock.

The Triassic section in DRB-9 is composed of a reddish-brown breccia that contain fragments of pink weathered gneiss in a claystone matrix. Marine and Siple (1974) classified the rock as a

fanglomerate representing talus and mudflows. In core weak bedding was noted having dips of 20° - 45° and an average dip of 35°. From the borehole sonic log the average acoustic velocity of the Triassic section is 4313 m/s. At the base of the Triassic section in DRB-9 a 0.9 m weathered zone was encountered, but no zone of broken rock, such as might be expected denoting a fault zone, was encountered (Marine 1974). The crystalline basement in DRB-9 is a multicolored gneiss having augen of pink feldspar in a green hornblende matrix. In DRB-9 the average acoustic velocity of the crystalline rock is 5286 m/s.

Both holes P5R and DRB-9 indicated that the Triassic basin fill is impermeable. Hole DRB-10 was drilled in 1971 to further investigate the the hydrologic properties of the Dunbarton basin. Hole DRB-10 (Elev. 76.4 m, TD 1281.8 m) drilled through 902 m of alternating red mudstone, fine-grained sandstone, and local conglomerate layers of apparent fluvial origin (Marine and Siple, 1974). The lithologic character of the Triassic fill at TD was similar to that at the top of the Triassic section. Marine and Siple noted that the source materials for the sediments in DRB-9 and DRB-10 appeared to be similar and suggested that the angularity of clasts and immaturity of sediments in DRB-10 indicated a distance of transport of less than 35 km.

The borehole velocity profile from DRB-10 (Figure 4) shows that beneath the weathered zone at the base of the Coastal Plain section the average acoustic velocity increases rapidly from 3572 m/s for the first 20 m to 3928 m/s for the first 40 m and then increases monotonically to 5681 m/s for the bottom 80 m of the borehole (1200-1280 m). The average acoustic velocity for 400-1200 m depth in the bore is 5226 m/s.

The investigation of suspected intrabasinal faults led to the drilling of holes P12R (Elev. 89.3 m, TD 388.2 m) and DRB-11 (Elev. 83.6 m, TD 999.8 m). These holes, separated by only 211 m, were designed to be deviated holes to intersect a fault interpreted from seismic reflection data (Parsons, Brinckerhoff, Quade & Douglas, Inc., 1973). Of the two holes, only hole DRB-11 was completed as planned. The difference in elevation of the top of Triassic between the two holes was only 0.6 m where the seismic reflection data indicated a fault of 6-15 m offset. Although no evidence for a fault offsetting the pre-Cretaceous surface was found, two 1 m wide zones of sheared

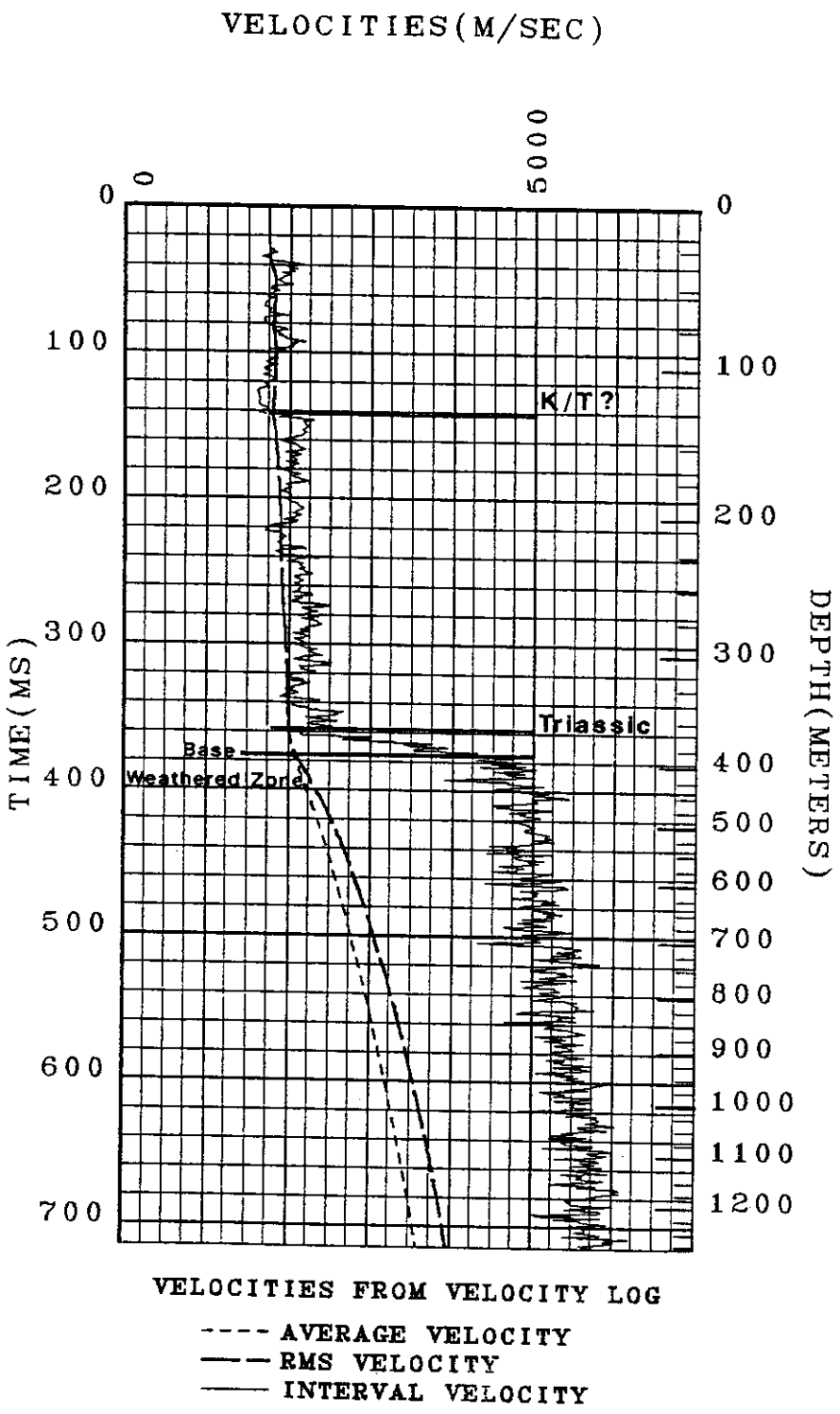

Figure 4. Velocity profile borehole DRB-10: Interval velocity, average velocity and RMS velocity from borehole DRB-10.

rock containing a large number of slickenslides were encountered in hole DRB-11 at depths of 713.5 m and 991.2 m. The lower sheared zone also contained a thin gouge.

The Triassic basin fill penetrated in hole DRB-11 was similar to that in DRB-10, albeit somewhat coarser and more poorly sorted. In core the dip of lithologic contacts was observed to be 5°-30°; with 7°-10° dips most common. The dip of joints and fracture surfaces range from 23° to 85°. The borehole acoustic velocity profile from DRB-11 is similar to that from DRB-10 (Marine, 1974).

The borehole velocity profiles from the DRB-10 and DRB-11 boreholes provide the only deep velocity information for the Dunbarton basin. These data confirm that the velocity of the deeper basin fill is well within the range of measured velocities for the crystalline basement at SRS. From the standpoint of the interpretation of seismic reflection data, a lack of acoustic impedance contrast between the basin fill and the crystalline basement might preclude seismic reflection imaging of the base of the Dunbarton basin. Seismic refraction measurements from the top of Triassic basement yield velocities from 4000 m/s-5000 m/s and average about 4500 m/s. From borehole sonic logs the weathered zone at the top of Triassic basement has an average velocity of 2143 m/s and is between 2 to 9 m thick, which similar is to that of the saprolite layer on crystalline basement.

Stratigraphy

The stratigraphic division of the Atlantic Coastal Plain section into formations is constantly in revision. Excellent summaries of the evolution of Coastal Plain formation nomenclature in South Carolina are those of Hattner and Wise (1980), Gohn (1992), and Fallaw and Price (1992). In this study the formation terminology used by Berkman (1991) and Snipes and others (1993a) is adopted (Figure 5).

The Late Cretaceous section at SRS is composed of weakly indurated, highly variable nonmarine sands and clays that range from Santonian to Maastrichtian in age (Snipes et al., 1993a). Generally, the lower section is representative of fluvial and delta plain depositional environments

AGE		UNIT		LITHOLOGY
TERTIARY	Miocene(?)	"upland unit"		Clayey, silty sands, conglomerates, pebbly sands, and clays; clay clasts common
	Late Eocene	Barnwell Group	Tobacco Road Sand	Red, purple, and orange, poorly to well-sorted sand and clayey sand with abundant clay laminae
			Dry Branch Formation	Tan, yellow, and orange, poorly to well-sorted sand with tan and gray clay layers near base; calcareous sands and clays and limestone in lower part downdip
			Clinchfield Formation	Biomoldic limestone, calcareous sand and clay, and tan and yellow sand
	Middle Eocene	Santee Limestone and correlatives		Micritic, calcarenitic, shelly limestone, and calcareous sands; interbedded yellow and tan sands and clays; green clay and glauconitic sand near base
	Early Eocene	Congaree Formation		Yellow, orange, tan, and greenish-gray, fine to coarse, well-sorted sand; thin clay laminae common
	Paleocene	Williamsburg Formation		Light gray, silty sand interbedded with gray clay
		Ellenton Formation		Black and gray, lignitic, pyritic sand and interbedded clays with silt and sand laminae
LATE CRETACEOUS	Maestrichtian	Lumbee Group	Peedee Formation	Gray and tan, slightly to moderately clayey sand; gray red, purple, and orange clays common in upper part
	Campanian		Black Creek Formation	Tan and light to dark gray sand; dark clays common in middle and oxidized clays at top
	Santonian		Middendorf Formation	Tan and gray, slightly to moderately clayey sand; gray red, and purple clays near top
		Cape Fear Formation		Gray, clayey sand with some conglomerates, and sandy clay; moderately to well indurated
LATE TRIASSIC		Newark Supergroup		Boulder conglomerate, red, arkosic, poorly sorted sandstone and red shale
PALEOZOIC and CRYPTOZOIC(?)		"crystallines"		Biotite gneiss, mica schist, amphibolite, chlorite schist, and granitoid rocks

Figure 5. Savannah River Site stratigraphy: (adapted from Snipes and others, 1993a).

and the upper section is representative of delta plain, delta front and prodelta sedimentation (Fallaw and Price, 1992). From oldest to youngest the formations are: Cape Fear, Middendorf, Black Creek and Peedee. The contacts between these formations are interpreted by Snipes and others (1993a) to be unconformable. Inasmuch as unconformities might give rise to correlatable seismic reflection markers, the nature of the formations and the formation boundaries is described briefly below. Most of the descriptive information that follows is derived from Fallaw and Price (1992) and Snipes and others (1993a).

The Cape Fear Formation is the most indurated of the Coastal Plain formations at SRS; it consists of poorly sorted, coarse and medium grained, silty and clayey sands interbedded with clays. The contact of the Cape Fear Formation with the underlying weathered layer at the top of basement is well defined on sonic and temperature logs, but can be difficult to distinguish in core. The contact with the overlying Middendorf Formation is denoted by a pebbly zone and on resistivity logs is recognized by a resistivity increase upon entering the overlying Middendorf Formation (Figure 6). In the center of SRS the Cape Fear Formation attains a thickness of 43 m.

The Middendorf Formation is composed of moderate to well sorted, coarse and medium grained sands that contain occasional clay clasts. In the northern part of SRS the Middendorf sands become less clayey. The top of the formation is defined by a clayey interval that consists of oxidized kaolinitic clays and sand. The Middendorf Formation is also about 43 m thick in the central part of SRS.

The Black Creek Formation consists of silts, clays and poorly to moderately sorted fine to coarse grained sands. The contact between the Black Creek Formation and the underlying Middendorf Formation is picked where the sands of the Black Creek Formation overlay the oxidized clays of the Middendorf Formation. According to Snipes and others (1993a) a pebbly layer, which they suggest marks an unconformity, is sometimes found at the base of the Black Creek Formation. They note that where the Middendorf clay layer is absent, the contact with the Black Creek Formation is difficult to pick. An intraformational unconformity, denoted by a thick oxidized clay layer, occurs in the Black Creek Formation in the western part of SRS. The Black Creek Formation is approximately 91 m thick in the central part of SRS.

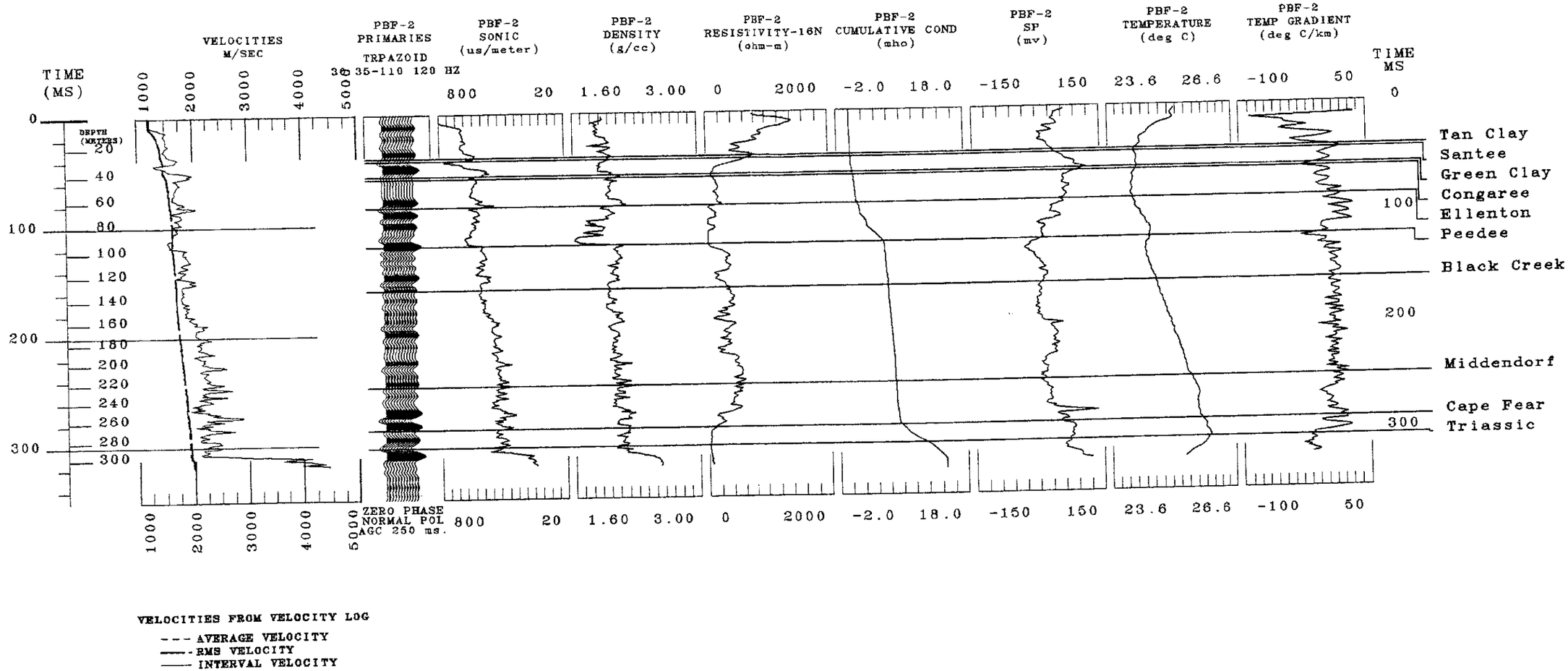

Figure 6. Geophysical log responses of the Coastal Plain sediments: Suite of geophysical logs from the PBF-2 borehole illustrating the log response of the Coastal Plain formations. Formation tops from Berkman (1991). Note that the top of basement and the top of the Peedee Formation (top of Cretaceous) are particularly well defined geophysical boundaries on the sonic, density, cumulative conductivity, temperature and temperature gradient logs. The top of the Cape Fear Formation is a distinctive boundary on the cumulative conductivity log.

The clay layers at the top of the Middendorf Formation and within the Black Creek Formation could be areally extensive seismic reflection markers. The identification of these layers in seismic reflection data would aid in stratigraphic identification of reflecting horizons in areas where borehole data are not available.

The lower Peedee Formation is composed of poorly to well sorted, fine to coarse grained sands that contain lignitic, pebbly, and clayey zones. The upper Peedee Formation is generally composed of oxidized clays interbedded with sands. The contact of the Peedee Formation with the underlying Black Creek Formation is placed at the bottom of a coarse sand layer that overlies sands interbedded with dark clays. Snipes and others note that the basal Peedee is pebbly, indicative of an unconformity. The Peedee Formation is about 21 m thick in the central part of the site.

The Tertiary section at SRS consists of highly variable, poorly consolidated nonmarine and marine sands, silts clays and limestones ranging from Paleocene to Miocene in age. The lower Tertiary section was deposited in fluvial, deltaic and marginal marine environments. During the Eocene deposition was mostly in shallow marine settings and by the Miocene nonmarine deposition was prevalent (Fallaw and Price, 1992). Most of the Tertiary section is poorly imaged in the seismic reflection data used in this study; hence, only the stratigraphic units likely to be imaged are described below. Most of the lithologic descriptions that follow are derived from Snipes and others (1993a).

The Paleocene Ellenton Formation consists of poorly and moderately sorted, silty and clayey sands, and pebbly sands interbedded with clays. Throughout most of SRS the contact between the Ellenton Formation and the underlying Peedee Formation is defined where sands in the Ellenton Formation overlie oxidized clays of the Peedee Formation. Where the Peedee clays are missing, however, the contact is difficult to pick. On sonic and temperature logs the contact, to within a few meters, is usually distinctive (Figure 6). Typically, on sonic logs a low velocity layer (clays in Peedee ?) separates variable, low velocity material above (Tertiary) from generally less variable, higher velocity material below (Cretaceous). In temperature logs a distinct break in the thermal gradient occurs at the K/T boundary indicating a change in thermal conductivity between poorly conductive Tertiary sediments and more highly conductive Cretaceous sediments.

The remainder of the Tertiary section, spanning the later Paleocene through the Miocene, is formed of sands, silts and clays that are fine to coarse grained, poorly to well sorted, and locally miceaous, lignitic, or gluaconitic. Of note is the middle Eocene Santee Formation, which consists in part of shallow marine limestones and calcareous silts and clays. The calcareous facies within the Santee Formation, and similar facies within the overlying Late Eocene Barnwell Group, could give rise to prominent discontinuous seismic reflections because of the generally higher velocity of the carbonates compared to the sands, silts and clays.

Pen Branch Fault

The Pen Branch fault defines the northwestern boundary of the Dunbarton basin (see Figure 2 on page 6). Seismic reflection profiling and drilling have established that the fault strikes N 53°-57° E at the base of the Coastal Plain and dips to the southeast (Chapman and DiStefano, 1989; Berkman, 1991). Within the Coastal Plain sediments the fault is a high-angle reverse fault, which implies reactivation of the fault under compression following infilling of the basin and peneplanation of the current basement surface. Displacement on the fault is approximately 30 m at the top of basement and decreases into the overlying sediments implying growth faulting. Seismic reflection data clearly show reflections offset as shallow as 50 ms ($\approx$ 50 m) above the basement reflection and drape folding of sediments above the fault (Chapman and DiStefano, 1989; Snipes et al., 1993a). The upward limit that the fault penetrates is unknown, although seismic data and borehole data indicate deformation associated with the fault persists to within a few tens of meters of the surface where Late Eocene age (38 m.y.) sediments are disturbed (Berkman, 1991; Stieve et al., 1991; Stieve et al., 1993).

Movement along the Pen Branch fault was ongoing through the Late Cretaceous to at least the Eocene as demonstrated by the thinning of isopachs over the hanging wall of the fault (Snipes et al., 1993a). Calculated rates of fault movement derived from borehole data are 0 to 1.5 m/m.y. and average about 0.4 m/m.y. over the last 85 million years (Snipes et al., 1993a). Recent

topographic and field studies conducted to study possible post-Eocene movements along the fault show no evidence for either a topographic expression of the fault or Quaternary fault movement (Geomatrix Consultants, 1993). Nevertheless, the analysis of stream drainages along the trace of the Pen Branch fault suggests rejuvenation of the drainages, but this has been attributed to more regional tectonic uplift and tilting and not specifically to post-Eocene movement along the Pen Branch fault (Hanson et al., 1994).

The attitude of the Pen Branch fault in the crystalline basement is uncertain. A dip calculation based on the location of the fault at the top of basement on seismic line PBF-18 and the intersection of the fault plane with borehole DRB-9 gives a minimum dip of 70° southeast. Deep seismic reflection profiling by Conoco in 1987-88 did not image the fault beneath the Coastal Plain. A drilling program by SRS in 1990-91 bracketed the Pen Branch fault, but was designed only to investigate faulting in the Coastal Plain sediments and the boreholes penetrated only a few meters into basement (Berkman, 1991). The SRS drilling program did, however, unequivocally establish the Pen Branch fault as the northwest boundary of the Dunbarton basin.

Other faults

Other named basement faults that offset the Coastal Plain sediments at SRS include the Crackerneck, Steel Creek, Ellenton and Atta faults (Stephenson and Stieve, 1992). Most of these faults were first detected on seismic reflection data. All of these faults are high-angle faults and many are only unambiguously identified on single seismic profiles. The time-offset of the Crackerneck, Steel Creek and Atta faults at the pre-Cretaceous unconformity is similar to that of the Pen Branch fault ($\approx$ 30 ms), whereas the Ellenton fault exhibits only 5-10 ms of offset. The Crackerneck and Steel Creek faults are interpreted to trend northeast-southwest and the Ellenton and Atta faults are interpreted to trend more north-south (Stephenson and Stieve, 1992; see also Figure 43 on page 103).

An abrupt increase in the slope of the basement surface north of Upper Three Runs has been interpreted as evidence for Late Cretaceous-Cenozoic activity of the Upper Three Runs fault (Cumbest and Price, 1989a). The Upper Three Runs fault is a basement structure identified from aeromagnetic and borehole data and interpreted as a Paleozoic fault that soles into the Augusta fault at depth (Cumbest and Price, 1989a; Stephenson and Stieve, 1992). No evidence for this fault offsetting Coastal Plain sediments was found during seismic reflection profiling by Conoco in 1987-88 (Chapman and DiStefano, 1989).

Seismicity

Because of the sensitive nature of the facilities at SRS seismic hazard is a prime concern. Following establishment of the SRS seismic network in 1976 two events have been recorded on site (see Figure 7 on page 26). The first earthquake was a duration magnitude (M_D) 2.6, intensity MM III-IV event on June 9, 1985, located at latitude 33° 13.38′ N and longitude 81° 41.73′ W (ERH 0.3 km) at a depth of 0.96 km (ERZ 1.6 km) that was recorded by over 20 stations in the southeastern United States (Stephenson et al., 1985; Talwani et al., 1985). The focal mechanism solution was interpreted as indicating left-lateral slip on a fault striking N 46° E and dipping 46° E (Talwani et al., 1985). The auxiliary nodal plane had a strike of N 46° W and dip 88° SW. The second earthquake was a duration magnitude (M_D) 2.0 event on August 4, 1988, located at latitude 33° 12.94′ N and longitude 81° 39.81′ W at a depth of 2.86 km (Stephenson, 1988). The 1988 earthquake, unlike the 1985 earthquake, was not felt on site and was only detected by seismic stations within 100 km of the epicenter. No focal mechanism solution could be obtained for this event. The epicenter of the 1988 earthquake is located approximately 4000 m southeast of the 1985 earthquake epicenter. The proximity of both events to the faulted northwestern border of the Dunbarton basin suggests that syntectonic structures might be involved.

Seismicity in South Carolina and Georgia is characterized by diffuse distribution of epicenters with notable concentration of earthquakes occurring in specific seismogenic zones (Tarr et al.,

1981). Many of the earthquakes occur near mapped faults or at the edges of intrusives and metamorphic belts. A significant number of events are associated with reservoir induced seismicity (RIS). Most of the foci are at shallow depths (< 8 km) and where focal plane solutions have been determined, thrust or strike-slip motion on steeply dipping fault planes is indicated. The calculated P-axes strike northeast and are subhorizontal. These data are consistent with *in situ* stress measurements in the region that indicate a northeast-southwest trending stress regime (Zoback et al., 1984).

The driving mechanism for neotectonism in the southeastern United States is generally accepted to be ridge push from the Mid-Atlantic ridge. Other proposed mechanisms and/or triggers include hydroseismicity, lithospheric cooling and contraction, depositional loading, and mantle hotspot migration (see reviews by Prowell, 1988; Gardner, 1989).

Geophysical Data

The Savannah River Site has been the focus of myriad geological and geophysical investigations since its establishment in the early 1950s. Most of these investigations, as a consequence of the defense-related activities of the site, have centered on earthquake hazard potential and groundwater flow. Geophysical surveys have included seismic reflection/refraction (Bonini and Woollard, 1960; Marine and Siple, 1974; Chapman and DiStefano, 1989; Berkman, 1991), ground penetrating radar (Sexton and Pirkle, 1993), aeromagnetic (Petty et al., 1965; Daniels, 1974), gravity (Anderson, 1990), transient electromagnetic soundings (Price et al., 1989) and various borehole investigations (Diment et al., 1965; Siple, 1967; Marine and Siple, 1974; Stieve et al., 1991; Stieve et al., 1993).

The primary focus of this study is the reprocessing and interpretation of a seismic reflection data set collected at SRS. These seismic reflection data are discussed in more detail below along with the other geophysical data sets used.

Seismic Reflection Data

SRS Vibroseis Data Set

Most of the seismic reflection data used in this study were collected during 1987-88 by Conoco, Inc., for the Environmental Sciences Division of Savannah River Laboratories (Chapman and DiStefano, 1989). The Conoco data set consists of 264 km (26 lines) of multifold vibrator seismic reflection data that were collected primarily to define basement structure in the central SRS area and thereby provide information necessary to locate future facilities (Figure 7 and Figure 8). Prime importance was attached to determining the areal and vertical extent of basement faults known to penetrate the Coastal Plain sediments. Other goals were to define further the Dunbarton basin and to image any geologic structure shallower or deeper than the prominent basement reflector. In addition to the seismic reflection data, vertical seismic profiles were recorded in three boreholes on site.

The Conoco seismic data, herein designated the SRS series of seismic lines, were recorded using a 96 channel recording system and split-spread cable geometry. Various combinations of source-receiver offsets, station intervals, and number of vibrators were used to image specific targets. These data were collected in three groups: Phase I, Phase II, and Experimental (Table 1). The Phase I data comprise 15 seismic lines (212.2 km) that were designed to provide regional coverage over the site. The Phase II data comprise 8 seismic lines (43.6 km) and were recorded as infill based on the results of the first phase. The experimental (EXP) seismic lines (8.5 km) were recorded over selected portions of Phase I seismic lines SRS-2, SRS-9, and SRS-12 with the intent to acquire higher resolution data to investigate specific geologic features or anomalies detected with other geophysical techniques.

The Conoco data set was the first quality regional seismic reflection survey of the Savannah River Site and interpretation of these data led to the delineation of basement faults believed to penetrate the Coastal Plain section on site. Specifically, the northwestern border fault of the

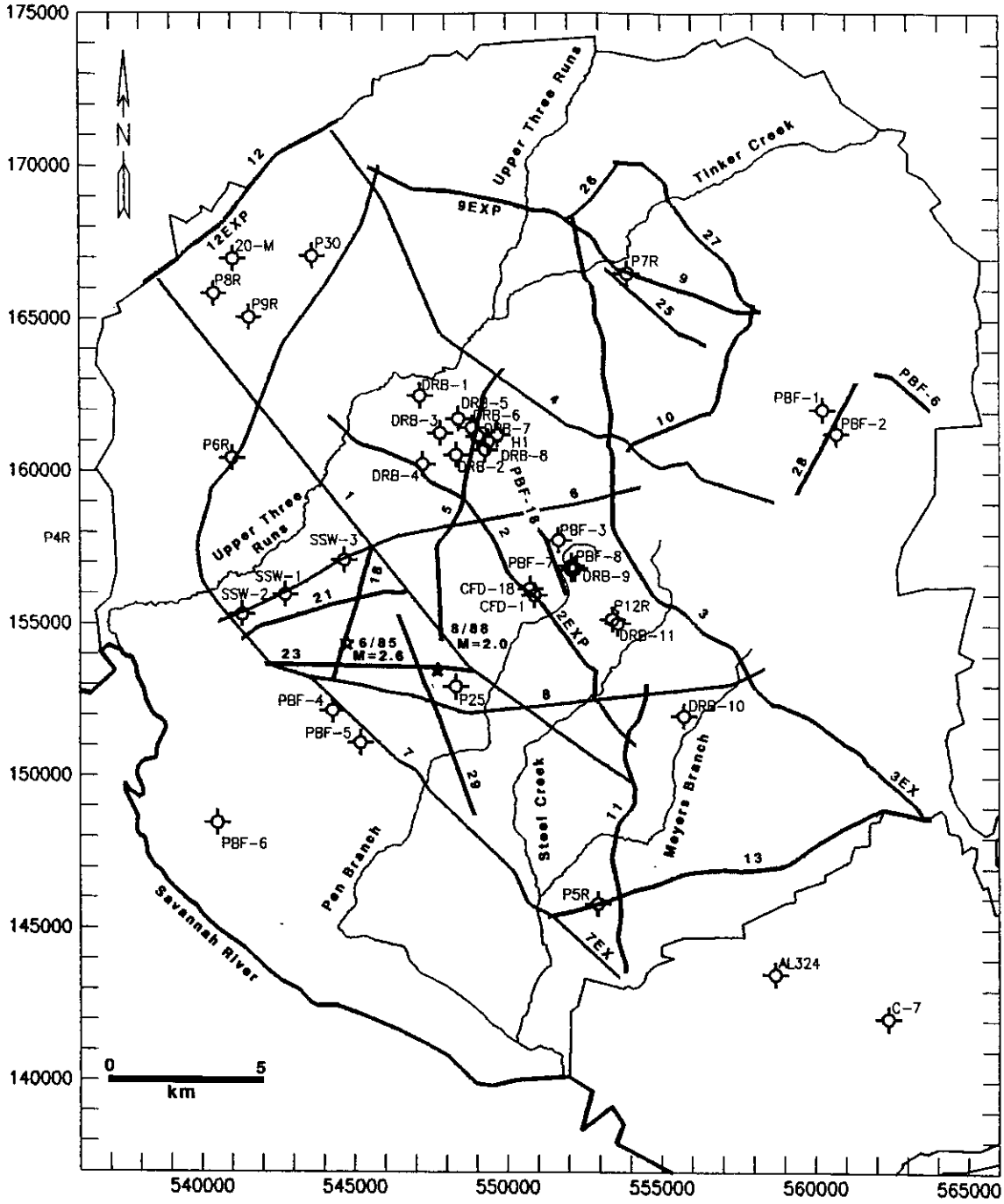

Figure 7. Seismic reflection survey and borehole basemap: Conoco Phase I lines are indicated in orange (12 m group interval) and red (16 m group interval). The Phase II lines are shown in green. Conoco experimental lines are indicated in brown atop seismic lines SRS-2, SRS-9, and SRS-12. The two EMEX high resolution seismic lines used in this study are shown in blue. All boreholes are tabulated in Table 2. Stars are earthquake epicenters annotated with date and magnitude of the event. Numbers around the edge of this map and succeeding maps are South Carolina state grid coordinates in meters (NAD 1983).

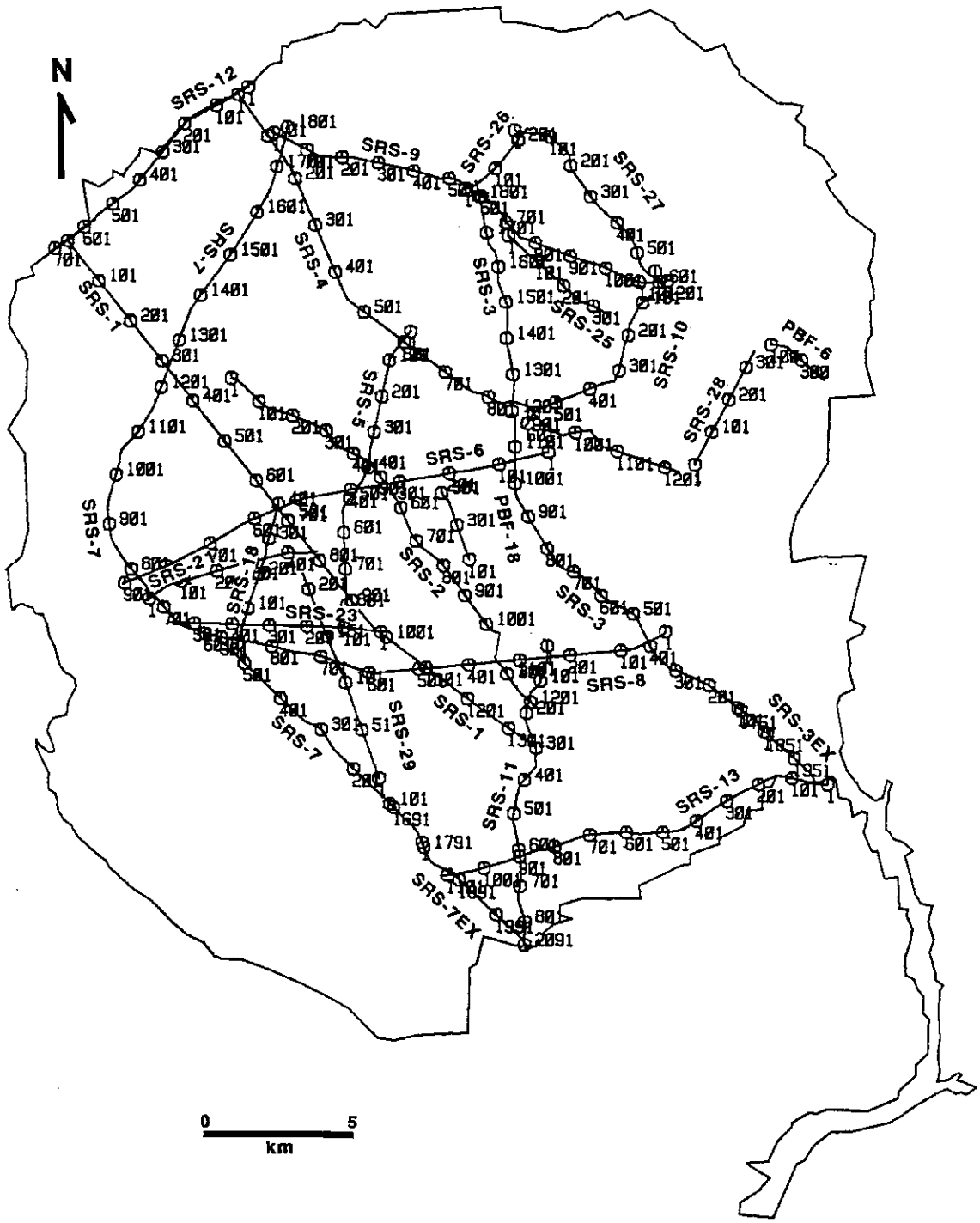

Figure 8. Seismic reflection survey shotpoint map: Station locations of the Conoco SRS and EMEX PBF seismic reflection lines used in this study are shown.

Dunbarton basin, the Dunbarton fault, later named the Pen Branch fault, was first clearly imaged and mapped. Nevertheless, these data were processed with the primary focus on imaging the top-of-basement reflection and this emphasis limited the information that could be extracted. In particular, the shallow time section was muted (0-100 ms, i.e., $\approx$ 0-90 m) in the data processing; hence, the upward limit of deformation associated with many of the faults could not be determined. Also, few reflections were detected from strata within the Dunbarton basin and the presence of the basin fill was indicated primarily by a decrease in amplitude of the reflection at the base of the Coastal Plain sediments. The detection of crustal reflections occurring at 2-3 s was noted on some lines, but the geometry of the reflections was unclear and was masked by multiple reflections generated within the overlying sedimentary cover. Furthermore, the data in several areas had severe static busts caused by failure of the residual statics program to align reflections properly. These busts mimic the appearance of faults and cast doubt on detailed interpretations made with these data.

PBF Shotgun Data Set

The results of the Conoco seismic reflection program prompted further investigation of the Pen Branch fault. Of particular concern was the limit of upward penetration of the Pen Branch fault into the Atlantic Coastal Plain sediments at SRS. Emerald Exploration Consultants (EMEX) in 1990-91 recorded 18 high resolution seismic reflection lines across the Pen Branch fault (Berkman, 1991). These seismic lines, herein designated the PBF series, were recorded with a 24 channel recording system and a buffalo gun source. The cable geometry was an asymmetric split spread with 6.1 m station intervals and shot points located at half station intervals to yield 1.5 m CDP spacings and nominal 12 fold data (Table 1, Figure 7). These seismic reflection data were supplemented by eight boreholes to basement designed to bracket the fault. Complete suites of geophysical logs were run in the holes and P and S-wave VSPs were recorded in four holes.

Table 1. Recording parameters of Savannah River Site seismic data.

Conoco 1987-88

Phase I

Line No.	Line Length (km)	Near-Far Offset (m)	Group Int. (m)	No. of Vibs.	Sweep Freq(Hz) swpl,recl (s)	CDP Fold	Sample Rate (ms)	Source Array vibxswp/(m)	Receiver Array Elem/(m)
1	22.8	42-830	16.8	3	20-120/10,14	48	2	3x6/29	14/16.8
2	14.9	42-615	12.2	3	20-120/10,14	24	2	3x6/24.4	14/16.8
3	22.4	42-615	12.2	3	20-120/10,14	24	2	3x6/24.4	14/16.8
3EX	2.9	42-615	12.2	3	20-120/10,14	24	2	3x6/24.4	14/16.8
4	20.6	42-830	16.8	3	20-120/10,14	48	2	3x6/29	14/16.8
5	9.7	42-615	12.2	3	20-120/10,14	24	2	3x6/24.4	14/16.8
6	14.9	42-830	16.8	3	20-120/10,14	48	2	3x6/29	14/16.8
7	29.8	42-830	16.8	3	20-120/10,14	48	2	3x6/29	14/16.8
7EX	5.2	42-830	16.8	3	20-120/10,14	48	2	3x6/29	14/16.8
8	15.2	42-830	16.8	3	20-120/10,14	48	2	3x6/29	14/16.8
9	14.2	42-615	12.2	3	20-120/10,14	24	2	3x6/24.4	14/16.8
10	7.3	42-615	12.2	3	20-120/10,14	24	2	3x6/24.4	14/16.8
11	10.3	42-615	12.2	3	20-120/10,14	24	2	3x6/24.4	14/16.8
12	8.5	42-615	12.2	3	20-120/10,14	24	2	3x6/24.4	14/16.8
13	13.5	42-615	12.2	3	20-120/10,14	24	2	3x6/24.4	14/16.8

Phase II

18	4.8	30-600	12.2	2	20-120/10,14	24	2	2x6/18.3	14/12.2
21	5.8	30-600	12.2	2	20-120/10,14	24	2	2x6/18.3	14/12.2
23	6.9	30-600	12.2	2	20-120/10,14	24	2	2x6/18.3	14/12.2
25	4.2	30-600	12.2	2	20-120/10,14	24	2	2x6/18.3	14/12.2
26	2.9	30-600	12.2	2	20-120/10,14	24	2	2x6/18.3	14/12.2
27	7.5	30-600	12.2	2	20-120/10,14	24	2	2x6/18.3	14/12.2
28	4.3	30-600	12.2	2	20-120/10,14	24	2	2x6/18.3	14/12.2
29	7.2	80-1584	33.5	4	15-100/12,16	48	2	4x8/33.5	28/33.5

Experimental

2EXP	2.4	15-300	6.1	1	30-150/8,10	48	2	1x4/0	14/bunch
9EXP	4.3	15-300	6.1	1	30-150/8,10	48	2	1x4/0	14/bunch
12EXP	1.8	15-300	6.1	1	30-150/8,10	48	2	1x4/0	14/bunch

Emerald Exploration Consultants (EMEX) 1990-91

PBF6	2.2	18-0-6-122 21-3-3-119	6.1	Buff. gun	409 ms	12	0.2	1 m hole 90 gr load	6/potted
PBF18	2.4	0-91-226 3-0-88-223	6.1	Buff. gun	409 ms	12	0.2	1 m hole 115 gr load	6/potted

The PBF high resolution data also suffer from severe statics problems. In addition, the processed data have a mixed appearance that renders horizon correlation difficult and ties to borehole seismograms uncertain.

Seismic Data Reprocessing

Interpretative reprocessing of the Conoco data set and part of the EMEX data set was undertaken to determine if additional geological information could be extracted from these data. In this study the entire Conoco SRS seismic reflection profile data set, with the exception of seismic lines SRS-2, SRS-6, and SRS-8, was reprocessed. Seismic lines SRS-2, SRS-6 and SRS-8 were reprocessed by Ashok K. Sen (1992) to 1000 ms using the processing flow developed by this author. Of the EMEX PBF seismic reflection data, only lines PBF-6 and PBF-18 were reprocessed. The other PBF seismic lines were reprocessed in a companion study by Çoruh and Costain (1994). No attempt was made to reprocess the vertical seismic profile data of either data package.

The details of the seismic data reprocessing for the SRS and PBF data are described in Appendix A. Copies of final stack, migrated, and automatic line drawing sections are collected in Appendix B. All the seismic data reprocessing was conducted at the Regional Geophysics Laboratory of Virginia Polytechnic Institute and State University using a VAX 11/780 (later a 11/785) mainframe computer and a Sun Sparc 10 workstation equipped with CogniSeis Digicon Interactive Seismic COmputer (DISCO) software and software developed by RGL personnel.

SRS Vibroseis Data Set: The generalized reprocessing sequence for the SRS vibroseis data is shown in Figure 9. All of the seismic reflection profiles were processed to an 80 m datum and a 50 ms bulk shift was added to the data such that the zero timing line on all the seismic sections is 50 ms above datum. In addition to the conventional CDP processing sequence of Figure 9, a refraction stack section of line SRS-1 was produced and experiments were conducted with prestack migration and partial prestack migration to image the Pen Branch fault on line SRS-2EXP.

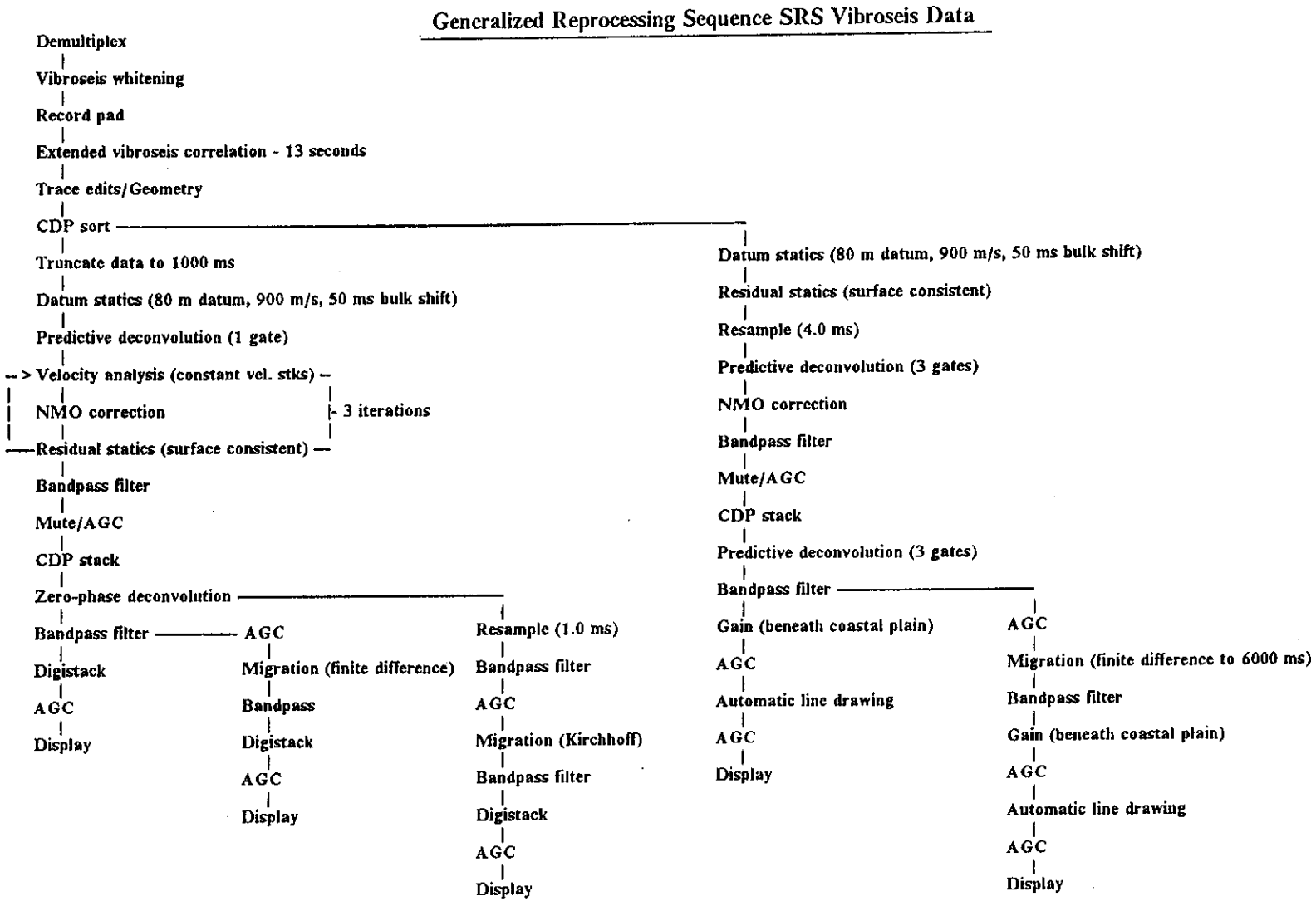

Figure 9. Generalized reprocessing sequence - Conoco SRS vibroseis data: Further details of the data reprocessing are given in Appendix A.

The reprocessing effort for the SRS data set was directed towards improving the continuity and resolution of reflections from the Coastal Plain sediments and the basal unconformity as well as enhancing the resolution of any basement faults that penetrate into the sedimentary section. It was of critical importance to recover as much as possible reflections from the shallow stratigraphic section that were muted in the original processing so that the limit of upward basement fault penetration could be determined. Care was taken to preserve reflection character to facilitate line-tying and stratigraphic correlations with borehole data. Secondary objectives of the reprocessing effort were to recover reflections from Triassic strata within the Dunbarton basin in order to define better the basin geometry and to recover any deep reflections through the use of extended vibroseis correlation (Pratt, 1982; Okaya and Jarchow, 1989) that could aid in interpretation of the regional tectonic framework.

The large number of seismic lines in the SRS data set required, for computer run-time considerations, creation of a subset of the data early in the processing sequence. After CDP sort a 1 s subset of the data was created and processed separately as the "shallow" data set. The stacking velocities and residual statics computed for the shallow data were later applied to the entire data record to the extended correlation time of 13 s - the "deep" data set.

Comparison between the reprocessed seismic reflection data and the original processed data is shown in Figure 10 for a part of seismic line SRS-10. In the reprocessed data the large static busts present in the original processed data have been eliminated. This is imperative if basement faults are to be reliably interpreted. Also, approximately 100 ms of the shallow time section muted in the original data processing have been recovered to within approximately 10-20 ms ($\approx$ 5-10 m) of the surface. In addition, examination of the time section below the basal unconformity shows that multiple reflections have been suppressed.

The consistency and reliability of the reprocessing effort is demonstrated by the excellent ties between intersecting seismic lines. The tie between lines SRS-4 and SRS-10 is shown in Figure 11. No time shift is necessary to tie the lines. Furthermore, subtle reflection waveform character correlates across the tie despite the different recording geometries used for the two lines.

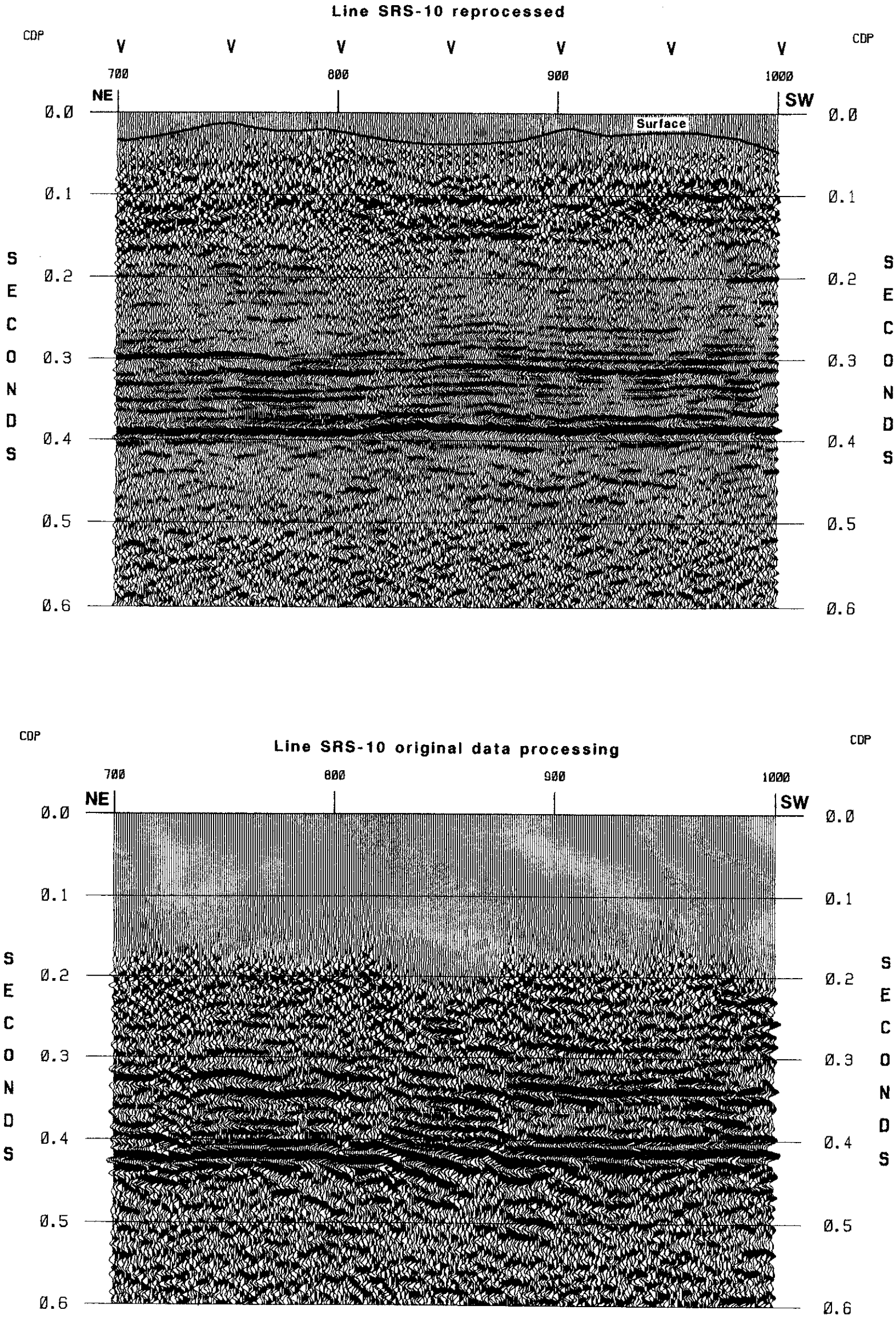

Figure 10. **Comparison reprocessed vs. original line SRS-10:** In the reprocessed data (top) the disruptions in reflection continuity present in the original data (bottom) are eliminated. These disruptions or "busts", caused by cycle skipping in residual statics computations, can be mistaken for faults. Note the recovery of approximately 100 ms of the shallow time section that was muted in the original processing. Surface topography has been converted to time using the datum correction velocity of 900 m/s.

Throughout the data set the line ties are of similar quality. In instances where seismic lines do not tie exactly, time shifts of 4 ms (2 samples) or less are typically required.

Comparisons between the reprocessed and original processed data for the subcoastal plain section are shown in Figure 12 and Figure 13 . In Figure 12 the upper crustal reflections present in the original processed version of line SRS-4 are enhanced in the reprocessed data to reveal a decollement and a fault splay. A similar data quality is obtained for data recorded over crystalline basement throughout the site, although north of Upper Three Runs the reflection continuity degrades for all lines. In Figure 13 the original processed version of line SRS-13 shows no evidence for the Dunbarton basin, although borehole P5R penetrated Triassic siltstone near station 963. In the reprocessed line SRS-13 reflections from the basin fill are clearly seen having a westward apparent dip. All of the reprocessed seismic lines recorded over the Dunbarton basin clearly show reflections, albeit typically weak reflections, from the basin fill. In general, the strongest reflections from within the basin occur along its southern margin. The imaging of the Dunbarton basin is a significant result because prior to this study the geometry of the basin fill was unknown.

PBF Shotgun Data Set: The generalized reprocessing sequence for the PBF high resolution seismic reflection data is shown in Figure 14. The reprocessing of the PBF high resolution data was guided by much the same principles as the SRS data, i.e. improvement of overall reflection resolution and continuity as well as reduction of false geologic structure created by statics problems. To conform with the SRS data both seismic lines were processed to an 80 m datum and a 50 ms bulk shift was added.

In the reprocessing of lines PBF-6 and PBF-18 it was necessary to apply a severe surgical mute to the CDP gathers to eliminate source generated noise and ground roll. This mute, while significantly improving reflection resolution in the stacked section, did result in elimination of about half the data in any CDP gather (see Appendix A).

To improve stacking velocity determinations and increase signal-to-noise ratio during the stacking process, traces from adjacent CDPs were combined to form nominal 24 fold data. This process resulted in some loss in spatial resolution (increase of CDP spacing to 3 m), but is justified

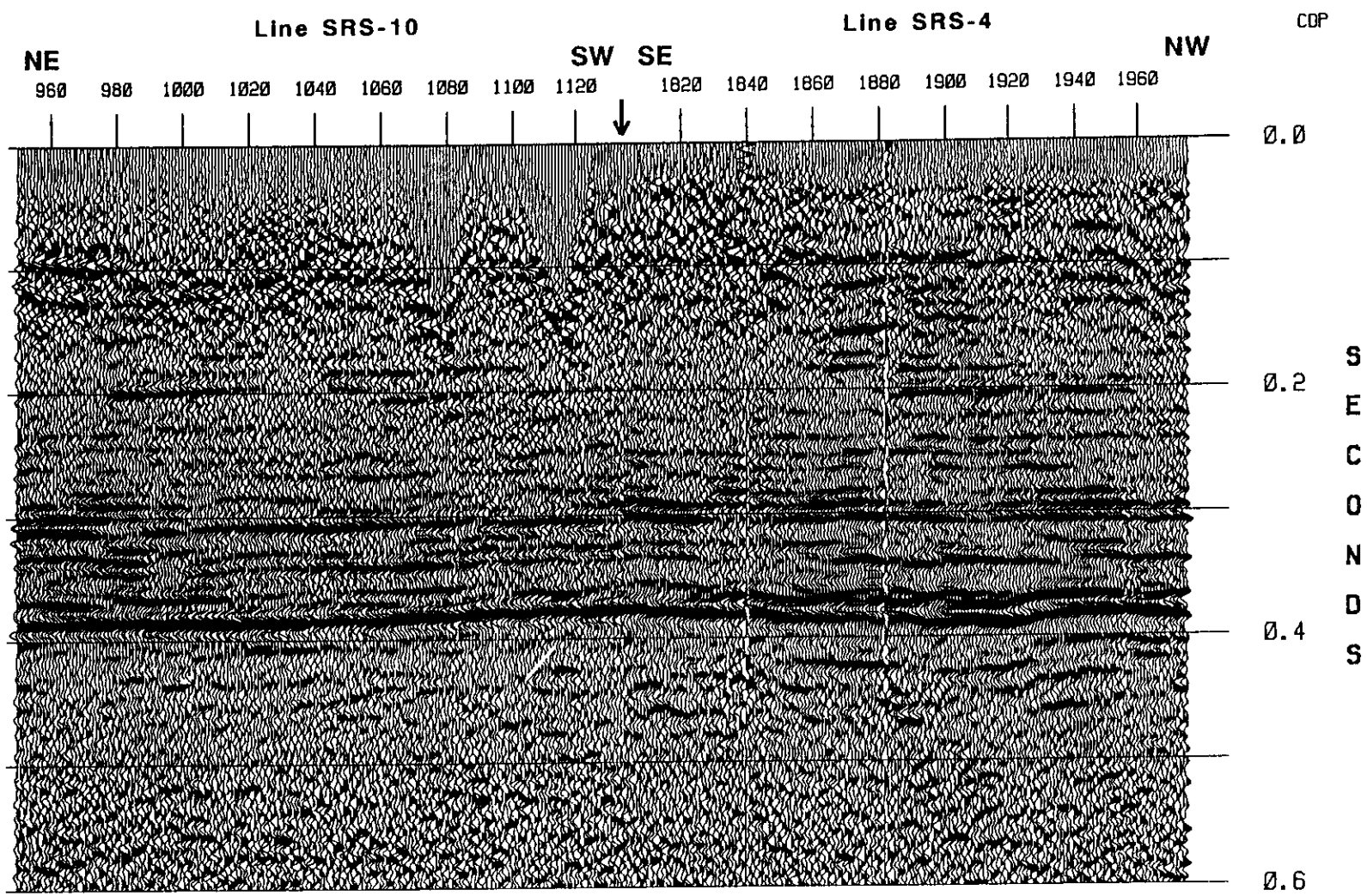

Figure 11. **Line tie between SRS-4 and SRS-10:** The excellent tie (arrow) between crossing seismic lines is indicative of the consistency and reliability of the data processing. Line SRS-4: 48 fold, 8.4 m trace spacing. Line SRS-10: 24 fold, 6.1 m trace spacing.

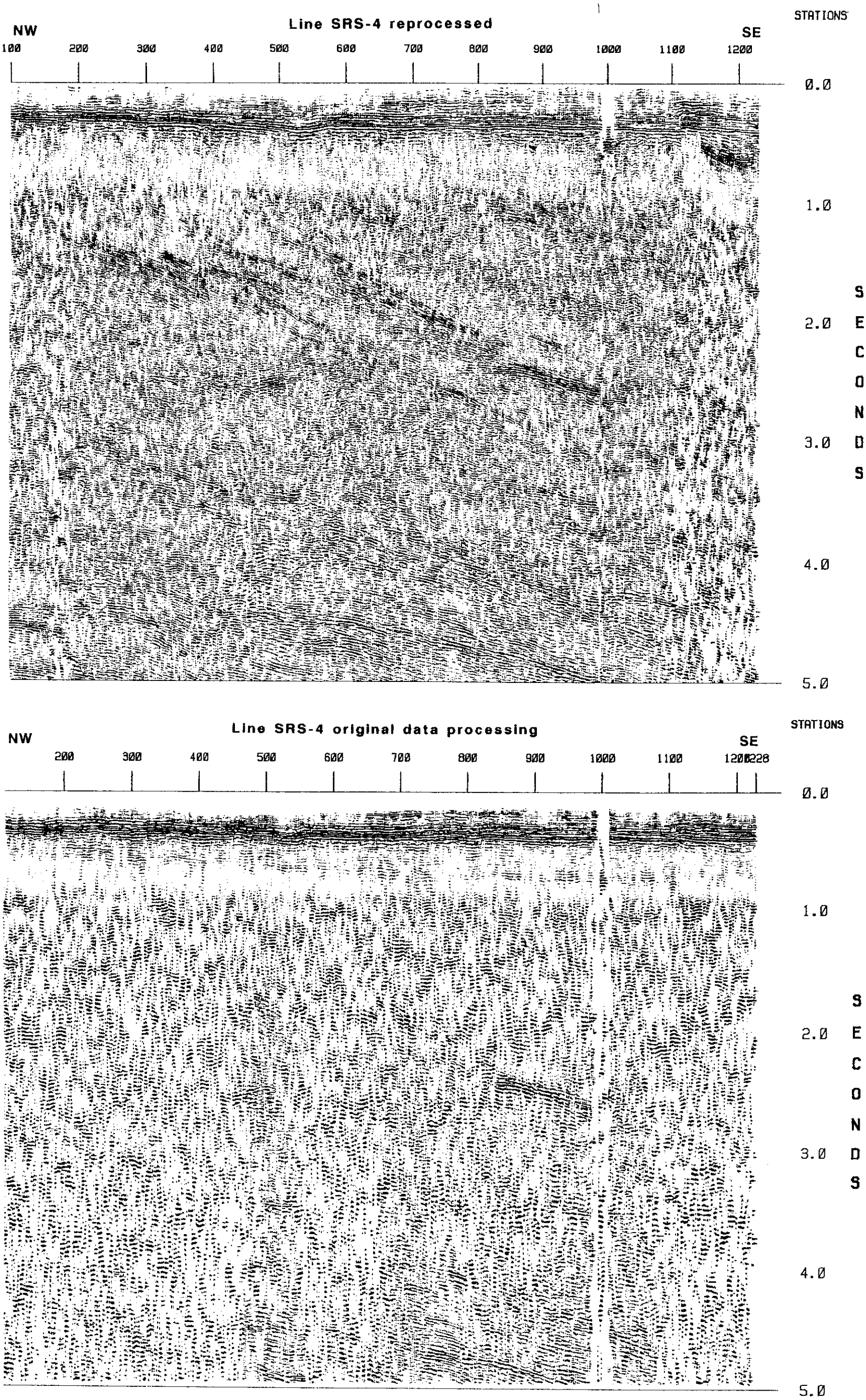

Figure 12. **Comparison reprocessed vs. original - crystalline basement:** Seismic line SRS-4. Upper crustal reflections are enhanced in the reprocessed data (top) which formerly were obscured by multiple reflections in the original processed data (bottom). Display is 1:1 for crustal of velocity 6 km/s. Every other trace plotted.

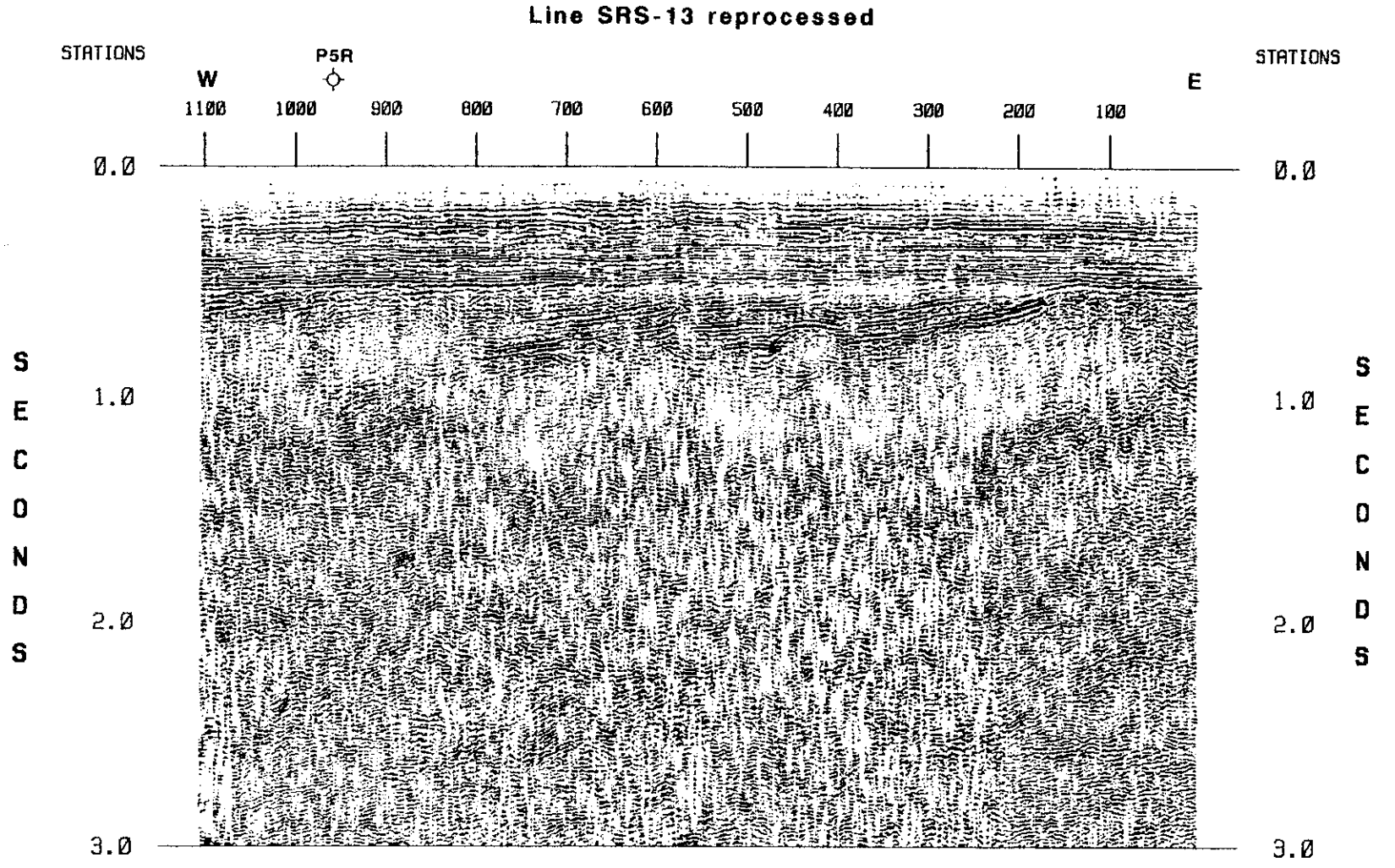

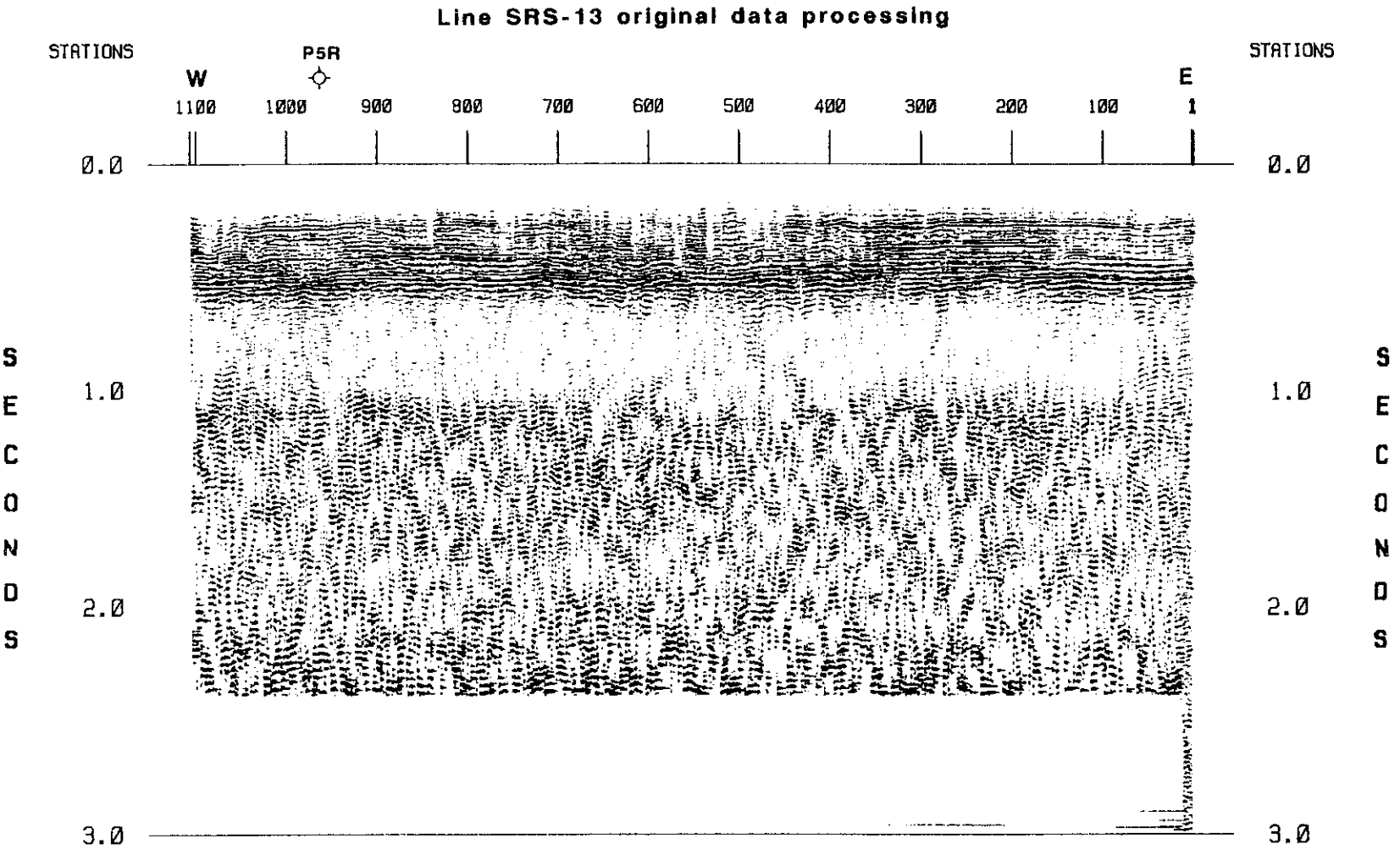

Figure 13. **Comparison reprocessed vs. original - Triassic basin:** Seismic line SRS-13. Reflections within the Dunbarton basin have been recovered in the reprocessed data (top) that were not present in the original processed data (bottom). Display is 1:1 for crustal velocity of 6 km/s. Every other trace plotted.

Figure 14. Generalized reprocessing sequence - PBF shotgun data: Further details of the data reprocessing are given in Appendix A.

by consideration of the Fresnel zone radius for the seismic wavelengths and depths involved (Appendix A).

Comparison between the reprocessed and original data is shown for seismic line PBF-18 in Figure 15. The reprocessed data show greater reflection continuity and reflection character than the original processed data. In addition, reflections from strata within the Dunbarton basin are apparent.

Other Seismic Reflection Data: In addition to the Conoco and EMEX seismic reflection data sets, displays and automatic line drawings (Çoruh et al., 1988) were generated of seismic profiles located near SRS in Georgia. These data were used in the interpretation of crustal structure and consist of two profiles recorded by Virginia Polytechnic Institute and State University for Southeast Exploration and Production Company (SEPCO) and regional seismic profiles recorded by the Consortium for Continental Reflection Profiling (COCORP). The COCORP lines, Line 5 and Line 8 (Cook et al., 1981) were composited and migrated as a single profile to 15 s for use in this study.

Borehole Data

The seismic reflection data sets were supplemented by information from 54 boreholes to basement in the Savannah River Site and environs (Table 2; see also Figure 3 on page 11 and Figure 7 on page 26). Much of the readily available information for holes off site consists only of top-of-basement picks and lithology at TD. In many cases it is not clear whether the top of basement is picked at the top of the weathered zone, as it is defined in this study, or at the top of unweathered basement rock. The problem is compounded inasmuch as lower Cape Fear Formation has often been interpreted as the weathered zone and vice-versa (D. Prowell, USGS, 1993, personal communication). Similarly, the description of the basement lithology is often cryptic, e.g. "crystalline". Nearly all the holes to basement, with the exception of the DRB series of holes, penetrate basement to a depth of only a few meters.

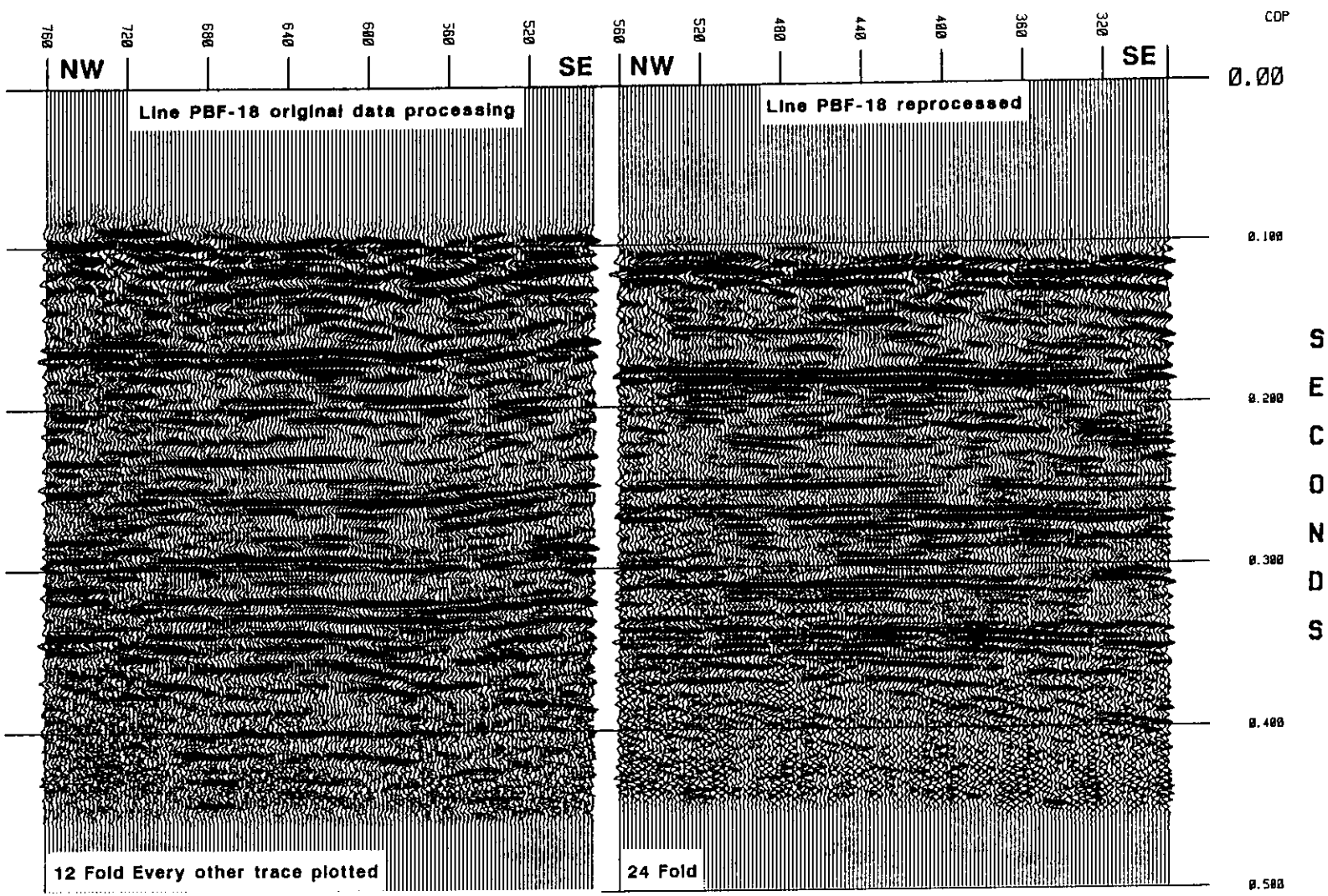

Figure 15. Comparison reprocessed vs. original line PBF-18: The reprocessed seismic data (right) exhibit greater reflection continuity and higher frequency content than the original processed data (left).

Table 2. Selected boreholes to basement in SRS study area.

Hole No.	Latitude	Longitude	TD (m)	Elev. (m)	Elev. BCP (m)	Basement Lithology	Ref.
PBF-1	33°17′36.28″	81°31′49.09″	324.6	84.2	-228.6	biotite + garnet gneiss	9,14
PBF-2	33°17′10.93″	81°31′31.36″	321.6	81.8	-208.0	Triassic strata	8,9
PBF-3	33°15′15.33″	81°37′19.10″	346.0	96.5	-232.7	biotite + garnet gneiss	9,14
PBF-4	33°12′11.88″	81°42′02.74″	328.7	63.4	-255.7	biotite + garnet gneiss	9,14
PBF-5	33°11′37.56″	81°41′27.72″	342.4	73.3	-244.0	Triassic strata	8,9
PBF-6	33°10′10.83″	81°44′26.60″	274.6	28.2	-238.2	Triassic strata	8,9
PBF-7	33°14′43.96″	81°37′03.19″	313.6	87.0	-211.4	Triassic strata	8,9
PBF-8	33°14′47.93″	81°37′03.37″	313.9	89.0	-210.4	Triassic strata	8,9
CFD-1	33°14′16.88″	81°37′48.36″	302.1	82.0	-215.4	Triassic strata	13
CFD-18	33°14′23.70″	81°37′53.34″	329.2	76.0	-240.9	crystalline	13
DRB-1	33°17′54.00″	81°40′18.00″	580.3	79.7	-178.0	quartz feldspar gneiss	1
DRB-2	33°16′42.00″	81°39′48.00″	604.1	85.8	-210.3	hornblende chlorite schist	1
DRB-3	33°17′12.00″	81°39′48.00″	591.9	87.0	-181.1	hornblende chlorite schist	1
DRB-4	33°16′42.00	81°38′06.00″	590.7	76.4	-193.9	quartzite + chlorite biotite schist	1
DRB-5	33°17′42.00″	81°39′36.00″	560.2	87.4	-184.4	epidote chlorite schist + quartzite	1
DRB-6	33°17′30.00″	81°39′24.00″	583.1	82.0	-189.3	hornblende chlorite schist	1
DRB-7	33°17′18.00″	81°40′30.00″	600.2	84.7	-197.8	hornblende chlorite schist + quartzite	1
DRB-8	33°16′54.00″	81°38′54.00″	607.2	79.9	-201.1*	crystalline	3
DRB-9	33°15′00.00″	81°37′00.00″	823.3	89.9	-215.8	Triassic fanglomerate/hornblende feld. gneiss	3
DRB-10	33°12′18.00″	81°34′48.00″	1281.8	76.4	-277.4	Triassic sandstone	3
DRB-11	33°13′30.00″	81°36′06.00″	999.8	83.6	-242.9	Triassic siltstone	4
P4R	33°15′00.00″	81°48′12.00″	233.3	32.1	-163.1	chlorite schist	2
P5R	33°09′00.00″	81°37′00.00″	400.3	63.5	-307.8	Triassic siltstone	2
P6R	33°16′40.00″	81°44′12.00″	317.6	77.1	-150.0	hornblende chlorite schist	5
P7R	33°20′00.00″	81°35′54.00″	.	.	.	crystalline	.
P8R	33°19′35.00″	81°44′36.00″	312.6	108.8	-121.6	hornblende schist	5
P9R	33°19′10.00″	81°43′51.00″	.	.	.	crystalline	.
P12R	33°13′54.00″	81°36′12.00″	388.2	89.3	-242.3	Triassic siltstone	4
SSW-1	33°14′14.88″	81°43′03.65″	317.4	94.9	-213.9	hornblende gneiss	7
SSW-2	33°13′53.68″	81°43′57.76″	396.5	51.0	-207.4	quartz feldspar gneiss	7
SSW-3	33°14′52.32″	81°41′49.33″	339.7	54.5	-213.5	hornblende gneiss	7
20-M	33°20′12.00″	81°44′12.00″	.	.	-108.8	chlorite schist	2
P25	33°12′39.00″	81°39′27.00″	.	.	.		.
P30	33°20′16.00″	81°42′31.00″	.	.	.		.
H1	33°17′07.50″	81°38′35.79″	.	.	.		.
AL324	33°07′37.00″	81°32′45.00″	.	.	-346.6	Triassic hornfels	12
SAL-1	33°26′18.00″	81°16′54.00″	350.2	62.5	-196.5	granite	6
C-2	33°26′17.00″	81°46′15.00″	.	.	-41.5	granite	11,14
C-5	33°19′14.00″	81°24′28.00″	.	.	-233.2	interlay. amphibolite/gneiss	12,14
C-6	33°10′42.0″	81°18′55.00″	60.0	420.6	-342.3	gneiss	12
C-7	33°06′48.00″	81°30′22.00″	.	.	-349.0	schist	12
C-10	33°01′30.00″	81°23′04.00″	.	.	-436.5	Paleozoic granodiorite	10,11
Girard	33°03′54.00″	81°43′13.00″	.	.	-342.9	Triassic	11
Millers Pond	33°13′48.00″	81°53′44.00″	.	.	-185.6	crystalline	11,12
AIK-858	33°24′41.01″	81°42′25.14″	268.7	132.6	-56.7	granite/granite gneiss	14
NPR	33°15′20.00″	81°38′15.00″	92.5	1219.2	.	biotite-garnet-hornblende-gneiss	14
SRS-905	33°13′40.00″	81°34′31.00″	95.5	306.9	.	.	14

References: (1) Diment et al., 1965; (2) Siple, 1967; (3) Marine and Siple, (1974) * Depth from sonic log - this study; (4) Marine, 1974; (5) Marine, 1976; (6) Speer, (1982) * Depth value apparently refers to top of hard rock; (7) Chapman and DiStefano, (1989); (8) Berkman, (1991); (9) Stieve et al., (1991); (10) Kish, (1992); (11) R. Cumbest, WSRC, personal communication (1993); (12) Snipes et al. (1993a); (13) Steive et al, (1993); (14) A. Steive, WSRC, personal communication, (1994).

The borehole data presented in Table 2 were compiled from original sources and supplemented with information obtained from the South Carolina Water Resources Commission, files of the Geothermal Project at Virginia Polytechnic Institute and State University, well log header blocks, and personal communication with individuals at SRS. In some instances the top of basement was repicked to conform with the convention used in this study. In those cases where the top of basement was repicked, sonic and temperature logs were used to identify the characteristic signature of the saprolite layer. Hence, the top of basement value listed might be at variance with values reported elsewhere in the literature. In addition, it was found that many borehole locations reported by Anderson (1990) were in error.

Of the holes listed in Table 2, thirty-five are located on Savannah River Site. Several of these holes had extensive suites of digital geophysical logs available. Complete suites of geophysical logs including sonic, density, nuclear, and resistivity logs were available for the PBF and CFD series of boreholes. For selected DRB and PR holes sonic and gamma ray logs were obtained. In addition, temperature logs recorded in certain of the DRB and PR holes as part of the Geothermal Program at VPI & SU were utilized (Costain, 1976).

Digital processing of geophysical logs was performed using the CogniSeis Digital Log Processing System (DLPS) software package operational on a Sun Sparc 2 work station at the Regional Geophysical Laboratory, VPI & SU. The DLPS software package has full capabilities for digital log processing, petrophysical calculations, log modelling, creation of synthetic seismograms and construction of cross-sections.

Synthetic Seismograms

To enable correlation of the borehole data to the seismic reflection data, synthetic seismograms were generated for 14 boreholes in the Savannah River Site (Table 3). Copies of the synthetic seismograms are included in Appendix C.

The synthetic seismograms, where possible, were constructed from both sonic and density logs. In several holes density logs were not available or were of poor quality. An attempt was made to

Table 3. Synthetic seismograms.

Hole No.	Log Reference (m)	Log Top (m)	Log Bottom (m)	Nearest Seismic Line
PBF-1	GL 84.2	55.5	322.17	SRS-28
PBF-2	GL 81.8	4.9	318.52	SRS-28
PBF-3	GL 96.5	0.3	343.81	PBF-18
PBF-4	GL 63.4	4.0	321.56	SRS-7
PBF-5	GL 73.3	47.2	338.94	SRS-7
PBF-7	GL 87.0	42.1 88.7	83.52 311.51	PBF-18
PBF-8	GL 89.0	22.9 93.3	76.8 311.51	PBF-18
CFD-1	GL 82.0	3.0	298.70	SRS-2EXP
CFD-18	GL 76.0	8.2	328.27	SRS-2EXP
DRB-4	GL? 76.4	275.5	610.82	SRS-2
DRB-6	GL? 82.0	336.5	610.82	SRS-5
DRB-8	KB 81.9	23.8	297.79	SRS-5
DRB-9	KB 92.1	336.5	824.18	PBF-18
DRB-10	KB 78.2	25.6	1280.16	SRS-8, SRS-11
DRB-11	GL 83.6	31.7	381.00	SRS-2, SRS-3
P12R	GL 89.3	55.5	366.98	SRS-2, SRS-3

generate synthetic density by computing average correlation coefficients for a common relation between density and velocity for the wells on site, i.e:

$$\rho = AV^b$$

where ρ is density, V is velocity and A and b are correlation coefficients determined empirically (Gardner et al., 1974). It was found that the fitted values for the A and b coefficients derived from the sonic and density logs varied widely among the boreholes. Furthermore, the fitted values poorly estimated the density of the Tertiary section; however, in practice the lack of density information did not pose a problem, inasmuch as synthetic seismograms computed with density and without density information were virtually indistinguishable.

The basic steps involved in constructing the synthetic seismograms included: (1) log editing; (2) resampling to one foot and conversion to metric units; (3) fill to surface with the last sample value; (4) datum shift to 80 m and fill to datum with the 900 m/s correction velocity or the last density sample value; (5) depth to time conversion and impedance log generation; (6) reflection coefficient series generation with and without multiples; (7) convolution of reflection coefficient series with a wavelet. The editing of the sonic logs was not without some subjectivity. Commonly, the upper 20 m of the logs exhibit extreme velocity excursions which, given the known low velocity of the near surface material, might be genuine. Hence, indiscriminate editing of these intervals could lead to timing errors during correlation to seismic data. The 80 m datum and 900 m/s correction velocity were used to conform with the datum corrections used for the seismic reflection data.

Potential Field Data

Gravity Data: The gravity data used in this study are derived from the Society of Exploration Geophysicists (SEG) gridded (4 km) Bouguer gravity data for the United States on the *Geophysics of North America* CD-ROM (Hittelman et al., 1989) and a detailed gravity survey of the Savannah River Site conducted by Anderson (1990).

To fully utilize the regional coverage afforded by the SEG gravity data set and the detailed coverage of the Anderson survey, both data sets were merged and new contour maps produced. To conform with the SEG data set, Anderson's data were converted to the GRS 67/ IGSN 71 datum using an empirically derived formula by Miller (1983). Grid points of the SEG gravity data set were eliminated where overlap occurred between the two data sets and the combined data set was gridded and contoured using the Surface III software package (Sampson, 1988). Both a regional Bouguer gravity map and a detailed Bouguer gravity map of the Savannah River Site were produced (Figure 16 and Figure 18 on page 50).

For regional coverage, i.e. outside the immediate vicinity of SRS, the gridding algorithm produced grid values at 2 km intervals employing a quadrant search and inverse distance squared

weighting. The detailed gravity map of the Savannah River Site area was generated using the same gridding algorithm as the regional map, but grid values were produced at 1 km grid intervals to take advantage of the denser distribution of control points (Figure 16). Both maps were checked versus the original SEG gravity data, the simple Bouguer gravity map of South Carolina (Long et al., 1975), and Anderson's map for veracity. There appear to be no discrepancies where the two data sets merge. Comparison of the computer-contoured gravity map of SRS with the original Anderson hand-contoured map shows the maps to be virtually identical, except for a slight discrepancy in the northeast part of the site where there is sparse gravity control.

Magnetic Data: The magnetic data used in this study are adapted from magnetic maps published by Petty and others (1965), Daniels (1974), and Daniels and others (1983).

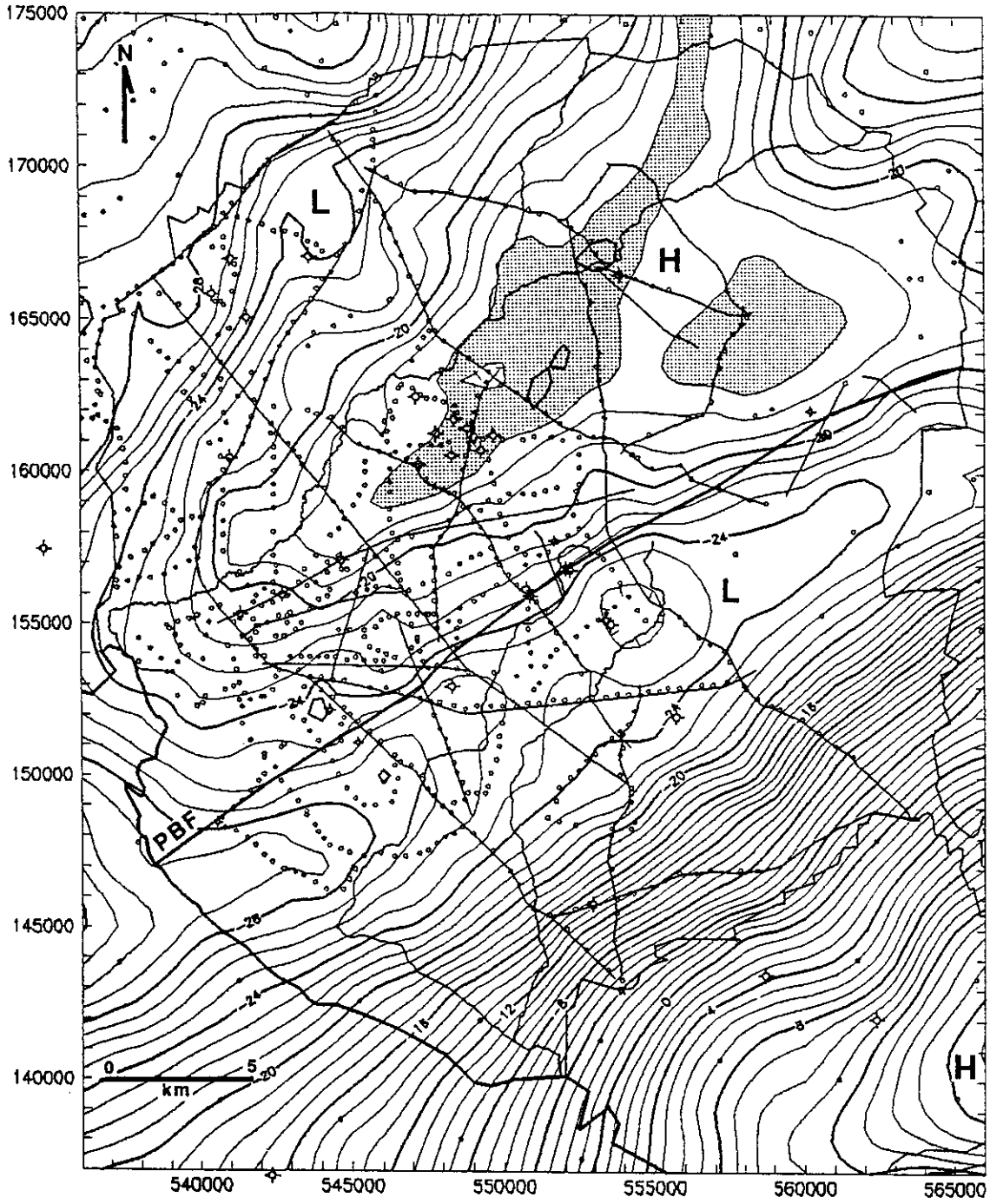

Figure 16. Simple Bouguer gravity map of SRS: Contour interval 1 mGal. Grid interval 1 km. Open circles indicate control points (gravity stations or grid points). Stippling denotes an area of gravity highs discussed in the interpretation. Gravity data from the *Geophysics of North America* CD-ROM (Hittelman et al., 1989) and Anderson (1990).

Interpretation

Deep Data Set

The relatively small areal extent of the Savannah River Site constrains the interpretation of the crustal seismic data. Foremost, the short profile lengths and the limitations inherent in the migration operator preclude obtaining an acceptable migrated image of the crust deeper than about 2.0-3.0 s (Appendix A). Therefore, interpretations made from the deep seismic reflection data, unless otherwise stated, are made from the unmigrated seismic sections. This being the case, the reflections are mispositioned by varying amounts and structural dips calculated from the seismic profiles and time maps are lower than in actuality. Also, inasmuch as the longest dip profile that can be generated by compositing the seismic lines is only 30 km, the interpretation of these data is heavily guided by comparisons among reflection events projected along inferred geologic strike to similar reflection events observed in nearby regional seismic reflection lines.

The nearest regional seismic reflection data to SRS are Seisdata Line 4 and Line 6 located 50 km and 20 km along strike from SRS in South Carolina and Georgia respectively and the composite COCORP profile Line 5 and Line 8 located 60 km along strike from SRS in Georgia (Figure 17). Of these data, the Seisdata lines were available only in small scale paper section format (Behrendt, 1985). Stack tapes of the COCORP lines were available from which a migrated section and an automatic line drawing (ALD) were produced for use in this study. The ALD of the migrated composite COCORP profile shows considerably more detail than seismic sections published by Cook and others (1981) and Iverson and Smithson (1983a).

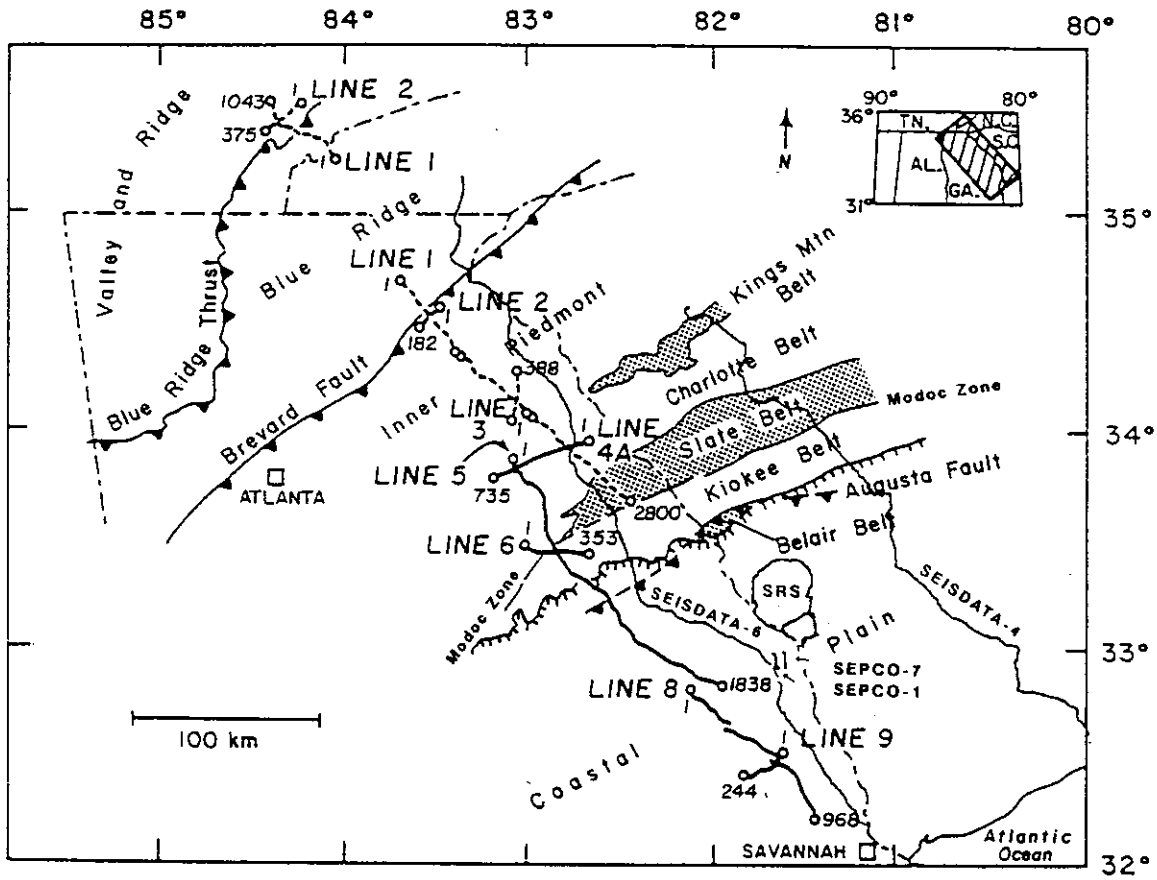

Figure 17. Location of regional seismic reflection lines: Figure adapted and modified from Cook and others (1981).

Interpretations of the COCORP data have been extensively published in the geologic literature (e.g. Cook et al., 1981; 1983; Petersen et al., 1984; Iverson and Smithson, 1983a, b; Heck, 1989; Costain and Çoruh, 1989; Phinney and Roy-Chowdhury, 1989). The traverse from northwest to southeast begins in the Piedmont in the Charlotte belt, crosses the Kiokee belt and the Fall Line onto the Atlantic Coastal Plain and terminates near the city of Savannah, Georgia. By projection of magnetic anomalies from known surface exposures it has been interpreted that the traverse crosses the Modoc zone and the Augusta fault. No surface exposures of the Belair belt or the Carolina Slate belt exist along the traverse, although the former is probably present beneath the Coastal Plain sediments.

Projection of the SRS deep seismic reflection data along inferred geologic strike, as determined from regional Bouguer gravity data (Figure 18), to the COCORP seismic traverse suggests that the crustal structure imaged at SRS should be similar to that imaged along the southern end of COCORP Line 5 (Figure 19). In this area most workers have interpreted reflections as from the Augusta fault and the Riddleville Triassic basin. Deeper southeast dipping reflections here and at other locations in the southeastern United States are usually interpreted to represent thrust surfaces indicative of pervasive Paleozoic deformation (e.g. Cook et al., 1981; Pratt et al., 1987; McBride and Nelson, 1991), although Heck (1989) suggested that these events are more related to Mesozoic rifting.

The deep SRS seismic reflection data (Appendix B) exhibit similar reflection configurations to the projected correlation with the COCORP data. The crust at SRS exhibits five main divisions that are bounded by dominantly southeast dipping reflections and reflection packages. These divisions are marked by the reflection Moho, interpreted at 11.0 s, subhorizontal reflections above the Moho, and southeast dipping reflections occurring from the base of the Coastal Plain to 8.0-10.0 s that are further divided by a 1.5-2.0 s wide band of bright, continuous reflection packages at 4.5-7.0 s in the midcrust and a 0.4 s wide band of high amplitude laminar reflections at 1.2-4.0 s in the upper crust. This shallowest band of reflections, which separates zones of complex reflection geometries above and below, probably represents the Augusta fault because of its similar

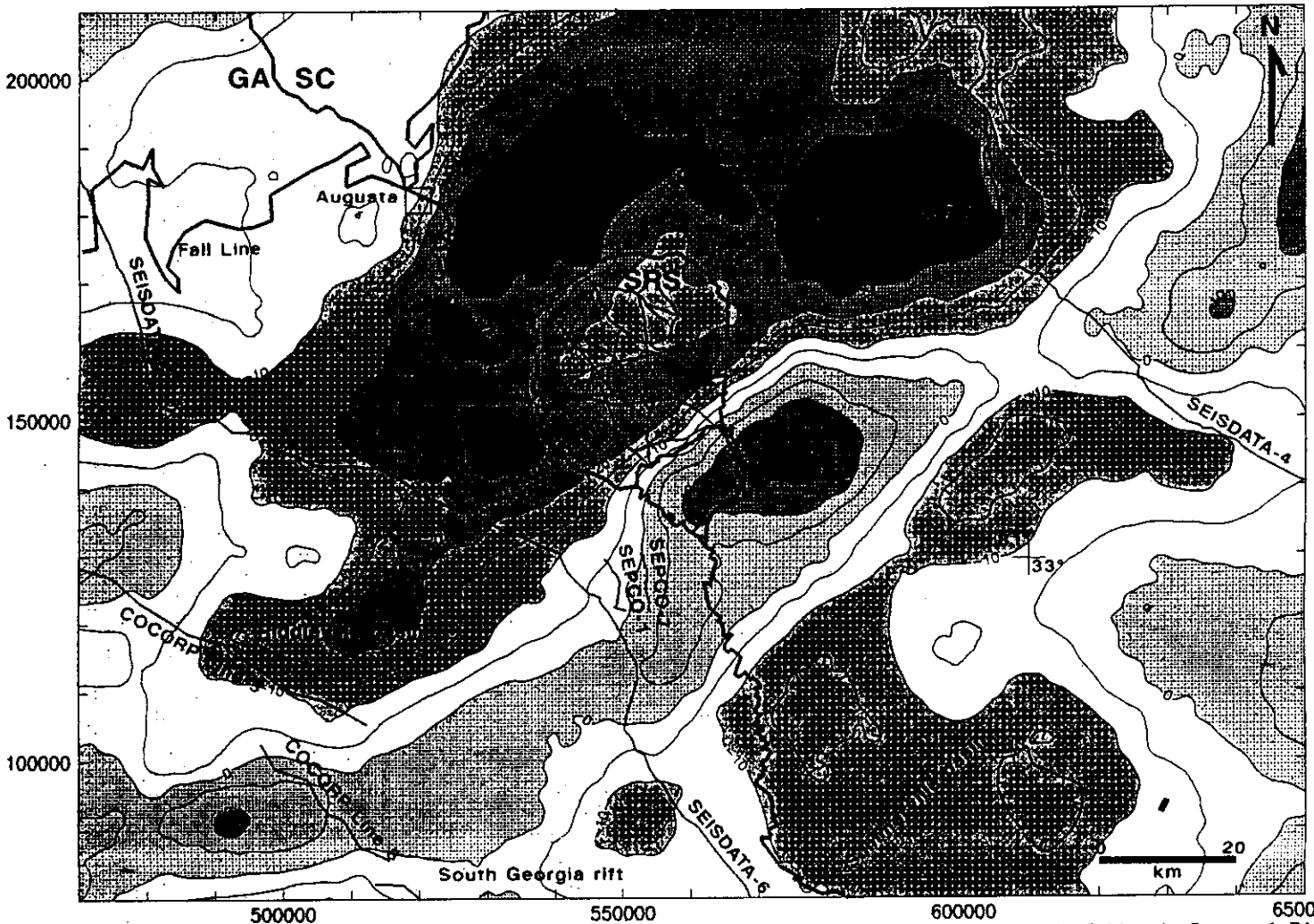

Figure 18. Regional Bouguer gravity map: Contour interval 5 mGal. Grid interval 2 km. The similarity in the gravity field at the Savannah River Site to that along the COCORP profiles indicates that the causal bodies (geologic structures) are similar at both locations. Note pronounced gravity lows associated with the concealed Dunbarton and Riddleville Triassic basins and a ridge of gravity highs on the south side of the basins. The ridge of gravity highs might represent upwelling of mafic material during Mesozoic extension as proposed by Bell and others (1998). Gravity data from the *Geophysics of North America CD-ROM* (Hittelman et al., 1989) and Anderson (1990).

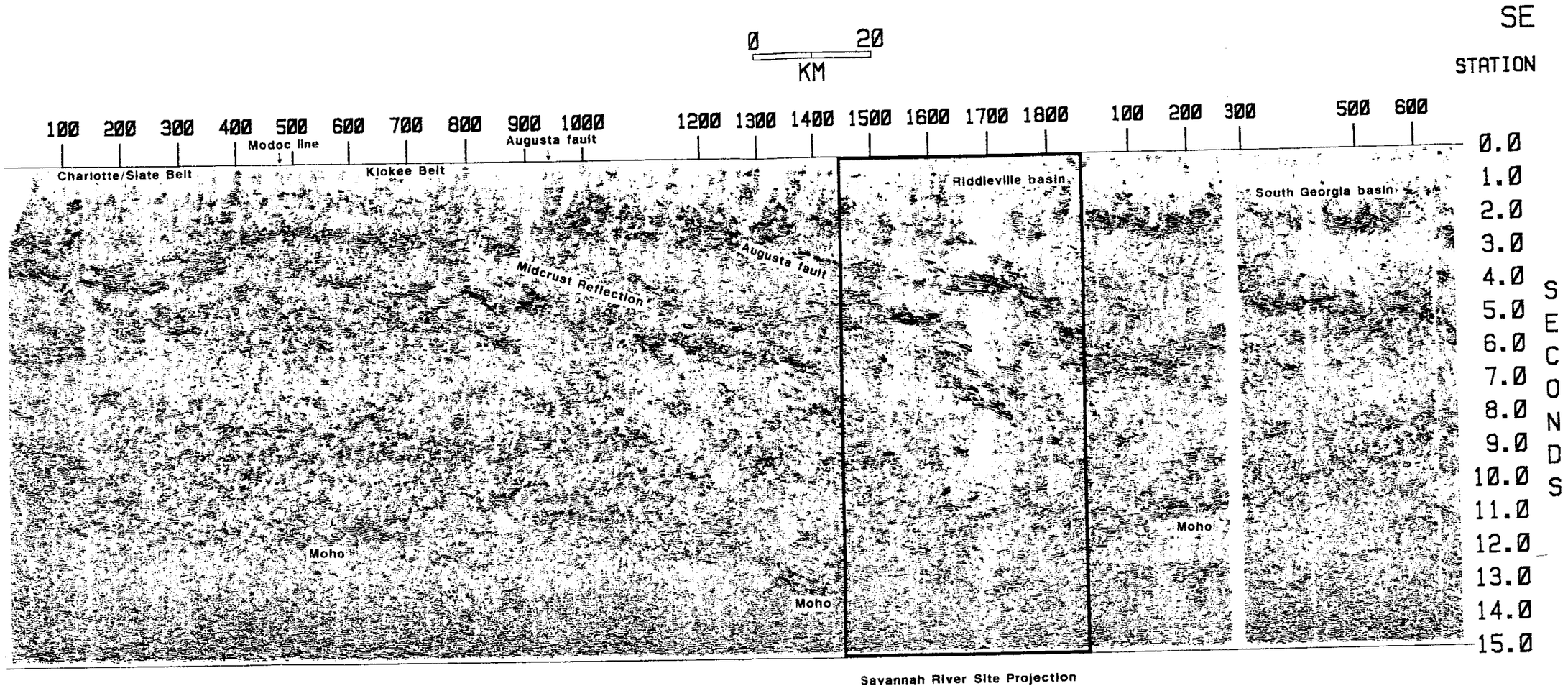

Figure 19. Automatic line drawing COCORP lines 5 and 8: The Savannah River Site seismic reflection data project to stations 1450-1838 on Line 5. The identification of the reflections is after Cook and others (1981). The Augusta fault and the Midcrust reflection are interpreted in the Savannah River Site seismic data. Kirchhoff migration of original COCORP stack data. Datum 120 m. Vertical exaggeration 2:1 for 6.0 km/s crustal velocity. Every other trace plotted.

seismic reflection character to the event identified in the COCORP data as the Augusta fault. The presumed Augusta fault and an event in the midcrust are correlatable surfaces throughout SRS.

Mohorovicic Discontinuity

The Moho at SRS is identified by a distinct 0.2-0.3 s wide band of laminated reflections occurring between 10.5-11.0 s (Figure 20). The corresponding depth, based on an average crustal velocity of 6.50 km/s, is 32.5-34.0 km. This range of depth values is shallower than the 38.0 km value obtained from on strike projection of Moho depths determined along the USGS seismic refraction profile located 10.0 km east of SRS (Luetgert et al., 1994), but is comparable to a 33.0 km depth to Moho determined by seismic refraction in the Charlotte and Carolina Slate belts (Kean and Long, 1980).

In the southeastern United States the Moho is found to exhibit variable reflection character. In the Valley and Ridge the reflection Moho is weak or absent; whereas in the Piedmont and under the Atlantic Coastal Plain the reflection Moho is locally prominent. The divide in Moho reflection character is associated with eastward crustal thinning marked by the Appalachian gravity gradient (Cook, 1984a) in the Piedmont. This crustal thinning has been variously interpreted to represent a relict Iaptean rifted margin, an early Paleozoic suture zone, or the edge of Mesozoic crustal thinning (see discussion by Hutchinson et al., 1983).

Areas that have undergone extension, such as SRS, or have young crust, typically are characterized by a reflective crust and a reflective Moho (Nelson et al., 1987; Goodwin and Thompson, 1988). In addition, the reflection Moho is often observed to be relatively continuous beneath complexly deformed crust and this presents the possibilities that either the Moho is a stable feature and unaffected by orogenesis, or that it is a young feature that reestablishes itself after an orogenic event. In the southeastern United States deep seismic reflection data have been interpreted as supporting at least a postcollisional age (Brown, 1987; Çoruh et al., 1988) or a Triassic-Jurassic age

for the Moho (McBride and Nelson, 1991). At present there is no consensus regarding the age of the Moho in the southeastern United States.

At SRS, seismic lines oriented parallel to the regional dip, i.e. northwest-southeast, exhibit numerous southeast dipping reflections below the reflection Moho (Figure 20; Appendix B). Most of these events have noticeably higher dip than the southeast dipping reflections in the mid- and lower crust. In places these dipping reflections cross the Moho, but are much lower in amplitude than the Moho band of reflectivity. On strike lines the sub-Moho events are parallel and subparallel to the Moho (e.g. line SRS-6, Appendix B). These observations suggest that the sub-Moho reflections are closely related to the southeast dipping reflections in the mid- and lower crust. A possible explanation is that the Moho is younger than the dipping reflections it truncates such that the upper mantle reflections denote relict structures; however, the subhorizontal reflections occurring above the Moho are clearly truncated by the southeast dipping reflections. Unless the subhorizontal reflections are part of the Moho, this argument must be rejected. Another explanation is that the sub-Moho reflections are multiple reflections from the southeast dipping reflectors in the lower crust and shallower. This interpretation would be consistent with the higher apparent dip of the events and their low amplitude. Another factor to be considered is that, if a proper migration could be performed on these data, many of these events would migrate to positions above the Moho.

Upwarping of the reflection Moho occurs northwest of the Dunbarton basin on most of the SRS seismic lines. This feature is best observed along line SRS-1 where the apex of the upwarp occurs at station 550 (Figure 20). This upwarping, i.e. local crustal thinning, is predicted by models of rift basin formation involving pure shear extensional deformation of the lower crust (Kusznir and Eagan, 1989; Bell et al., 1988). In regard to the SRS data, the short profile lengths makes attribution of this phenomena to crustal thinning during Mesozoic extension tenuous. No abrupt change in the depth of the Moho under the Dunbarton basin was detected in the USGS seismic refraction profile (Luetgert et al., 1994), although seven kilometers of crustal thinning (39-32 km) was observed under the Summerville basin. The detection of relatively small wavelength crustal

thickness variations, such as observed in the SRS reflection data, however, might not have been resolvable by that survey.

Part of the Moho upwarp at SRS can be attributed to velocity push-down caused by low velocity strata in the Dunbarton basin. Such velocity push-down would account for the observation that the apex of the upwarp occurs north of the basin rather than under the basin. In addition, diffraction event geometry and the size of the Fresnel zone at Moho depths are factors to be considered. Whether the Moho warp at SRS is caused by local crustal thinning or is a reflection travel-time anomaly cannot be determined from these data.

The reflection Moho observed in the migrated COCORP data shows crustal thickening in the vicinity of the Riddleville basin and crustal thinning to the northwest and southeast (Figure 19). The crustal thinning to the southeast is similar to that interpreted from seismic refraction data southeast of SRS. In the COCORP data the reflection Moho beneath the Riddleville basin occurs at 13.0 s. No localized upwarping of the reflection Moho is observed under the Riddleville basin, although such a feature might not be resolvable in these data because of the relatively large trace spacing.

The transition zone where the crust thins south of the Riddleville basin is not well imaged in the COCORP data (Figure 19, Line 5 station 1800 to Line 8 station 200). This zone coincides with a 20 mGal Bouguer gravity high and vergence of the southeast dipping reflections with the base of the crust. The transition zone has been interpreted as a root zone for the large thrust sheets to the west under the Piedmont, Blue Ridge, and the Valley and Ridge (Cook et al., 1981; 1983) and/or the (an) Alleghanian suture (Phinney and Roy-Chowdhury, 1989). Costain and Çoruh (1989) suggested that this area was also a locus of Mesozoic extension. Cumbest and others (1992) interpreted the gravity high as related to Mesozoic rifting and expressive of Bell and others (1988) model for whole crustal extension via simple shear and mafic intrusion along the detachment.

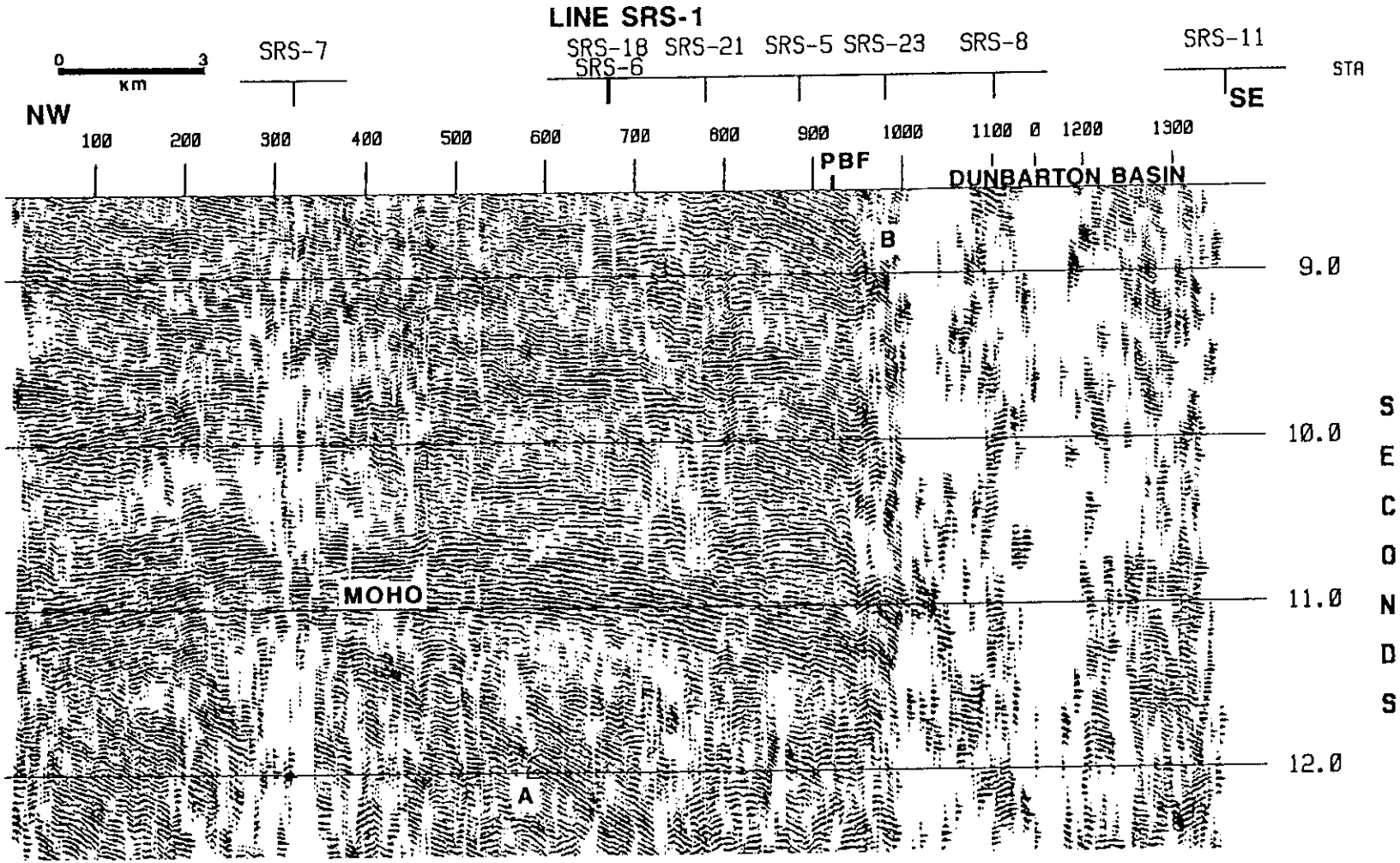

Figure 20. **Reflection Moho line SRS-1:** Reflection Moho as imaged on line SRS-1. Many of the dipping reflections (A) below the Moho would migrate to positions above the Moho. Subhorizontal reflections above the Moho are truncated by southeastwardly dipping reflections (B). Loss of reflectivity occurs beneath the Dunbarton basin. PBF = Pen Branch fault. Every other trace displayed.

Lower Crust

The lower crust at SRS, i.e. below 7.0-8.0 s, is relatively transparent and lacks the higher amplitude reflections of the middle and upper crust (Appendix B). Above the reflection Moho, weak subhorizontal reflections that demark a distinct reflective unit are truncated at 8.0-10.0 s by discontinuous southeast dipping reflections (Figure 20). Many of the crossing events and steep dips observed in this area would migrate to higher structural levels. In the midcrust the dipping events become remarkably continuous, laminated, high amplitude, and correlatable between seismic lines. The reflection geometries within the dipping layers strongly suggest a thrust and duplex geometry.

The reflections immediately above the Moho are similar, albeit lower amplitude, to reflections detected in the COCORP data and interpreted to represent late Precambrian or early Paleozoic age oceanic or transitional rift-stage crust (Cook et al., 1983), or thinned Grenville crust (Phinney and Roy-Chowdhury, 1989; Nelson and McBride, 1991). The southeast dipping reflections that truncate these lower subhorizontal events represent thrust surfaces formed during the various Paleozoic compressional deformations known to have affected the Appalachian orogen.

The transparency of the lower crust might not be entirely geological, but rather could result from insufficient signal as a consequence of the restricted bandwidth of these data. The full correlation time of the SRS seismic data is 4.0 s. Extended vibroseis correlation to yield output beyond this time results in linearly decreasing bandwidth of the correlated output with increasing time, i.e. the effective sweep is both shorter in duration and bandwidth. The increase in signal-to-noise ratio through use of vibroseis correlation is as per the square root of twice the product of the sweep length and the sweep bandwidth (Schneider, 1983). Therefore, at late times in extend correlated data the signal-to-noise ratio can be expected to be less than at earlier times in the correlated trace. Furthermore, the poststack bandpass filters applied to the data (Appendix A, Table 5) begin to cut severely into the passband at about 7.0 s.

Midcrust

The reflection patterns in the midcrust are similar in form to the southeast dipping reflections in the upper part of the lower crust and indicate a common structural history for both regions. Within the midcrust a 3.0-4.0 s wide zone of southeast dipping high amplitude laminar reflections occurs that defines an easily recognizable seismolithologic unit (Figure 21; see also Appendix B). Subdividing the zone are distinct bands of reflectivity 0.5-0.7 s wide that exhibit duplex geometry. The presumed thrusts are sharp discrete boundaries that are correlatable throughout much of SRS. Most of these thrusts are parallel or subparallel to the laminar reflections, although certain thrusts are observed to truncate the reflective bands.

One of the interpreted thrust surfaces is a continuous mappable reflection that dips southeastward from 4.6-7.0 s across SRS (Appendix B). This reflection is easily recognizable and is usually defined by only one or two wavelet cycles. Throughout most of the site the event is parallel to the laminar bands of reflectivity, but splays updip and flattens north of line SRS-7 (Figure 21). Below the thrust the reflection packages become gradually less distinct and less laminar, perhaps as a result of restricted bandwidth, and merge into the more steeply dipping reflections of the lower crust. Above the thrust the bright laminar reflection packages persist for 1.0-1.5 s before also becoming less distinct and less continuous. That this midcrustal reflection is continuous throughout the site and cuts across reflection packages suggests that it is a major structure.

The COCORP profile (Figure 19 on page 51) shows continuous high amplitude southeast dipping midcrustal reflections at times comparable to the events observed in the SRS data. One of these events (Figure 19 on page 51, Midcrust Reflection), which defines the upper bound of a 1.5-2.0 s wide reflection package, can be traced nearly the length of the profile, over 160 km, and appears to be correlative to the midcrustal thrust imaged at SRS. This reflection is identified as the Alleghanian Appalachian master decollement (Harris and Bayer, 1979; McBride and Nelson, 1991). The continuity of these reflection events along geologic strike, if proved to be genuine, would sup-

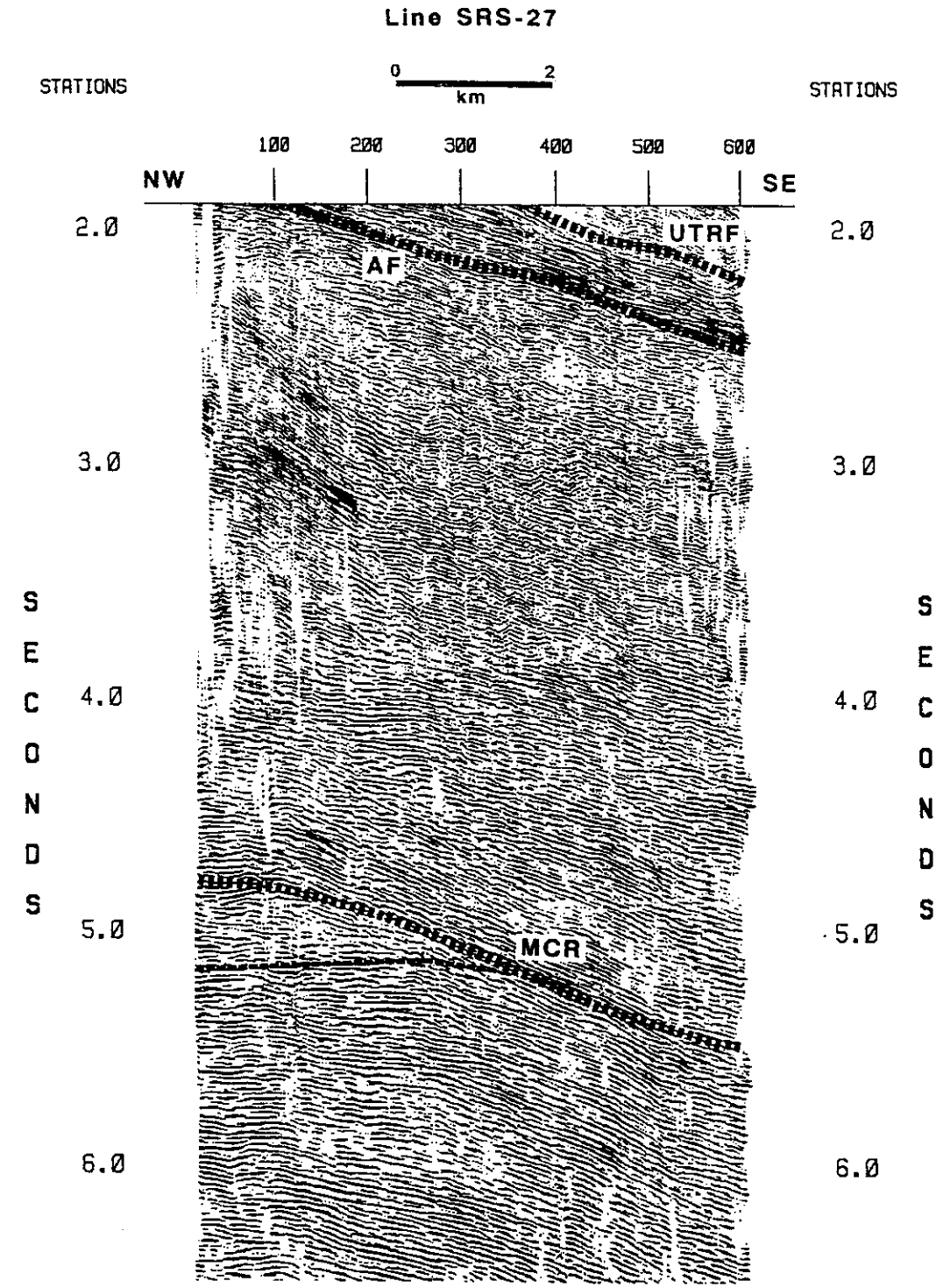

Figure 21. Midcrustal seismic reflection discontinuity: Reflection seismic expression of a probable major midcrust thrust (MCR). On line SRS-27 the event truncates deeper reflection packages as it splays updip. AF = Augusta fault, UTRF = Upper Three Runs fault. Display is 1:1 for crustal velocity of 6 km/s. Every other trace plotted.

port geologic models for evolution of the Appalachian orogen that incorporate large scale, presumably Paleozoic age, thrusts beneath the Piedmont and under the Atlantic Coastal Plain (e.g. Hatcher, 1971; Clark et al., 1978, Harris and Bayer, 1979; Cook et al., 1981, 1983; Pratt et al., 1987; Phinney and Roy-Chowdhury, 1989).

The assignation of specific lithologies or protoliths to any of the deep crustal data is, at best, speculative. The midcrustal reflections in the COCORP data were interpreted to be metamorphosed Precambrian and Paleozoic shelf strata. These rocks were interpreted to be overridden by the Piedmont and Blue Ridge along the Appalachian master decollement (Cook et al., 1981, 1983). Alternative interpretations of the midcrustal reflections are that of layered metasediments or layered intrusives and not fault surfaces; however, the geometry of the reflections imaged in the SRS data strongly suggest that many of the reflections are indeed fault bounded (Figure 21).

Upper Crust

The upper crust at SRS, defined as the upper 3.5-4.0 s of the time section, is dominated by southeast dipping reflections and reflection packages that have noticeably different reflection character than those observed in the middle and lower crust (Appendix B). The most complex reflection geometries observed in the SRS deep data set occur within the upper crust.

The most prominent reflection package of the upper crust is a 0.4 ms wide band of high-amplitude laminar reflections that dips southeastward across the site from 1.2-3.5 s (e.g. see Figure 26 on page 68 and Figure 27 on page 69). This band of reflectivity, which separates distinctly different reflection patterns above and below, is correlatable and mappable throughout SRS. Below the reflective band reflections are indistinct, discontinuous, and, in the northern third of the site, appear to have local northeast dips (truncated folds?). Above the reflective band, reflections are higher amplitude, continuous, correlatable, and exhibit complex reflection geometries.

The main band of reflectivity is strikingly similar to the reflection identified in the COCORP data as the Augusta fault and traceable for over 80 km. The similarity between the COCORP event interpreted as the Augusta fault and the reflective band at SRS is remarkable, although the SRS seismic lines are too short to verify whether or not these are indeed reflections from the Augusta fault. At SRS the presumed Augusta fault occurs at earlier reflection times than in the COCORP data, which implies a southwest component of dip on the fault surface.

In the northern third of SRS a fan-shaped, concave upward, southeast dipping wedge of reflectivity merges or soles into the Augusta fault (Figure 22). The reflection character of the wedge is similar to a reflection package imaged in Lumberton, North Carolina and confirmed by drilling to be interlayered mafic and felsic lower amphibolite grade metavolcanic rocks similar to that found in the Carolina Slate Belt (Pratt, 1982; Pratt et al., 1985). Boreholes 20-M and P8R at SRS penetrated chlorite schist and hornblende schist in the area of the wedge and confirm a similar origin for the reflections in this area (Figure 2, Table 2). The southern flank of this feature appears to correspond to the Upper Three Runs fault of Cumbest and Price (1989a). Along some of the seismic lines, particularly seismic line SRS-1 (Appendix B), the Upper Three Runs fault appears to offset the Augusta fault where the former soles into the latter. During Mesozoic extension the Upper Three Runs fault might have been locally reactivated in preference to the Augusta fault to cause the observed geometry.

In the middle and southern thirds of the site occur several prominent, locally correlatable, often concave upward, southeast dipping reflections and reflection packages that merge into, or are subparallel to, the Augusta fault (e.g. Figure 27 on page 69; Appendix B). These reflections trend northeast-southwest and are interpreted to be faults that sole into the Augusta fault. Some of these structures project upward to where faults are interpreted offsetting the Coastal Plain sediments. Borehole data indicate that these faults bound lithologies of differing metamorphic grade similar to the faults of the Eastern Piedmont fault system. The fault slices are characterized by variably reflective and laminar wedges of dipping reflections. In the center of SRS one of these fault slices bounds a large antiform (Figure 27 on page 69, stations 500-800). The Pen Branch fault is poorly imaged in these data, probably as a consequence of its high dip angle.

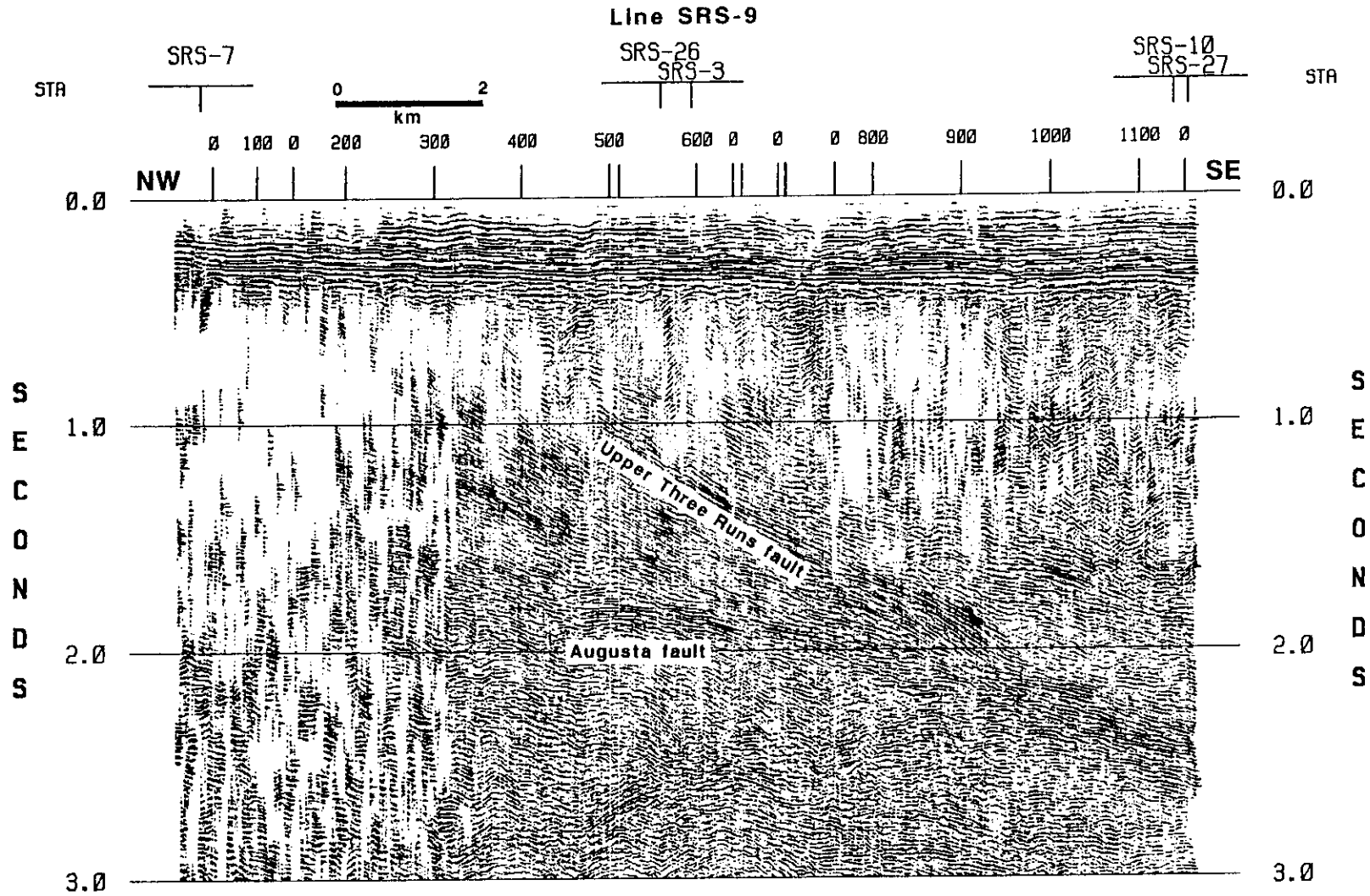

Figure 22. **Augusta fault-Upper Three Runs fault:** Seismic line SRS-9. The Upper Three Runs fault splays off the Augusta fault and bounds a fan-shaped wedge of laminar reflections.

One of the reflection packages that subparallels the Augusta fault can be followed under the Dunbarton basin where it truncates northwest dipping reflections that occur above it (e.g. see Figure 23 on page 63 and Figure 27 on page 69). This reflection package defines the detachment along which the basin developed and confirms that the pre-existing structural fabric was exploited during rifting to form the Dunbarton basin. Along the southern margin of SRS the reflection package merges into laminar reflections occurring 0.3-0.4 s above the base of the Augusta fault. On seismic lines SRS-1 and SRS-7 the detachment does not appear to be offset by the Pen Branch fault and on line SRS-8, a quasi-strike profile, it can be clearly followed under the basin westward to the base of the Coastal Plain northwest of the Pen Branch fault (Appendix B). In the eastern part of the site, on line SRS-3, the detachment does appear to be offset by the Pen Branch fault, but this faulting does not offset the Augusta fault.

In many models of basin development extension creates listric normal faults that sole into a detachment surface (e.g. Wernicke and Burchfiel, 1982; Withjack et al., 1995). As extension progresses, the upper plate collapses and rotates downward and away from the border fault. The northwest dips above the the detachment observed at SRS show this geometry, but as discussed in a later section, the Pen Branch fault is near vertical where it bounds Triassic strata and such a structure does not easily fit into these models. The Pen Branch fault could become listric within the crystalline basement, but the seismic data are inconclusive.

If the hypocenters from the 1985 and 1988 Savannah River Site earthquakes are projected onto seismic line SRS-1 they fall on the detachment (Figure 23). This suggests the possibility that this structure is seismogenic; however, the error associated with the depth determination of the earthquakes is larger than the calculated depth values. More earthquakes and a denser network of receiver stations are required to determine the relationship between seismicity and geologic structure in this area.

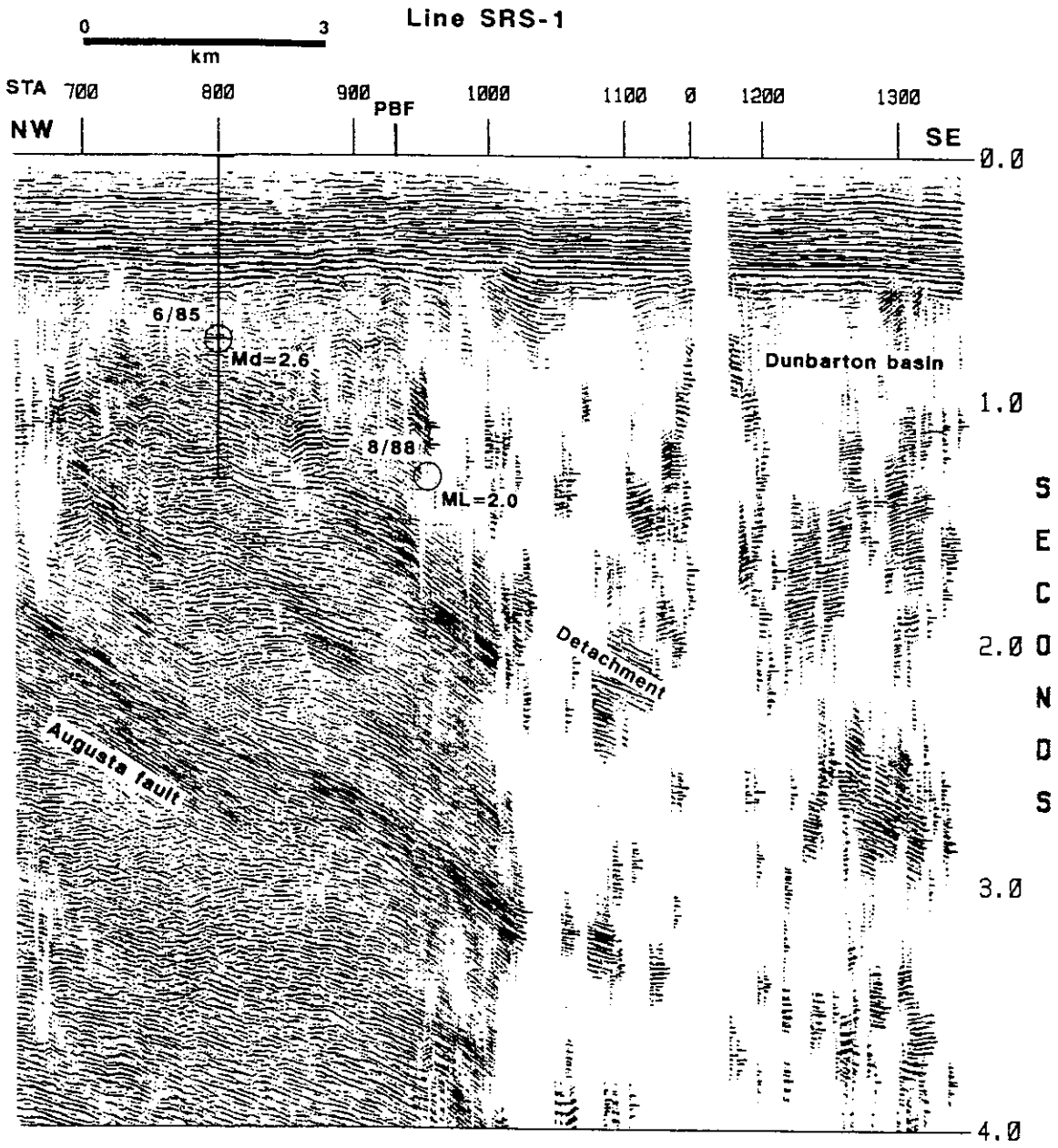

Figure 23. Earthquake foci line SRS-1: The foci for the 1985 and 1985 earthquakes at SRS are plotted on seismic line SRS-1. The events appear to fall on a detachment that underlies the Dunbarton basin. Earthquakes: June 9, 1985, depth 0.96 km, ERZ 1.6 km, ERH 0.3 km; August 4, 1988, depth 2.86 km. PBF = Pen Branch fault. Display is 1:1 for crustal velocity of 6 km/s. Every other trace plotted.

Gravity and Magnetic Data

The individual fault slices of the upper plate of the Augusta fault give rise to identifiable gravity and magnetic signatures. In particular, the aeromagnetic map of the Savannah River Site shows two prominent linear magnetic anomalies north of the trace of the Pen Branch fault that form a Y-shaped pattern (Figure 24). The "Y" has been variously interpreted as a southwest plunging fold (Daniels, 1974), continuation of the Eastern Piedmont fault system under the Coastal Plain (Cumbest and Price, 1989b), and evidence for near vertical Mesozoic age faults offsetting a slab of mafic schist/gneiss underlying SRS at 1.0-2.0 km depth (Anderson, 1990). In detail, the reprocessed SRS seismic data reveal the origin of the anomaly to be more complex.

The lower limb of the Y anomaly is interpreted to originate from the truncation at the base of the Coastal Plain of the detachment that underlies the Dunbarton basin (Figure 26 and Figure 27). This structure is the boundary between amphibolite, biotite gneiss and penetratively deformed mafic and ultramafic rocks (Figure 2 on page 6). The corresponding magnetic lineament is parallel to the trace of the Pen Branch fault and is traceable to the northeast and southwest off SRS. Southwest of SRS the magnetic lineament merges into a magnetic lineament that farther eastward is associated with the Augusta fault (Figure 25). Northeast of SRS the amplitude of the anomaly diminishes and the limbs of the Y converge defining a sigmoid. Cumbest and Price (1989b) recognized the parallelism between the magnetic anomaly and the northwest border of the Dunbarton basin and suggested that the former denoted a detachment that led to the formation of the basin. Furthermore, they interpreted the magnetic lineaments at SRS as extensions of the Eastern Piedmont fault system under the Coastal Plain and that, by inference, the proposed detachment was a reactivated Alleghanian structure. A similar interpretation is proffered herein.

The upper limb of the Y is roughly coincident with the Upper Three Runs fault. In Figure 26 and Figure 27 the inflection point of this anomaly is to the south of the Upper Three Runs fault and appears to be associated with the fault slice that bounds the fan-shaped structure, but to the northwest (line SRS-9, Appendix B) the lineament follows the trend of the Upper Three Runs fault. The intervening area between the limbs of the Y is indeed an antiform as interpreted

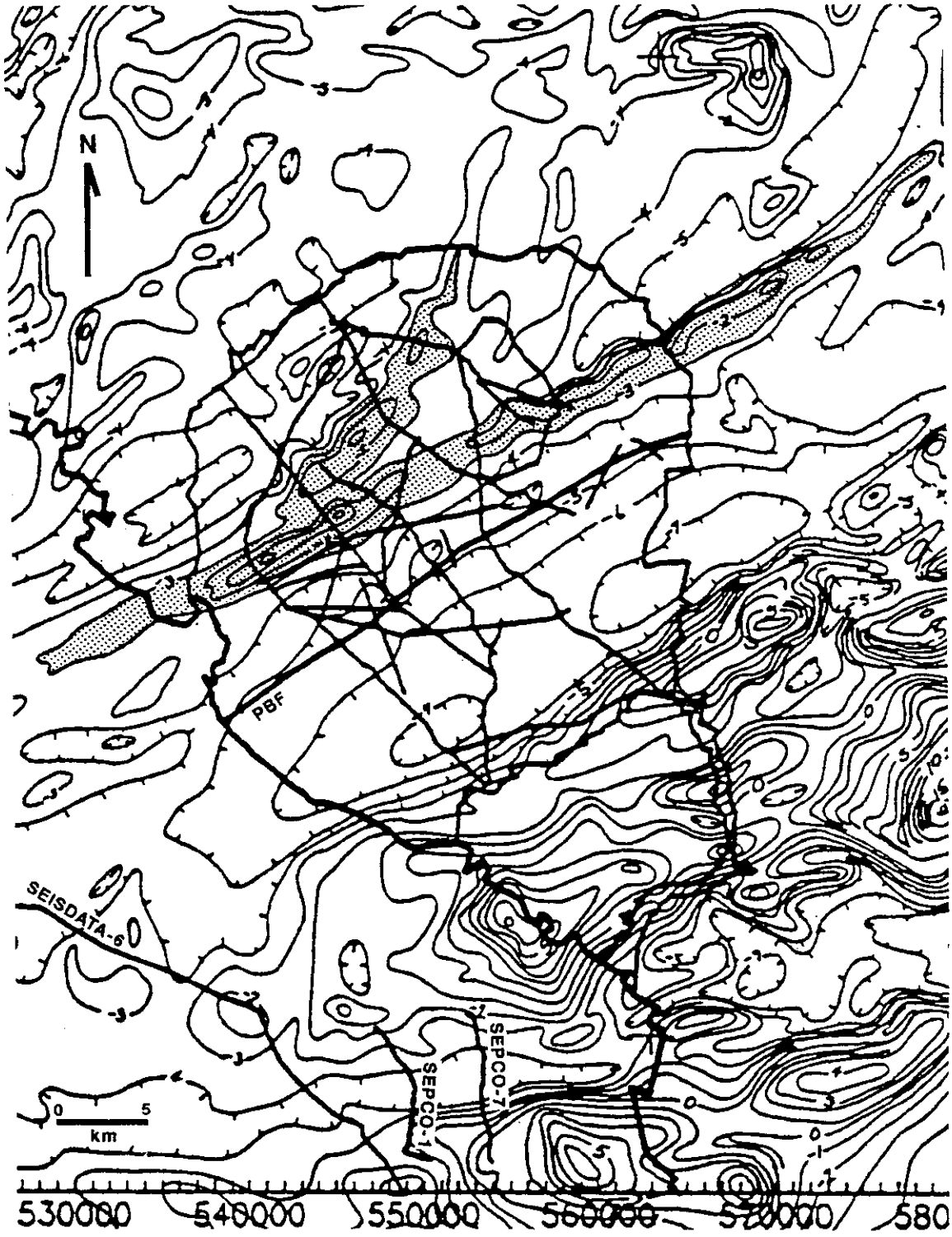

Figure 24. Aeromagnetic map of SRS study area: Aeromagnetic data from Daniels and others (1983) The Y-shaped anomaly is highlighted. The contours are scaled values of residual field intensity and are not directly convertible to nanoTeslas.

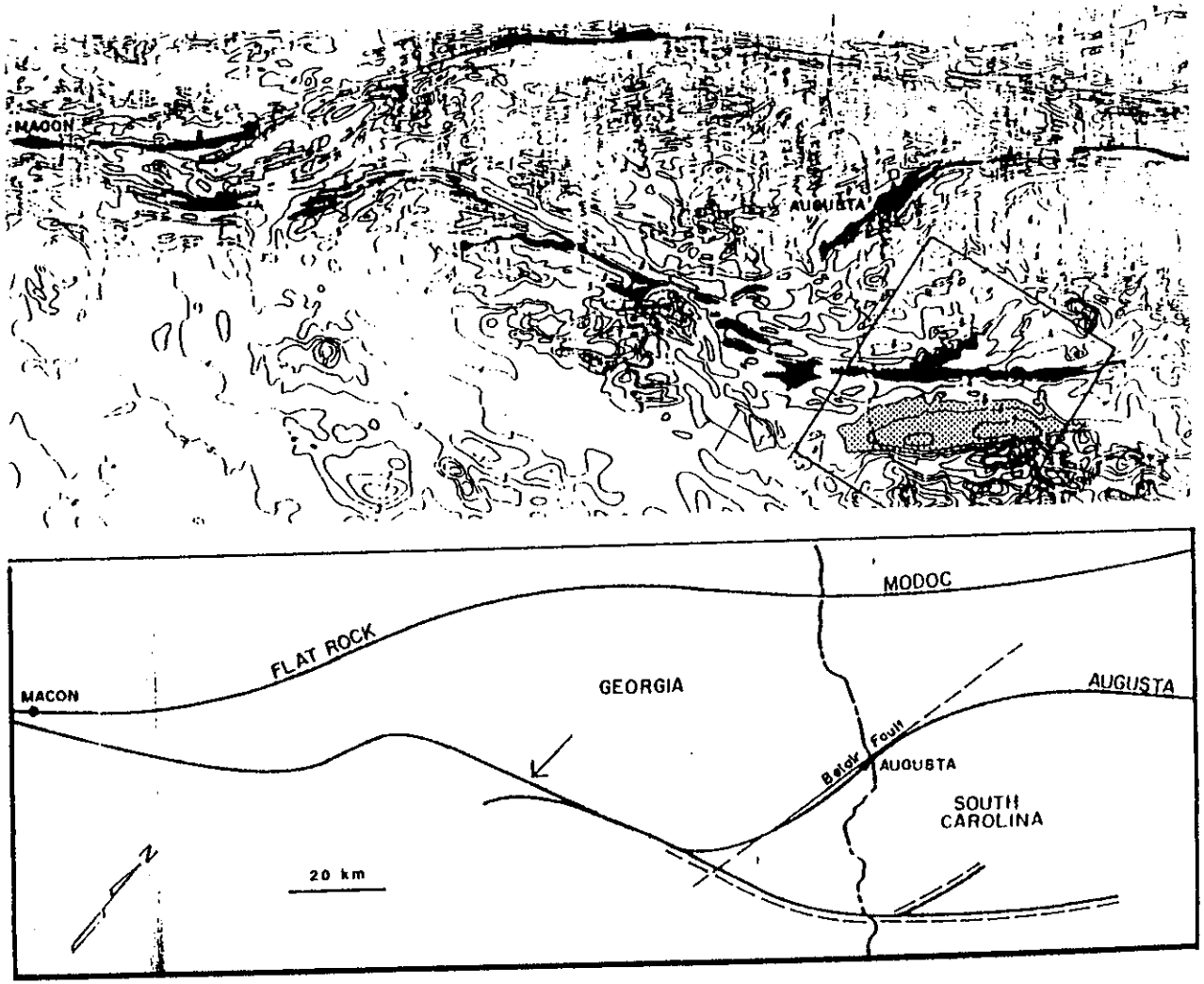

Figure 25. Regional aeromagnetic map: Residual regional aeromagnetic data (top) and interpretation of the Eastern Piedmont fault system (bottom). The SRS study area is outlined and the magnetic low over the Dunbarton basin is stippled. The limbs of the "Y" magnetic anomaly at SRS converge to the southwest and merge into a magnetic lineament that is associated with the Augusta fault. Figure from Cumbest and Price (1989b, Figure 2).

by Daniels (1974) (Figure 26, stations 500-800). This structure is developed in the penetratively deformed mafic and ultramafic rocks and is bounded on the northwest by the Tinker Creek fault. The Tinker Creek fault penetrates into the Coastal Plain sediments where it is a mappable structure across SRS (see "Time-structure Maps - Shallow Data Set"). The mafic and ultramafic rocks of the interior of the Y give rise to a prominent northeast-trending gravity high (Figure 16 on page 46). Northeast of seismic line SRS-9 the gravity anomaly bifurcates. In this area seismic lines SRS-9, SRS-10 and SRS-27 show complex reflection patterns that suggest that the structure has split into two folds (Appendix B).

A small gravity low occurs along the northwest boundary of SRS defined by the northeast half of line SRS-12, south to line SRS-7, and line SRS-4 to the juncture with line SRS-7 (Figure 16 on page 46). This area is also coincident with a local high in basement time-structure, a topographic high, and a basement reflection amplitude anomaly (Figure 41 on page 101, Figure 55 on page 124, and Figure 61 on page 133). Along seismic line SRS-12 (Appendix B) loss of reflection signal occurs in the upper crust in this area. Eight kilometers to the north of this anomaly granitic basement was penetrated in the AIK-858 borehole and farther to the north the Alleghanian Graniteville-Vaucluse pluton is interpreted from borehole and gravity data (Speer, 1982). The gravity low is perhaps indicative of granitic rock related to the Graniteville-Vaucluse body, but no hole to basement exists to confirm the interpretation.

The above interpretation of gravity and magnetic anomalies is speculative. In the reprocessed seismic reflection data the probable sources of the potential field anomalies observed at SRS have been identified. These seismic data should constrain detailed gravity and magnetic modelling of the anomalies, which is beyond the scope of the present investigation.

Dunbarton Basin

The Dunbarton basin is revealed to be a half-graben with the northwest border defined by the Pen Branch fault. In overall geometry, the Dunbarton basin is similar to the Riddleville basin as

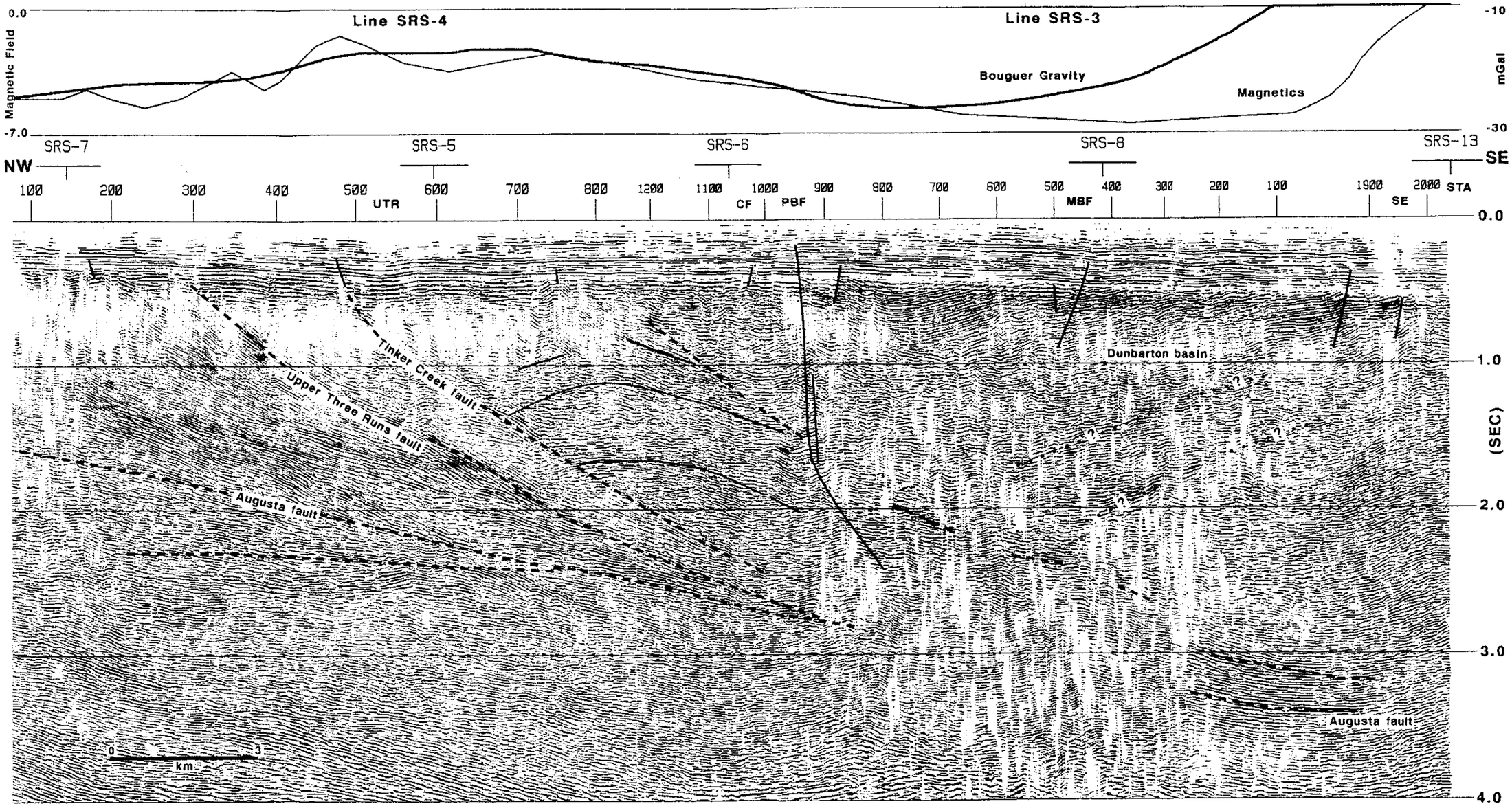

Figure 26. **Upper crustal structure along lines SRS-3, SRS-4:** The short wavelength gravity and magnetic anomalies observed at SRS originate from geologic boundaries/structures above the Augusta fault. PBF = Pen Branch fault, MBF = Meyers Branch fault, CF = C Line fault, UTR = Upper Three Runs. Migrated seismic data. Display is 1:1 for crustal velocity of 6 km/s. Every other trace plotted.

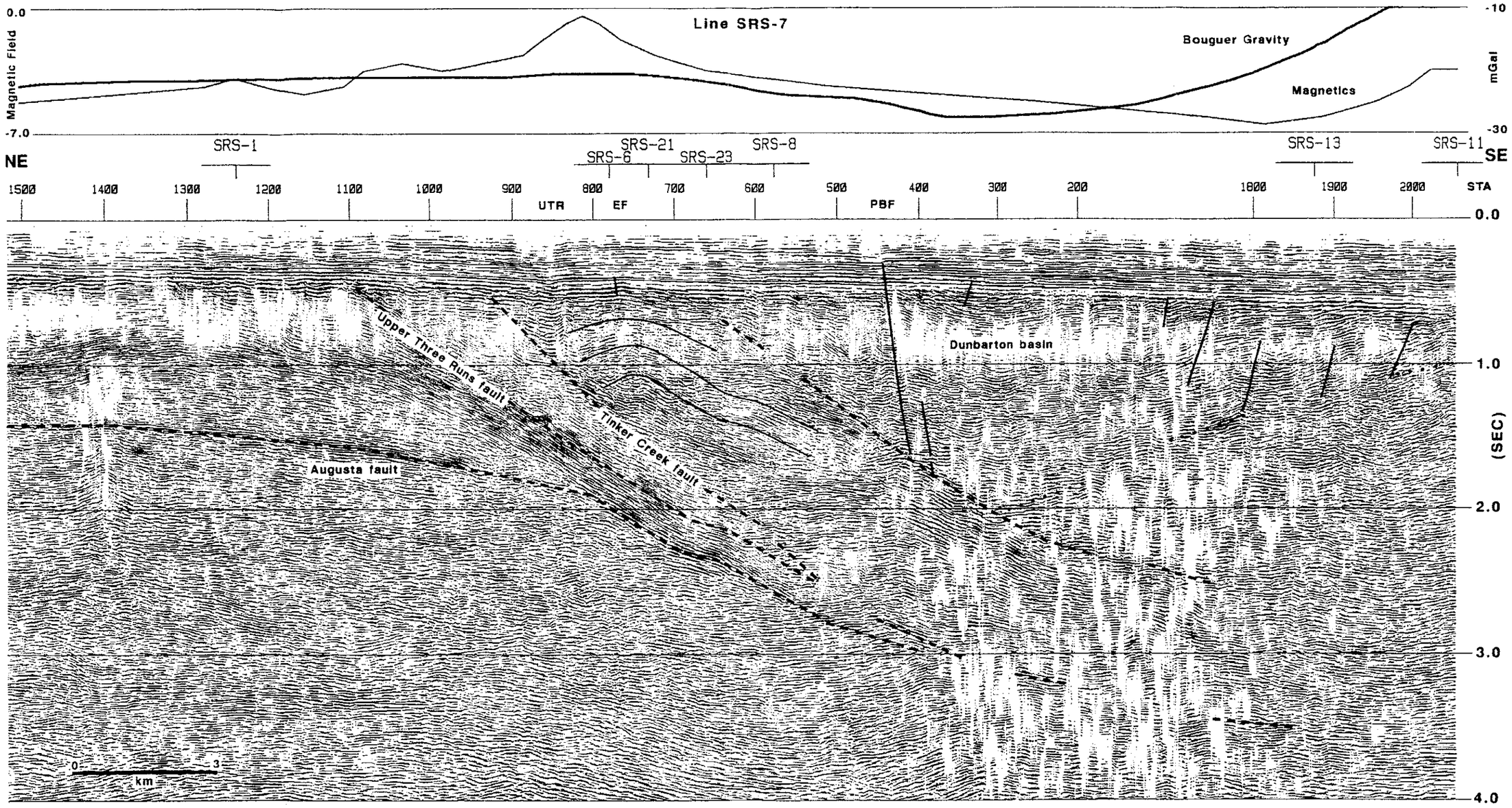

Figure 27. **Upper crustal structure along line SRS-7:** The short wavelength gravity and magnetic anomalies observed at SRS originate from geologic boundaries/structures above the Augusta fault. PBF = Pen Branch fault, EF = Ellenton fault, UTR = Upper Three Runs. Migrated seismic data. Display is 1:1 for crustal velocity of 6 km/s. Every other trace plotted.

interpreted from COCORP line 5 (Petersen et al., 1984). The basin strata dip 10-15° to the northwest and along the northwestern border of the basin, within 2 km of the Pen Branch fault, the sedimentary units undergo dip reversal and dip 15-20° to the southeast (Figure 26 and Figure 27). The local southeast dip near the Pen Branch fault is prevalent throughout the site and is consistent with borehole data from DRB-9 (Siple and Marine, 1974). In general, the Dunbarton basin strata are weakly reflective, unlike the highly reflective Triassic strata belonging to the South Georgia sequence described by McBride and others (1989). The strongest reflections from the basin fill occur along the southern margin of SRS and near the Pen Branch fault on lines SRS-4 and SRS-28. The southeastern border of the basin was not detected in the SRS seismic data and evidently occurs offsite.

On lines SRS-13, SRS-3EX, SRS-11 and SRS-7EX (Appendix B) there occur within the basin high-amplitude, short (< 500 m) reflection segments concordant with the basin reflections. These events are probably igneous sills and/or flows similar in origin and age to those commonly found in the Triassic rift basins of eastern North America (Manspeizer and Cousminer, 1988). Several of these sills appear in conjunction with faults, which suggests that the fault planes might have acted as conduits for the igneous material. One such example occurs on line SRS-13 (Appendix B) between stations 385 and 465 at 0.7-0.8 s where high amplitude reflections are observed emanating on either side of a fault block within the basin. The overall high reflectivity of the basin sediments in the south of SRS is probably caused by sill injection and intercalation of igneous material with the basin fill. No boreholes at SRS have encountered igneous material, although just south of the site borehole AL-324 encountered metamorphosed Triassic strata (Snipes et al., 1993a).

Many of the Mesozoic rift basins of eastern North America have characteristic gravity anomalies parallel to their eastern margins consisting of a short wavelength (≈50 km) 25 mGal "inner gravity high" along the edge of the basin and a broad wavelength (≈100 km) 20 mGal "outer gravity high" farther seaward (Bell et al., 1988). Model studies of these gravity anomalies led Bell and others (1988) to propose a model for rifting involving simple shear through the entire crust. In this model extension is accommodated by movement along pre-existing Paleozoic age thrusts in the midcrust and by simple shear in the lower and upper crust. The outer gravity high corresponds

to the location where the detachment cuts through the base of the crust and crustal material is replaced by mantle material by flexural isostasy. The inner gravity high is caused by diabase intruded along the detachment in a layer up to 2.0 km thick during the later stages of rifting. If the detachment is steeply dipping, the inner and outer gravity highs are coincident.

The gravity profile across the Dunbarton basin is similar to profiles across other Mesozoic basins to the northeast of SRS as modelled by Bell and others. As previously noted, the linear 20 mGal gravity high south of SRS (Figure 18 on page 50) has been interpreted to be Mesozoic in age and related to rifting. This gravity high continues southwestward to where it defines the southern margin of the Riddleville basin. In the COCORP data this region is a discontinuity in the southeast dipping reflection patterns where the reflections steepen and verge into a "root zone" at the base of the crust (Figure 19 on page 51, Line 5 station 1800 to Line 8 station 200). Undoubtedly, a similar geometry exists south of SRS.

Gravity modelling of the Dunbarton basin and its associated inner gravity high by Cumbest and others (1992) indicated that the gravity high could be modelled by a mafic mass that is at least 9.0-10.0 km in thickness, 20.0 km in breadth and extends partly beneath the basin. The top of the modelled mafic body is as shallow as the base of the Coastal Plain. If the model of Bell and others is invoked, Mesozoic extension was localized along the root zone and caused failure of the entire crust in simple shear. Intrusion of mafic material along the steeply dipping root zone and into the hanging wall of the detachment beneath the basin during the later stages of rifting results in a single linear gravity high south of the basin that can be modelled as a simple, vertical extensive mafic mass. Diabase intrusion along the detachment and into its hanging wall is the source of the sills and high reflectivity along the southern margin of the Dunbarton basin.

The geometry of the higher amplitude reflections detected on lines SRS-4 and SRS-28 (Appendix B) at the Pen Branch fault is similar to those imaged elsewhere along the northwest border of the Dunbarton basin; the only distinguishing characteristic of these reflections is the amplitude. None of the other seismic lines that cross the Pen Branch fault exhibit as high amplitude reflections from the Triassic sediments. It might be that these reflections represent particularly well indurated fanglomerate layers or could also be evidence for igneous material intercalated with the basin strata.

An enigmatic phenomenon associated with the high reflectivity of the basin sediments in the the south of SRS is the sharp transition between the highly reflective and weakly reflective strata in the northwest-southeast direction (see Appendix B, line SRS-3 stations 40-160 and line SRS-7EX stations 1860-1960). This sharp boundary occurs over a distance of only a few meters beginning near the top of Triassic basement and persists through the length of the data. At 1.0-1.5 s and later in the time section the time to reflection events on either side of transition begins to differ, becoming less for those events to the southeast. Some of this time difference can be attributed to intrabasinal faulting; however, to attribute all the time difference to faulting would require a fault with throw similar to, or greater than, the Pen Branch fault. No compelling evidence exists for such a fault. A possible explanation for the time difference is velocity pull-up. If the average velocity of the basin sediments is increased to that of the crystalline rocks as a consequence of sill injection, the time difference might be accounted for.

No evidence for large intrabasinal unconformities appears on any of the SRS seismic lines. This is in contrast to some of the basins of the South Georgia rift where unconformities separating syn-rift (Triassic) and post-rift (Jurassic) sedimentation have been interpreted (McBride et al., 1989). Hence, all the strata in the Dunbarton basin are syn-rift deposits and the later post-rift deposits have been eroded or were not deposited as far west as the Dunbarton basin.

Petersen and others (1984) noted a distinct bimodal seismic stratigraphy to the Riddleville basin where the lower section is well layered and dips 6-10° north toward the border fault and the upper section, that forms most of the basin fill, is weakly layered and subhorizontal. They suggested, by analogy to other rifts, that the lower, layered sequence represented lacustrine sedimentation or clastics interlayered with basalt flows. No such bimodal seismic stratigraphy is observed for the Dunbarton basin. Where reflections from the Dunbarton basin strata are detected, the reflection character, except for the amplitude variations previously described, is uniform and layered. The reflection patterns noted from within the Riddleville basin could merely represent a local feature, given that the interpretation by Petersen and others is based on a single seismic profile.

The strata within the Dunbarton basin are locally faulted and some of these intrabasin faults penetrate into the Coastal Plain sediments as reactivation structures (see Figure 26 on page 68 and

Figure 84 on page 171). Most of these faults appear to be northwest dipping antithetic normal faults that bound discrete fault blocks formed contemporaneously with the basin graben. It appears that faulting and sedimentation were occurring at roughly similar rates, inasmuch as the dip angles of reflections within the basin are similar wherever basin fill can be unambiguously interpreted.

The southeastern boundary of the Dunbarton basin was not traversed by the SRS lines, with the exception that the character of the basement reflection on the first 50 traces of line SRS-13 (Appendix B) is similar to that observed where crystalline basement is known to exist. The pattern of multiple reflections beneath the basement reflection for these traces is similar to that for crystalline basement; however, autocorrelograms produced from stacked traces and undeconvolved CDP gathers were not noticeably different than those from other areas throughout the site. No refraction velocity measurements could be obtained from this area as the critical distance for the basement refraction is nearly the same as the distance represented by these traces. The nearest basement refraction velocity measurement to this location is 4826 m/s, which is calculated at the southeastern end of line SRS-3EX and is characteristic of the Triassic strata.

The location of the southeastern boundary of the basin can be roughly estimated from the Bouguer gravity map (Figure 18 on page 50). It is known that the boundary passes between the AL-324 and C-7 boreholes, i.e. the Martin fault of Snipes and others (1993b). The gravity contours between these boreholes trend northeastward near the eastern terminus of line SRS-13, and trend southwestward and south west of the southern terminus of line SRS-7. To the south and east of SRS seismic line SEPCO-1 shows clear evidence for a Triassic basin (Figure 28). Four kilometers to the east of this profile seismic line SEPCO-7 also shows what could be basin strata beneath the Coastal Plain, but the interpretation of basin strata is less clear (Figure 29). The gravity contours in the vicinity of the SEPCO lines trend nearly north-south and the contour values are similar to those where Triassic strata are known to be present. Thus, in a general sense, the 4-10 mGal contours denote the southern edge of the Dunbarton basin.

North of the Pen Branch fault there is no evidence for a peripheral basin such as that interpreted in the COCORP data by Cook and others (1981). A refraction stack section of line SRS-1 shows that the top of basement refractor uniformly stacks in at velocities above 5500 m/s north

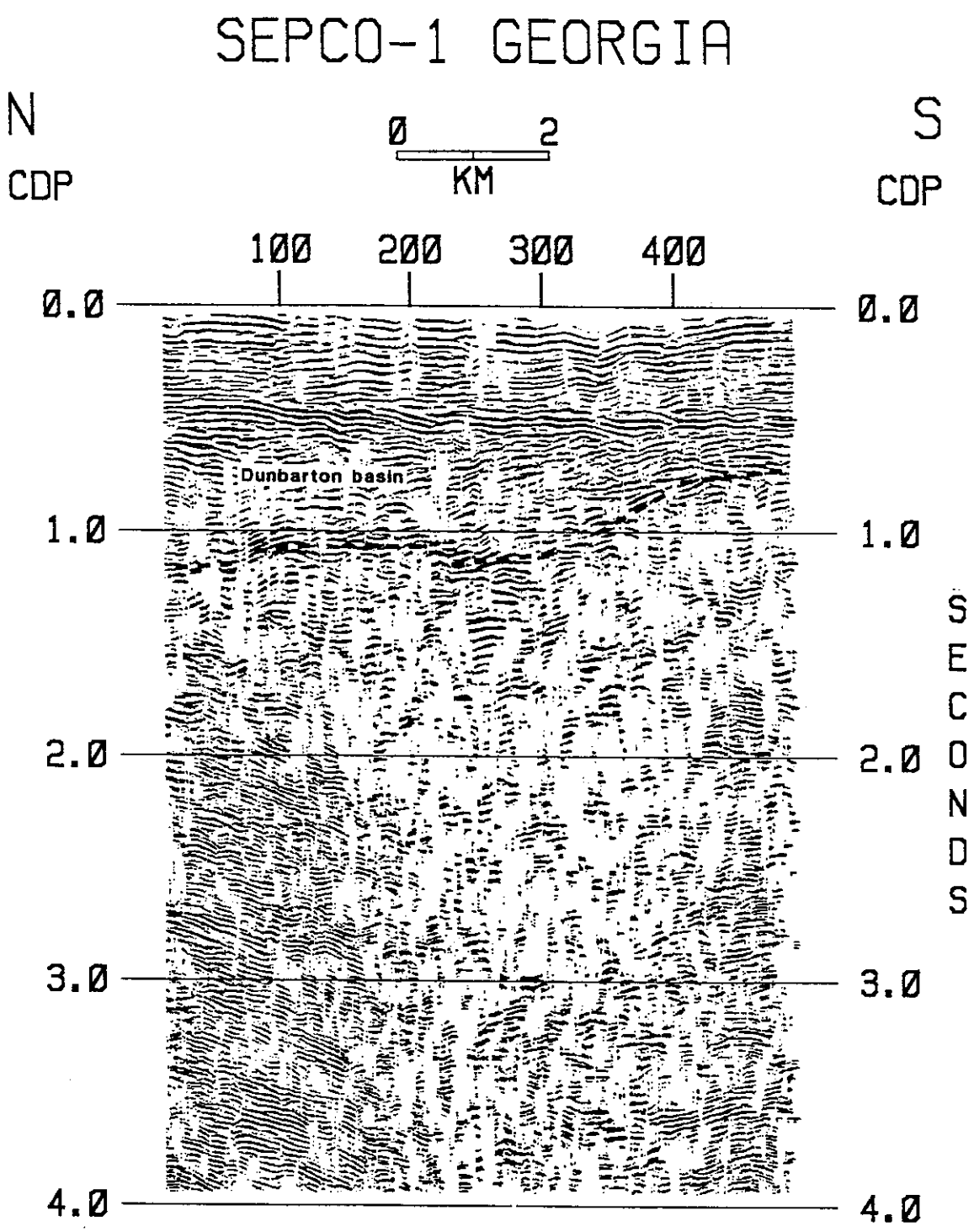

Figure 28. **Automatic line drawing SEPCO line 1:** Reflections from basin strata are clearly evident beneath the Coastal Plain. Reflections originating from within the basement dip toward the center of the profile from both sides of the line. In aeromagnetic data a magnetic lineament that splays from the Goat Rock fault passes through this location (Figure 24). Trace spacing 16.76 m.

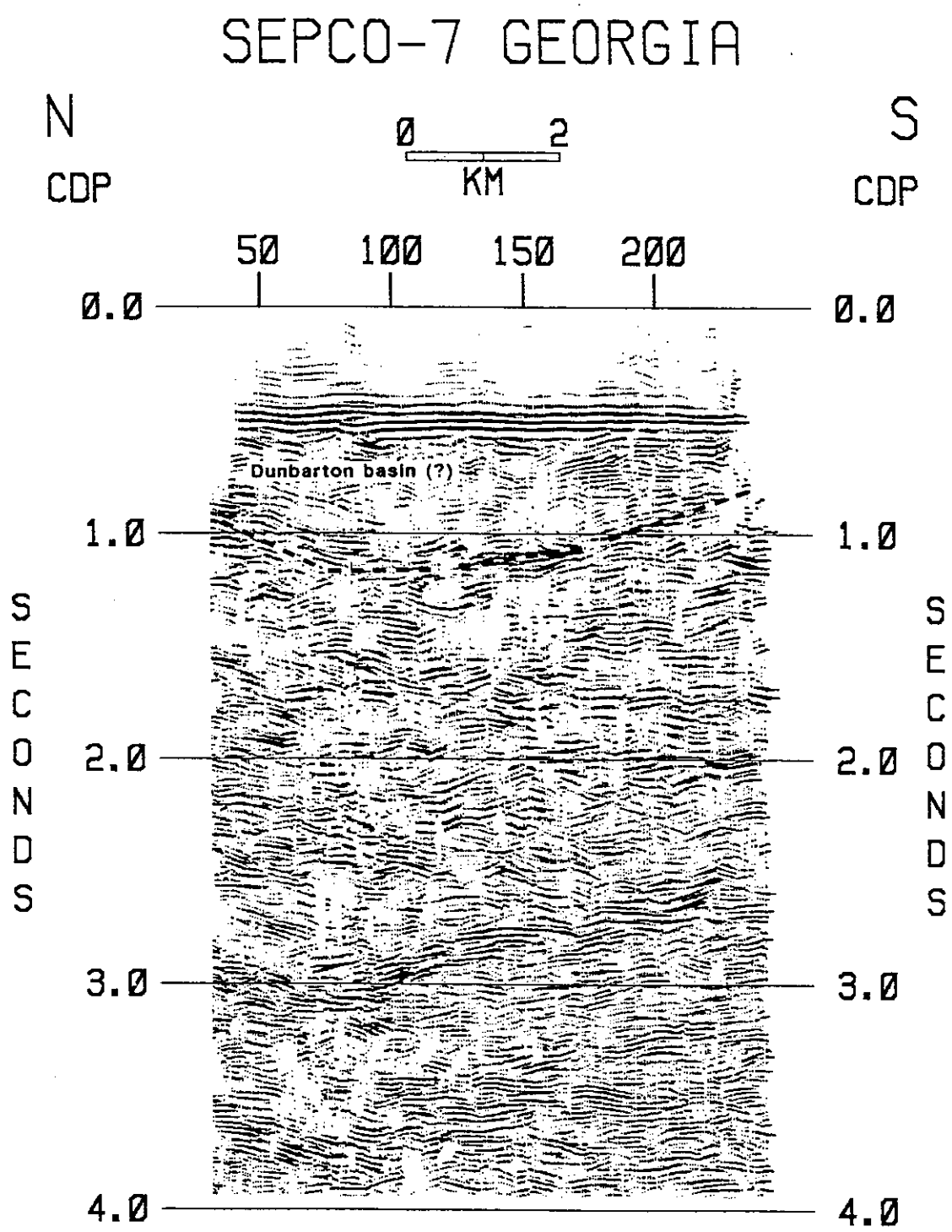

Figure 29. Automatic line drawing SEPCO line 7: The identification of Triassic basin strata beneath the Coastal Plain on this line is less clear than on SEPCO-1. The interpreted thickness of basin strata at this location is less than that on line SEPCO-1 implying eastward shallowing of the basin toward the gravity high. Note that reflections originating from within the basement dip toward the center of the profile similar to those observed on line SEPCO-1. Trace spacing 33.53 m.

of the Pen Branch fault. South of the fault a coherent stack can only be obtained for slower velocities (Figure 30). Therefore, at least along line SRS-1, no outliers of Triassic strata exist north of the Pen Branch fault. Furthermore, none of the basement refraction velocity values measured north of the Pen Branch fault at SRS are in the range of values for Triassic strata (Bonini and Woollard, 1960; Chapman and DiStefano, 1989; Demirbag, 1990). North of SRS the Graniteville-Vaucluse pluton is concealed beneath the Coastal Plain and is exposed in stream drainages along the Fall Line; thus, the Dunbarton basin defines the western limit of preserved Triassic strata in this part of the southeastern United States.

The thickness of the basin fill is not well constrained. On none of the seismic lines is the base of the basin imaged, i.e., the transition between Triassic strata and crystalline rock in the hanging wall of the detachment is unclear. On seismic line SRS-3 between stations 600 and 800 basin strata are clearly interpreted to 1.0 s (Figure 26). If the average velocity of the Triassic strata is taken to be 5400 m/s, by extrapolation of the velocity profile from the DRB-10 borehole, then the lower bound for the maximum thickness of Triassic strata is 1.6 km. On seismic line SRS-8 between stations 100 and 400 segments of northward dipping reflections at 1.9 s can be interpreted to mark the bottom of the basin (Appendix B). In that case, the thickness of the basin fill is calculated to be 3.7 km. Therefore, the range of probable values for the maximum thickness of the basin fill is 1.6-3.7 km. The 1.6 km thickness value is similar to the results obtained from transient electromagnetic soundings (1.80 km; Price et al., 1989) and gravity modelling (1.62 km; Marine and Siple, 1974); however, in the case of gravity data, the density of the strata near the base of the basin is probably similar to that of the crystalline rock, which would lead to an under estimation of the strata thickness. Costain and Çoruh (1989) noted that for many of the Triassic basins of eastern North America the base of the basin fill, as imaged in seismic reflection data, seldom exceeds 1.8-2.0 s reflection time. They speculated that this characteristic time boundary or limit corresponds in depth to the brittle-ductile transition when the basins were formed. Thus, by inference, it is unlikely that basin fill in the Dunbarton basin much exceeds 4.5 km.

The seismic reflection character of the contact between the Triassic basin fill and the base of the Atlantic Coastal Plain sedimentary sequence is variable. On many seismic lines this reflection

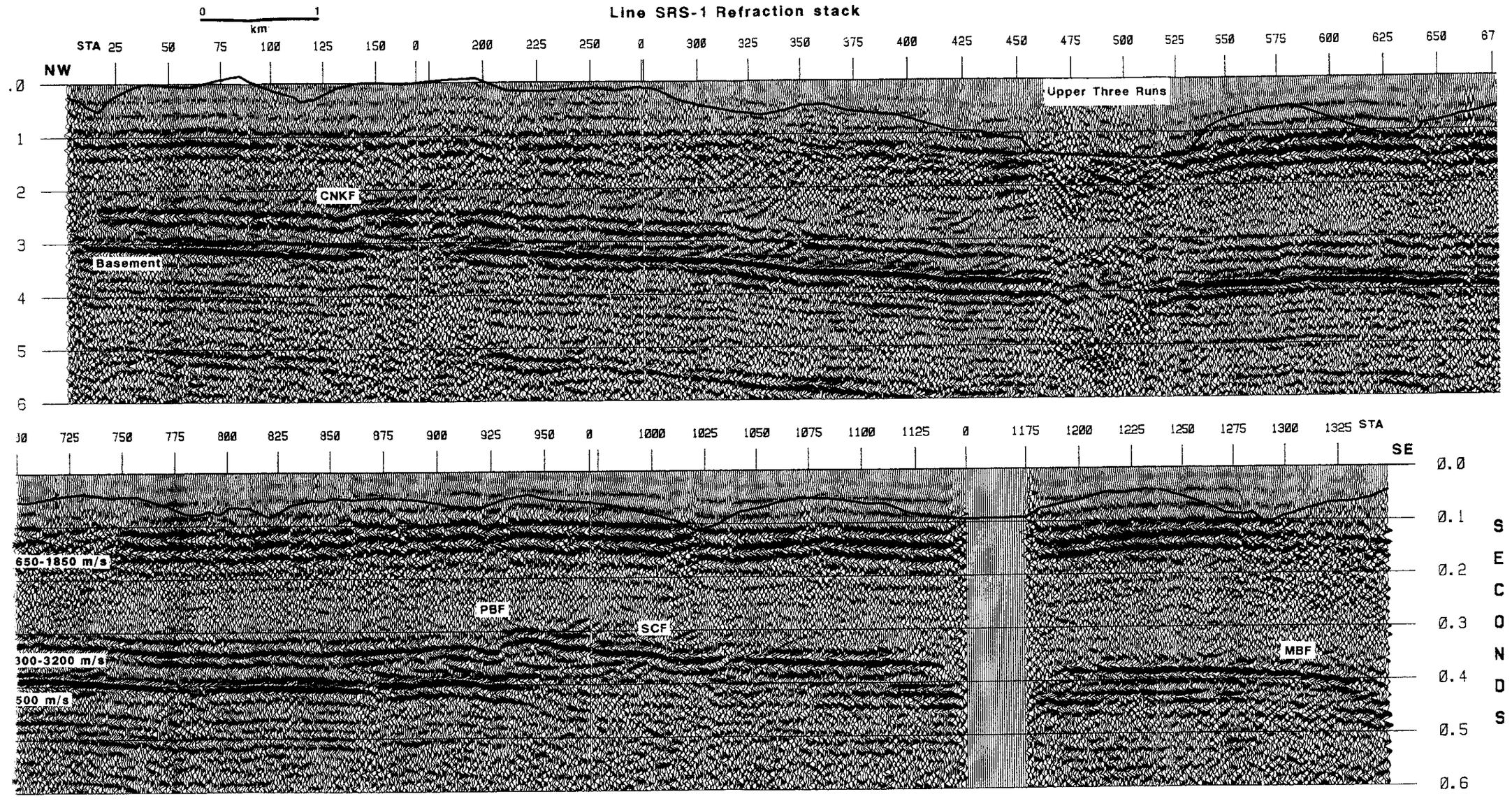

Figure 30. Refraction stack line SRS-1: The refraction stack is produced by applying linear movement (LMO) to the CDP gathers using the appropriate refraction velocity (Appendix A). At the Pen Branch fault (PBF) the top-of-basement refraction no longer stacks in at 5500 m/s indicating a change in basement lithology (velocity) caused by the lower velocity Triassic strata in the Dunbarton basin. CNKF = Crackerneck fault, SCF = Steel Creek fault, MBF = Myers Branch fault.

is a stark angular unconformity (e.g. line SRS-4, Appendix B); on other lines the boundary is a continuous, distinct, two-cycle reflection where the lower cycle eventually becomes dominant (e.g. line SRS-2, Appendix B). The two cycle reflection observed at SRS is similar to a reflection occurring at or near the base of the Atlantic Coastal Plain section over Triassic sediments of the South Georgia rift (McBride et al., 1989; Figure 3). McBride and others (1989) interpreted this reflection to be an areally extensive Middle Jurassic basalt and/or diabase sill sequence, the "J" reflector, which is correlatable throughout the South Georgia basin and offshore South Carolina and Georgia. The J reflector demarks the post-rift unconformity, i.e. the initiation of drift stage sedimentation.

In the SRS area, synthetic seismograms constructed from borehole sonic and density logs demonstrate that the two-cycle reflection arises from interference between reflections from the basal Cape Fear Formation and reflections from the top and bottom of the weathered zone at the top of Triassic basement (see section "Correlation of Borehole Data to Seismic Reflection Data" and figures contained therein). At some of the locations where the J reflector was identified by McBride and others, and not independently verified by borehole or seismic refraction data, the two-cycle reflection could have a similar origin. Therefore, the J reflection might be less areally extensive than previously thought.

Time-structure Maps - Deep Data Set

The details of construction of the time-structure maps are discussed later in this report as part of the interpretation of the shallow data set. Three reflection events were found to be mappable in the crust throughout SRS; the Midcrust reflection, the Augusta fault, and the Upper Three Runs fault.

Midcrust Reflection Time-structure Map

The time-structure map prepared on the Midcrust reflection reveals a relatively uniform dip of the surface to the southeast across SRS (Figure 31). Northeast of line SRS-7 from the intersection with line SRS-1 the reflection surface is less steep and a local flattening of the thrust surface occurs along line SRS-4 near Upper Three Runs. A trend surface fit to the map where the dip is uniform indicates a dip of 16.5° southeast (migrated, V = 6.35 km/s) and a strike of N 45° E. In the middle of the map area, coincident with the trace of the Pen Branch fault at the top of crystalline basement, the thrust surface rapidly steepens for a distance of 1.5-3.0 km before resuming a constant dip. The southern boundary of the map is more complex. At the intersection of line SRS-13 with lines SRS-7, SRS-11 and SRS-3 occur time-structure highs.

Many of the local perturbations in time-structure demonstrably correspond to variations in the velocity field caused by overlying geology, i.e. velocity push-downs or pull-ups. This effect is accentuated by the small maximum source to receiver offset used to record the SRS data. Static anomalies caused by shallow velocity variations generally decrease with increasing time because, as time increases, the time anomaly is progressively averaged over a larger number of traces in the summing fold as governed by the mute pattern (Musgrove, 1994). With a short maximum recording offset, however, the smoothing effect applies to shallower sources of the velocity variation only; for deeper sources the static effect is present on all traces in a gather. The flattening of the thrust surface along SRS-4 near Upper Three Runs correlates with the velocity push-down observed in marker reflections in the Coastal Plain section. The coincidence of the steepening in time of the thrust surface with the trace of the Pen Branch fault at the top of crystalline basement suggests that the steepening results from velocity push-down related to the lower velocity fill of the Dunbarton basin compared to the higher velocity of crystalline basement.

The velocity push-down in time-structure suggests a method to recover the shape of the Dunbarton basin by isolating from the trend of the thrust a time residual that represents the seismic travel-time delay through the basin. Figure 32 was produced by subtracting from the time-structure map of the thrust (Figure 31) the time-structure map of the top of basement

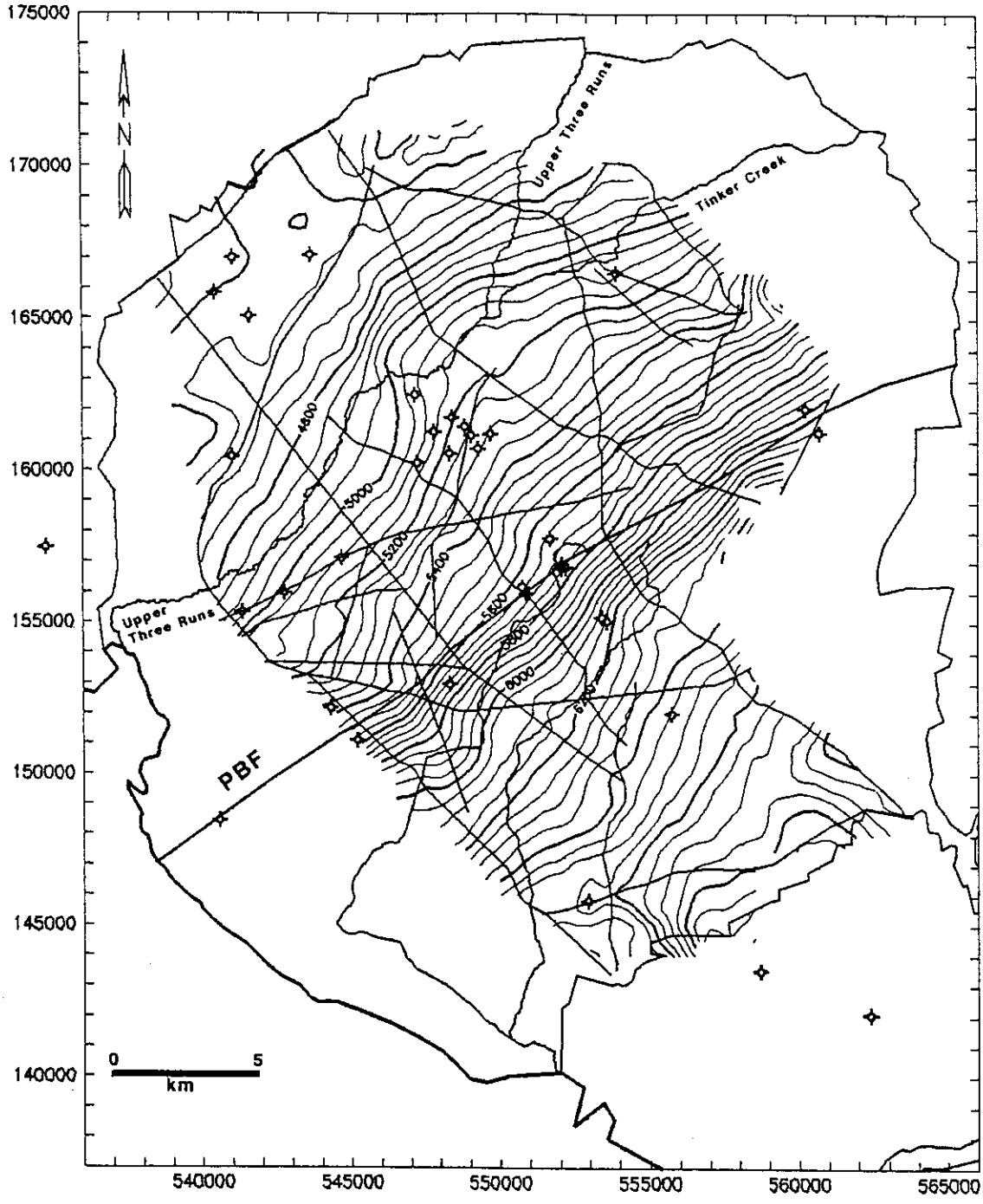

Figure 31. Time-structure map of the Midcrust reflection: Contour interval 50 ms. Grid interval 500 m. Reflection geometries indicate that this surface is a major midcrustal thrust; possibly correlative to an event in COCORP line 5 that is traceable for 160 km and interpreted to be the Appalachian master decollement. Map was produced from unmigrated seismic data. The trace of the Pen Branch fault (PBF) at the top of crystalline basement is plotted for reference.

(Figure 41) and subtracting from that difference a trend surface fit from Upper Three Runs-Tinker Creek to the trace of the Pen Branch fault at the top of basement. The subtraction of the top of basement time-structure map is performed to remove the velocity push-down effect of the Coastal plain sediments. The residual map is a time-delay structure map of the base of the Dunbarton basin under the assumptions that the dip of the thrust is constant under the basin and that the velocity field within and below the basin does not vary significantly.

The smooth gradient in the residual map (Figure 32) southeast of the trace of the Pen Branch fault indicates that the northwest boundary of the Dunbarton basin is abrupt and is defined by the Pen Branch fault zone. The time-delay associated with Pen Branch fault zone is consistently about 160 ms along its length, which further suggests that the northwestern boundary of the Dunbarton basin is structurally simple. In detail, residual time-structure profiles along seismic lines SRS-3 and SRS-7 show similar minor time variations that point to the existence of narrow fault-block slivers forming the basin border (Figure 33).

The time-residual map shows the basin to shallow to the southeast. Breaks in slope and enclosed lows in the time residual suggest the presence of intrabasinal fault blocks. The maximum push-down, defined from the trace of the Pen Branch fault, is 260 ms in the enclosed low along line SRS-3. Along the other seismic lines the maximum push-down is less than 200 ms. If the assumptions concerning the interpretation of this map are valid, then the deepest part of the Dunbarton basin within the map area is in the enclosed low along line SRS-3. Lending credibility to this interpretation are the Bouguer gravity data which show an enclosed gravity low at this location (Figure 16 on page 46).

The time residual low at the intersection of line SRS-1 with line SRS-8 corresponds to a nose of low Bouguer gravity values (Figure 16 on page 46) and probably represents local deepening of the basin in that area. The broadening of the time residual along line SRS-7 to the north of the intersection with line SRS-13 can be interpreted as less throw on intrabasinal faults as the basin widens to the southwest. In this area the Bouguer gravity contours also exhibit less relief.

The southern border of the basin is dominated by two positive time residuals at the intersection of line SRS-3 with line SRS-13 and at the conjunction of lines SRS-7, SRS-11, and SRS-13.

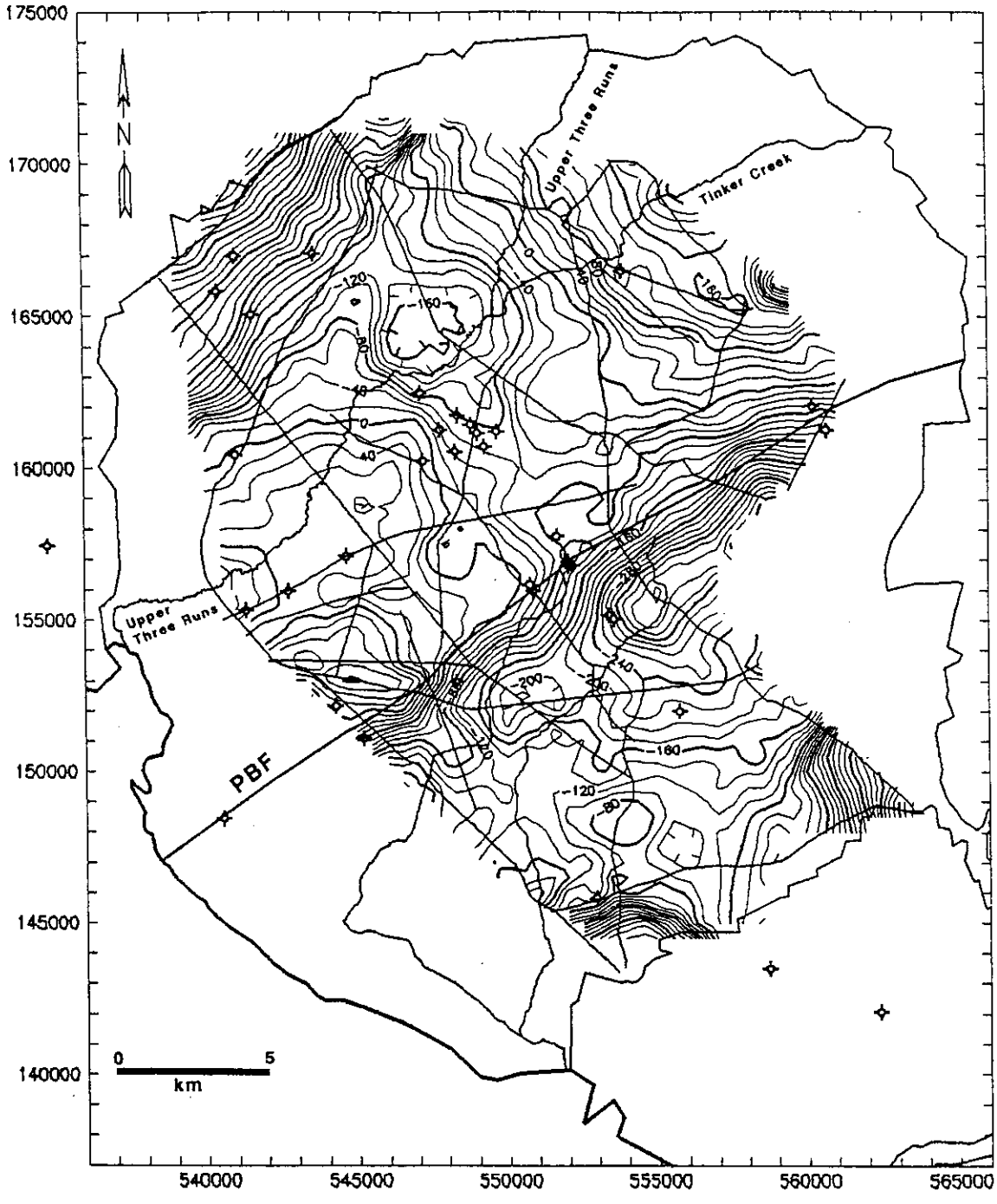

Figure 32. Residual of Midcrust reflection time-structure map: Contour interval 20 ms. Grid interval 500 m. Map was produced by subtracting the Basement time-structure map (Figure 41) from the time-structure map of the Midcrust reflection (Figure 31) and subtracting from that residual map a trend surface fit to that part of the residual map between Upper Three Runs and the trace of the Pen Branch fault (PBF) at the top of basement. South of PBF this map is a time-delay structure map of the base of the Dunbarton basin.

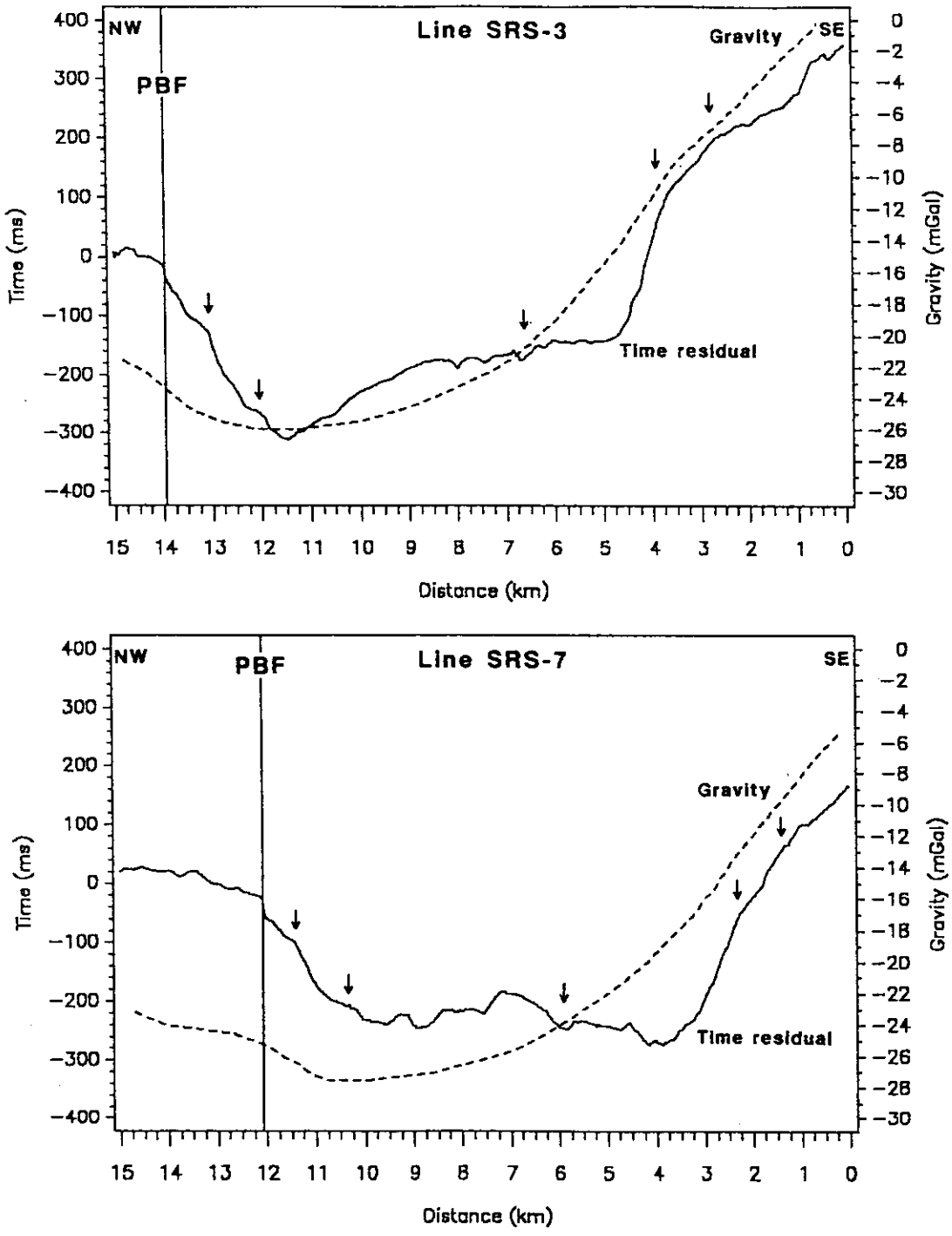

Figure 33. **Bouguer gravity and time residual profiles:** Bouguer gravity and Midcrust reflection time residual profiles along seismic lines SRS-3 and SRS-7. Some of the minor perturbations in the time residual are continuous along strike indicating possible intrabasinal faults (arrows). The close correspondence between gravity (density) and the time residual (velocity) suggests similar sources. This correspondence is especially noted for the south side of the basin where high Bouguer gravity and positive time residuals might relate to injection of mafic material related to rifting. PBF = Pen Branch fault.

Although intrabasinal faults are interpreted near where the dip reversal occurs (Figure 26 on page 68), the throw of these faults is interpreted to be less than the offset of the Pen Branch fault and therefore cannot account for the 0.3-0.4+ s of time-structure Two possibilities are presented: (1) the dip of the thrust flattens; (2) the velocity structure changes to produce velocity pull-up. In support of the former, the thrust does flatten in the northeastern part of the site and consideration of how duplexes form would require the thrust to flatten eventually downdip. That a change in velocity structure creates the positive time residuals is supported by the observation that the dip reversal in time-structure occurs where the seismic reflectivity of the basin fill increases. The increase in reflectivity might result from sill injection as previously proposed. The sill injection could increase in average velocity of the basin strata such that the velocity contrast between the basin strata and the crystalline basement is decreased, and lead to velocity pull-up of reflections within the basin. The Bouguer gravity field shows higher values corresponding to these areas and supports the hypothesis that higher velocity (denser) material is present above the thrust surface (Figure 33 and Figure 16 on page 46).

Augusta Fault Time-structure Map

The time-structure map of the Augusta fault shows the surface to generally dip to the southeast, although a strong secondary southwestward dip is apparent (Figure 34). A first order trend surface fit to the map north of the trace of the Pen Branch fault indicates that the surface strikes N52.8°E and dips 18.0° to the southeast. As expected, a gradient in time-structure occurs at the trace of the Pen Branch fault denoting velocity push-down related to the low velocity Dunbarton basin strata. Under the Dunbarton basin poor reflection signal prevents the interpretation of the fault all on the seismic lines, but it appears that the fault flattens. The fault surface also flattens northeast of line SRS-7 from the junctions with SRS-1 and SRS-4, SRS-9. An enclosed positive time anomaly occurs on seismic line SRS-11 and on part of seismic line SRS-13.

The southwestward dip on the Augusta fault, defined by the map area bounded by seismic line SRS-6 east to the juncture with line SRS-2 and south to the trace of the Pen Branch fault, is

strikingly similar to the gross features of the Bouguer gravity map that show decreasing gravity values in that area (Figure 16 on page 46). A qualitative interpretation is that the basement rocks above the Augusta fault are less dense than those below to give rise to the Bouguer gravity anomaly, i.e. the Augusta fault bounds lithologic units of differing physical properties. In field exposures north of SRS the Augusta fault bounds amphibolite grade metamorphic rocks of the Kiokee belt to the northwest from lower metamorphic grade greenschist rocks of the Belair belt to the southeast. The similarity between the Bouguer gravity map and the time-structure map of the August fault supports the suggestion that the Augusta fault is a major geologic boundary.

The parallelism between the trace of the Pen Branch fault and the time-structure contours of the Augusta fault indicates a syntectonic relationship between the two structures. Petersen and others (1984) interpreted the Augusta fault to have undergone backslip in extension during the Mesozoic to create the Magruder fault and the Riddleville basin. If a similar scenario applies to the Pen Branch fault and formation of the Dunbarton basin, it is likely that the trend of the Pen Branch fault would be similar to that of the Augusta fault; however, as previously noted, within the confines of SRS the Pen Branch fault does not sole into the Augusta fault. Thus, the relationship between the Pen Branch fault and the Augusta fault is less clear. Nevertheless, both basins are localized above ramps on the Augusta fault and are similar in cross-sectional form. The greater detail afforded by the SRS seismic data could account for any differences observed between the two locations.

The enclosed positive time anomaly on seismic lines SRS-11 and SRS-13 is in the same location as the positive time residual noted for the Midcrust reflection (Figure 32). This indicates that the velocity anomaly is located above the Augusta fault. In a preceding section it was noted that the increase in reflectivity in the basin, the positive time residual of the Midcrust reflection, and the gravity gradient on the south side of the basin were all coincident. These occurrences suggest that the velocity pull-up is caused by an increase in the average velocity of the Dunbarton basin fill.

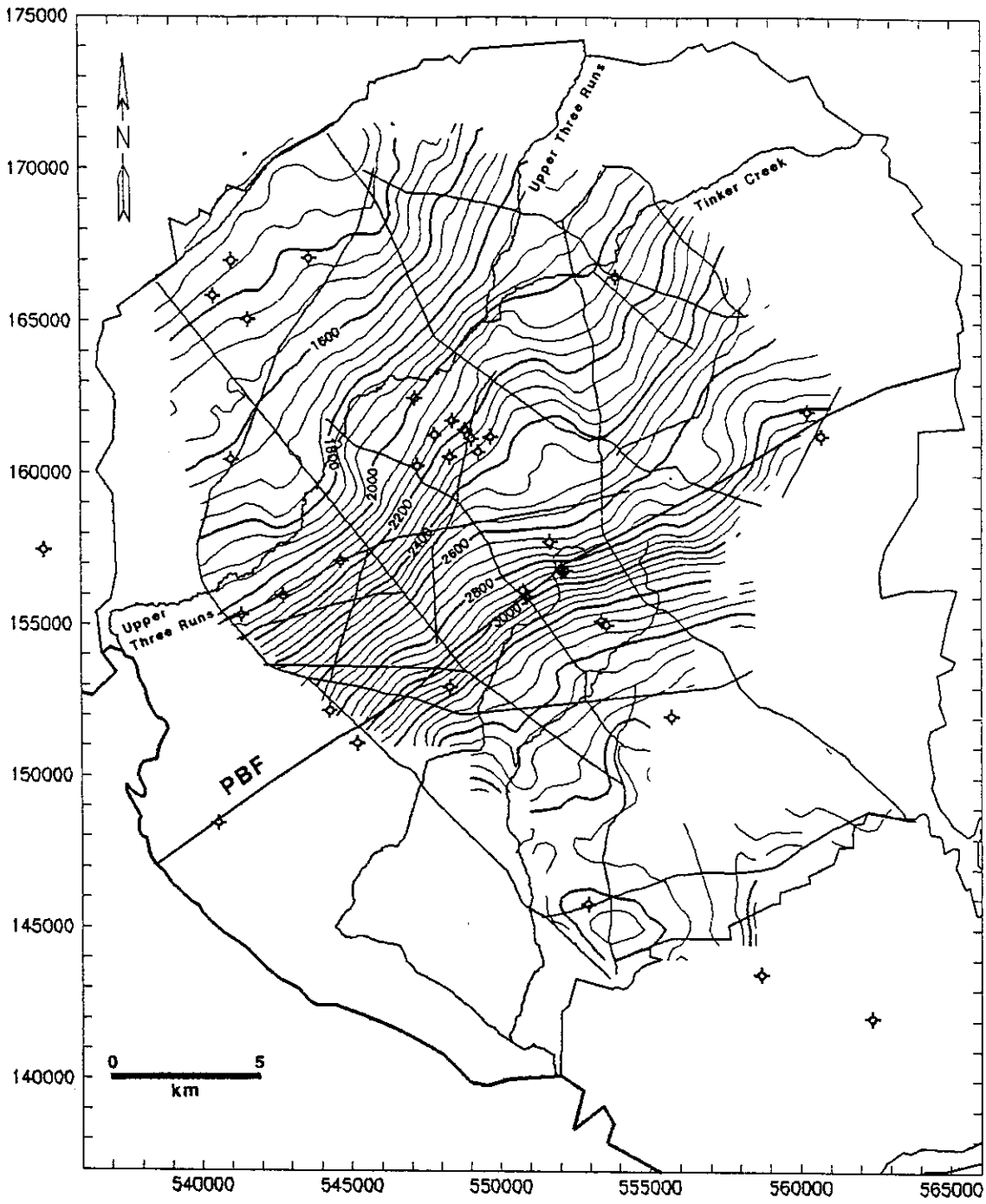

Figure 34. Time-structure map of the Augusta fault: Contour interval 50 ms. Grid interval 500 m. Map was produced from unmigrated seismic data. The trace of the Pen Branch fault (PBF) at the top of crystalline basement is plotted for reference.

Upper Three Runs Fault Time-structure Map

For purposes of time-structure map construction, the Upper Three Runs fault is defined as the southeastern boundary of the fan-shaped band of reflectivity in the northern third of SRS (Figure 22 on page 61). This event is correlatable line-to-line from just south of the trace of the Pen Branch fault to 1.0-3.0 km north of Upper Three Runs where it is truncated at the base of the Coastal Plain sediments. Under the Dunbarton basin the Upper Three Runs fault cannot be reliably mapped, but it appears to flatten and sole into the Augusta fault either beneath the basin or immediately to the south of SRS.

The fault surface trends N52.5°E and dips 30.6° SE (Figure 35). A slight component of southwestward dip is also noted in the same area where the southwestward dip on the Augusta fault occurs. In that area, the dip of the Augusta fault and the dip of the Upper Three Runs fault are nearly the same. This observation might lend support to the hypothesis that the Upper Three Runs fault was selectively reactivated over the Augusta fault during the Mesozoic extension that formed the Dunbarton basin.

Seismic Modelling

To investigate the effect of velocity push-down caused by the Dunbarton basin on deep time horizons, zero-offset normal incidence ray tracing seismic modelling was performed using the Advanced Interpretive Modelling System (AIMS) software by GeoQuest. The goals of the modelling were to find the depth of the Dunbarton basin necessary to reproduce the maximum amount of velocity push-down observed in the data and to determine the attitude of the Pen Branch fault below the Coastal Plain.

For simplicity, the Dunbarton basin was modelled as a half-graben basin bounded on the northwest by the Pen Branch fault. The Midcrust reflection and the Augusta fault were modelled as surfaces with dips of 16.5° and 24° respectively and a horizontal Moho was put in for a reference

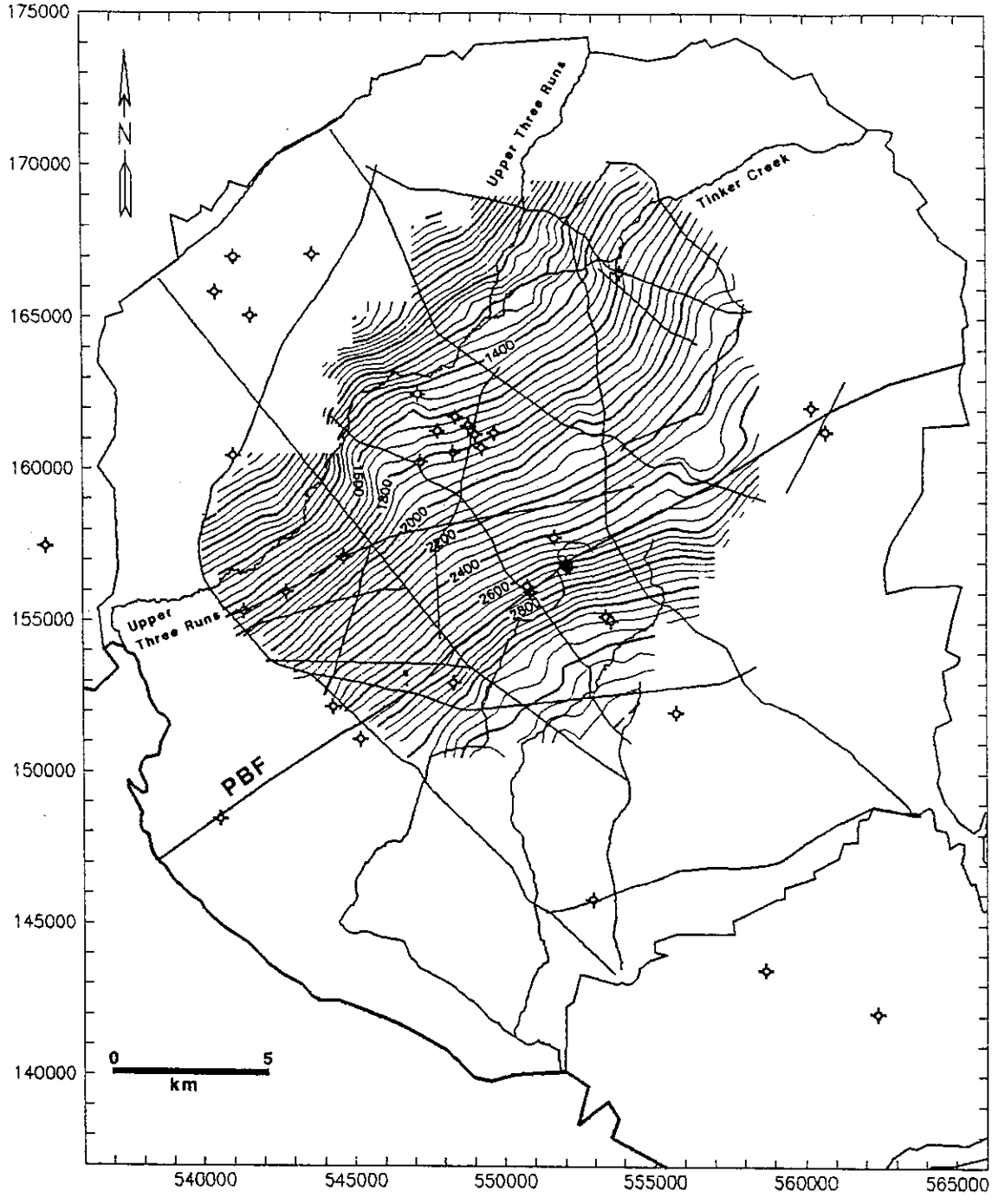

Figure 35. Time-structure map of the Upper Three Runs fault: Contour interval 50 ms. Grid interval 500 m. The reflection event is truncated at the base of the of Coastal Plain sediments north of Upper Three Runs and cannot be reliably followed more than 2-3 km beneath the Dunbarton basin. Map was produced from unmigrated seismic data. The trace of the Pen Branch fault (PBF) at the top of crystalline basement is plotted for reference.

horizon (Figure 36). The velocity of the basin fill was fixed at 5.40 km/s, adapted from the velocity profile of the DRB-10 borehole (Figure 4 on page 15). The velocity of the crystalline basement was 6.35 km/s, based on an average of seismic refraction velocity values for the mid- and upper crust from the USGS seismic refraction profile (Luetgert et al., 1994). The deep interfaces were placed so that the model time-section would mimic the observed average reflection time to the interfaces for a profile 25 km long centered on, and normal to, the Pen Branch fault. The dip of the Pen Branch fault and the thickness of the Dunbarton basin were varied in successive models.

The seismic model (Figure 37) reproduces the salient characteristics of the field data. Of particular note is the contribution of the Atlantic Coastal Plain sediments to the velocity push-down observed in deeper time horizons; in effect, the Coastal Plain imprints a regional time push-down that must be accounted for in the interpretation of these data. Thus, from a simple model such as Figure 37 the interpretation of deep reflections is not straight forward; the interpreted geometry of any reflector must include removal of the push-down effect. The observed warping of the reflection Moho, previously commented upon, might in large part be caused by these effects. The model also reproduces the increase in amplitude noted in deep reflections at the edge of the push-down at the Pen Branch fault and examination of the ray tracing model demonstrates that the amplitude increase is caused by the focusing of rays at this boundary (Figure 38).

To ascertain the dip of the Pen Branch fault beneath the Coastal Plain sedimentary cover, the shape of the flank of the push-down from the model was compared to the shape of the the push-down observed on the Midcrust reflection on line SRS-3 (Appendix B) for various angles of fault dip. The results from the modelling indicate that the Pen Branch fault is nearly vertical where it is the boundary between Triassic and crystalline basement (Figure 39). It should be noted that the shape of the velocity push-down varies as per the dip of the interface such that a shallower or steeper dip assigned to the Midcrust reflection would require altering the dip angle of the Pen Branch fault to achieve a match to the field data. Furthermore, the dip of the Pen Branch fault within the crystalline basement cannot be determined with this method.

The model results also indicate that the depth of the basin fill is between 4.0-5.0 km, which supports the interpretation of the seismic reflection data presented earlier. If the average velocity

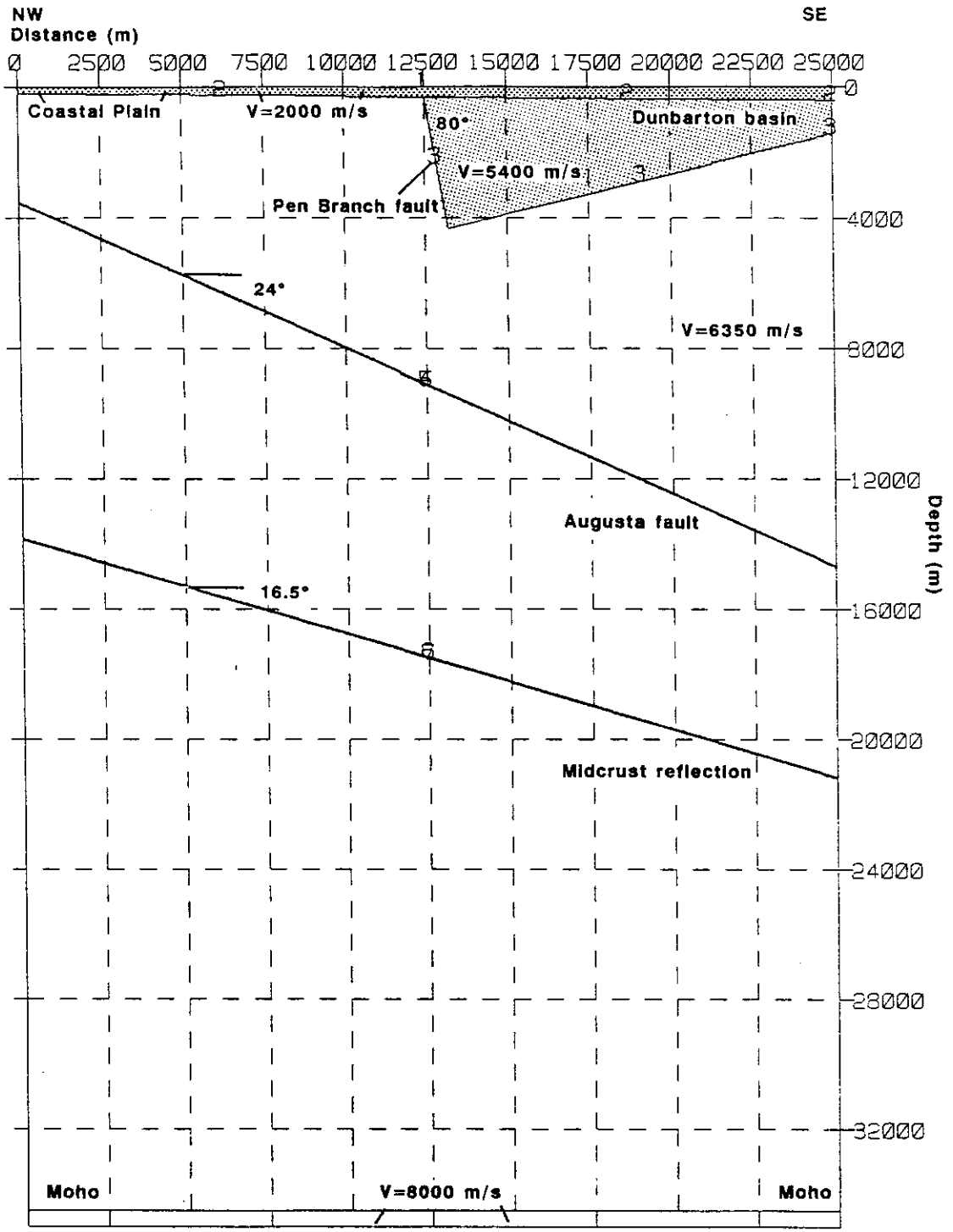

Figure 36. **Depth model used for seismic modelling:** The model is designed to represent a 25 km long cross-section centered on and perpendicular to the Pen Branch fault. The model velocities are adapted from borehole and seismic refraction measurements.

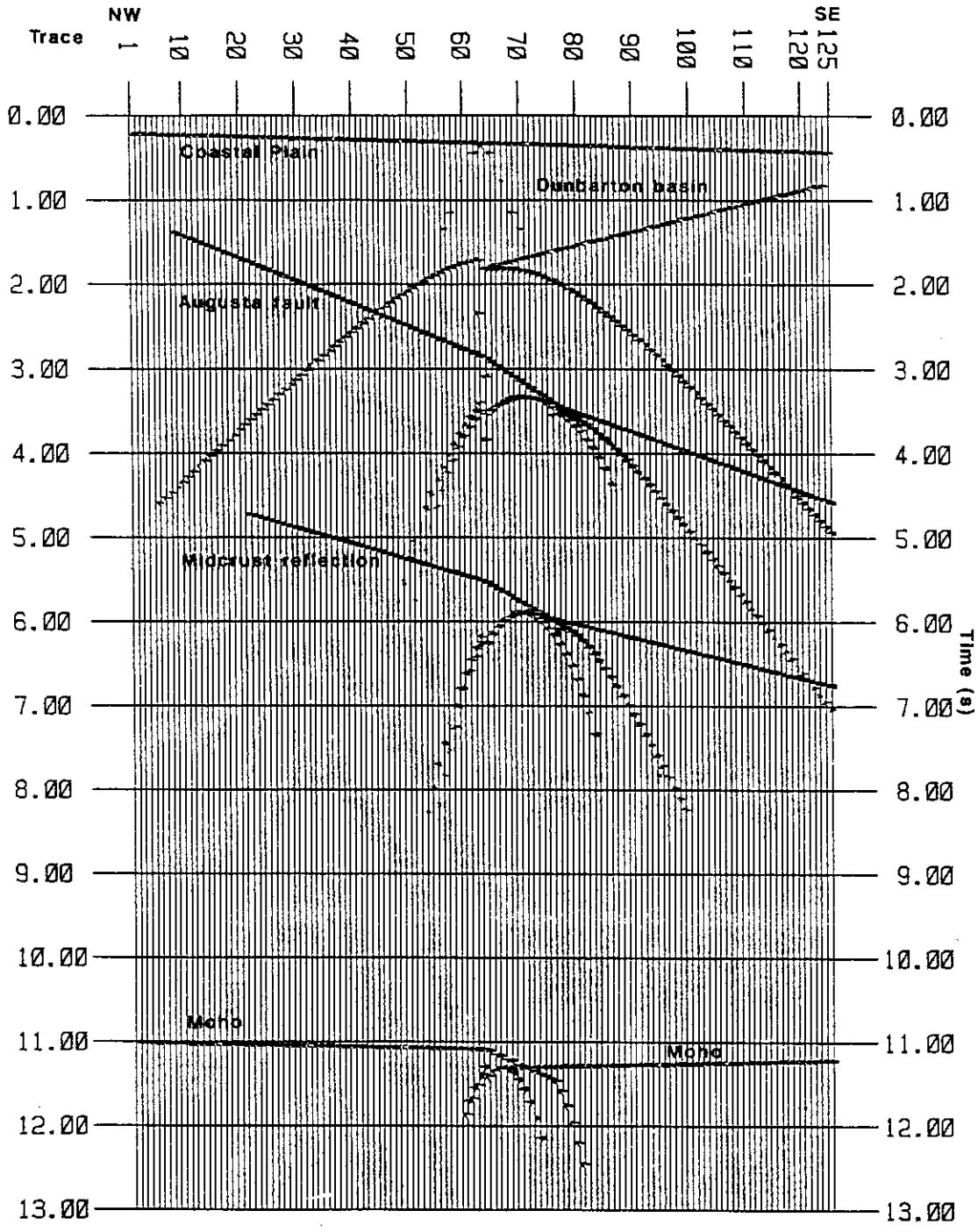

Figure 37. Seismic time model: Result of zero-offset normal incident ray tracing seismic modelling using depth model of Figure 36. Trace interval is 200 m. Reflection coefficients are convolved with a 20 Hz Ricker wavelet. Geometric spreading and transmission effects have been neglected. Note the velocity push-down effects caused by the Coastal plain sediments and the Dunbarton basin. The shape of the velocity push-down associated with the Dunbarton basin partly depends on the dip of the subsurface interfaces.

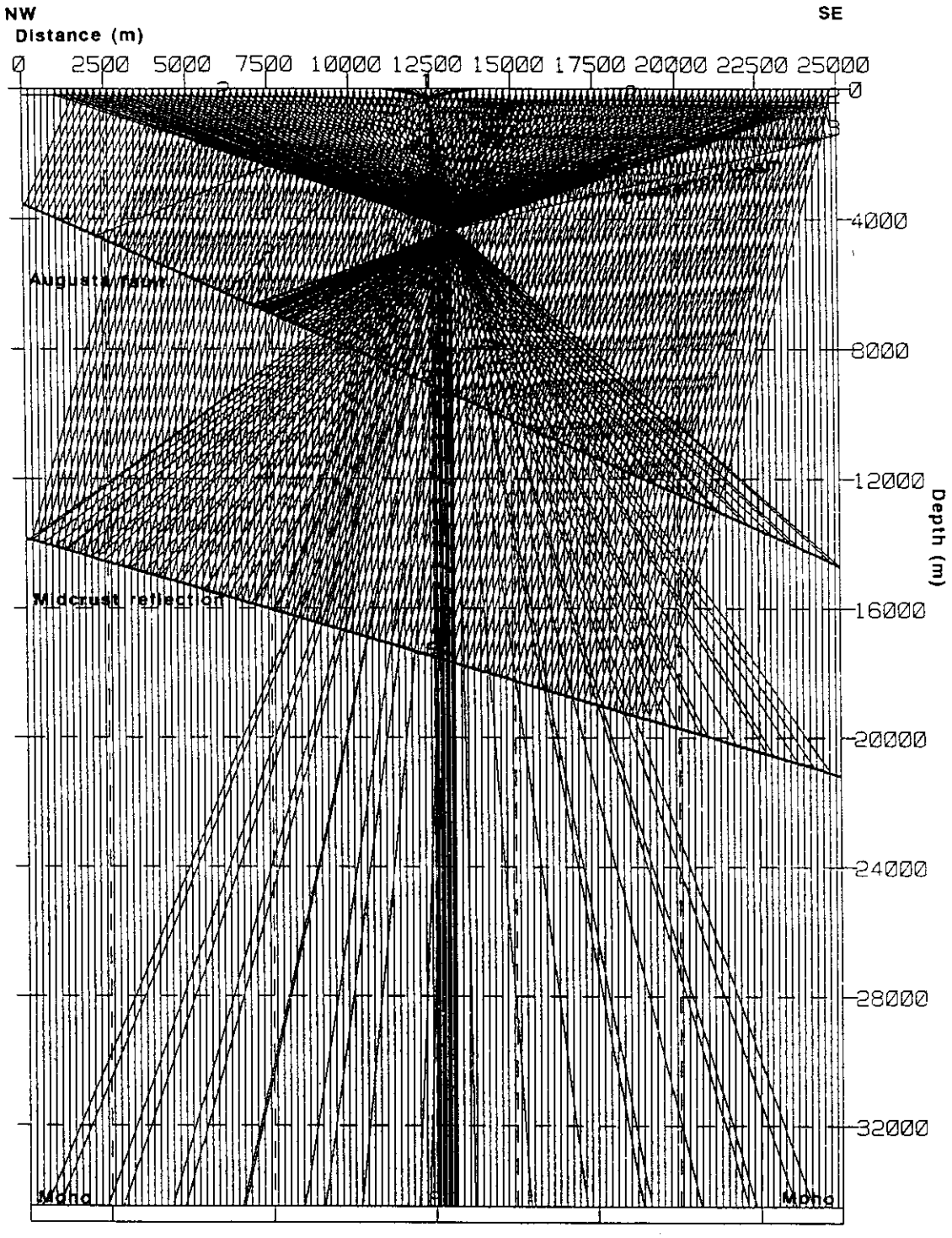

Figure 38. Seismic rays traced: Normally incident rays traced to produce seismic time model of Figure 37. Refraction of rays through the edge of the basin produces a focusing effect noted in the time model (Figure 37).

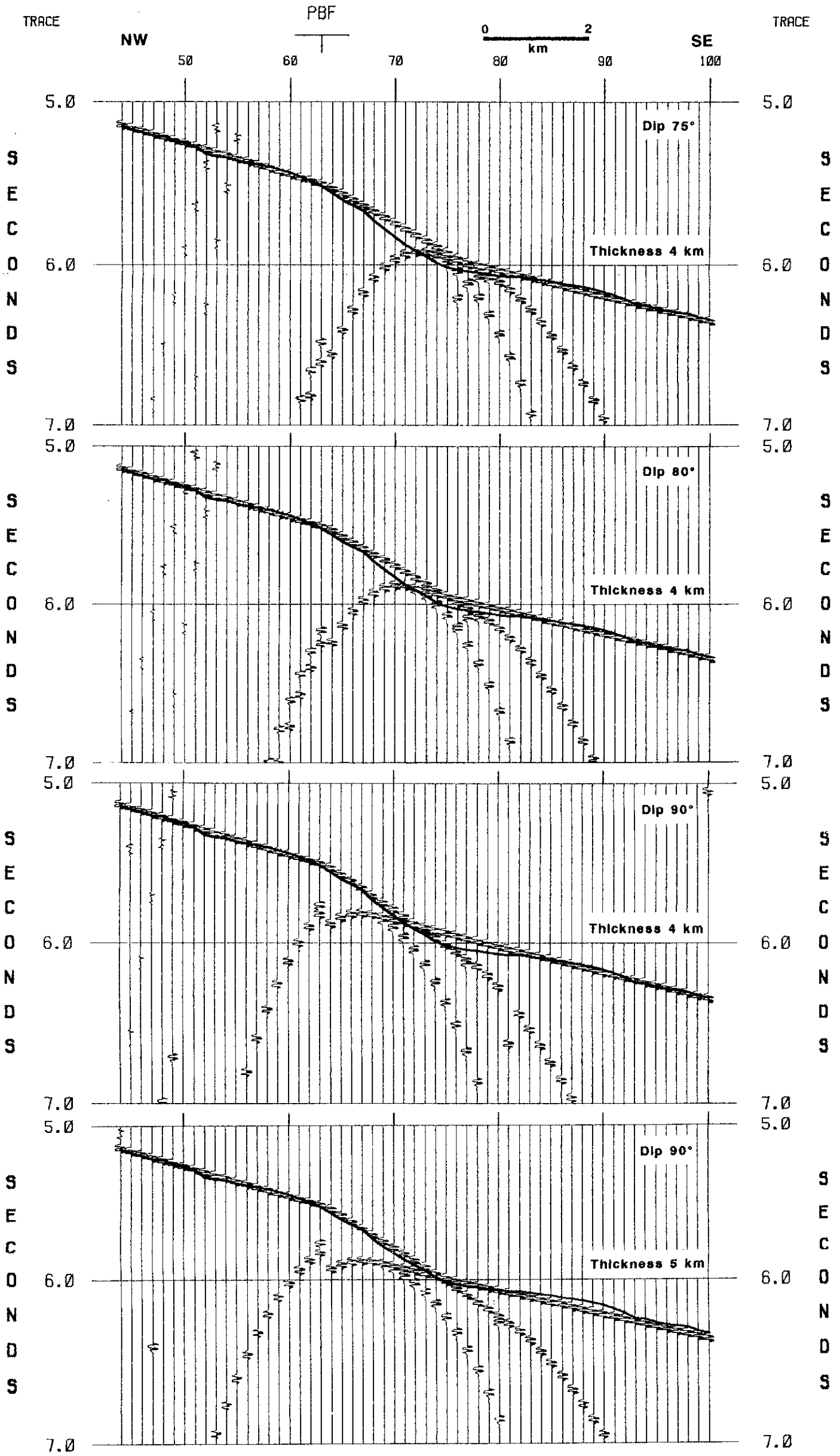

Figure 39. **Determination of dip of the Pen Branch fault:** Comparison between velocity push-down observed on seismic line SRS-3 (solid line) and modelled results for varying dip of the Pen Branch fault (PBF). A -310 ms bulk shift was applied to the digitized values on line SRS-3 to match the time-model. The models indicate that the dip of the Pen Branch fault is near vertical and that the maximum thickness of Triassic strata in the Dunbarton basin is 4-5 km.

contrast is larger than in the model, then the basin would be shallower; however, the velocity profile of the DRB-10 borehole indicates that the velocity of the basin fill rapidly approaches values similar to the crystalline rock, which would require a deeper basin to account for the observed amount of push-down. The 4.0 km value is deeper than depth estimates previously determined for the Dunbarton basin from gravity (1.4-1.6 km; Marine, 1974; Anderson, 1990), magnetic (1.0 km; Daniels et al., 1983), and transient electromagnetic (1.8+ km; Price et al., 1989) data.

Shallow Data Set

The interpretation of the shallow SRS seismic reflection data set entailed the construction of time-structure, isochron and reflection amplitude maps, as well as trend surface analysis, correlation analysis between time-structure with topography, and correlation of synthetic seismograms to various seismic profiles followed by depth conversion of the digitized interpretations.

General Data Observations

Stratigraphic identification of specific reflection horizons is dubious at best given the fact that previous workers have not been able to tie synthetic seismograms to seismic reflection data at SRS (see discussions by Chapman and DiStefano, 1989; Berkman, 1991) and the ongoing revision of Coastal Plain stratigraphy. Furthermore, the two sets of formation tops available for use in this study are in conflict and do not consistently correspond to the same geophysical signatures seen on either sonic logs or seismic reflection data. This suggests that the formation tops are in error or that the seismic reflection markers do not necessarily represent formation boundaries or unconformities. Further work to resolve this issue is warranted. In this study the mapped reflections are assumed to represent time-stratigraphic boundaries.

The seismic reflection data of the shallow data set were interpreted prior to correlation with the synthetic seismograms. Three reflection events were found to be mappable throughout SRS. These time horizons are designated (1) Basement, (2) Blue Marker, and (3) Yellow Marker, and were later found to correspond to (1) the top of unweathered basement rock, (2) the top of the Middendorf Formation, and (3) the top of the Peedee Formation respectively. For the latter two markers the actual reflection traced was the wavelet trough above the reflection peak that usually denotes these boundaries. Therefore, the time horizons mapped are actually in the basal Black Creek Formation and basal Ellenton Formation for the Blue Marker and Yellow Marker respectively.

Two other reflecting horizons are locally mappable in the site area. These horizons occur at the top of the Cape Fear Formation, called the Green Marker, and within the middle Black Creek Formation, called the Orange Marker. The Green Marker is difficult to follow north of Upper Three Runs where it merges with reflections that are found approximately 20 ms above the Basement reflection. The Orange Marker typically disappears 3-4 km north of the Pen Branch fault.

Reflections from the Basement, Blue Marker (the top of the Middendorf Formation) and Yellow Marker (the top of the Peedee Formation) can to be tied with some certainty from line to line within the SRS vibroseis data set. On those seismic lines that do not intersect other lines, jump correlation between adjacent profiles was guided by matching reflection character and preserving isochron times along strike. North of Upper Three Runs-Tinker Creek all reflections within the Coastal Plain sediments tend to become less distinct and reflection identification, except for the Basement reflection, is less reliable. This effect probably results not only from stratigraphic thinning updip, but also decreasing CDP fold as the time to the various horizons lessens. Reflection horizon ties to the PBF series lines are somewhat imprecise owing to the different seismic source used and the higher frequency content compared to the SRS data. Low-pass filtering of the PBF lines and matching both reflection character and isochron times minimized this problem. At most, reflection misties of a half a cycle might be expected.

The identification of faults is based on time offset of reflections and is almost exclusively restricted to offsets that originate in the basement and penetrate upward into the Coastal Plain

sediments. Excluded from this definition are those faults that result from depositional loading and are not demonstrably related to basement faulting. Recent high resolution seismic reflection profiling at SRS has identified many shallow faults confined to the Tertiary section (M. Waddell, ESRI, 1995, personal communication); however, because the recording parameters of the SRS Conoco seismic lines were optimized to image the deeper section, many of these faults are poorly resolved and cannot be reliably interpreted. The identification of basement faults is not always unambiguous; small time offsets and fault planes oblique to the line of profile complicate the issue. Furthermore, some faults of considerable offset are detected on only one or two profiles; thus, the orientation of these structures is subjective. Minor static busts can imitate the appearance of faults and can lead to the misinterpretation of the sense of fault movement (Appendix A). Forced folding or drape folding (Stearns, 1978) of sediments over a basement fault is not mapped as a fault penetrating to the level of the folding regardless of the radius of curvature of the folding. That is, deformation by faulting (offset) is distinguished from deformation by folding; however, the amplitude of such folding is used to determine rates of fault movement in addition to offset.

It must be emphasized that if a particular time horizon is not observed to be offset by a fault, it does not preclude the possibility that the reflector is offset in depth. The statement of whether or not a time horizon is faulted must be qualified as to whether or not such an offset is within the resolution limit of the data. Generally, the resolution of two events separated by greater than an eighth or quarter wavelength is possible (Sheriff, 1977). Therefore, for the SRS data, given an average dominant frequency of 50 Hz, and an average velocity of the Coastal Plain sediments of 2000 m/s, the vertical resolution limit is 5-10 m. That is, faults of less than 5 m throw are unlikely to be detected with these data and basement-related faulting undoubtedly penetrates higher into the Coastal Plain sediments than what can be interpreted from these data.

A further caution with regard to the interpretation of these data arises from the use of a single velocity for the datum static correction. In some instances reflection geometry mimics topography either in a direct or inverse sense indicating that the datum correction velocity was either too low or too high. This long wavelength static anomaly is easily discernible on highly compressed horizontal scale seismic sections. Simple poststack time horizon flattening can yield a more interpretable

section; however, the problem can be treated adequately only prestack (Sen, 1991; Pickard, 1992). Where highly localized near surface velocity variations exist a static anomaly is created that in stacked data broadens in width and decreases in amplitude with increasing time (Musgrove, 1994). An example of this effect is illustrated in Figure 40 for a part of line SRS-9 recorded over Upper Three Runs. For this type of static anomaly artificial flattening of time horizons to remove the effect of near surface velocity variation can lead to the interpretation of false time-structure.

Time-Structure Maps - Shallow Data Set

Time-structure Map Construction: The three reflection horizons were hand-digitized from paper seismic sections at an average of one point per four traces, linearly interpolated between traces, and written into the seismic trace headers that contain the X-Y positioning information. Inasmuch as the SRS seismic lines were surveyed referenced to South Carolina state plane coordinates, this geographic base was used to produce all the maps in this study. All geographic locations were converted to the South Carolina state grid (North America Datum 1983) using the computer program CORPSCON developed by the U. S. Army Engineer Topographic Laboratories.

Time-structure maps were produced using the Surface III mapping package by Interactive Concepts, Inc. (Sampson, 1988). For data management and run-time considerations the digital data were decimated one in two before gridding thereby reducing the number of data points for a given horizon to approximately 18,000. The gridding procedure utilized an inverse distance squared weighted algorithm with an octant search pattern to minimize bias caused by the closely spaced data points along the seismic lines. Grid points were computed every 200 m and the maps were contoured at 5 ms (2.5 time samples) intervals. In two areas, between lines SRS-11, SRS-13 and between lines SRS-9, SRS-4, a few grid nodes did not satisfy the the grid operator requirements. In each of these areas it was only necessary to insert three synthetic data points, determined by projecting trends from nearby seismic lines, for adequate control before the were regridded.

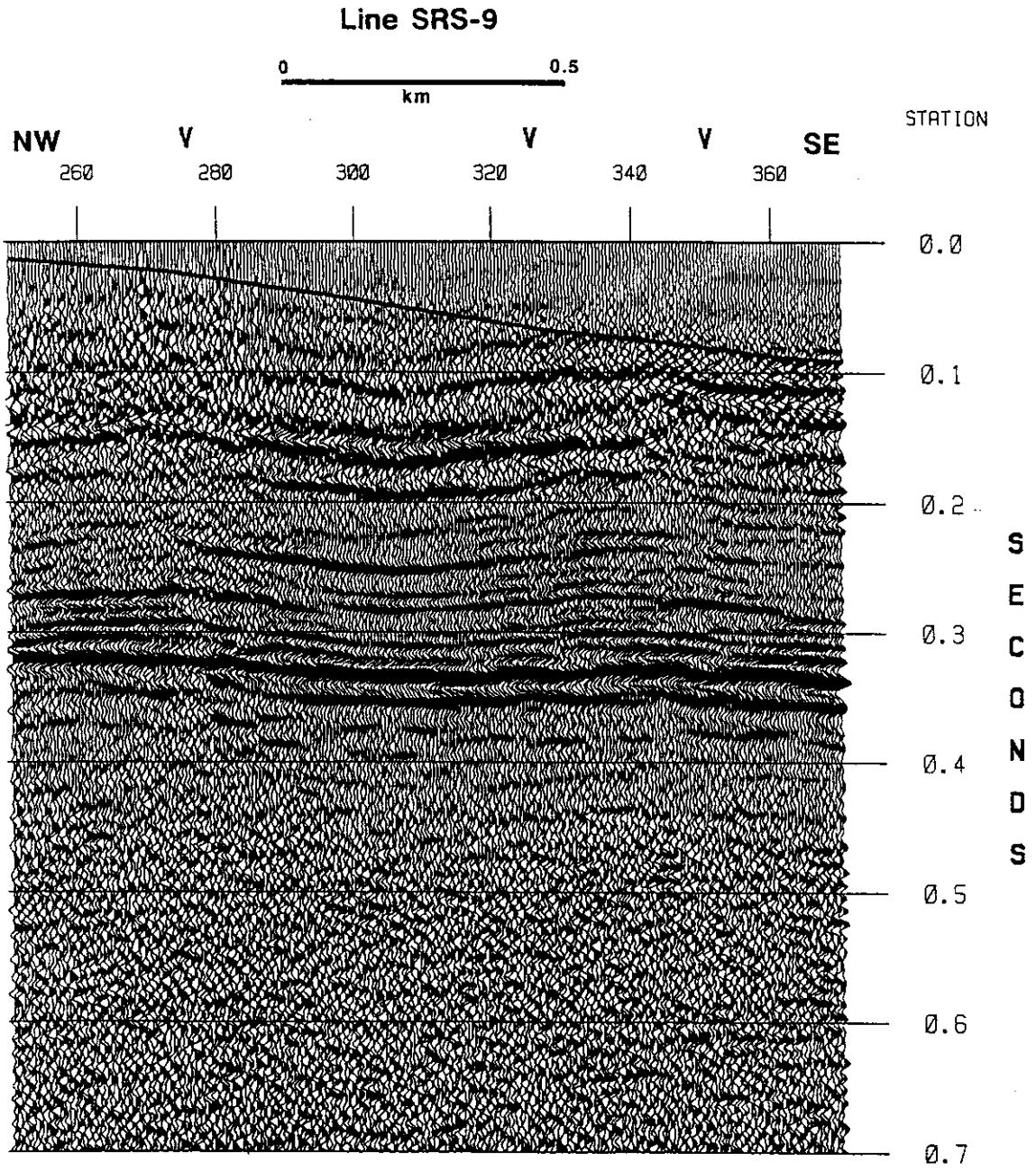

Figure 40. Static anomaly line SRS-9: The velocity pushdown encountered from stations 280 to 320 broadens in width and decreases in amplitude with increasing time. This effect is a consequence of the effective spread length governed by the mute pattern. This type of pushdown should not be eliminated by simple poststack time horizon flattening.

The gridding and contouring intervals were chosen empirically to represent a balance between loss of map detail and spatial aliasing of structural features. Along the edges of the time-structure maps, and in regions removed from the seismic line control, the gridding occasionally generated contours that are unsupported by the data. Furthermore, the Surface III mapping package does not allow contouring of across faults; thus, the time-structure maps are smoothed across faulted areas. In short, the computer generated maps have inherent limitations and caution must be exercised in the interpretation of these data in areas far removed from the seismic lines.

Basement Time-structure Map

The reflection from the top of unweathered basement is the most prominent event on all the seismic lines from the SRS vibroseis data set and can readily be correlated line to line with little difficulty (e.g. Figure 44 on page 104). Where the reflection is from crystalline basement the wavelet is characteristically a sharp, well defined peak with well developed sidelobes. The amplitude of the reflection exhibits local variations that could indicate basement lithology changes, fracturing/faulting, or differing thicknesses of the saprolite layer. Over Triassic basement the reflection is weaker and locally becomes discontinuous. In these areas the angular unconformity between the dipping Triassic sediments and the overlying subhorizontal Coastal Plain sediments is often clearly imaged.

On the PBF seismic lines the Basement reflection is usually less clear and the time picks are less reliable (e.g. Figure 68 on page 146). Neither line PBF-18 nor line PBF-6 intersects any of the SRS seismic lines and identification of the Basement reflection is based on reflection amplitude, jump correlation from nearby SRS seismic lines, and geometric relationships between reflections occurring earlier and later in the time section.

The Basement reflection time-structure map and fault map (Figure 41 and Figure 42) show three distinct divisions delineated by changes in basement slope bounded by Upper Three Runs-Tinker Creek and the Pen Branch fault. These divisions, marked by similar slopes of the reflection surface in the upper and lower divisions of the map and much lower slope for the middle division,

are the same remarked upon by Chapman and DiStefano (1989) in the interpretation of the original processed SRS data set.

In contrast to the basement time-structure map produced by the interpretation of the original processed SRS seismic lines (Figure 43), more detail is present in the time-structure map produced from the reprocessed seismic data - especially in numbers of faults detected and mapped. Most of these newly mapped faults offset the Basement reflection less than 10 m (10 ms two-way time) and do not penetrate far upward into the sedimentary cover (see succeeding maps). The map of Figure 42 should be regarded as something of a minimum with regard to detection of basement faults; higher resolution techniques would undoubtedly lead to the discovery of more faults.

Most of the faults are interpreted to trend northeast-southwest subparallel to the trend of the Pen Branch fault. Generally, faults northwest of the Pen Branch fault are down-to-the-northwest whereas faults southeast of the Pen Branch fault are down-to-the-southeast. All of the faults are high-angle faults within the Atlantic Coastal Plain sediments; thus, the determination of the sense of fault movement, i.e. normal or reverse, is difficult. Of those faults where sense of the fault movement can be determined, only reverse faults have been found. None of the mapped faults can conclusively be termed a normal fault. Typically, the faults can be paired, where a down-to-the-northwest fault is paired with a down-to-the-southeast fault to form a discrete fault block, although often one of the faults of the pair exhibits much less throw (antithetic fault?) than the other (Figure 44).

One of the faults mapped at the top of basement is interpreted to reverse its sense of throw from west to east across the site. This fault, herein named the C Line fault, trends northwest-southeast and joins the Pen Branch fault. From west to east across SRS the throw of the fault increases and the sense of movement changes from down-to-the-northeast to down-to-the-southwest. This fault appears paired with a northeast trending fault parallel to Upper Three Runs, herein named the Tinker Creek fault. The Tinker Creek fault also increases in throw toward the northeast, which suggests that the block bounded by these faults has undergone a tilt up to the northeast; that is, rotation has accompanied faulting.

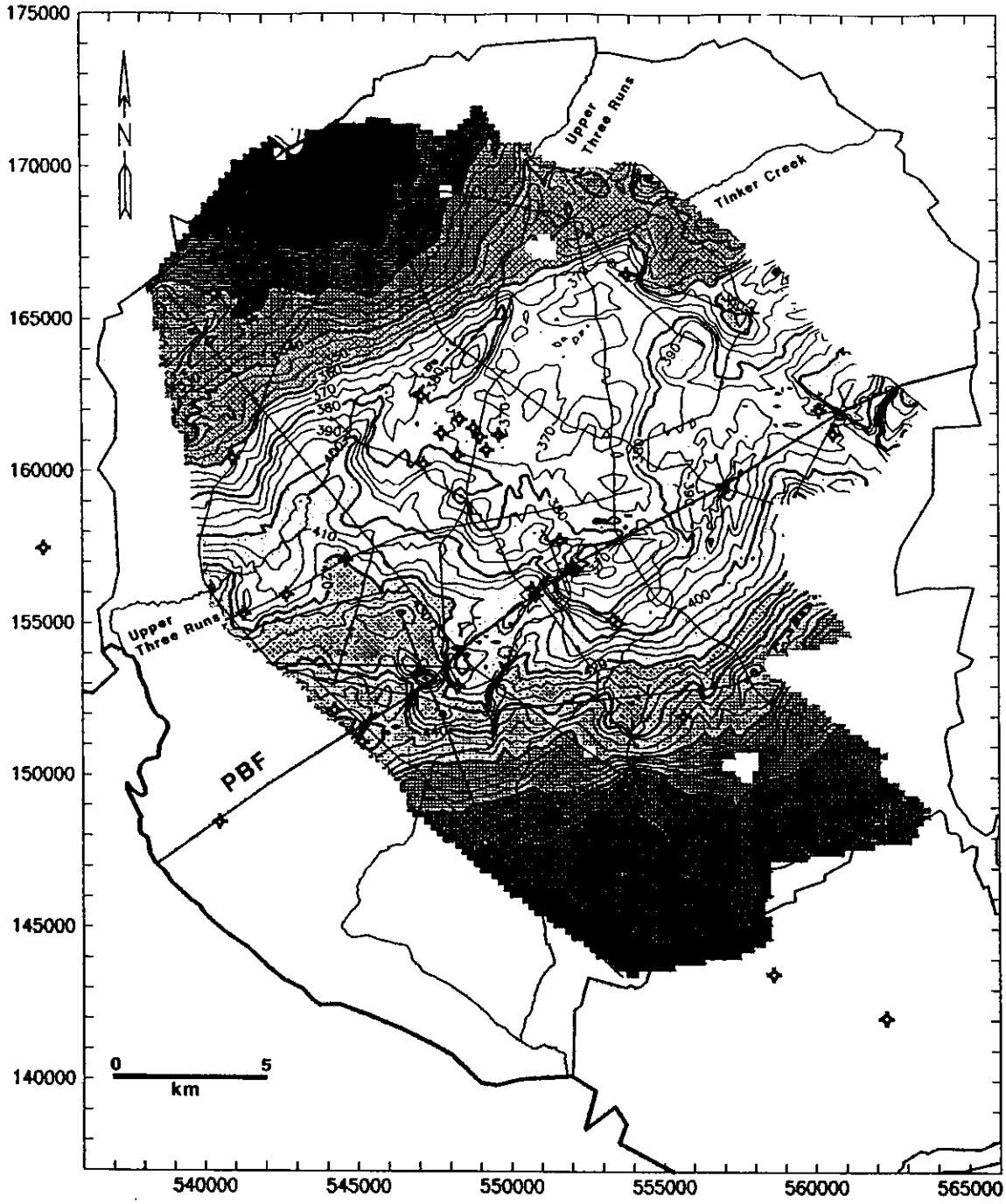

Figure 41. Time-structure map of Basement reflection: Contour interval 5 ms. Grid interval 200 m.

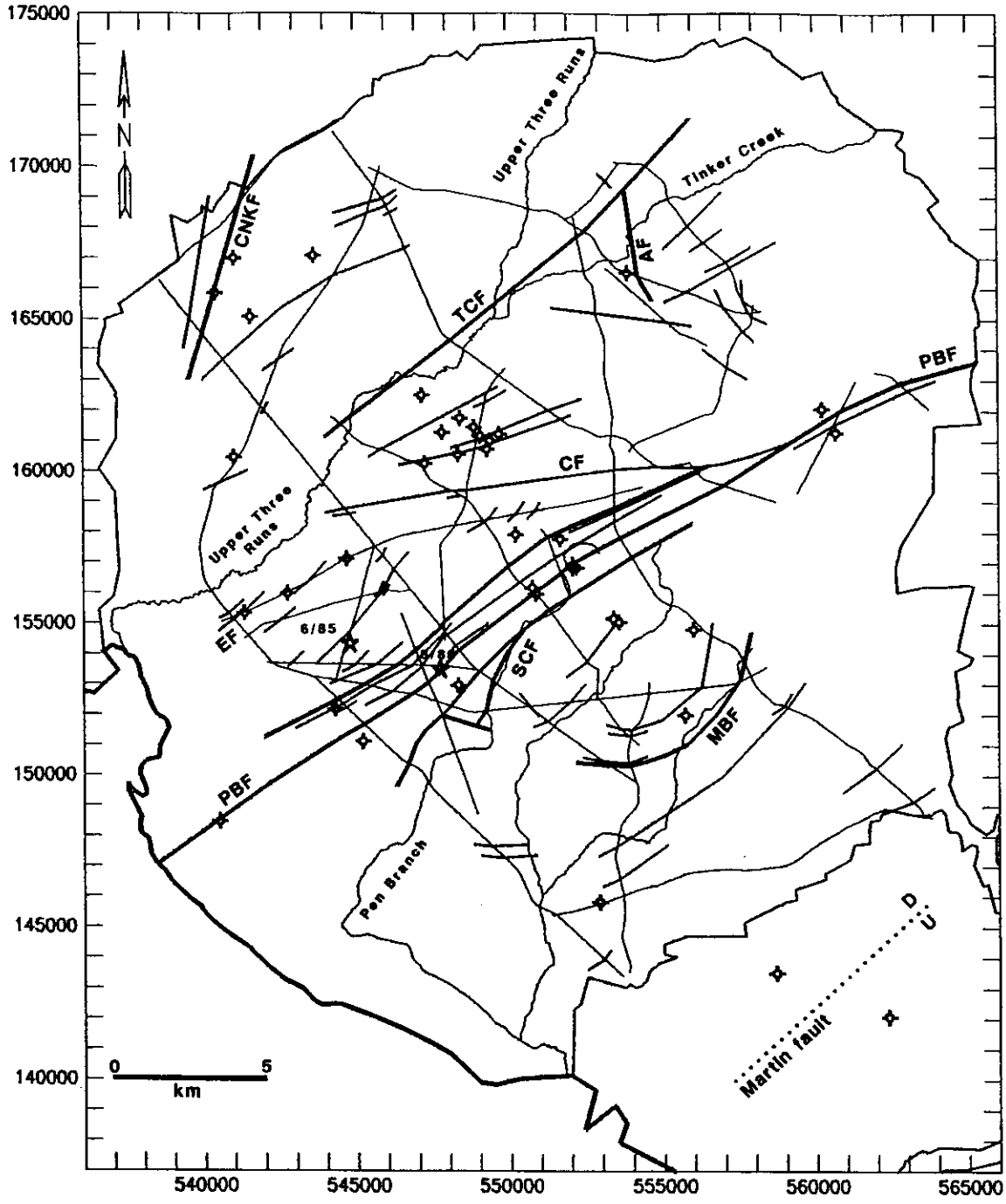

Figure 42. Basement fault map: Faults that offset the Basement reflection are shown. Faults that are down-to-the-northwest are indicated in orange and faults that are down-to-the-southeast are indicated in green. Faults with time offsets greater than 15 ms anywhere along the fault trace are denoted by thicker lines. PBF = Pen Branch fault, TCF = Tinker Creek fault, SCF = Steel Creek fault, MBF = Meyers Branch fault, AF = Atta fault, CNKF = Crackerneck fault, EF = Ellenton fault, CF = C Line fault.

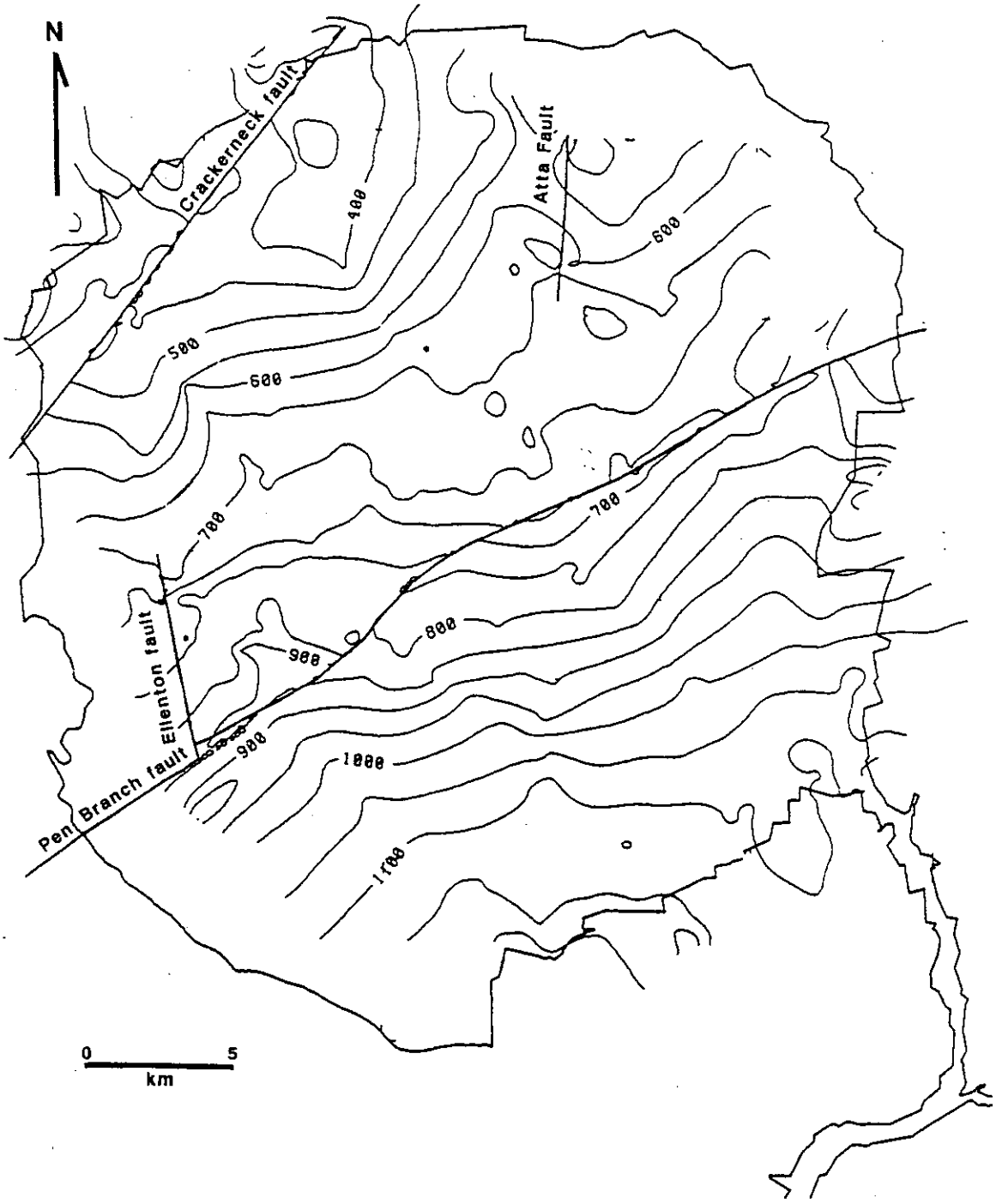

Figure 43. Basement fault map from Chapman and DiStefano (1989): Structural contour map of the pre-Cretaceous surface based on interpretation of the original processed Conoco SRS seismic reflection data. Contour interval 50 ft.

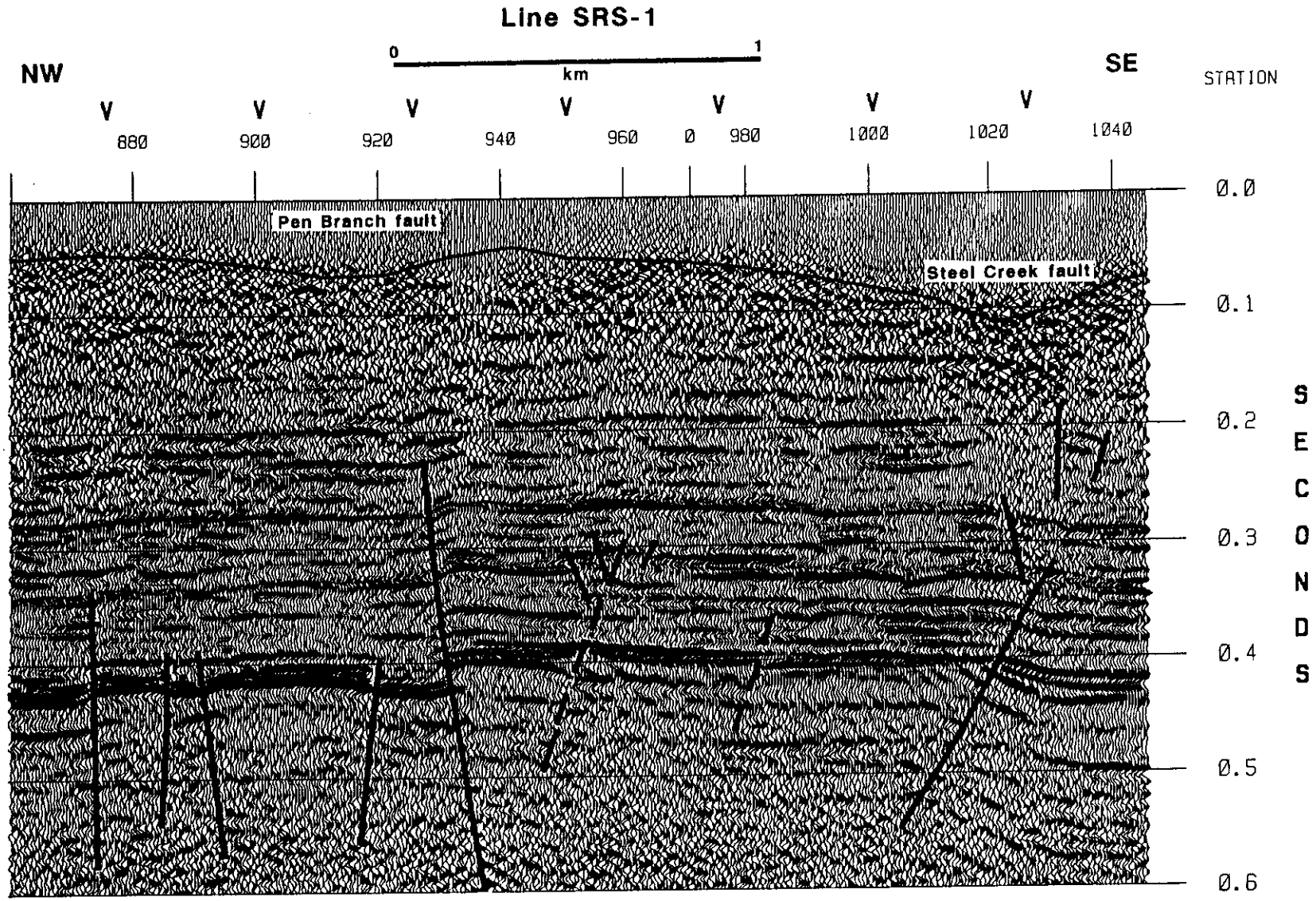

Figure 44. Fault blocks: Seismic line SRS-1. Pen Branch fault zone. Down-to-the-northwest faults are paired with down-to-the-southeast faults to form discrete fault blocks. The Pen Branch fault and the Steel Creek fault define a small pop-up block.

No unambiguous evidence of translation is seen on any of the faults mapped, although many faults in cross section exhibit the characteristics of flower structures. Such criteria for strike-slip faulting as differing seismic reflection character and differing time thicknesses on either side of a fault are present throughout the dataset, but can also be explained as resulting from the variable lithology of the Coastal Plain sediments and growth faulting (Harding, 1990). Nevertheless, strike-slip faulting would be consistent with the focal plane mechanism of the 1985 SRS earthquake (Talwani et al., 1985).

The most dominant structural feature at this map horizon is the Pen Branch and related faults that comprise a fault zone at least 3 km wide, herein named the Pen Branch fault zone (PBFZ). The Pen Branch fault is the main through-going fault in the PBFZ. Offset on the Pen Branch fault is down-to-the northwest and increases to the northeast along the fault. Nowhere does the trace of the fault at the top of basement level appear to be offset, contrary to earlier interpretations (Chapman and DiStefano, 1989; Anderson, 1990). Furthermore, unlike the Belair fault described by Prowell and O'Connor (1978) and Bramlett and others (1982) near Augusta, Georgia, the Pen Branch fault is not comprised of *en echelon* fault segments, but is a single fault within the PBFZ. Faults of much less throw occur subparallel to the Pen Branch fault. Northwest of the Pen Branch fault these faults occur in paired bands of down-to-the-northwest and down-to-the-southeast faults where the down-to-the-northwest fault typically exhibits greater offset and mappable extent. Southeast of the Pen Branch fault (i.e. away from the border fault) the faults in the PBFZ are fewer in number, down-to-the-southeast, and posses lesser throw than the faults northwest of the Pen Branch fault. An exception is the Steel Creek fault, as imaged on seismic lines SRS-1 (Figure 44) and SRS-8 (stations 540-585, Appendix B), where the time-offset of the Basement reflection is greater than 15 ms.

The faults mapped where Triassic basement underlies the Coastal plain sediments are mostly down-to-the-southeast. One of these faults, herein named the Meyers Branch fault (MBF in Figure 42; see also Figure 84 on page 171), appears to involve greater than 70 m (70 ms two-way time) displacement of the basement surface. Most of that displacement, however, is not expressed

as offset along a discrete fault, but rather as the amplitude of the basement warp bounded by the fault.

The division in time-structure defined by Upper Three Runs-Tinker Creek is partly delineated by the Tinker Creek fault previously mentioned. This fault, as noted in a preceding section, is apparently not the Upper Three Runs fault of Cumbest and Price (1989b), but is a related feature. The name Tinker Creek fault is adopted to distinguish between the two structures. This terminology is different than that previously used by this author (Domoracki, 1994a; Domoracki et al., 1994b). The Tinker Creek fault is a high-angle down-to-the-northwest fault across SRS and can be mapped unambiguously for a distance of 15 km on seismic lines SRS-2, SRS-4, SRS-3, SRS-9 and SRS-27. The time offset of the basement reflection along the fault increases to the northeast.

In this map, and succeeding maps, a low in time-structure occurs along Upper Three Runs valley. At seismic line SRS-4 (stations 500-570, Appendix B) the low is at minimum. The low in time-structure is attributed in this report to velocity push-down (see "Correspondence between Time-structure and Topography" and Appendix A); however, recent field mapping and analysis of borehole data in the vicinity of line SRS-4 has revealed an area of northwest dip in the Middle Eocene Warley Hill Formation on the southeast side of Upper Three Runs valley. The area of northwest dip roughly coincides with the apparent northwest dip of the mapped reflections (D. Snipes, Clemson Univ., 1994, personal communication; Fallaw et al., 1994). At the present time it is not known whether the mapped shallow structure is present at deep structural levels or is tectonic in origin.

Many of the mapped basement faults parallel contours of the Bouguer gravity field (Figure 45). This correspondence suggests that these faults parallel density contrasts in the basement, i.e. structural discontinuities, faults. In the interpretation of the deep data set it was noted that some of the fault slices on the hanging wall of the Augusta fault penetrated upward into the Coastal Plain. The correspondence between the gravity field and the mapped basement faults supports the interpretation of the deep seismic reflection data presented and the idea of the reactivation of deep crustal structures during the Late Cretaceous.

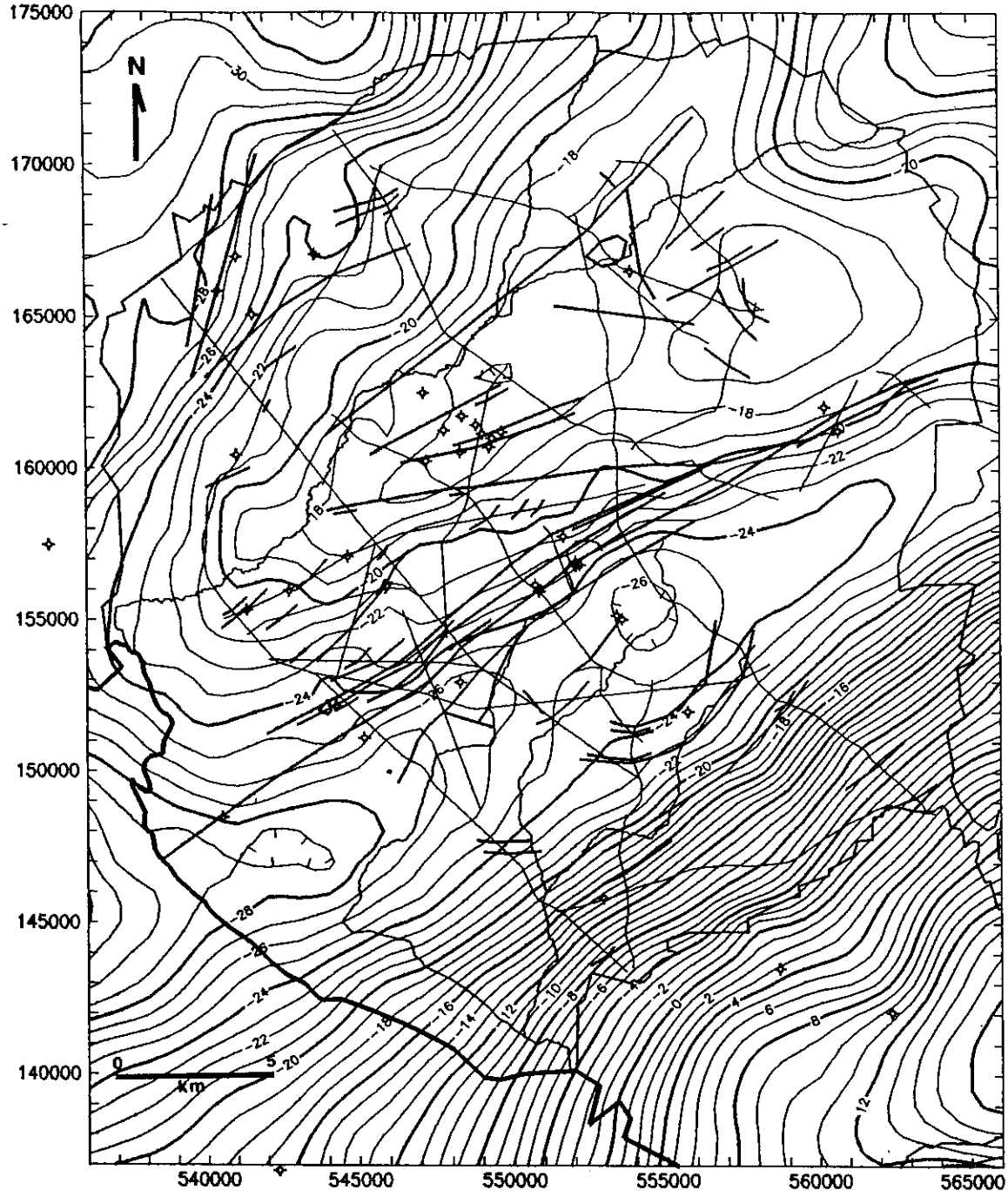

Figure 45. Basement faults superposed on the Bouguer gravity map: Note that many of the faults parallel contours of the gravity field. Contour interval 1 mGal.

Blue Marker Time-structure Map

The Blue Marker reflection throughout most of SRS is defined as a wavelet trough above a wavelet peak that is generally continuous 65-115 ms above the basement (e.g. Figure 44). The Blue Marker reflection separates zones of higher amplitude reflections below from zones of lower amplitude reflections above. The trough of the wavelet is mapped for convenience. Stratigraphically, the wavelet peak originates at the unconformity between the Middendorf and Black Creek Formations. In sonic logs this boundary is marked by a distinct increase in interval velocity upon entering the Middendorf Formation (Figure 6 on page 19).

In the southern and central parts of SRS this reflection is easily interpreted from line to line. North of Upper Three Runs the reflection begins to merge with other reflections as the sedimentary section thins updip. Occasionally, the reflection changes polarity and in some instances scour and fill structures cause local relief on the unconformity surface.

The Blue Marker time-structure map and fault map (Figure 46 and Figure 47) exhibit much the same structure as the Basement time-structure map shown in Figure 41, albeit somewhat more subdued. Most of the major faults that offset the top of crystalline basement also offset the Blue Marker. The Pen Branch, Crackerneck, and Tinker Creek faults all offset this level as do some of the faults that originate within the Dunbarton basin. In addition, several of the faults that penetrate upward from the basement level begin to split or splay upward as faulting propagates into higher stratigraphic levels. Several of the subsidiary faults within the Pen Branch fault zone cause deformation of this time marker through folding, although offset is not observed. The Steel Creek fault is similar in this regard to other faults within the Pen Branch fault zone.

Yellow Marker Time-structure Map

The Yellow Marker is denoted by a large-amplitude trough 160-250 ms above the basement reflection (e.g. Figure 44). Throughout the site area this marker is the shallowest coherent reflection that can be mapped and as such defines a major change in reflection character in the seismic

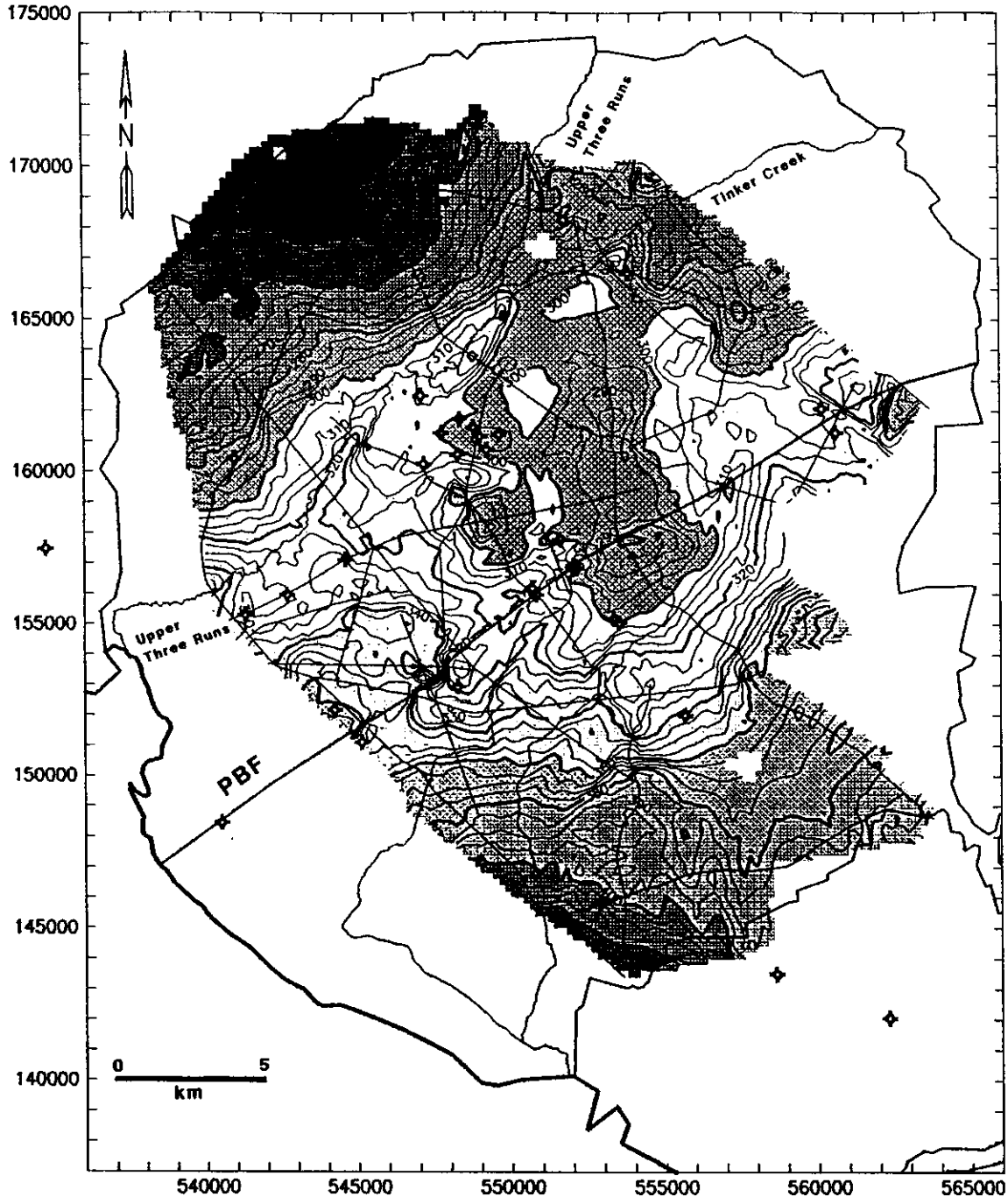

Figure 46. Time-structure map of Blue seismic marker: Contour interval 5 ms. Grid interval 200 m.

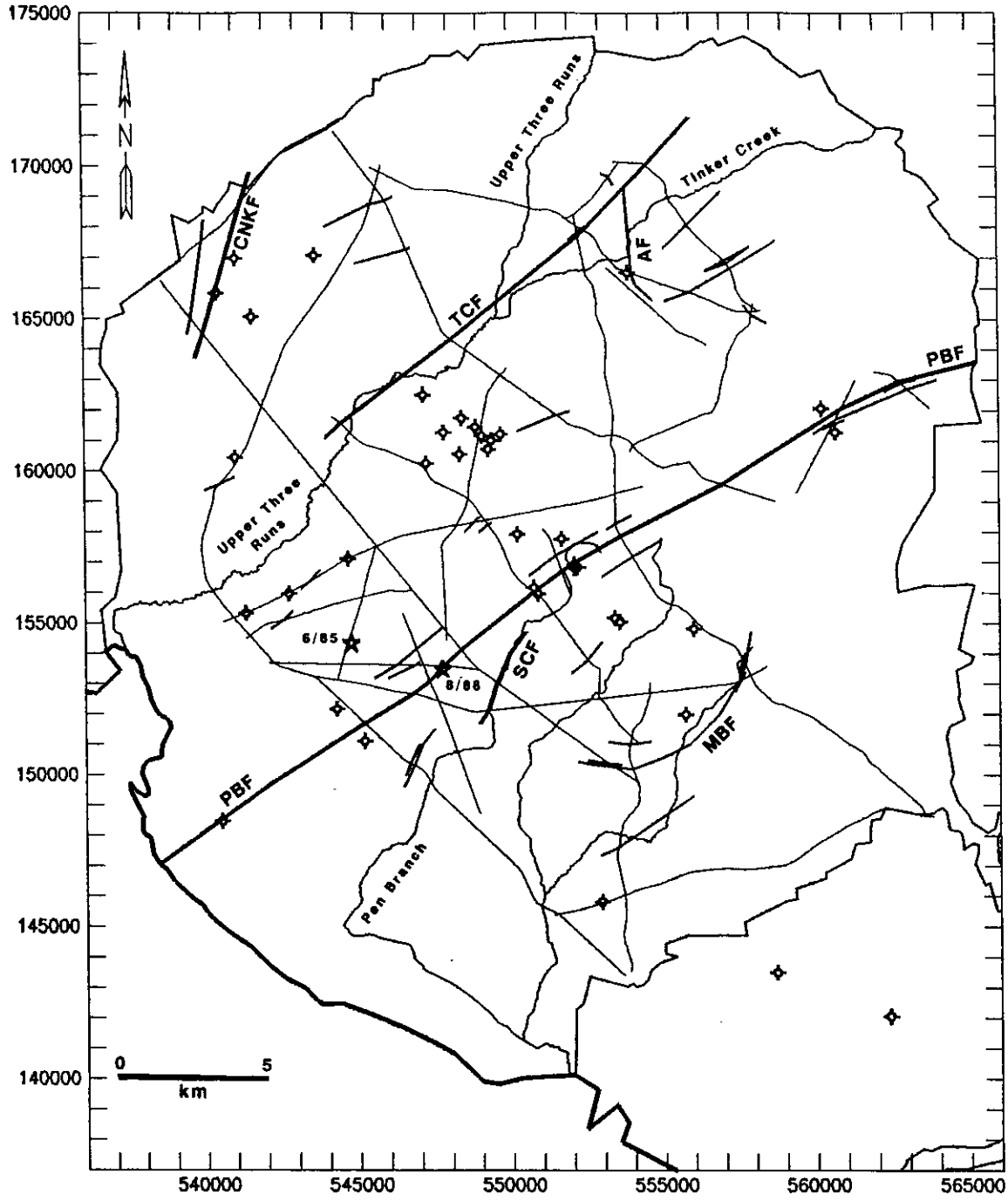

Figure 47. Blue Marker fault map: Faults that offset the Blue Marker reflection are shown. Faults that are down-to-the-northwest are indicated in orange and faults that are down-to-the-southeast are indicated in green. Faults with time offsets greater than 10 ms anywhere along the fault trace are denoted by thicker lines. PBF = Pen Branch fault, TCF = Tinker Creek fault, SCF = Steel Creek fault, MBF = Meyers Branch fault, AF = Atta fault, CNKF = Crackerneck fault.

data. Above the Yellow Marker reflections are generally weak and discontinuous; below the Yellow Marker reflections are higher in apparent amplitude and more continuous.

Correlation of the Yellow Marker to geophysical logs shows the reflection to originate near the top of the Cretaceous Peedee Formation in the basal Paleocene Ellenton Formation (Figure 6 on page 19 and Figure 70 on page 149). The Tertiary section at SRS is composed of relatively unconsolidated low velocity sands and clays of marine and nonmarine origin; this variability probably gives rise to the observed low-amplitude discontinuous reflections. Another factor to be considered is that, as a result of the recording geometry and the mute pattern, most of the seismic reflection lines do not build up significant CDP fold until Yellow Marker time or later. Seismic lines recorded with shorter near offsets, such as the EXP lines (e.g. line SRS-2EXP, Figure 67 on page 145) or line PBF-6 (Appendix B), do exhibit coherent reflections above the Yellow Marker.

Examination of the Yellow Marker time-structure map and fault map (Figure 48 and Figure 49) shows similar, yet even further subdued, structure as the preceding two maps (Figure 46 and Figure 41). Some of the variation in time-structure at this level results from near surface velocity variations as previously discussed. Only the Pen Branch, Tinker Creek, and Meyers Branch faults are observed to offset this time horizon. The Steel Creek and Crackerneck faults do cause appreciable deformation of the Yellow Marker (in time), but do not appear to offset it within the resolution of these data.

The Yellow marker reflection was mapped by Chapman and DiStefano as their "orange" marker reflection in the interpretation of the original processed SRS seismic data. In that study, the reflection was muted in the data processing and consequently could not be mapped in the northern part of SRS

Trend Surface Analysis of Time-structure

Trend surface analysis of the time-structure maps was undertaken to investigate the possibility that the uplift of the basement fault blocks bounded by the Pen Branch fault and the Tinker Creek

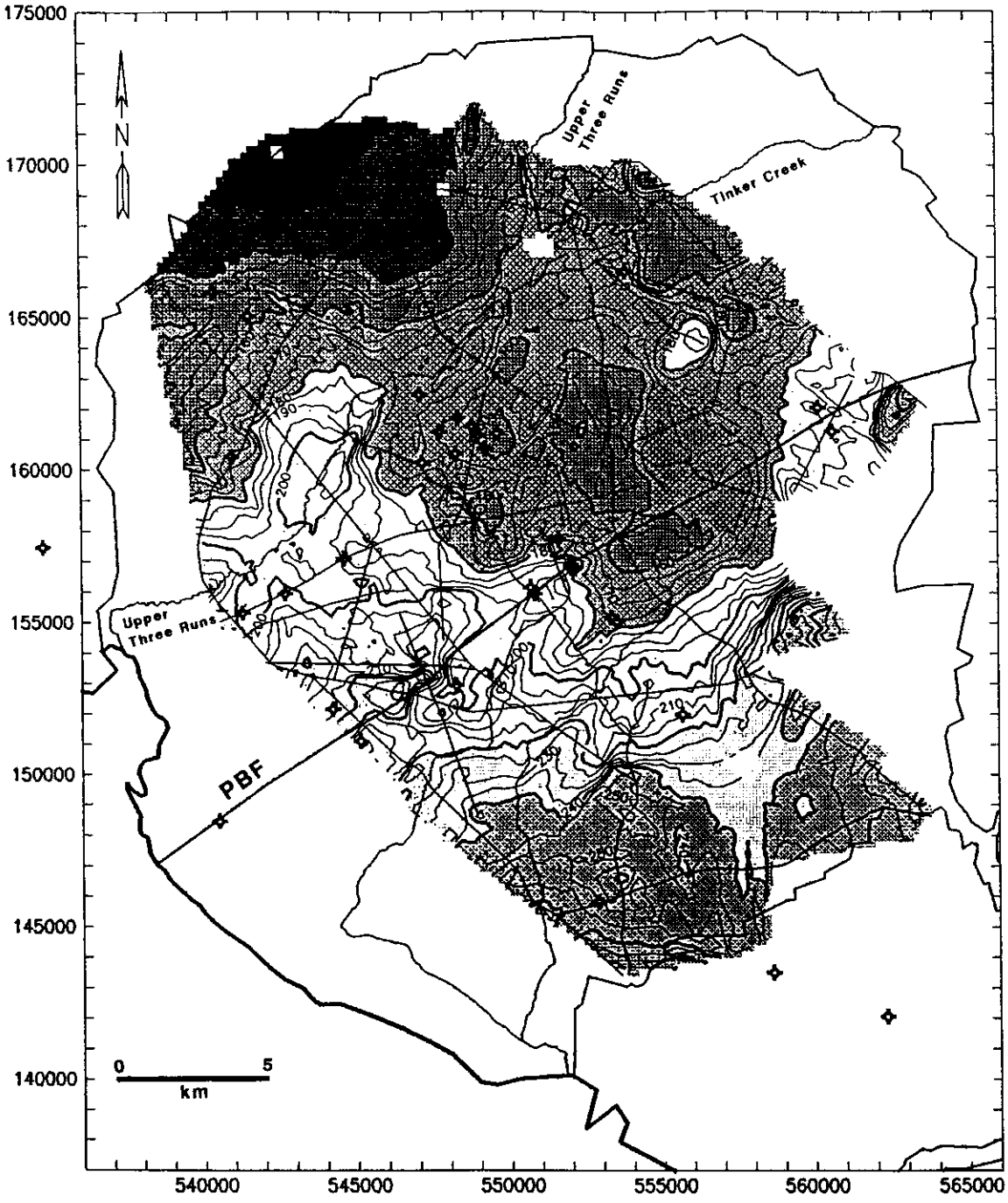

Figure 48. Time-structure map of Yellow seismic marker: Contour interval 5 ms. Grid interval 200 m.

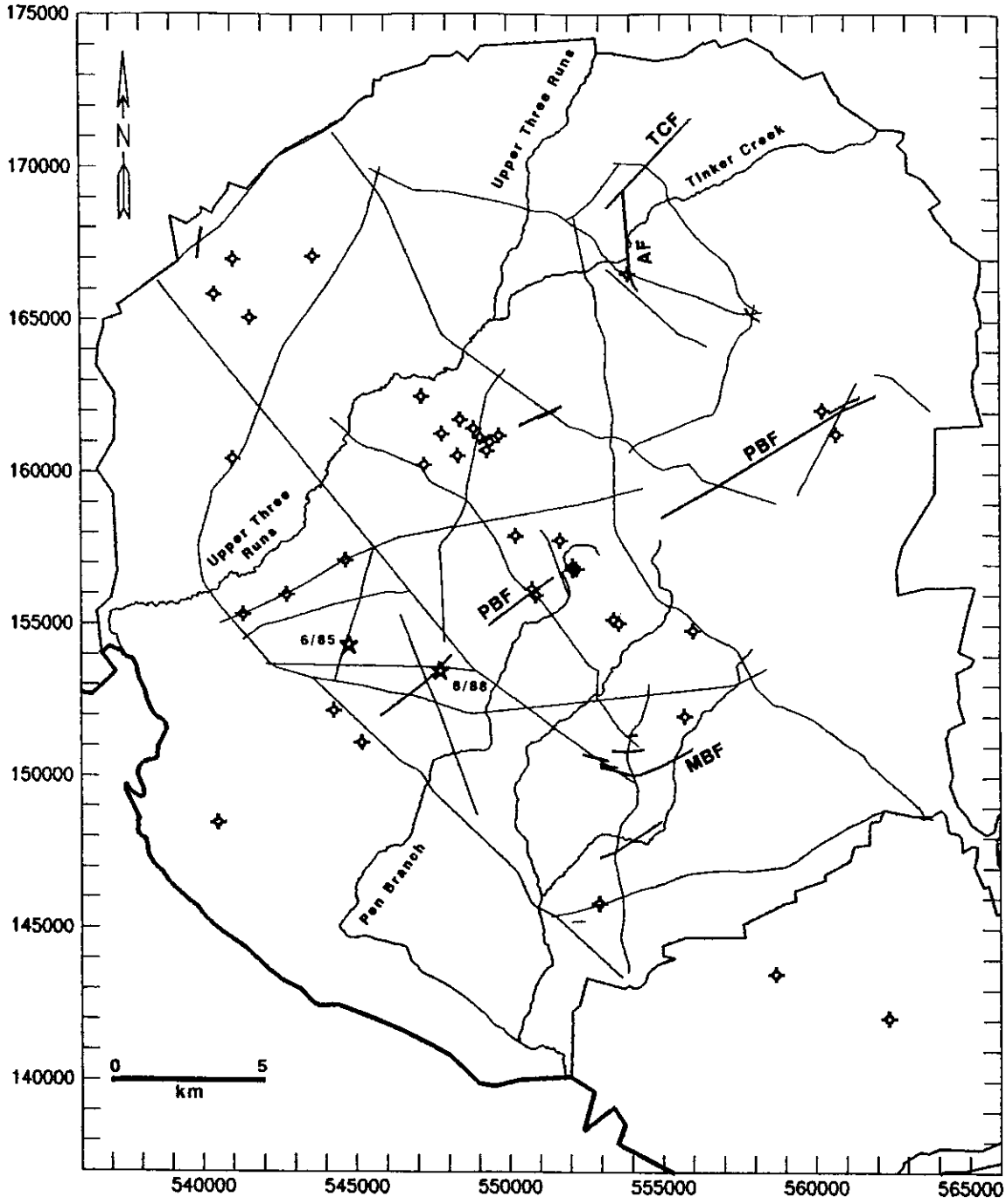

Figure 49. Yellow Marker fault map: Faults that offset the Yellow Marker reflection are shown. Faults that are down-to-the-northwest are indicated in orange and faults that are down-to-the-southeast are indicated in green. PBF = Pen Branch fault, TCF = Tinker Creek fault, MBF = Meyers Branch fault, AF = Atta fault.

fault might have been accompanied by components of rotation in a horizontal plane. Plane surfaces were fitted to three areas of the time structure-maps defined by (1) north of Upper Three Runs-Tinker Creek; (2) between the Pen Branch fault and Upper Three Runs-Tinker Creek; (3) south of the Pen Branch fault (Figure 50). At each structural level the strike and dip (in time) of the fitted surfaces was noted. These data, compiled in Table 4, show that the strike directions of the surfaces fit to the middle and southern areas (Area 2 and Area 3) exhibit consistent rotation directions up through the time section. In particular, the middle area shows clockwise rotation and the southern area counterclockwise rotation. These results suggest that Cretaceous-Tertiary movement on the Pen Branch fault and related structures was not pure dip-slip, but was transpressional. This would be consistent with the earthquake focal mechanism for the 1985 earthquake at SRS that indicated left lateral strike-slip motion on a fault parallel to the Pen Branch fault (Talwani et al., 1985).

The strike directions of time horizons in Area 1 do not exhibit consistent rotation directions. This result might be caused by an inadequate sample area, or that the analysis is invalid. The interpretation of the trend surface data is predicated on the assumptions that the seismic markers represent time-stratigraphic horizons as opposed to lithostratigraphic horizons and that these surfaces can be described by planes. No tests of statistical significance of fit other than "goodness of fit" were performed; however, intuition suggests that the fact the strike directions of the fitted surfaces on either side of the Pen Branch fault zone exhibit consistent rotation directions through the time section is more than coincidental.

Isochron Maps

Isochron maps were created by contouring the difference in grid values between the time-structure maps. Isochron maps were produced for the following intervals: Basement-Blue Marker, Blue Marker-Yellow Marker and Basement-Yellow Marker.

Table 4. Subsurface trends.

Surface	Strike	Slope	Goodness of Fit	Multiple Correlation
Topography	N 77.5° E	1.0 ms/km SE	0.738	0.859
Yellow Marker	N 82.5° E	4.8 ms/km SE	0.854	0.924
Blue Marker	N 79.0° E	5.8 ms/km SE	0.870	0.933
Basement	N 78.5° E	8.0 ms/km SE	0.920	0.959
Subsurface Divisions				
Yellow - Blue -Basement				
Area 1	N 67.5° E	8.2 ms/km SE	0.862	0.928
Area 1	N 60.5° E	9.4 ms/km SE	0.904	0.951
Area 1	N 64.0° E	10.0 ms/km SE	0.928	0.963
Area 2	N 81.0° W	3.2 ms/km SW	0.594	0.771
Area 2	N 84.0° W	3.6 ms/km SW	0.652	0.807
Area 2	N 88.0° E	5.5 ms/km S	0.750	0.866
Area 3	N 72.0° E	6.8 ms/km SE	0.805	0.897
Area 3	N 74.0° E	8.4 ms/km SE	0.844	0.919
Area 3	N 77.0° E	10.6 ms/km SE	0.911	0.955
Isochron Yellow-Blue	N 55.0° E	1.1 ms/km SE	0.519	0.720
Isochron Blue-Basement	N 79.0° E	2.2 ms/km SE	0.912	0.955
Isochron Yellow-Basement	N 71.0° E	3.2 ms/km SE	0.887	0.942

Basement-Blue Marker isochron map: The Basement-Blue Marker isochron map (Figure 51) shows thickening of the Middendorf- Cape Fear interval from north to south across SRS. A subtle decrease in the isochron occurs over the hanging wall of the Pen Branch fault that indicates the fault was active at this time as a reverse fault. At seismic line PBF-18 the isochron decreases 10 ms with respect to surrounding values. This decrease might be evidence for movement of the Pen Branch fault, but the "bulls-eye" nature of the contours suggests that more control is needed.

Near a line from Tinker Creek to Upper Three Runs an increase in the gradient of the isochron occurs over a 1-2 km interval and indicates thickening of the Middendorf-Cape Fear isopach. Similar gradients occur in the isochron map trending from the intersection of seismic lines SRS-2

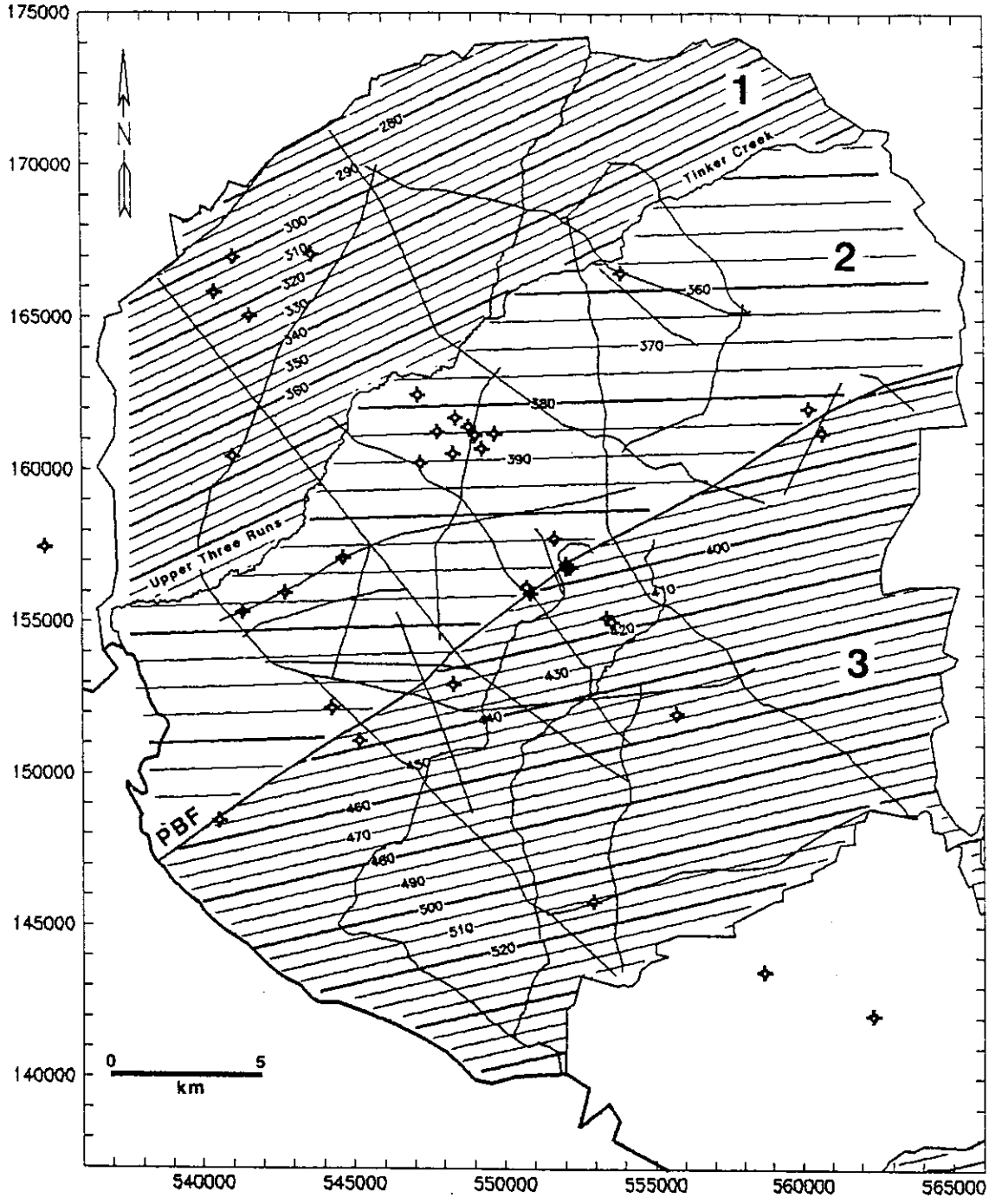

Figure 50. Trend surfaces: Trend surfaces fit to the Basement reflection. Contour interval 5 ms. Strike and dip of the trend surfaces fit to the Basement, Blue Marker, and Yellow Marker time horizons are tabulated in Table 4. The central block exhibits clockwise rotation of strike directions upward through the time section; whereas the southern block exhibits counterclockwise rotation of strike directions.

and SRS-5 to the intersection of seismic lines SRS-6 and SRS-7 and from the intersection of seismic lines SRS-3 and SRS-8 to the intersection of seismic lines SRS-1 and SRS-23. These gradients in the isochron map could be evidence for growth faulting and tilting of basement fault blocks. Another explanation are that the gradients denote erosional features.

Blue Marker-Yellow Marker isochron map: The Blue Marker-Yellow Marker isochron map (Figure 52) shows unmistakable thinning of the Peedee-Black Creek interval over the hanging wall of the Pen Branch fault. Clearly, the Pen Branch fault was an active growth fault during this time as previously confirmed by borehole data (Snipes et al., 1993a).

The abrupt increase in isochron thickness southward of Tinker Creek-Upper Three Runs is evidence for Late Cretaceous growth faulting in the northwestern third of SRS. The isochron gradient is located northwestward of the Tinker Creek fault mapped in Figure 42, which indicates that movement along that structure was not responsible for the isochron changes (Figure 53). The projected trace of the Upper Three Runs fault to the top of basement, however, is roughly coincident with the isochron gradient. Cumbest and Price (1989a) proposed that the flexure of the basement surface north of Upper Three Runs was caused by movement along the Upper Three Runs fault and was evidence for continued extension of the Dunbarton basin. This extension would cause normal movement on the Upper Three Runs fault and lead to thickening of sedimentary units on the hanging wall. Nevertheless, extension is inconsistent with the post-rift movement history of the Pen Branch fault. Moreover, all the faults at SRS, where the sense of movement can be determined, are reverse faults.

The isochron gradient near Upper Three Runs-Tinker Creek can also be thought of as thinning of sedimentary units to the northwest. The thinning might originate by reverse movement along a deep structure, perhaps by ramping up of the Augusta fault or reverse movement on the splays that sole into the Augusta fault. In this model, the isochron gradient is caused by a fault-bend fold resulting from reverse movement on a southeast dipping basement ramp - possibly the Crackerneck fault or a fault northwest of SRS. The wedge bounded by the Upper Three Runs fault (Figure 22 on page 61) is largely a passive structural element in this scenario. The localization of

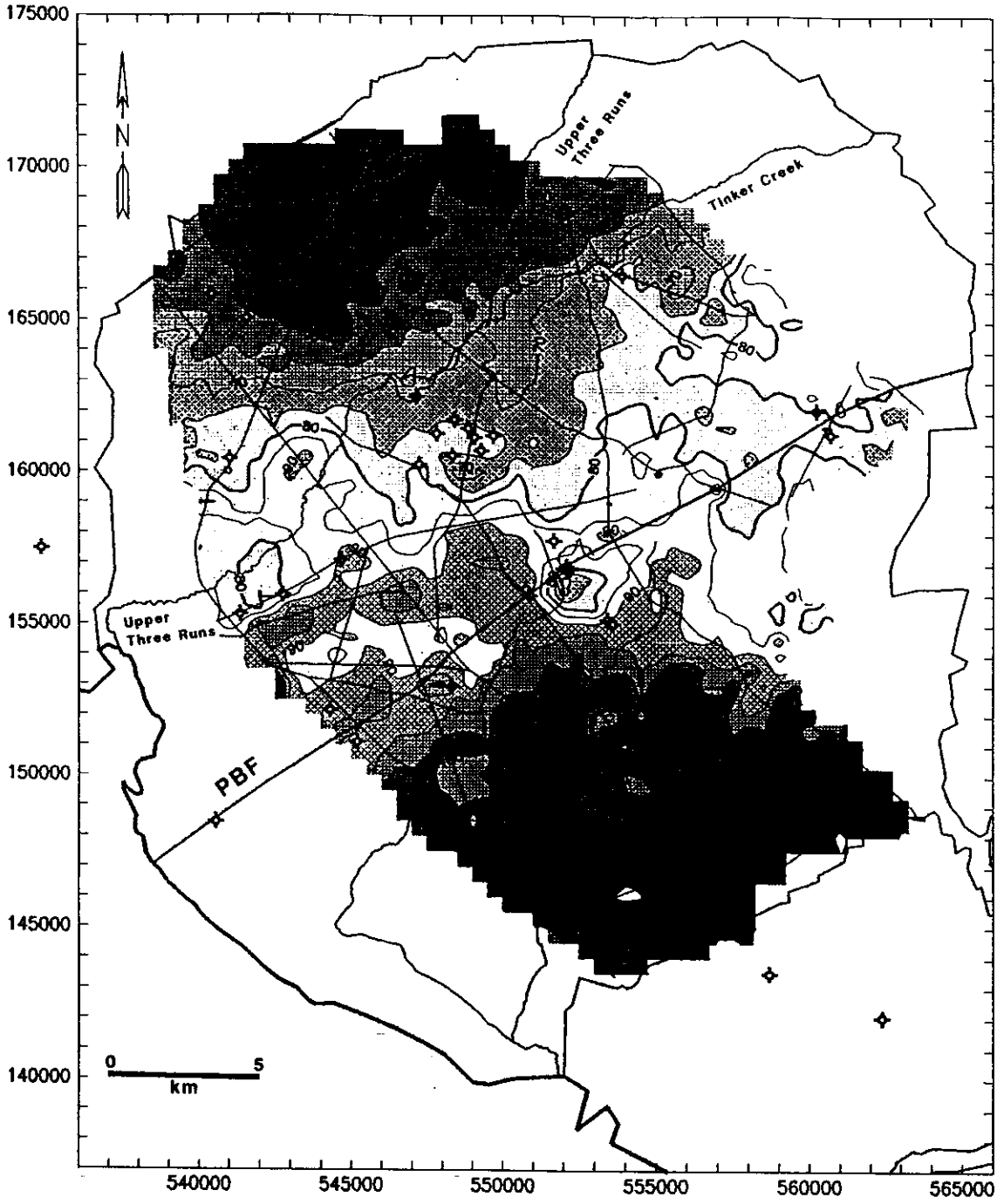

Figure 51. Isochron Basement reflection-Blue Marker: Contour interval 5 ms. Grid interval 500 m.

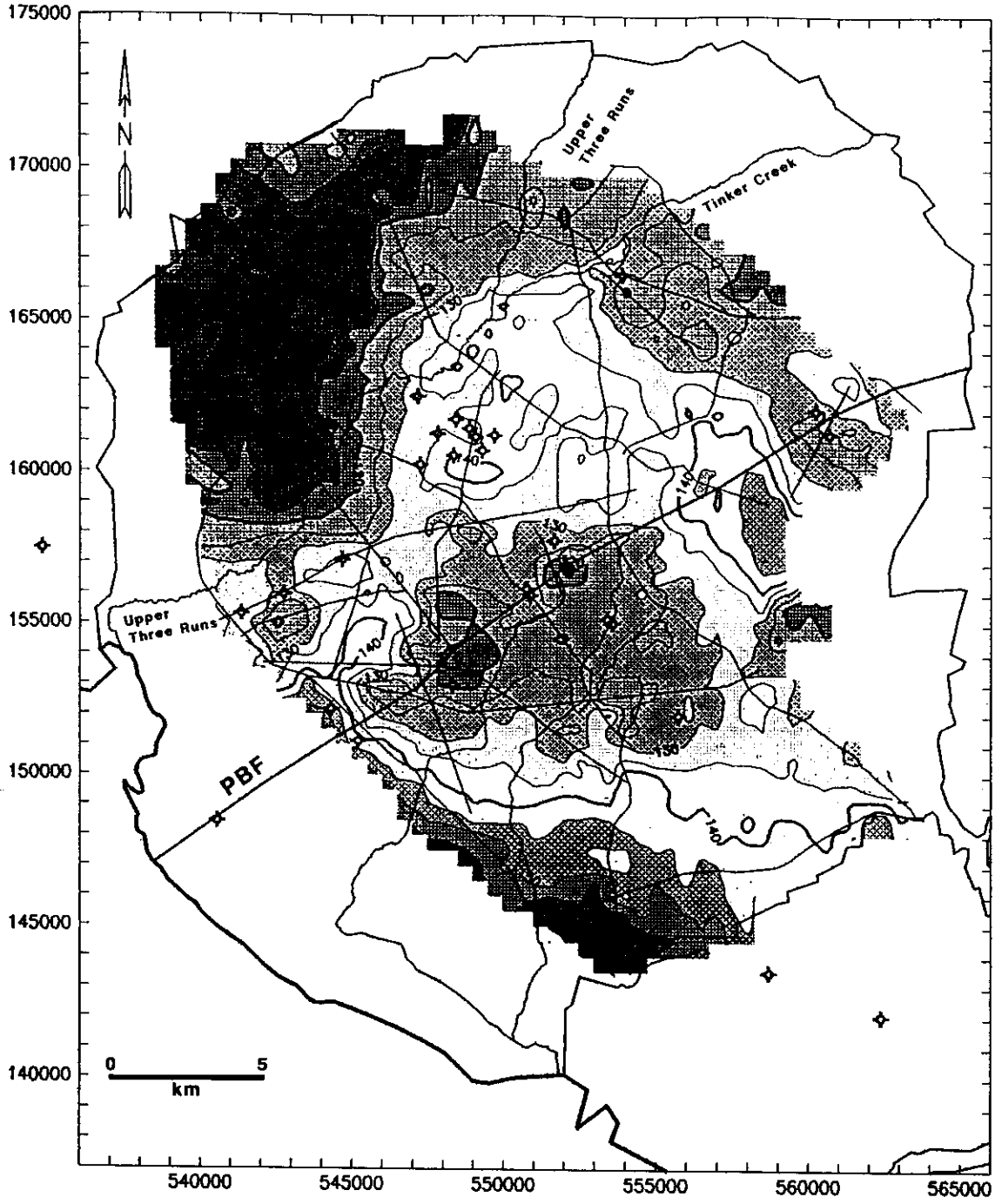

Figure 52. Isochron Blue marker-Yellow Marker: Contour interval 5 ms. Grid interval 500 m.

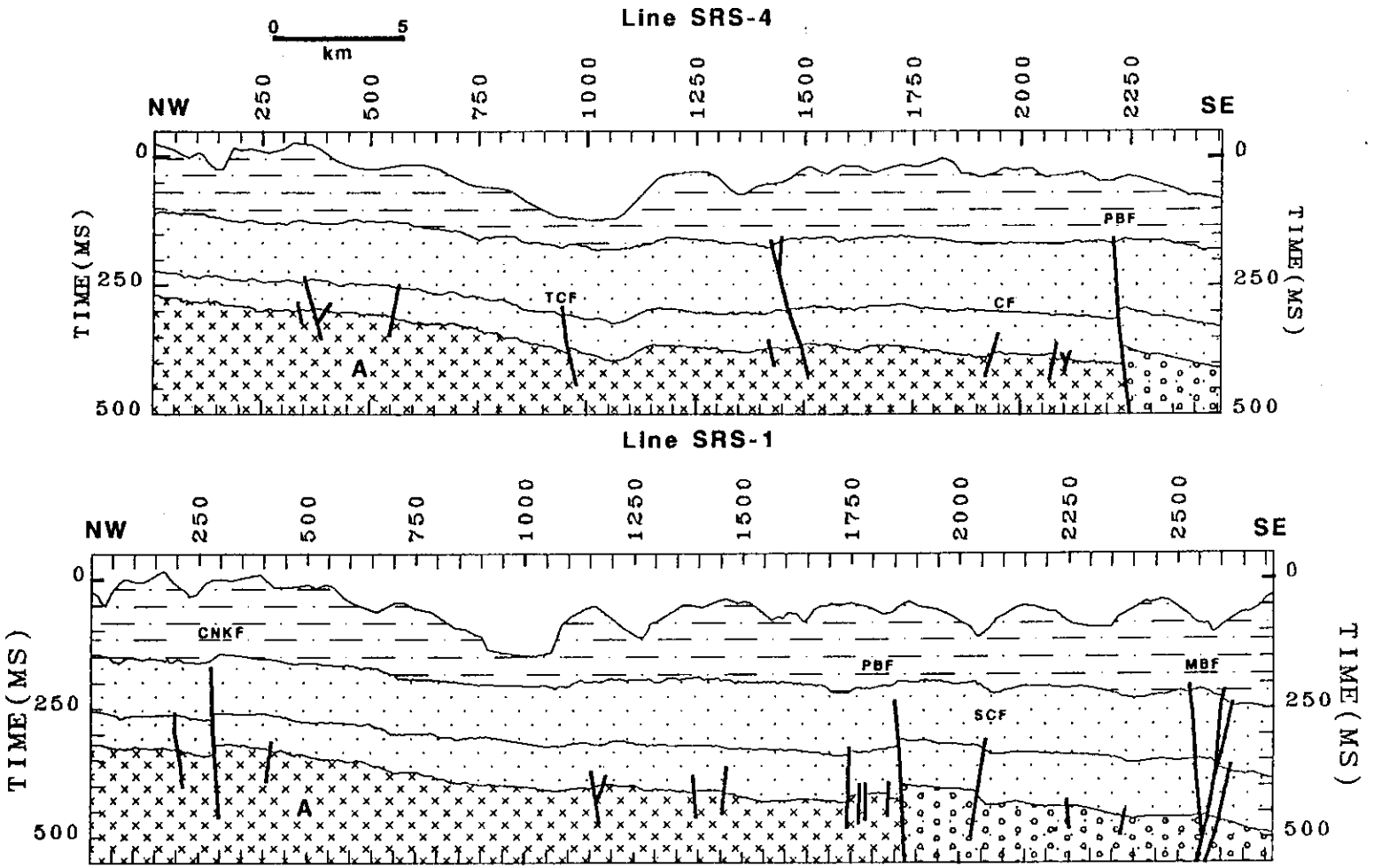

Figure 53. Reflection horizons interpreted across SRS: Seismic lines SRS-1 and SRS-4. The basement flexure (A) associated with the isochron thinning in the Cretaceous time section is not coincident with the Tinker Creek fault (TCF) mapped in the Coastal Plain sediments. Note the continuation of the basement flexure from line SRS-4 to line SRS-1. The Tinker Creek fault does not appear to extend southwestward as far as line SRS-1. PBF = Pen Branch fault, CNKF = Crackerneck fault, MBF = Meyers Branch fault, SCF = Steel Creek fault, CF = C Line fault. Vertical exaggeration 10:1 for V = 2000 m/s.

the gradient is caused by the inhomogeniety between the wedge and its bounding unit and not specifically by movement on the Upper Three Runs fault. This model would also explain why the location of the isochron gradient shifts position slightly for shallower isochrons (see previous and following isochron maps). Furthermore, the model is is consistent with reverse motion on all the major faults at SRS. In other areas of the Atlantic Coastal Plain changes in structural dip and isopach thickness could reflect ramps, flats and fault-bend folds of basement structures and be demonstrative of reactivation tectonics.

Southwestward of the Pen Branch fault another abrupt gradient in the isochron map occurs and denotes thickening of the Blue Marker-Yellow Marker isochron to the southwest. This gradient is roughly coincident with the Meyers Branch-Steel Creek faults mapped in Figure 42. Thus, the area between the Pen Branch fault and the Meyers Branch fault can be interpreted to have undergone uplift during deposition of the Peedee-Black Creek formations.

Basement-Yellow Marker isochron map: The isochron map of the Cretaceous time section, Basement-Yellow Marker (Figure 54), shows essentially the same features of Figure 51 and Figure 52, albeit somewhat better defined. The thickening of the Cretaceous section south of Upper Three Runs-Tinker Creek is a pronounced linear feature on this map.

Correspondence between Time-structure and Topography

Examination of the time-structure maps and the surface topography (Figure 55) suggests a correspondence of large scale features between the data sets. Under Upper Three Runs valley the time-structure maps uniformly have lower values. In the area bounded by seismic line SRS-4 to the intersection with line SRS-5 and southwestward along line SRS-5 to line SRS-2 both maps define higher values. Similarly, the higher time-structure values defined by the northeastern half of line SRS-12 and the intersections of lines SRS-9 and SRS-7 with SRS-4 correspond to a topographic high. In addition, the gradient in time-structure delineated from the intersection of line

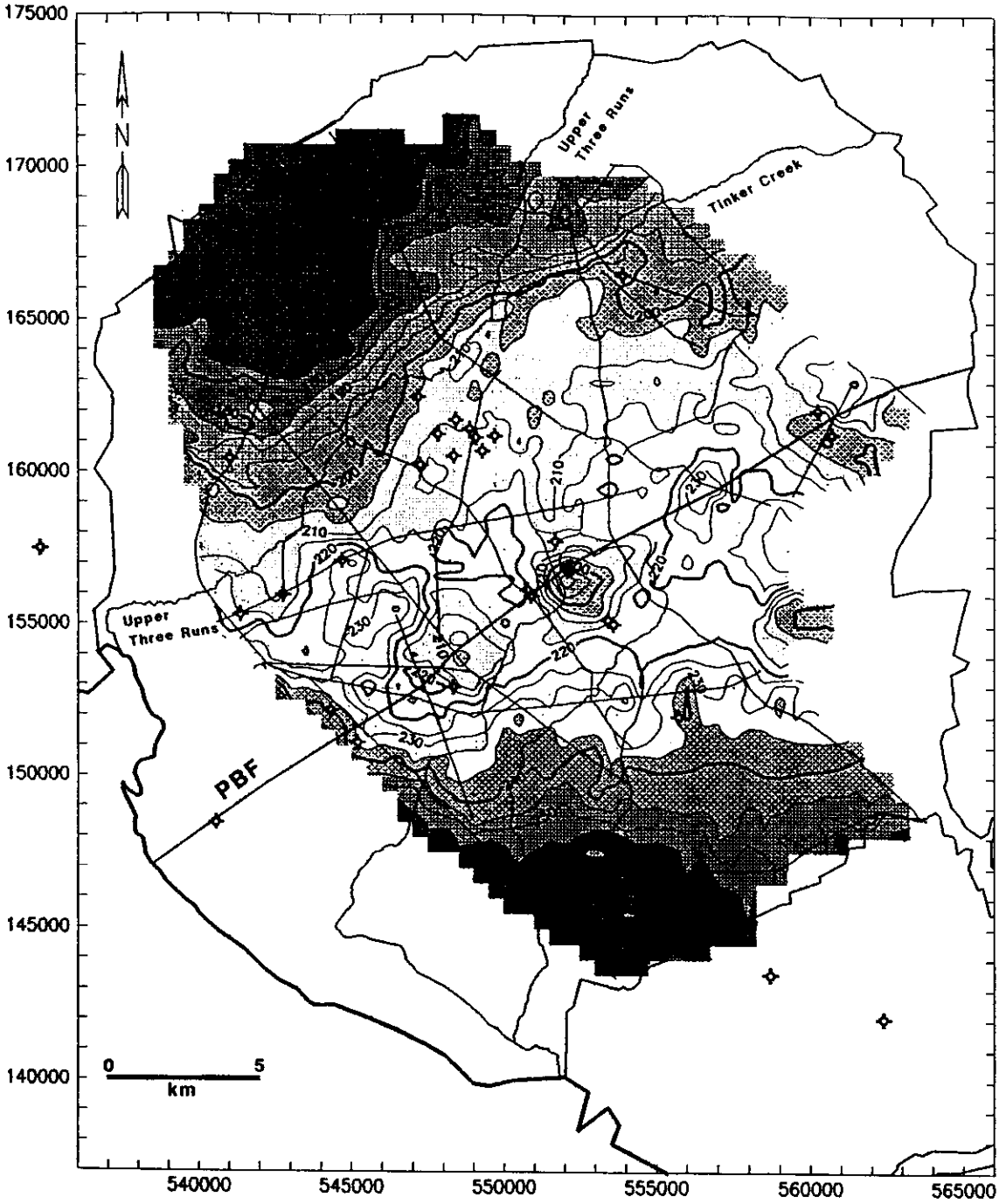

Figure 54. Isochron Basement reflection-Yellow Marker: Contour interval 5 ms. Grid interval 500 m.

SRS-2 with SRS-11 to the intersection of line SRS-3 with SRS-8 also appears to correlate with a topographic gradient.

The apparent correspondence of time-structure to surface topography can be attributed to either an incorrect datum static or basement uplift affecting present-day topography. The time-structure lows under Upper Three Runs valley are probably a result of velocity push-down caused by too low a datum velocity used to correct the seismic data to datum. To correct seismic reflection data to datum a correction velocity must be chosen to represent the rock that is either "cut" or "filled" above or below datum. In Upper Three Runs valley much of the Tertiary section has been eroded, which requires that the datum correction velocity be higher than that used elsewhere to represent the missing older, higher velocity strata. The relationship between time-structure and topography for the other areas mentioned above is less clear.

To study the possible correspondence between time-structure and topography a simple form of two-dimensional correlation analysis was performed. The analysis involved the generation of product maps that result from the multiplication of the residualized topographic and time-structure maps reduced to standard normal form (Davis, 1973). These product maps indicate areas where surface topography and time-structure correspond. Positive correlation between the maps (high to high or low to low) is indicated by positive products and negative products indicate inverse correlation.

The topography and time-structure maps were both gridded at 500 m intervals and residualized by fitting and subtracting a plane surface from each data set using the Surface III software package. The trends removed from the data are listed in Table 4. Standardization of the maps to convert the data to dimensionless form entailed subtracting the mean of the variable from each grid point and dividing by the standard deviation (σ) of the variable. That is,

$$Z_j = \frac{X_j - \overline{X}}{\sigma}$$

where X_j is the grid point, $\overline{X}$ is the mean of the variable. The product maps are contoured in products of the standard deviation of the variables from their respective means.

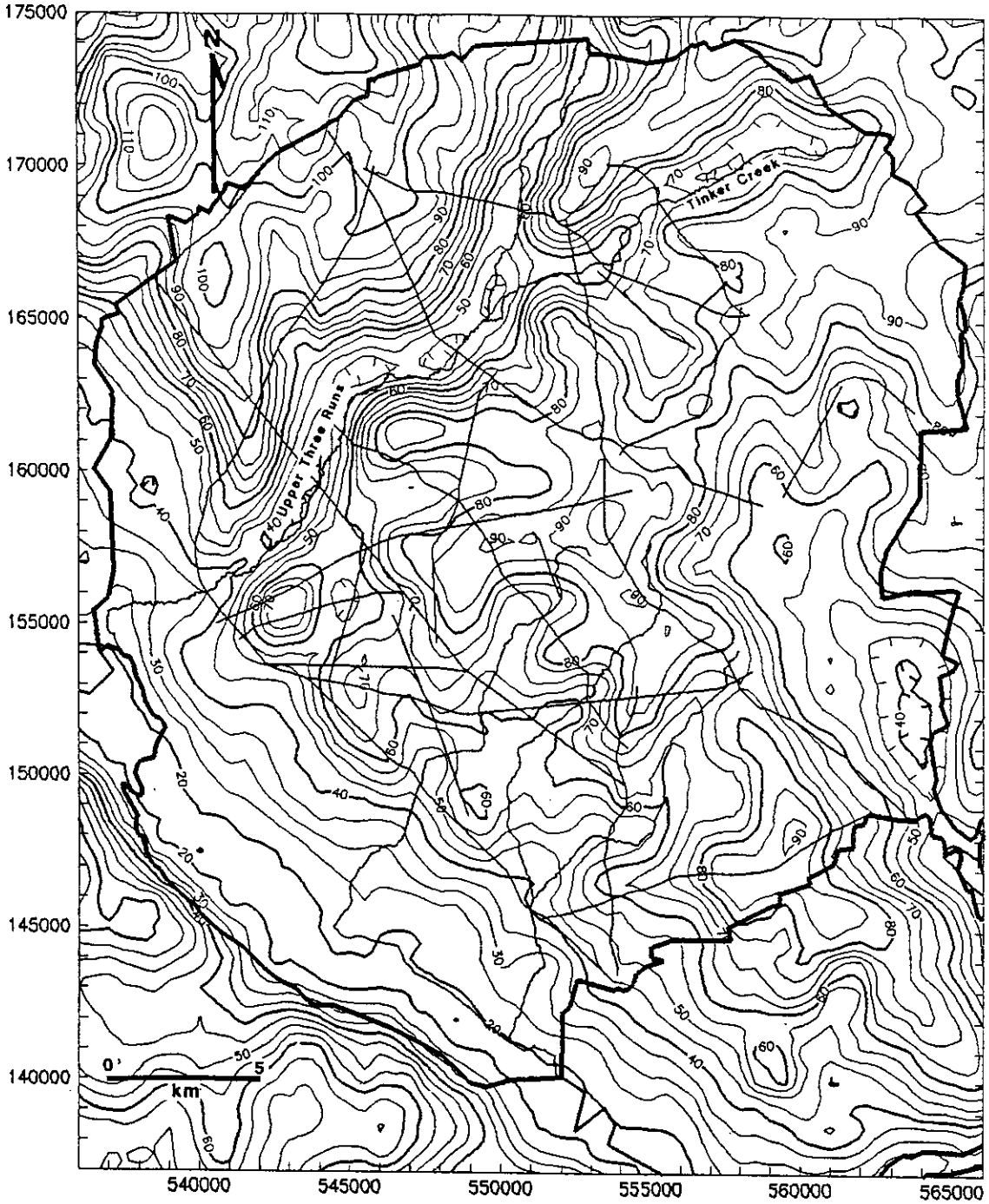

Figure 55. Topographic map of SRS: Contour interval 5 m. Grid interval 500 m. Digital (30 seconds grid interval) topography from the *Geophysics of North America* CD-ROM (Hittelman et al., 1989).

In Figure 56 the correlation between topography and basement time-structure is shown. Only positive products are contoured, i.e. positive correlations between topography and time-structure. Along Upper Three Runs valley, time-structure and topography coincide; this result is apparent from visual inspection of the seismic sections. Another area where time-structure and topography coincide is on the hanging wall of the Pen Branch fault from seismic line SRS-3 to SRS-8 and from seismic line SRS-2 to SRS-11. Also, positive correspondence between time-structure and topography occurs along the northern half of seismic line SRS-12 and southward to the intersections of seismic lines SRS-7, SRS-4 and SRS-9.

The correlation of the Blue Marker time-structure with topography (Figure 57) and the correlation of the Yellow Marker time-structure with topography (Figure 58) are both similar to the correlation of Basement time-structure with topography (Figure 56). The demonstrated correspondence between time-structure and topography is inconclusive. At a minimum, the origin of the positive correlation between topography and time-structure affects all three time horizons. This result is not inconsistent with either near surface velocity variation or Cenozoic uplift.

If the preceding analysis is performed on the isochron maps, the effect of near surface velocity variations should be minimized. The correlation of the Basement-Blue Marker isochron with topography and the correlation of the Blue Marker-Yellow Marker isochron with topography are shown in Figure 59 and Figure 60 respectively. In this case, isochron thins show positive correlation to topographic highs and vice-versa. The Basement-Blue Marker isochron shows little correspondence to topography other than an area on seismic line SRS-1 at Upper Three Runs and two areas on seismic lines SRS-3 and PBF-18. The Blue Marker-Yellow Marker isochron shows two areas that have correspondence to topography: at Upper Three Runs valley on seismic line SRS-4 and on the hanging wall of the Pen Branch fault on seismic lines SRS-3, SRS-2 and SRS-11. This latter area, previously identified in the time-structure (Figure 41 on page 101) and isochron maps (Figure 52 on page 119), is bounded in part on the southeast by the Meyers Branch fault (Figure 42 on page 102). It could be argued that this area has undergone uplift not only in the Cretaceous, but also during the Cenozoic to account for the correspondence between the time-structure maps, isochron maps and topography. It must be noted, however, that near surface static

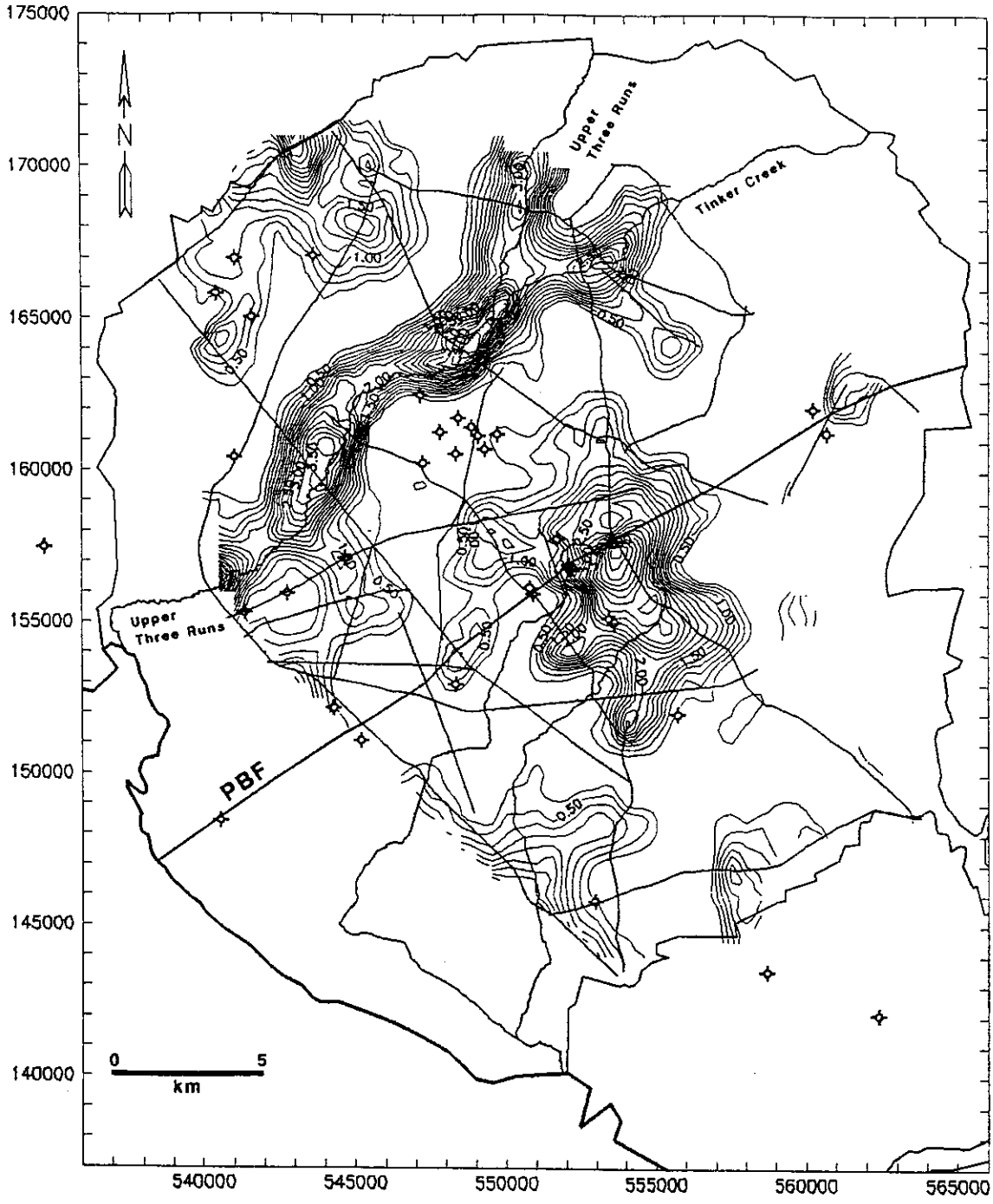

Figure 56. Product of standardized maps: Topography-Basement: Positive products shown only. Grid interval 500 m. Contours in product of standard deviations from the mean. Map indicates areas where topography and basement time-structure are both above or below their respective means in standardized form, i.e. areas where topography and basement time-structure correlate. Areas of correlation represent either (1) basement uplift affecting topography (Cenozoic uplift), or (2) long wavelength statics anomalies caused by incorrect datum correction velocity.

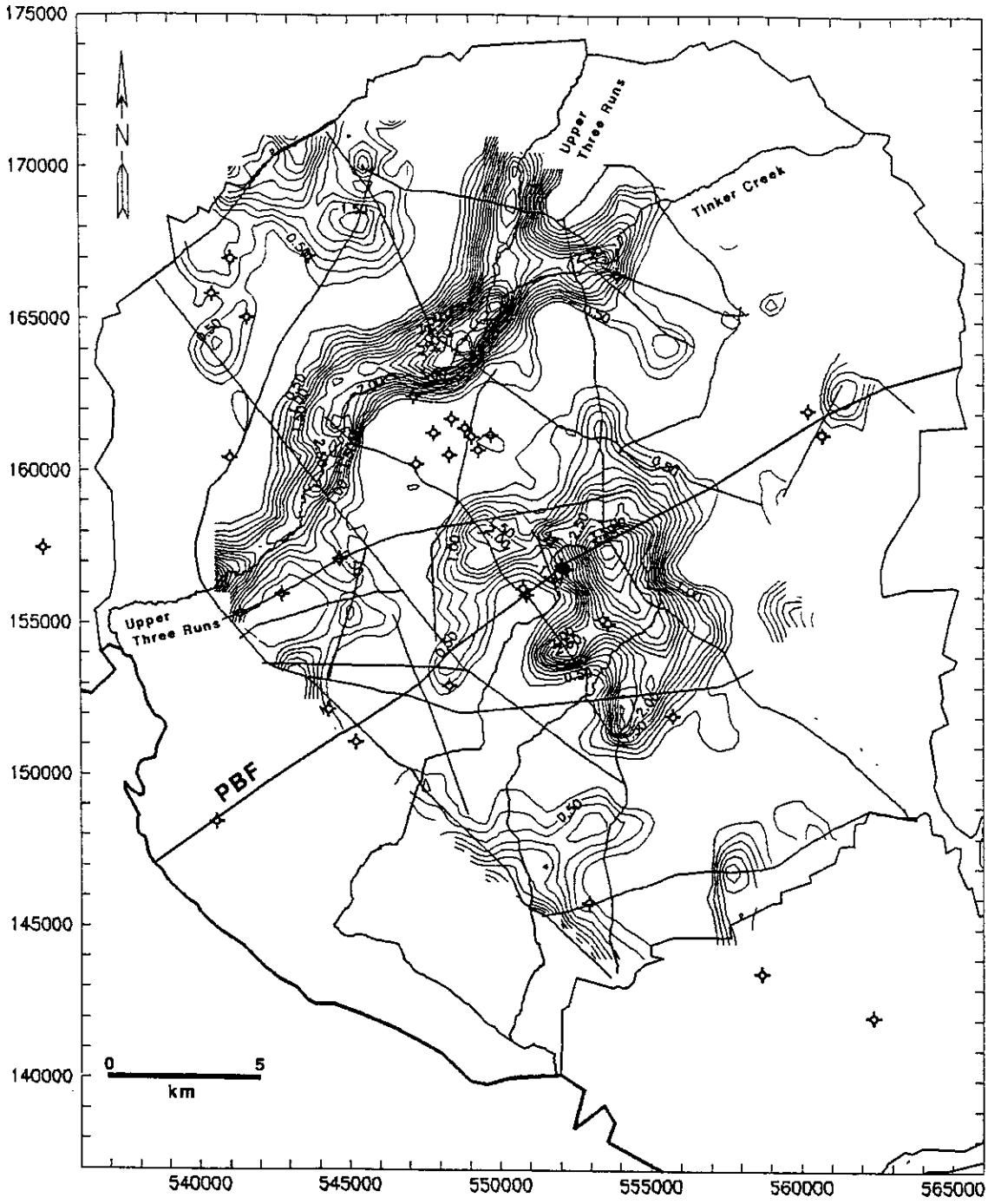

Figure 57. **Product of standardized maps: Topography-Blue Marker:** Positive products shown only. Grid interval 500 m. Contours in product of standard deviations from the mean. Comments as per Figure 56.

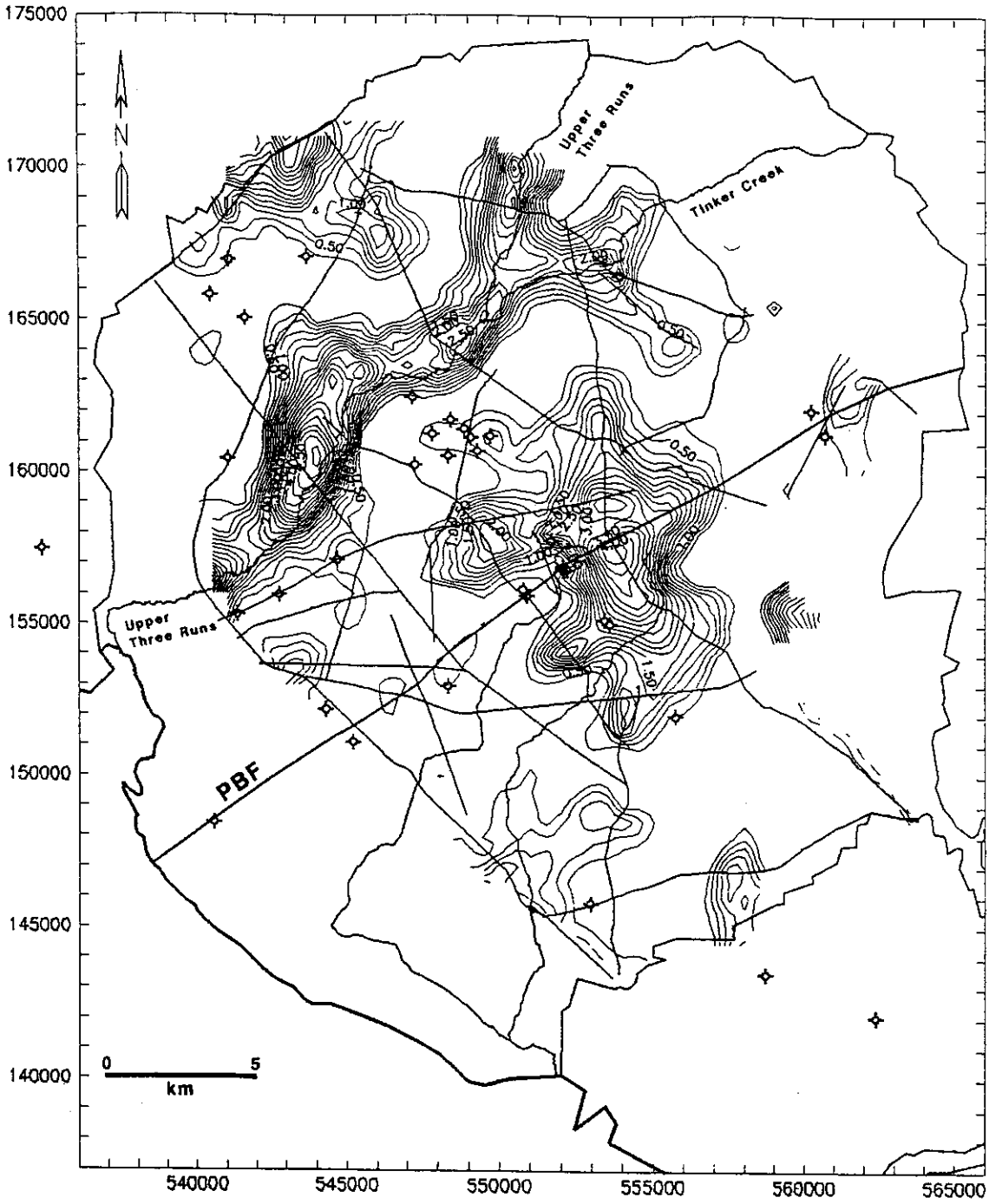

Figure 58. **Product of standardized maps: Topography-Yellow Marker:** Positive products shown only. Grid interval 500 m. Comments as per Figure 56. The similarity among Figure 56, Figure 57 and this figure is consistent with either Cenozoic uplift or near surface velocity variations leading to incorrect datum static.

anomalies decrease with increasing time (Musgrove, 1994), which could also account for the apparent noncorrespondence of the Basement-Blue Marker isochron with topography (at the limit of resolution) and the correspondence with the the shallower Blue Marker-Yellow Marker isochron. The results of this analysis are not conclusive with regard to the possibility of Cenozoic uplift at SRS, but are intriguing, and bear further study.

Amplitude Maps

Amplitude of Basement Reflection

The amplitude of the Basement reflection, as previously noted, is observed to vary across SRS. The most obvious amplitude variation is the marked decrease in reflection amplitude where the basement changes from crystalline to Triassic and the velocity at the base of the weathered layer changes from about 5700 m/s (crystalline) to about 3200 m/s (Triassic). The resulting decrease in acoustic impedance contrast leads to the lower reflectivity seen in the stacked data. In detail, however, the amplitude variations are more subtle and the velocity structure at the top of basement is more complex. Various workers have noted that refraction velocities within the crystalline basement at SRS exhibit a wide range of values (Bonini and Woollard, 1960; Chapman and DiStefano, 1989; Demirbag, 1990). The variation in the basement refraction velocity values suggests that a corresponding variation in the amplitude of the basement reflection should exist as a result of the changing acoustic impedance contrasts. Therefore, it might be possible to characterize divisions of the crystalline basement by reflection amplitude. These variations in reflection amplitude might denote lithologic/ structural boundaries or different depths of weathering and development of the saprolite layer. Variations in amplitude of the Triassic basement reflection might represent lithologic changes associated with specific depositional environments that relate to the structural development of the basin.

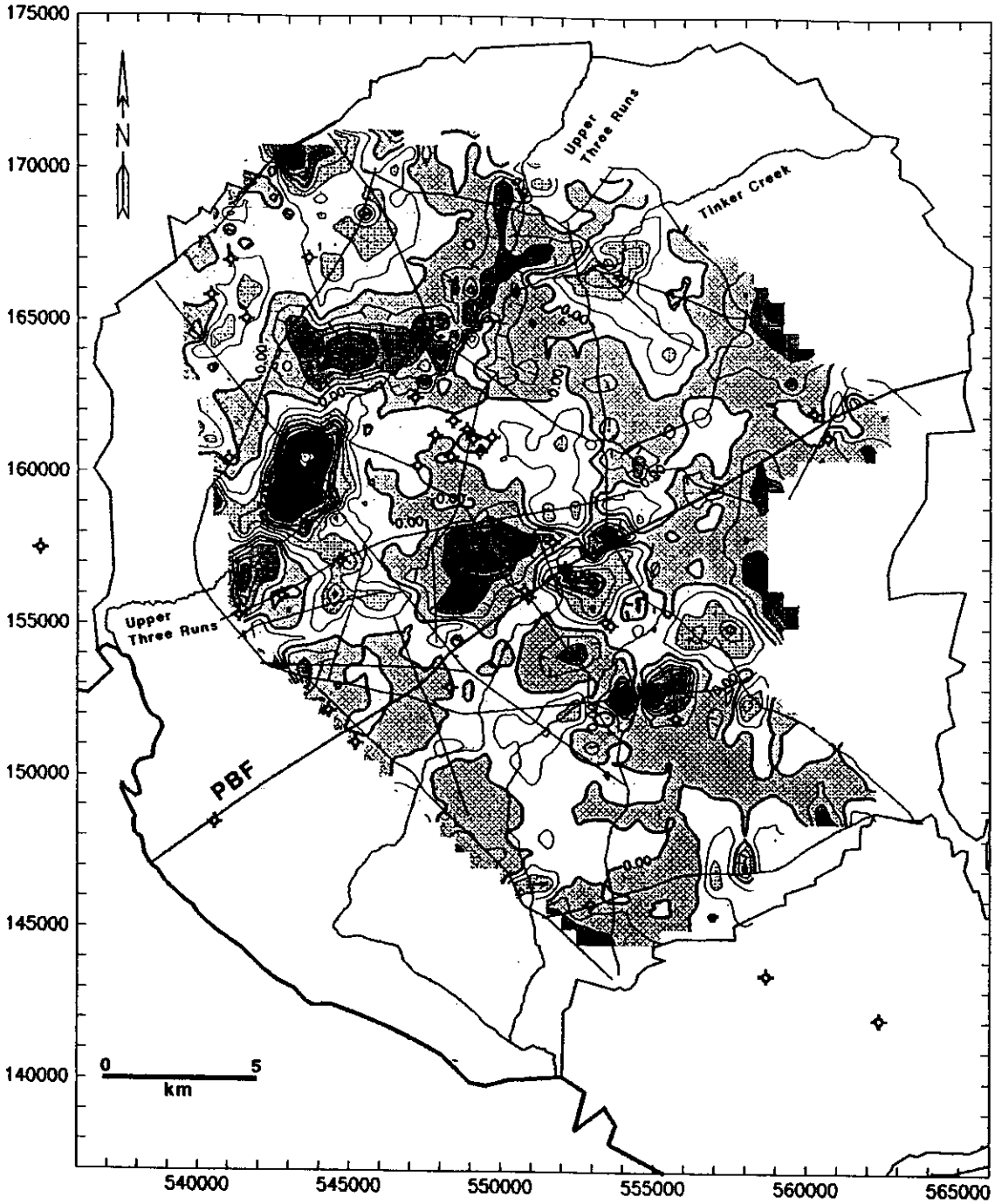

Figure 59. Product of standardized maps: Topography-isochron Basement-Blue: Positive products indicate areas where a decrease in isochron time-thickness corresponds to a topographic high. Isochron lows would correspond to topographic highs if uplift is ongoing or has been episodic since deposition. Positive products are indicated by yellow and warmer colors.

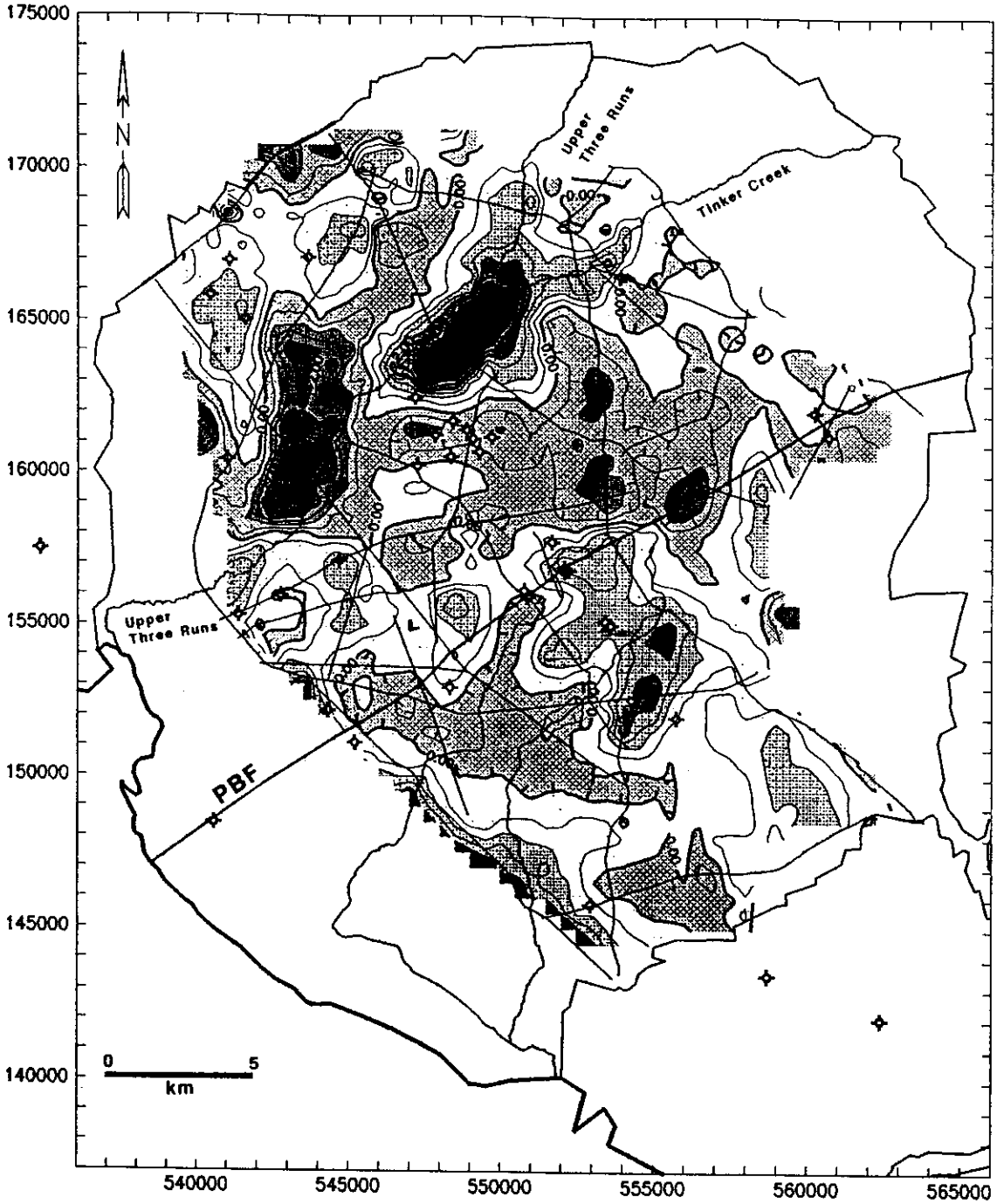

Figure 60. Product of standardized maps: Topography-isochron Blue-Yellow: Comments as per (Figure 59). Positive products are indicated by yellow and warmer colors.

The basement reflection amplitude map (Figure 61) was constructed from the final migrated seismic sections after display filters and AGC were applied. For each trace in a seismic line the reflection amplitude was defined as the sum of the absolute value of the sample values within a 40 ms window centered on the digitized basement reflection. These values were subject to a 15 point smoothing filter and decimated one in four before gridding and contouring. Line SRS-18 was eliminated from the data set because of anomalously high amplitude values compared to lines SRS-21 and SRS-23. The PBF lines were also eliminated from the data set because of the different seismic source, recording system, and frequency band used from the SRS lines.

The amplitude contours clearly delineate two major zones: lower amplitude values south of the Pen Branch fault where Triassic strata underlie the Coastal Plain sediments and higher amplitude values north of the fault where crystalline basement is present. The amplitude values from the crystalline basement can be further subdivided north and south of Upper Three Runs-Tinker Creek where generally higher reflection amplitudes exist to the north. Thus, the basement reflection amplitude map defines the same divisions as the Basement time-structure map (Figure 41 on page 101). From this result it can be inferred that the Upper Three Runs fault bounds a major change in basement velocity (lithology), which would be consistent with the assumption that it is a major geologic structure.

The interpretation of the shorter wavelength features in the reflection amplitude map as representing local basement velocity changes is lent credibility from the correspondence between seismic refraction velocity values and seismic reflection amplitude. Demirbag (1990) determined basement refractor velocities along line SRS-1 by measurement of shot record first arrivals. Demirbag's refraction velocity profile (Figure 62) shows good correspondence with the reflection amplitude values along line SRS-1. In addition, the basement refraction velocity values reported by Bonini and Woollard (1960) and Chapman and DiStefano (1989) are also consistent with the reflection amplitude map.

The arcuate band of higher amplitudes from the southern terminus of line SRS-29 through lines SRS-1, SRS-8, and SRS-2 probably represents the subcrop of a higher velocity rock type at the top of Triassic basement. This conclusion is supported by Demirbag's refraction velocity pro-

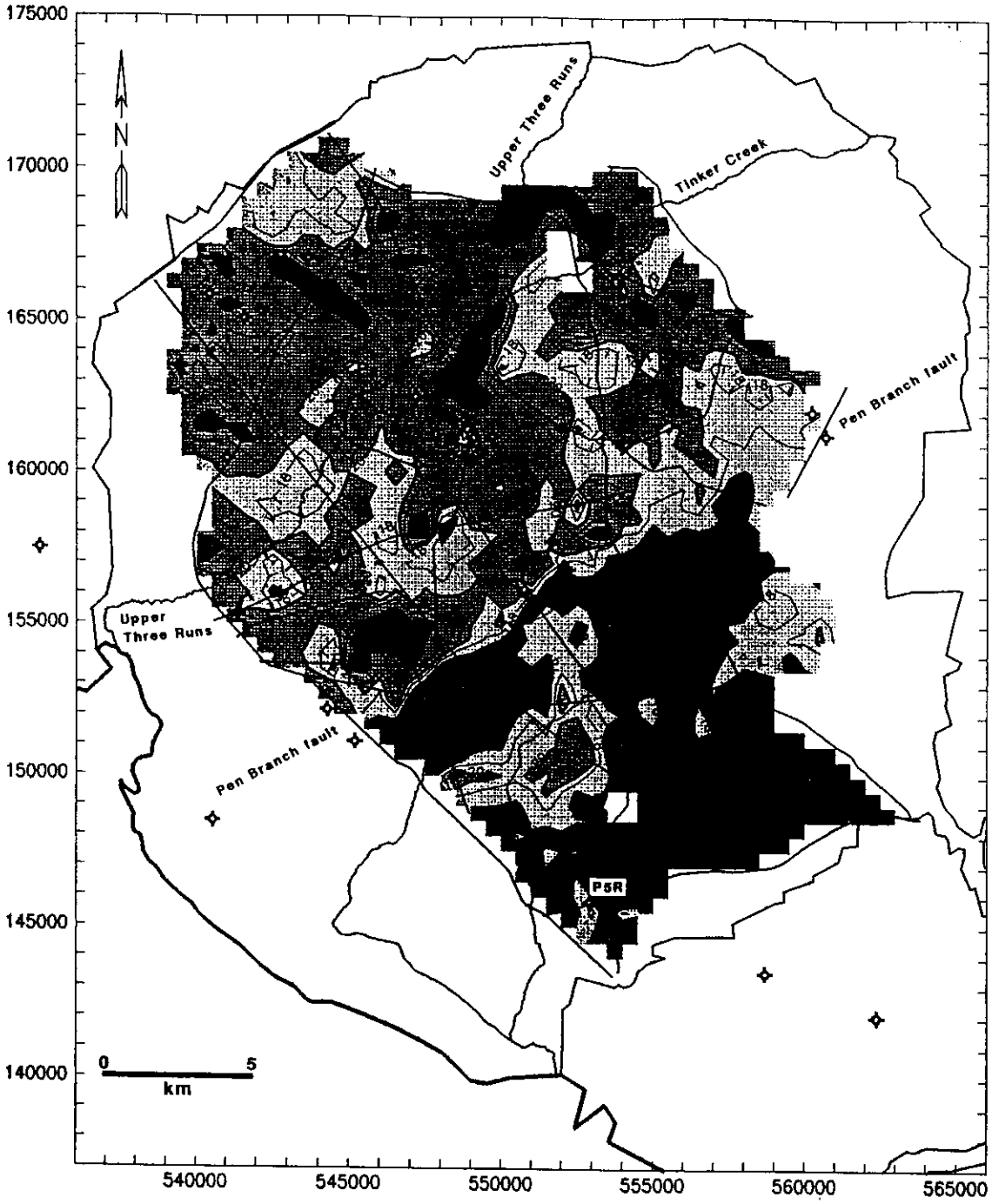

Figure 61. Amplitude of Basement reflection: Higher amplitudes are indicated by warmer colors, lower amplitudes by cooler colors. Contours are amplitude divided by 1,000,000. Grid interval 500 m. The reflection amplitudes appear to define three zones bounded by the Pen Branch fault and Upper Three Runs similar to the time-structure maps.

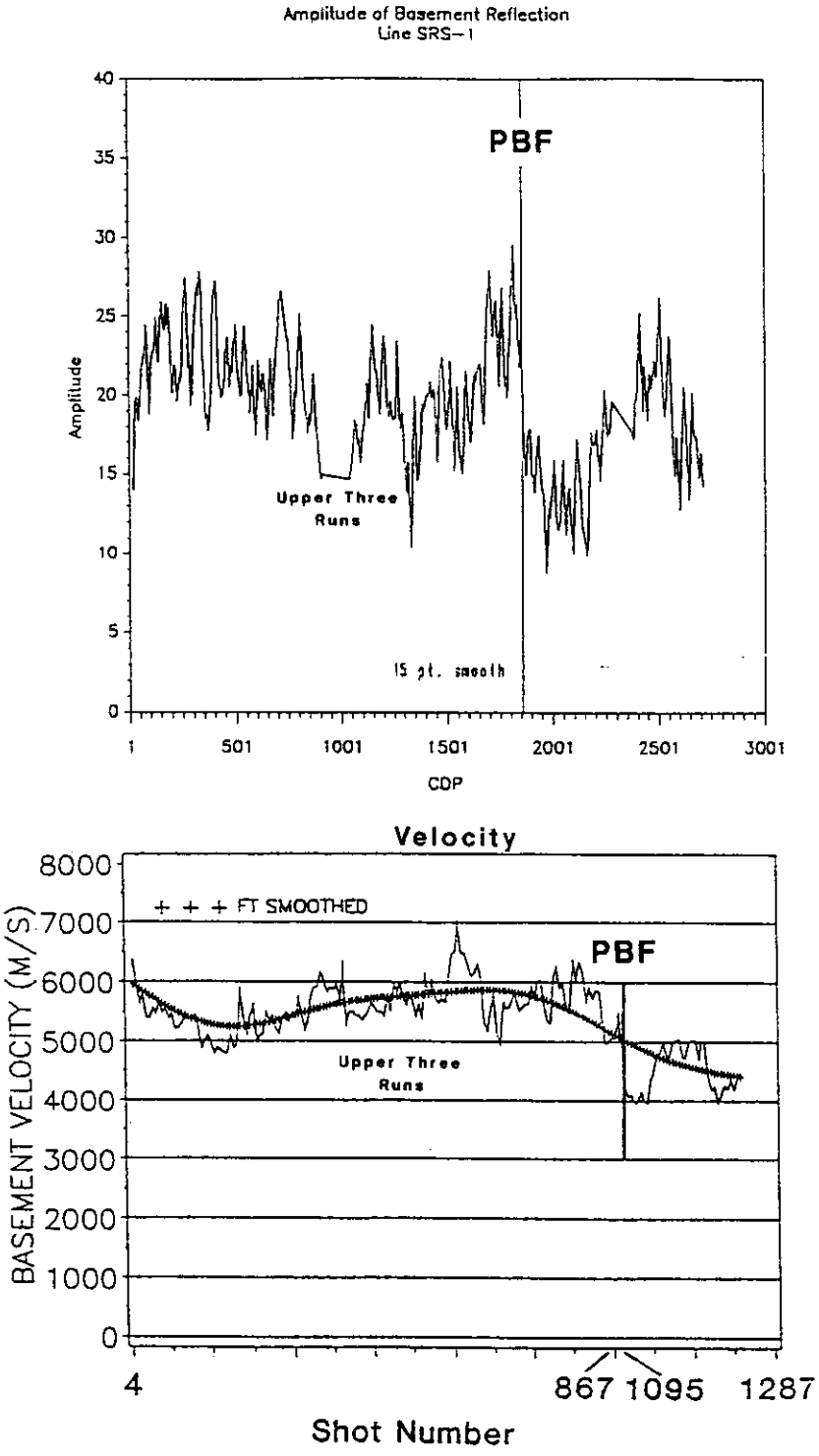

Figure 62. Refraction velocity vs. reflection amplitude: Line SRS-1. Basement reflection amplitude (top) correlates favorably to basement refraction velocity (bottom). Note especially good correspondence between refraction velocity and reflection amplitude from Upper Three Runs southward. Refraction velocity profile information from Demirbag (1990, Figure 27).

file, which shows higher refraction velocities in this area. Although no borehole to basement exists near this amplitude anomaly to confirm the basement lithology, the reflection amplitudes near borehole P5R also exhibit similar high amplitudes, but in a much smaller, restricted zone. Furthermore, the basement refraction velocity (4831 m/s) determined near P5R (Bonini and Woollard, 1960) is similar to that from Demirbag's profile (4800-5000 m/s) for the anomaly. In P5R the Triassic section was red claystone and siltstone containing calcareous nodules that was interpreted to represent subaerial caliche deposits (Marine and Siple, 1974). Possibly, these reflection amplitudes could denote similar lithology to that encountered in P5R.

Several small areas of low reflection amplitude are present north of the Pen Branch fault. Many of these areas can be identified as areas of low signal resulting from surface conditions (SRS-23, SRS-6 west end, Appendix B). At other locations the low amplitude values appear to be associated with faulting and might denote the presence of fractured rock (juncture of SRS-5 with SRS-6, west end of line SRS-6). The absence of any large areas of low amplitude basement reflections north of the Pen Branch fault would seem to preclude the possibility of any outliers of Triassic strata. Refraction stack sections could be used to further bear out this assertion.

The area of lower reflection amplitude defined by the northern half of seismic line SRS-12 south to the conjunction of lines SRS-4, SRS-7, and SRS-9 is strikingly similar in outline to the basement high in time-structure (Figure 41 on page 101) and a gravity low (Figure 16 on page 46). This area probably also defines a lithologic/structural boundary, perhaps associated with the Graniteville-Vaucluse pluton.

Amplitude of Yellow Marker Reflection

The amplitude variation of the Yellow Marker reflection, identified as representing the basal Ellenton Formation or the top of the Peedee Formation, was mapped in the same manner as the Basement reflection (Figure 63). All of the Conoco SRS seismic lines were used to construct the amplitude map; the PBF seismic lines were excluded for reasons discussed previously. Sonic logs and synthetic seismograms of this interval show that the amplitude anomaly is caused by thickness

variations of a low velocity clay layer at the K/T boundary. Two principal areas of northeast trending high reflection amplitudes exist. The first area occurs between Upper Three Runs and the Pen Branch fault with the highest values just southwest of the DRB borehole cluster. The second area is well localized, defined by the area along line SRS-3 south of Steel Creek to the junction with line SRS-8 and along line SRS-8 to the junction with line SRS-11 and including the northern half of that line.

The first area exhibits a branching pattern that interconnects isolated patches of higher amplitude across SRS. This pattern does not have any obvious relation to time-structure; however, a weak correlation with the Blue Marker-Yellow Marker isochron (Figure 52 on page 119) seems to be present. The amplitude anomaly occurs just southeast of the hinge line of isochron thickening, which suggests that the uplift north of Upper Three Runs led to localization of the clay layer - possibly as a stream channel. Hence, this clay interval might be evidence for an ancestral Upper Three Runs creek.

The location of the second area of higher amplitude appears to be in part structurally controlled. The southeastern boundary of the area is defined by the Meyers Branch fault (Figure 42 on page 102). The higher amplitudes are on the up block. In time-structure this area is a local flattening on the fault block defined by the Pen Branch fault and the Meyers Branch fault (Figure 41 on page 101). Unlike the first amplitude anomaly, this anomaly is localized on a structural high. The seismic data, isochron maps, and time-structure maps indicate that fault movement at SRS was ongoing during the Cretaceous and Tertiary with a consistent sense of movement; thus it is problematic that the clay facies, if it is indicative of stream channels, would be localized on a structural high. Perhaps the low velocity interval at this location denotes a different depositional environment.

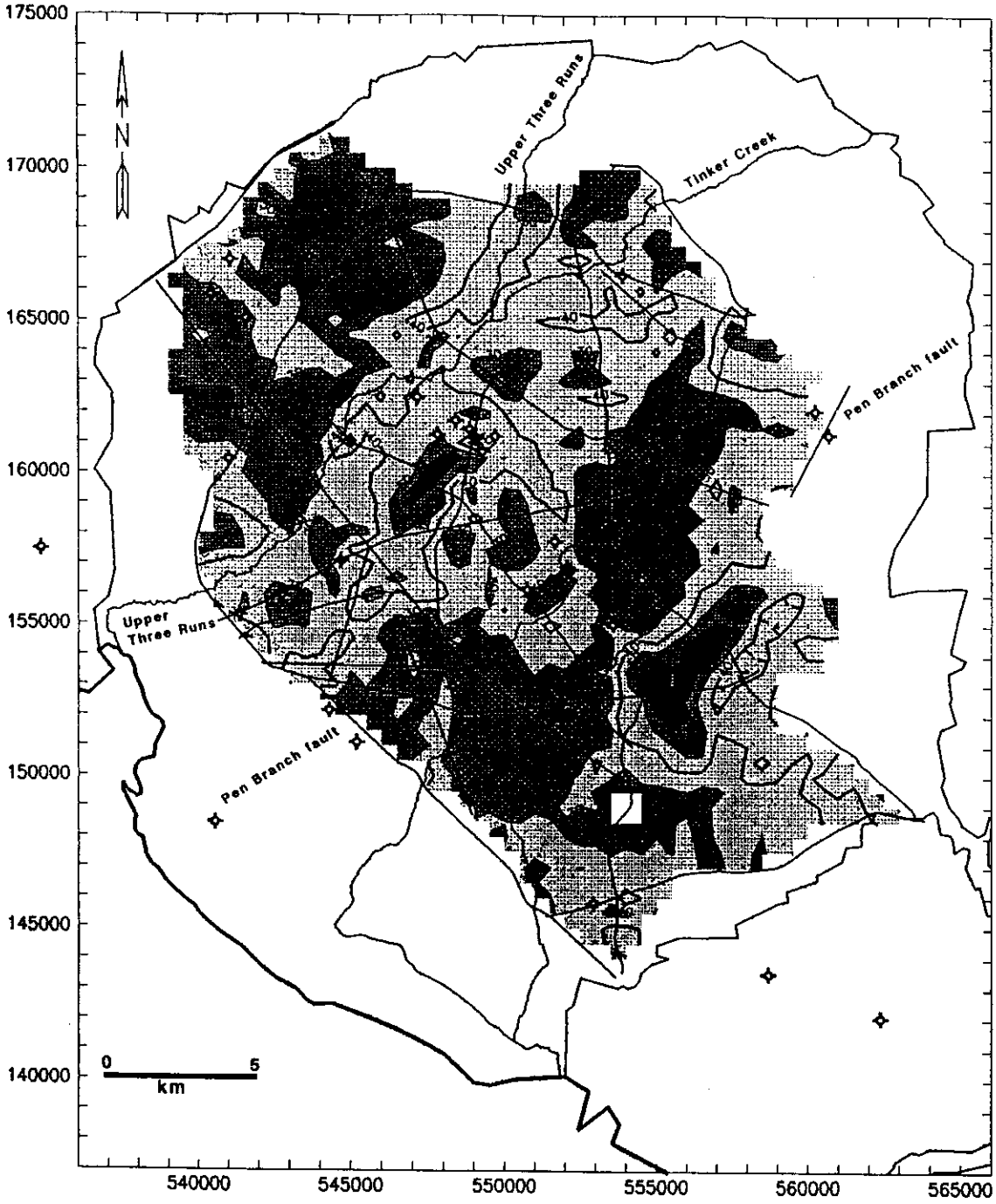

Figure 63. Amplitude of Yellow Marker reflection: Higher amplitudes are indicated by warmer colors, lower amplitudes by cooler colors. Contours are amplitude divided by 100,000. The high reflection amplitudes represent thickening of a low velocity clay layer at the K/T boundary, perhaps a stream channel facies within the basal Ellenton Formation. Note the northeast trend in the amplitude values.

Correlation of Borehole data to Seismic Reflection data

Correlation of the synthetic seismograms to the seismic reflection data to enable stratigraphic identification of the reflecting horizons was done interactively using the DLPS software previously described. Eleven of the synthetic seismograms listed in Table 3 on page 43 were correlated to the seismic reflection data. Nine of these synthetic seismograms were used to constrain the interpretation of four seismic profiles across the Pen Branch fault and a tenth synthetic seismogram was correlated to a nearby seismic line. Reflection horizons digitized from these seismic profiles were converted to depth using the time-to-depth relation developed from the synthetic seismograms and the results plotted as depth cross sections. For convenience only, the annotated formation tops are those tabulated by Berkman (1991) for the PBF boreholes.

A considerable body of geophysical literature is available on the correlation of synthetic seismograms to seismic reflection data (e.g. Sengbush et al., 1961; Anstey, 1977; Goetz et al., 1979). In essence, the problem is that rarely does a synthetic seismogram correlate directly to a reflection profile. The proposed reasons for misties include: violation of the zero-offset assumption, anelastic attenuation, poor velocity/depth sampling in the borehole domain, reflection smearing caused by CDP stacking, borehole invasion, etc.. Much of the problem with time-to-depth conversion and synthetic seismogram correlation can be avoided through the use of checkshots or vertical seismic profiles. As previously mentioned, in selected PBF series boreholes vertical seismic profiles were recorded; however, the geophones in these borehole surveys were placed only to a maximum of 100 m depth and high-fidelity time-to-depth conversion would require geophone locations along the entire length of the wellbore.

To obtain a usable correlation between a synthetic seismogram and a seismic profile the synthetic seismogram can be alternately stretched or compressed until a suitable correlation is reached. This process, done interactively in DLPS, also stretches or compresses the time-to-depth relation obtained by integrating the borehole sonic log. That is, the interval velocities are altered as per stretching in time; whereas the depth scale is unaltered. In this study, unless otherwise stated, all

of the synthetic seismograms correlated to seismic reflection profiles have been so stretched. The synthetic seismograms collected in Appendix C have not been stretched.

The correlation of synthetic seismograms with the seismic reflection data began with identification of the top-of-basement reflection. This reflection, actually the top of unweathered basement, is the most prominent reflection event throughout SRS and is usually unambiguously interpreted, although where Triassic basement is present the pick is occasionally less clear. Ties to reflections that originate from the Cretaceous section can generally be accomplished with a minimum of time shifting or stretching of the synthetic seismogram. Those reflections interpreted as probable unconformities, identified on the basis of lateral continuity of the reflection in the stacked section and sharp boundaries in the sonic log, are correlated with little difficulty. Other reflections in the Cretaceous section are more difficult to correlate and particularly those to boreholes located more than a few tens of meters from a seismic line. The correlation of synthetic seismograms to reflections that originate from the Tertiary section is uncertain owing to the lack of resolution of the vibroseis reflection data within 150-100 ms of the surface and the extremely variable velocity of the units. For the Tertiary formations often time shifts of several milliseconds were required to obtained a suitable correlation. As a result, the time-to-depth relation and reflection ties for units younger than Paleocene age should be approached with caution.

The problem of extreme velocity variations in the Tertiary strata is illustrated by correlation of the synthetic seismograms from the Confirmatory Drilling Project (CFD) holes to seismic line SRS-2EXP. For each of the eight boreholes along line SRS-2EXP synthetic seismograms were generated in the manner previously described and the time-to-depth relation from the sonic logs was used, without time shifting or stretching, to convert the seismic section to depth (Figure 64). The resulting depth section shows an irregular, wavy reflection geometry that is not borne out by correlation between various geophysical logs in depth (Stieve et al., 1993). Hence, the time-to-depth relation is suspect and the problem probably arises because of the factors previously mentioned as well as from the velocity values used to fill to the surface and/or datum. It was for this reason that the synthetic seismogram correlation for the deeper boreholes proceeded from first tying to the top of basement reflection.

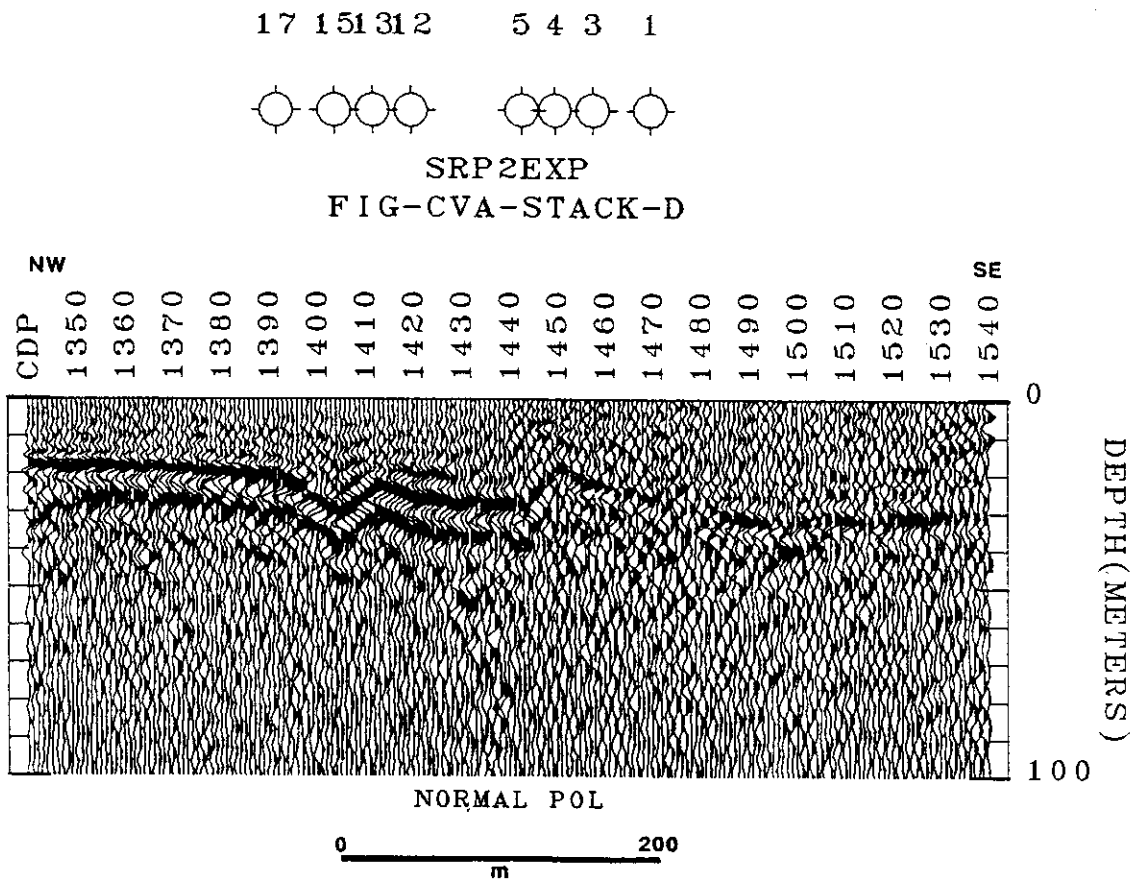

Figure 64. Seismic line SRS-2EXP converted to depth: Result of depth conversion of part of line SRS-2EXP using depth-to-depth relations developed from the synthetic seismograms without either stretching the seismograms or using variable datum correction velocities.

Cross Sections

Synthetic seismograms from boreholes PBF-1, PBF-2, PBF-3, PBF-4, PBF-5, PBF-7, CFD-1, CFD-18, DRB-8, and DRB-9 were correlated to the following seismic profiles: SRS-7 (PBF-4, PBF-5), SRS-2EXP (CFD-1, CFD-18), PBF-18 (PBF-3, PBF-7, DRB-9), SRS-28 (PBF-1, PBF-2) and SRS-5 (DRB-8). The time-to-depth relations were derived from the time stretched synthetic seismograms and were linearly interpolated between the boreholes. Because most of boreholes do not penetrate basement rocks more than a few meters, the bottom of the time-to-depth logs were padded with average velocities of 5700 m/s for crystalline basement and 5000 m/s for Triassic basement. The location of the tie between a borehole and a trace on a seismic profile was based on the projection along geologic strike of the borehole location to the seismic line followed by lateral shifting of the synthetic seismogram to match the reflection character of the seismic profile.

SRS-7: Boreholes PBF-4 and PBF-5 tie to seismic line SRS-7 at CDPs 1559 and 1394 respectively (Figure 65 and Figure 66). The Pen Branch fault at this location is a relatively simple structure and does not exhibit the complex antithetic faulting found at other locations. The growth fault nature of the Pen Branch fault is evident from the thinning of units on the hanging wall. Minor faults bounding small fault blocks are imaged northwest of the Pen Branch and southeast of the Pen Branch fault a splay of the Steel Creek fault is imaged. In the depth cross section, the thickness of the saprolite zone on the footwall of the Pen Branch fault is probably exaggerated by the fill velocity used to pad the time-to-depth log. Similarly, the thickness of the Green Marker is also exaggerated southeast of borehole PBF-5.

SRS-2EXP: The two deep boreholes from the Confirmatory Drilling Project, CFD-1 and CFD-18, tie to line SRS-2EXP at CDPs 1470 and 1394 respectively (Figure 67). The Pen Branch fault develops a minor splay and antithetic faults are imaged at this location. The results of the Confirmatory Drilling Project indicated that at this location the deformation associated with the

Line SRS-7

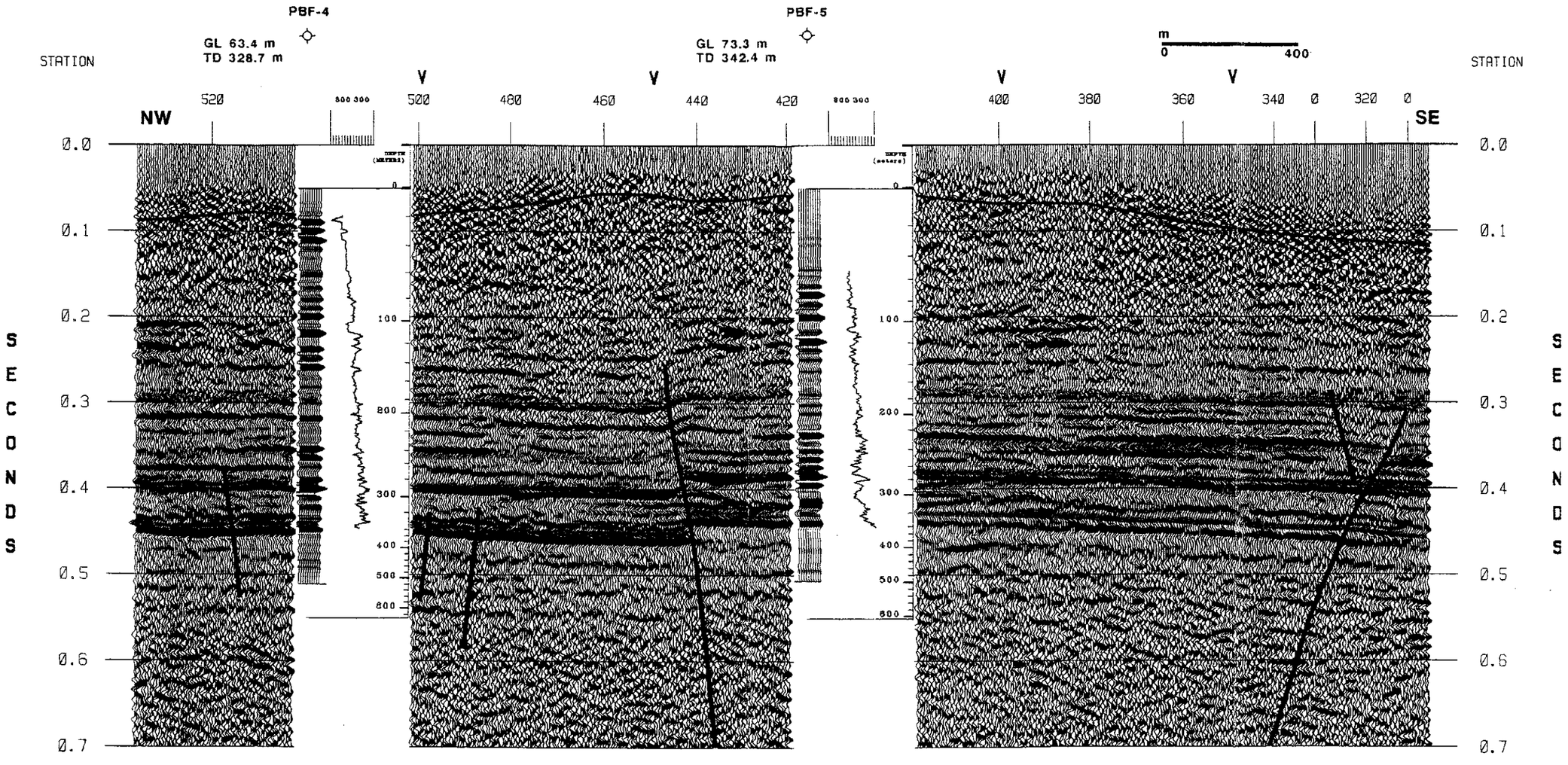

Figure 65. Synthetic seismogram ties to line SRS-7: Ties of synthetic seismograms and sonic logs from boreholes PBF-4 and PBF-5 to seismic line SRS-7. Wavelet 30-35-110-120 Hz bandpass.

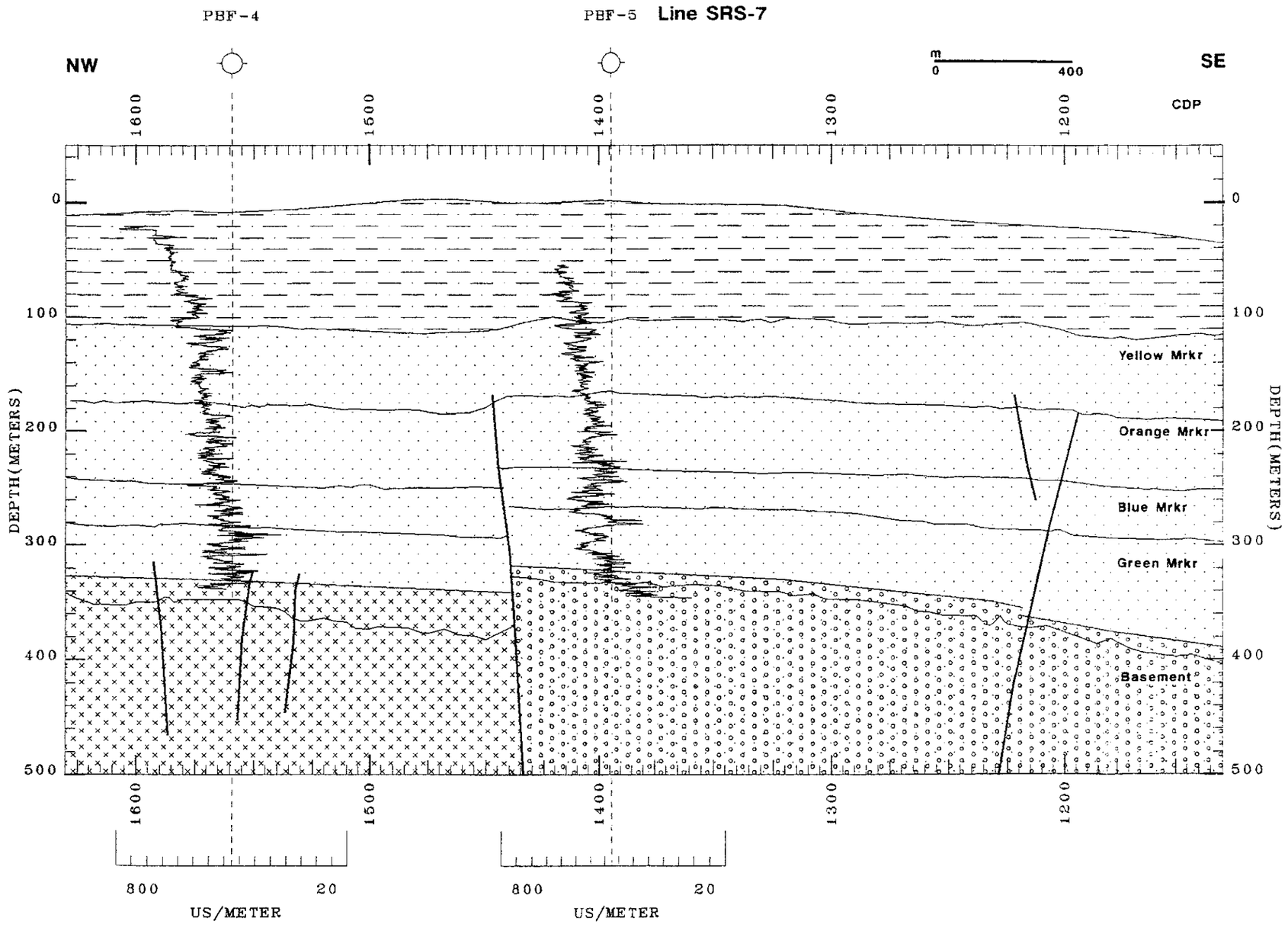

Figure 66. Depth cross section along line SRS-7: Zero depth corresponds to 80 m.

Pen Branch fault extends upward to at least the base of the Congaree Formation and perhaps as high as the Eocene Dry Branch Formation (Stieve et al., 1993).

PBF-18: Boreholes PBF-3 and PBF-7 tie to seismic line PBF-18 at CDPs 1376 and 598 respectively (Figure 68 and Figure 69). The deep sonic log from DRB-9 was spliced into the sonic log from PBF-7 to create nearly complete velocity coverage from the Coastal Plain into basement. A minor down-to-northwest fault is imaged within the Pen Branch fault zone. The geometry of the Pen Branch fault along line PBF-18 is similar to what was observed along line SRS-7.

SRS-28: The PBF-1 and PBF-2 boreholes tie to seismic line SRS-28 at CDPs 544 and 356 respectively (Figure 70 and Figure 71). The correlation of the synthetic seismogram from PBF-1 to line SRS-28 revealed that several meters of the lower Black Creek Formation were missing in the borehole. This missing section, possibly caused by translational movement along the Pen Branch fault, results in an incorrect time-to-depth relation. For this reason the Orange Marker is thinner on the footwall than on the hanging wall of the Pen Branch fault in the depth converted cross section. The time section, however, shows that Orange Marker is indeed thicker on the footwall as would be expected for growth faulting.

Unlike the other cross sections across the Pen Branch fault, no faults appear to be be present northeastward of the Pen Branch fault; however, because of the oblique strike of line SRS-28 to the fault the profile might be insufficiently long to detect their presence. Two small faults are detected that originate within the Dunbarton basin and penetrate upward into the Coastal Plain sediments. These faults are down-to-the-northeast faults similar to the Pen Branch fault.

The Pen Branch fault imaged along line SRS-28 is a complex structure (zone) consisting of three closely spaced faults that propagate upward from the basement or splay just above basement. Movement along the two northwesternmost faults was not sufficient to affect sedimentary units above the Green Marker (Cape Fear Formation). The northwestern branch of the southeastern fault was active through Blue Marker (Middendorf Formation) deposition to cause thinning of the

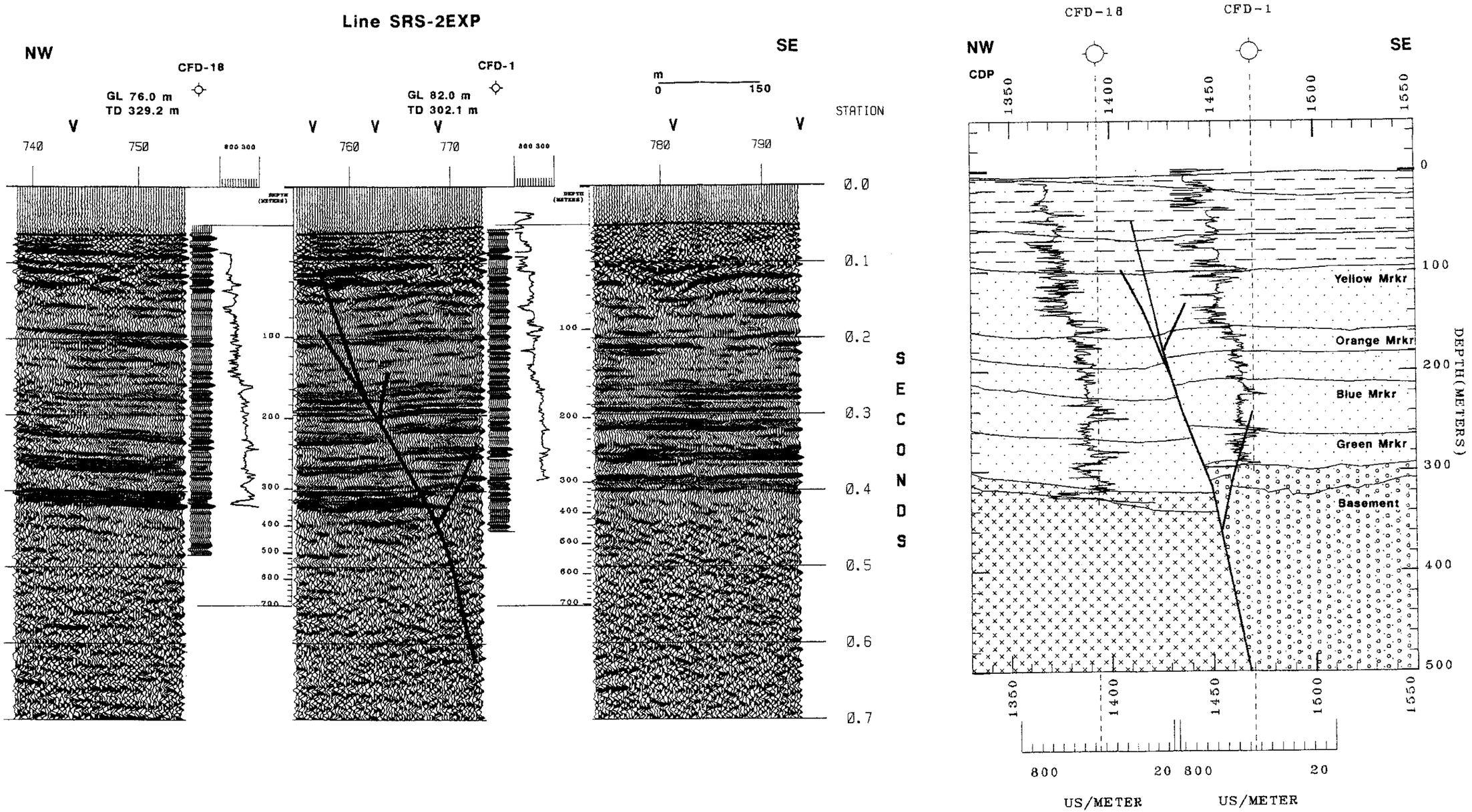

Figure 67. Time and depth cross section along line SRS-2EXP: Ties of synthetic seismograms and sonic logs from boreholes CFD-18 and CFD-1 to seismic line SRS-2EXP and depth cross section. Wavelet 35-40-150-160 Hz bandpass. Zero depth corresponds to 80 m

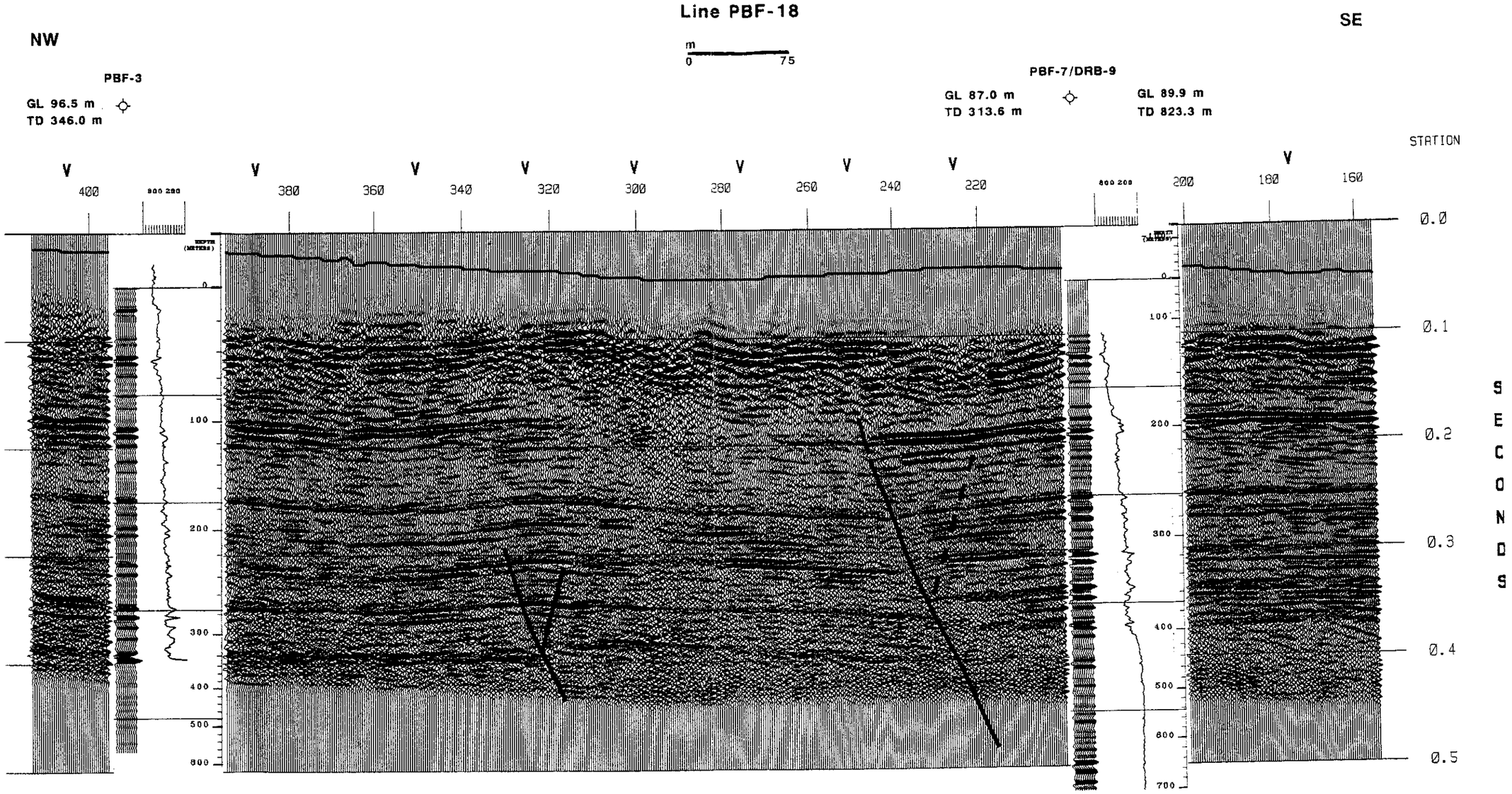

Figure 68. Synthetic seismogram ties to line PBF-18: Ties of synthetic seismograms and sonic logs from boreholes PBF-3, PBF-7 and DRB-9 to seismic line PBF-18. Wavelet 90 Hz Ricker.

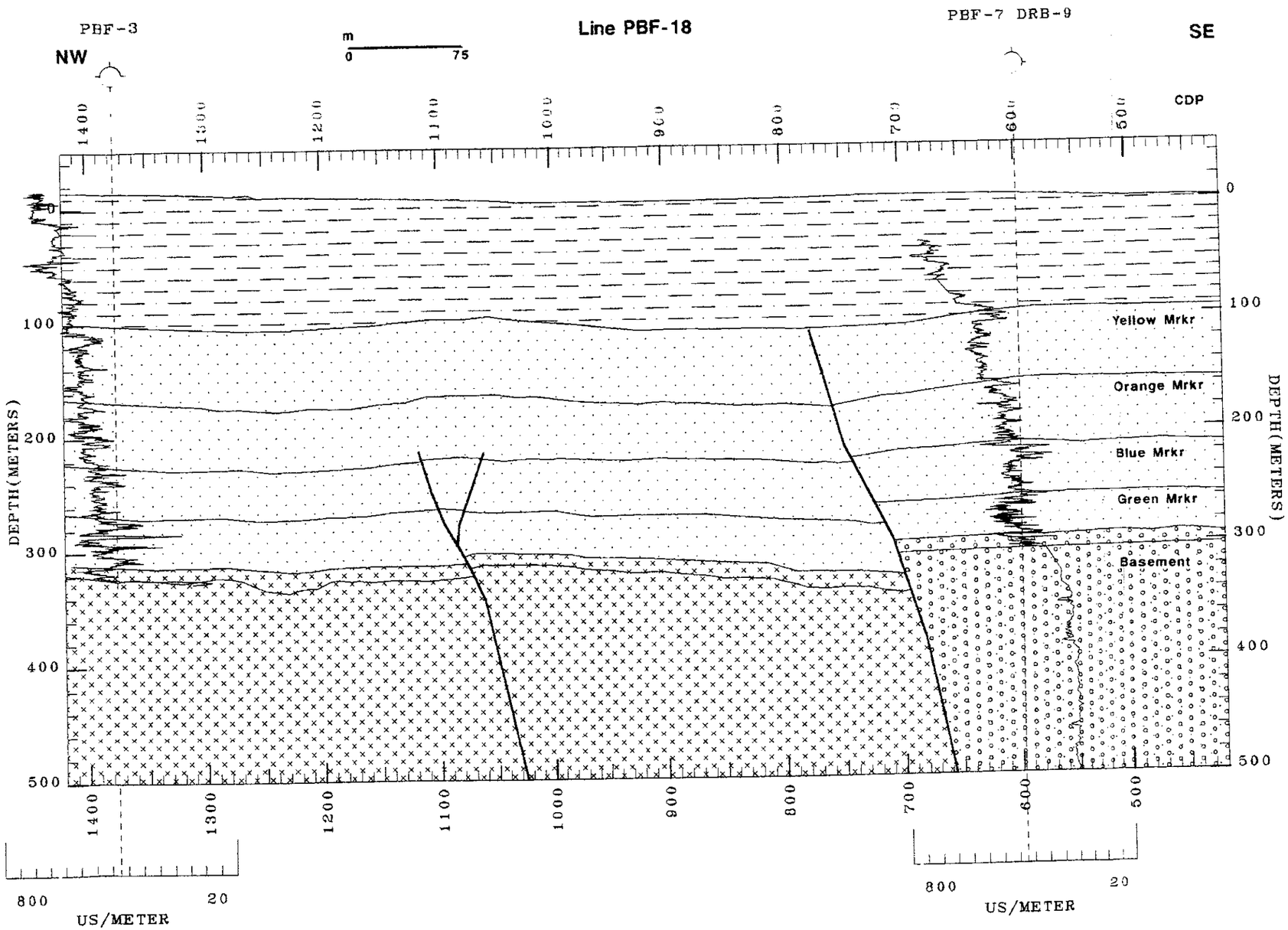

Figure 69. Depth cross section along line PBF-18: Zero depth corresponds to 80 m.

isopach across the fault, but later movement caused minimal disruption of younger layers. The southeastern branch of the fault shows mostly post-Blue Marker activity.

SRS-5: Borehole DRB-8 from the Bedrock Depository Program ties to line SRS-5 at CDP 508 (Figure 72). The change in reflection amplitude of the Yellow Marker in this area of line SRS-5 is not seen in the DRB-8 synthetic seismogram or sonic log, which suggests that the amplitude decrease of this marker from CDP 420 to CDP 480 extends eastward to this location.

The top of basement in DRB-8 was repicked in this study after initial attempts to tie the synthetic seismogram to line SRS-5 using the value published by Siple (1967) and Marine (1976) were unsuccessful. The new top of basement pick of -201.1 m (BSL), based on sonic log and temperature log character, is similar to those reported for the other DRB boreholes.

At least two small down-to-the-northeast faults were detected on this profile in the vicinity of the DRB cluster. These faults trend north-northeastward (Figure 42). Marine (1976) reported fluid flowing in fractures in DRB-8 (KB 81.9 m) at 329.2 m, 422.1 m, 475.5 m and 481.6 m depth. Possibly the faults mapped north of DRB-8 are penetrated by the borehole, which would confirm these faults as reverse faults.

Faults in the Coastal Plain - Summary and Discussion

Pen Branch Fault: The Pen Branch fault is the northwestern boundary fault of Dunbarton basin; however, within the Coastal Plain sediments the fault is a high-angle, southeast-dipping reverse fault. The Pen Branch fault is an example of structural inversion where the original normal fault has been reactivated under compression following infilling of the basin (Triassic) and peneplanation of the current basement surface (Late Cretaceous). The Pen Branch fault is the dominant throughgoing fault in a 3 km wide fault zone parallel to the northwestern margin of the Dunbarton basin (Figure 42 on page 102). Within this zone faults occur subparallel to the Pen Branch fault and locally develop splays. The trace of the Pen Branch fault does not appear to be offset along

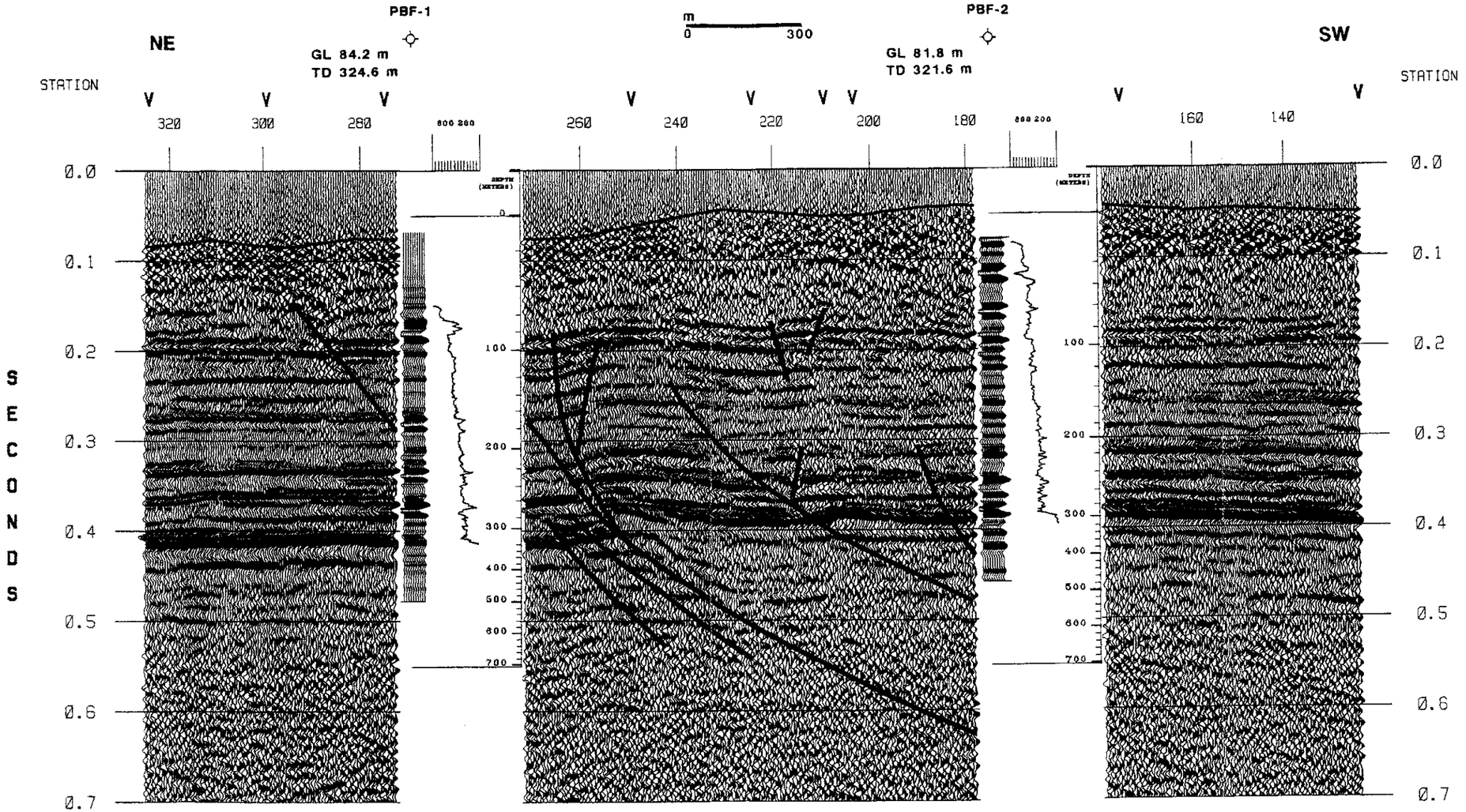

Figure 70. Synthetic seismogram ties to line SRS-28: Ties of synthetic seismograms and sonic logs from boreholes PBF-1, and PBF-2 to seismic line PBF-28. Wavelet 30-35-110-120 Hz bandpass.

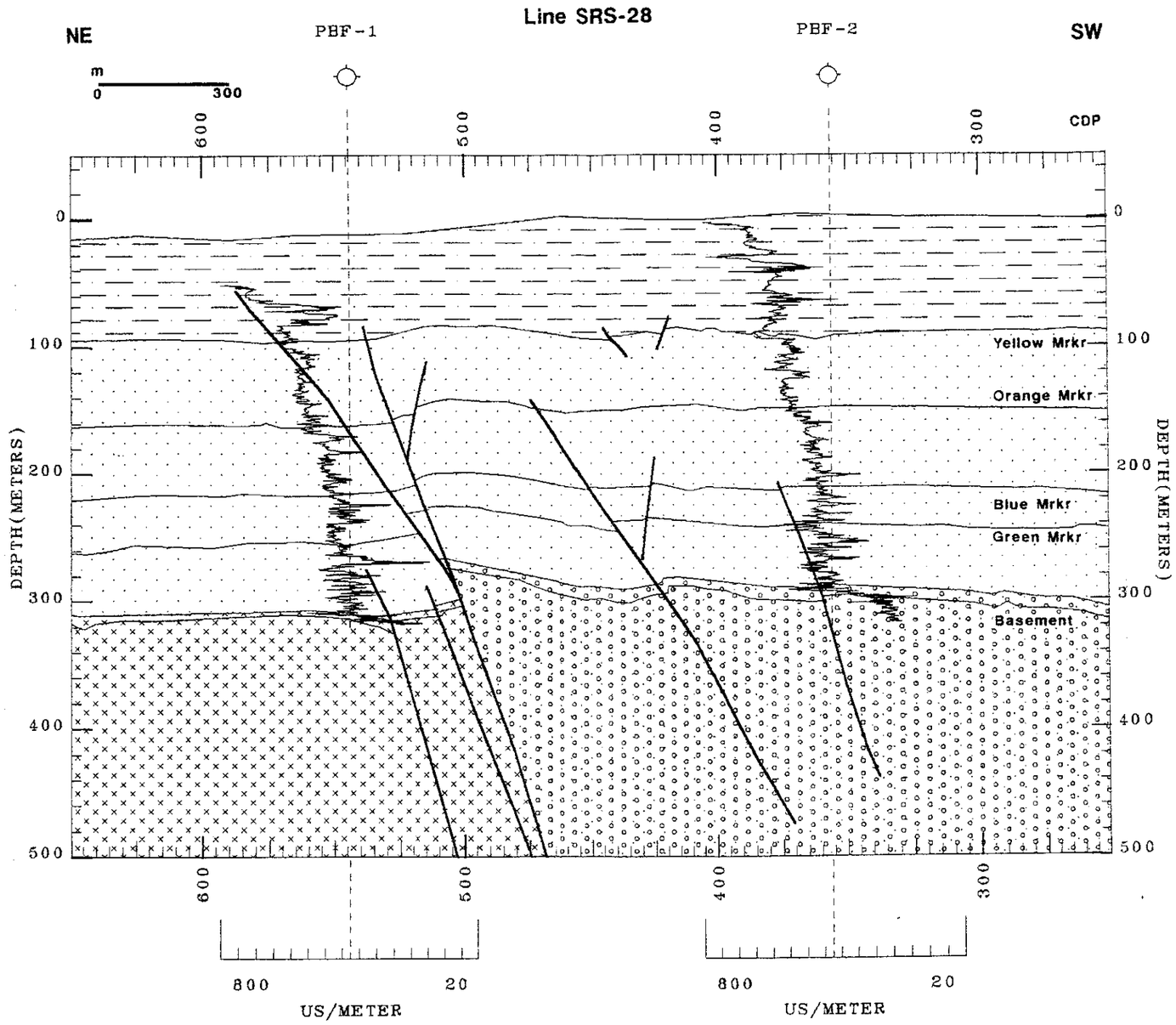

Figure 71. Depth cross section along line SRS-28: Zero depth corresponds to 80 m.

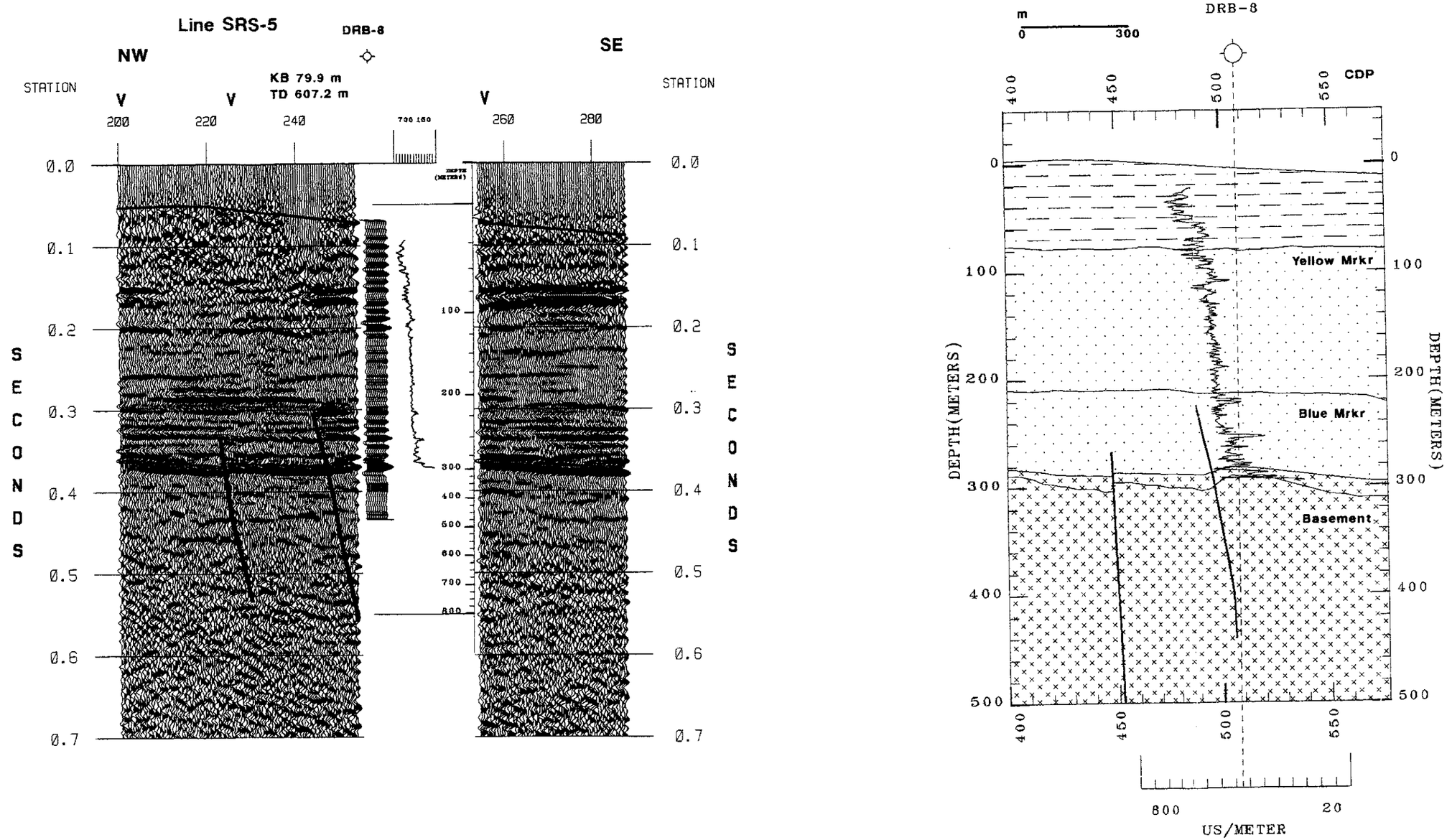

Figure 72. Time and depth cross section along line SRS-5: Tie of synthetic seismogram and sonic log from borehole DRB-8 to seismic line SRS-5 and depth cross section. Wavelet 30-35-110-120 Hz bandpass. Zero depth corresponds to 80 m

its length at any structural level, contrary to interpretations by Chapman and DiStefano (1989) and Anderson (1990). Any transfer faults that exist along the northwestern boundary of the Dunbarton basin occur outside the coverage of the seismic data set. Faults within crystalline basement parallel to the Pen Branch fault tend to be down-to-the-northwest reverse faults, whereas faults in the Triassic basement tend to be down-to-the-southeast reverse faults, i.e. backthrusts (Figure 42 on page 102). The Steel Creek fault appears to be one of these backthrusts (Figure 44 on page 104).

The Pen Branch fault is defined only at SRS; its extension to the northeast and southwest is a matter of conjecture. Northeastward of seismic line SRS-28 through seismic line PBF-6 the strike of the fault changes to N70°E. Berkman (1991) interpreted the fault as present on seismic line PBF-7, 0.5 km northeastward of line PBF-6. The C-5 borehole 9 km east-northeastward of line PBF-6 encountered crystalline basement rock (Snipes et al., 1993a) and near C-5 the USGS seismic refraction experiment detected low velocity basement rocks interpreted to be the Dunbarton basin (Luetgert et al., 1994). If the Dunbarton basin extends eastward as far as the C-5 borehole, then projection of the Pen Branch fault through line PBF-7 to hole C-5 gives a strike for the fault of N 78°E.. Bouguer gravity data shows the gradient associated with the fault parallels this trend northward and eastward through the southern edge of gravity low associated with the Springfield pluton (Figure 18 on page 50). Speer (1982) interpreted the alteration of granite in the SAL-1 borehole core as probably Mesozoic in age and perhaps related to the border fault of the Dunbarton basin. Examination of seismic line Seisdata Line 4 (Behrendt, 1985) does not show evidence of faulting at an interpreted projection of the Pen Branch fault; however, the scale of presentation of this line makes a detailed interpretation difficult. Evidence for continuation of the Pen Branch fault to the southwest off SRS is also uncertain. No conclusive evidence for the Pen Branch fault is seen on line Seisdata Line 6, but the small size display is difficult to interpret. Again, the gravity data would suggest that the anomaly associated with the flank of the basin continues to the southwest into Georgia.

Movement along the Pen Branch fault was ongoing through the Late Cretaceous (Santonian) to at least the Late Eocene (Priabonian). Graphs of the offset of horizons by the Pen Branch fault versus depth and age of offset horizon derived from borehole and seismic data illustrate the growth

fault nature (Figure 73). The rate of vertical movement along the Pen Branch fault during 85-38 Ma ranges from 0.0-1.0 m/m.y. for selected horizons. The average rate of vertical movement during that time was 0.22 m/m.y. as determined by linear fit to the offset versus age of offset horizon graph. This rate is less than the average 0.4 m/m.y. rate determined by Snipes and others (1993a) using borehole data. Movement along the Pen Branch fault during this time was at a slower rate than along the nearby Belair fault zone, and indeed, was slower than along any of the fault zones in the Atlantic Coastal Plain compiled by Prowell (1988) (Figure 74). Interestingly, the age of offset horizon versus offset curves for the Pen Branch fault and other Atlantic Coastal Plain faults appear to project through the origin, which suggests ongoing fault movement. Moreover, because most of these faults exhibit similar rates of vertical movement (0.2-0.8 m/m.y.), Prowell (1988) proposed that this result points to a common causative mechanism for the faulting - ridge push. If the state of crustal stress is assumed to have been relatively constant since the post-Jurassic development of the passive margin, then ongoing movement of these faults is likely.

The absolute limit of upward penetration of the Pen Branch fault into the Atlantic Coastal Plain sediments is uncertain. Within the resolution of these seismic data, no clear disruption of reflections shallower than 10-20 ms above the K/T boundary is observed; however, deformation associated with the fault appears to affect the shallowest resolvable time horizons (e.g. see Figure 67 on page 145 and Figure 70 on page 149). The results of the Confirmatory Drilling Project along seismic line SRS-2EXP indicate that deformation associated with the Pen Branch fault persists to at least the level of the Late Eocene Dry Branch Formation (Stieve et al., 1993). Above this level the interpretation of the borehole data is less certain, and any scour and fill structures in the shallow sedimentary units can confuse the issue. Topographic profiles across the Pen Branch fault taken from the SRS seismic lines show the suggestion of a topographic anomaly associated with the fault (Figure 75). Furthermore, recent geomorphic work suggests that drainages along the projected surface trace of the Pen Branch fault have been rejuvenated, perhaps as a consequence of local tectonic uplift and tilting (Hanson et al., 1994) These phenomena, as with the map standardization analysis presented earlier, are compelling, but not conclusive evidence that deformation associated with the Pen Branch fault persists to the surface.

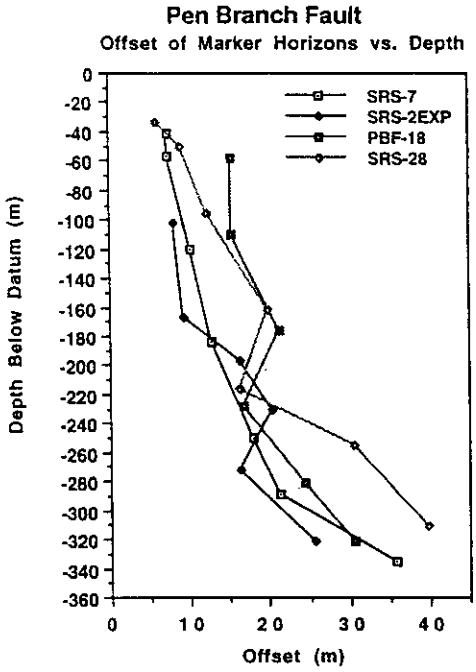

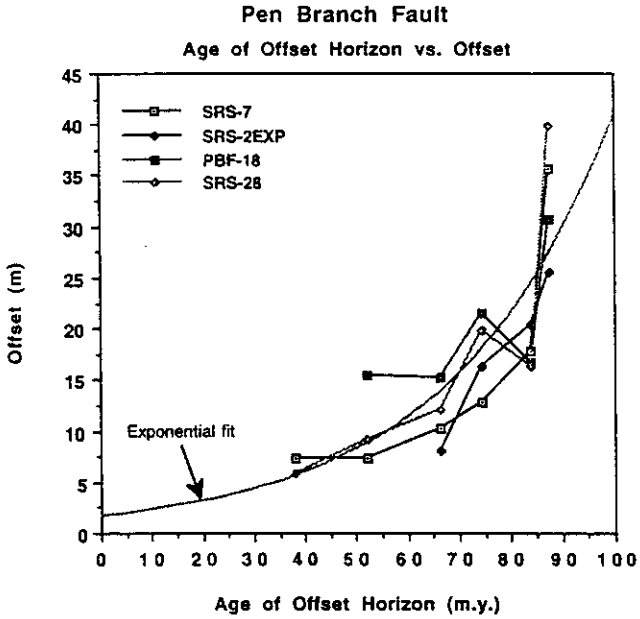

Figure 73. Pen Branch fault: Offset vs. depth and Offset vs. time: The movement history of the Pen Branch fault is plotted for the four depth converted cross sections across the fault. The Pen Branch fault is a growth fault; thus, these graphs represent the cumulative offset of any given marker. The average rate of vertical movement along the Pen Branch fault is 0.22 m/m.y. For Cretaceous age markers, fault offset is measured from the cross sections, where offset is defined as the maximum displacement of a marker either as a break or as the amplitude of a drape fold. For the Tertiary age markers (Green Clay and Tan Clay), the fault offsets are calculated from borehole picks reported by Berkman (1991). The geologic age of the markers are as reported by Fallaw and Price (1992) and Snipes and others (1993a).

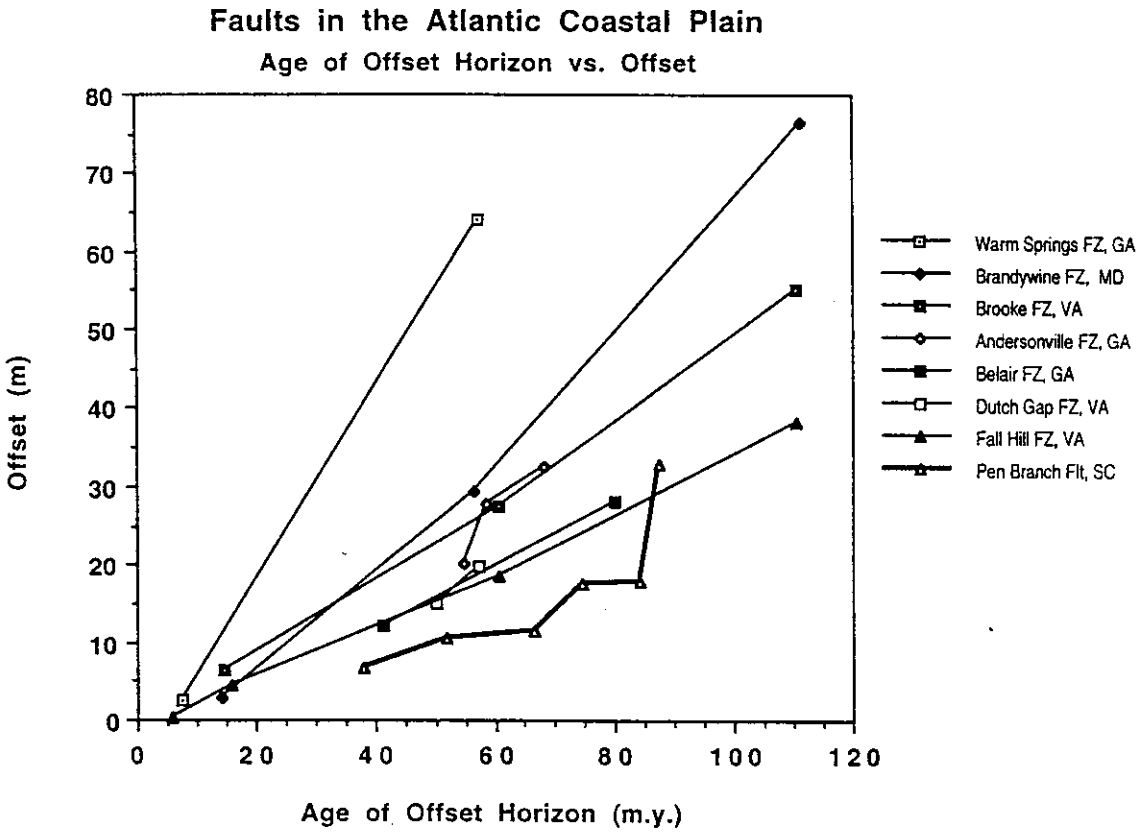

Figure 74. Atlantic Coastal Plain faults - Fault offset vs. time: Vertical movement along the Pen Branch fault was at a slower rate than for other faults in the Atlantic Coastal Plain. Note that the curves appear to project through the origin, which suggests ongoing fault movement. The data presented for the Pen Branch fault are averages for selected horizons. Data for the other fault systems are as compiled by Prowell (1988).

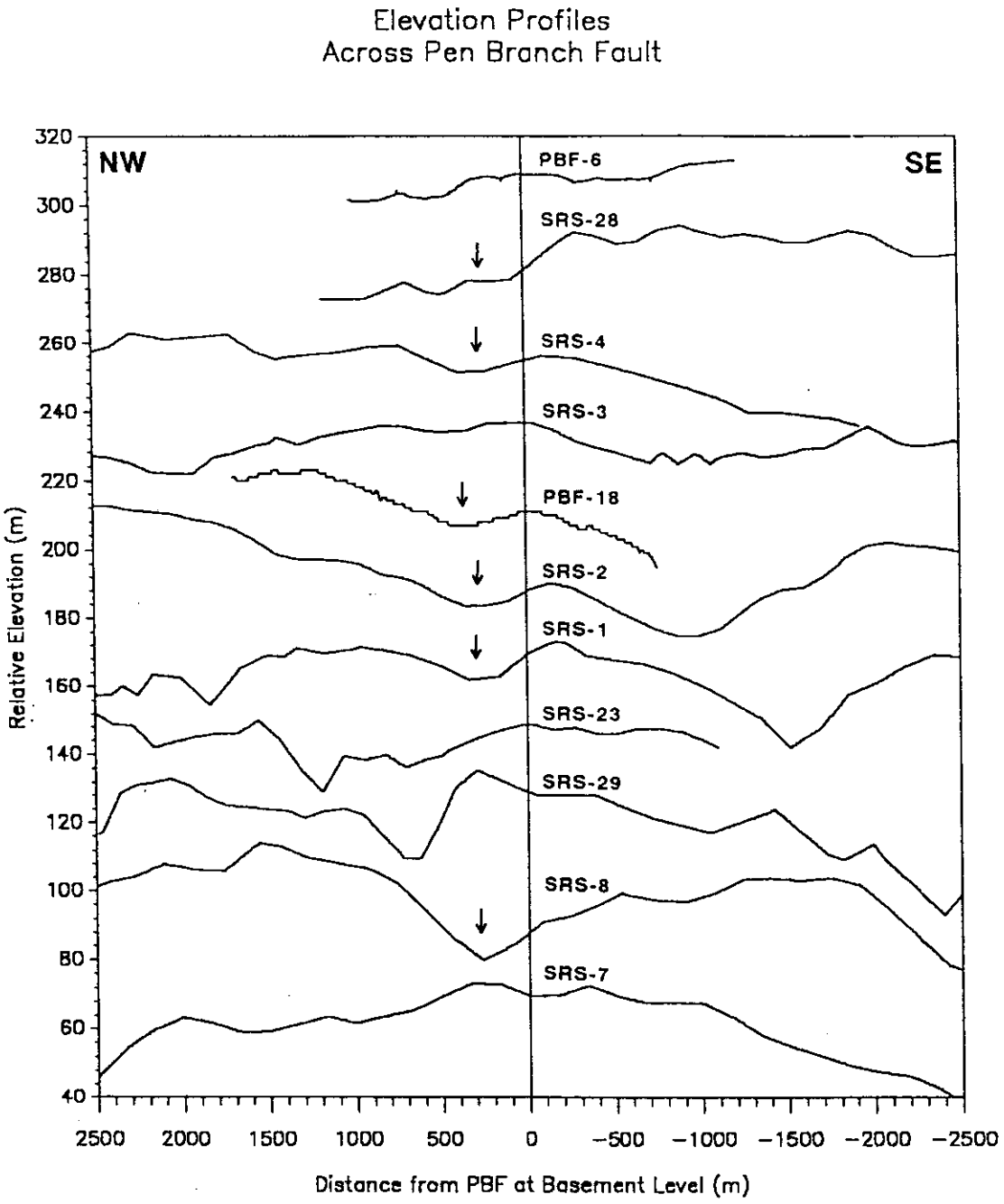

Figure 75. **Elevation profiles across the Pen Branch fault:** Elevation profiles from seismic reflection lines crossing the Pen Branch fault. Profile directions are north to south left to right and west to east bottom to top. The zero distance reference is where the fault offsets the top of basement reflection. Note on many of the profiles a shallow ≃4-6 m depression occurs ≃200 m north of the zero line (indicated by arrows) suggestive of a topographic anomaly associated with a southeast dipping Pen Branch fault. This feature is best exhibited on seismic lines SRS-8, SRS-1, SRS-2, SRS-4, SRS-28 and PBF-18.

Investigations conducted elsewhere in South Carolina have shown that deformation associated with reactivated basement faults is part of present-day topography (Marple and Talwani, 1993; 1994). The Pen Branch fault in this regard would not be unusual if this were the case. Given that rates of erosion in the Coastal plain are approximately 20 m/m.y. (Geomatrix Consultants, 1993), two orders of magnitude greater than the rates of faulting, any topographic expression associated with the fault is most likely exhumed.

Tinker Creek fault: The Tinker Creek fault (TCF) is a new discovery. The fault on seismic line SRS-27 was previously interpreted to be the ATTA fault, a north-south trending feature (Chapman and DiStefano, 1989; Stephenson and Stieve, 1992). The TCF is unambiguously interpreted on seismic lines SRS-27, SRS-9, SRS-3, SRS-4 and SRS-2 where it is a down-to-the-northwest fault subparallel to the Pen Branch fault (Figure 42 on page 102 and Figure 76). On seismic line SRS-27 the TCF develops secondary faults above the Middendorf Formation that are reminiscent of flower structures and suggests possible strike-slip movement along the fault. The maximum offset of the basement reflection, 24 ms ($\approx$ 24 m) on line SRS-27, is similar to that of the major faults at SRS. The throw of the Tinker Creek fault within the Coastal Plain sediments increases to the northeast at about the same rate as the Pen Branch fault (Figure 77). From this it is inferred that both faults share a common movement history, albeit dip-slip movement on the Pen Branch fault is at a higher rate. Examination of the deep seismic reflection data reveals the fault to be a southeast dipping thrust that faults the northwest limb of an antiform (Figure 26 on page 68); thus, the TCF is a reactivation structure similar to the Pen Branch fault.

West of seismic line SRS-2 the trace of the TCF projects to the skip in the seismic coverage on line SRS-1 at Upper Three Runs. If the trend of the time offset of the fault as shown in Figure 77 is considered, then it is likely that any offset present at this location is below the resolution limit of these data. In addition, correlation of the deep TCF structure across SRS places the fault near the bend in seismic line SRS-7 at Upper Three Runs. Inspection of line SRS-7 no conclusive evidence for a fault in the Coastal Plain sediments near that location (stations 950-1050, Appendix B); therefore, the Tinker Creek fault probably dies out in the Coastal Plain sediments

Seismic Expression of Tinker Creek Fault

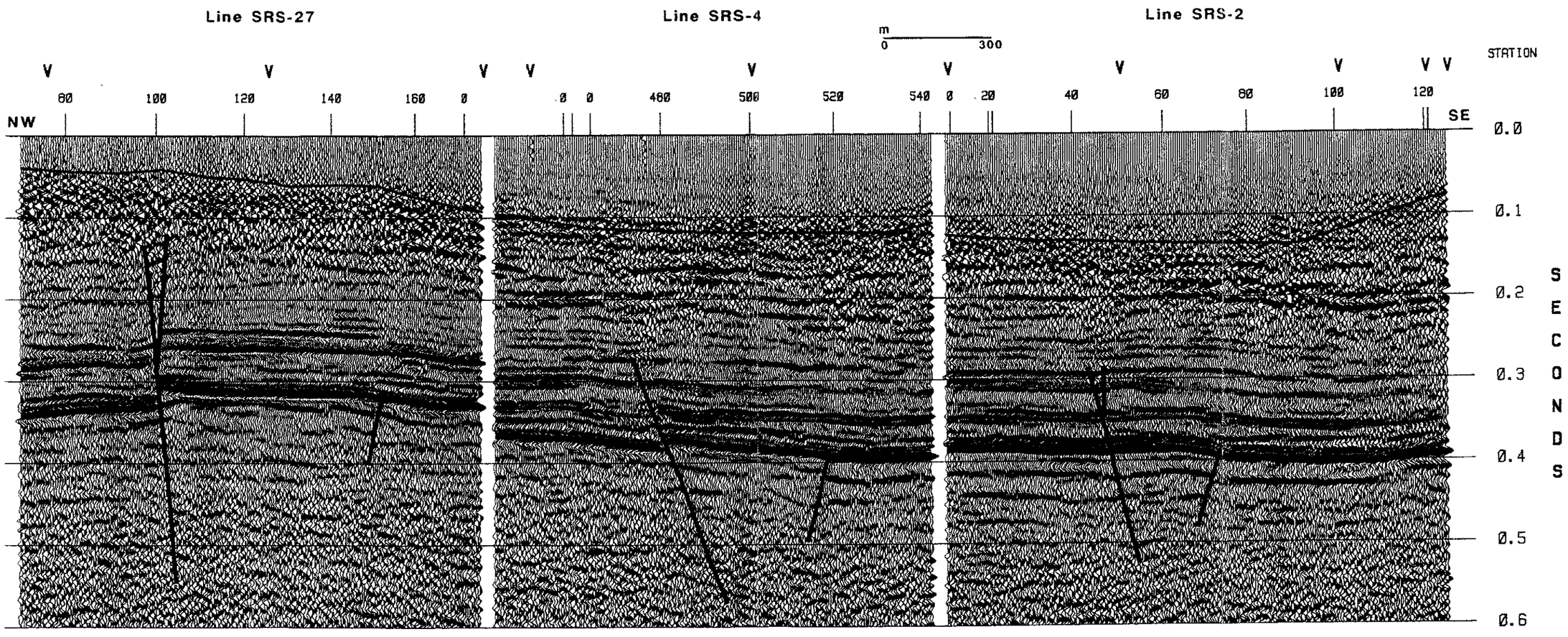

Figure 76. Seismic expression of the Tinker Creek fault: Seismic lines SRS-27 (left), SRS-4 (middle), and SRS-2 (right). The time offset of reflections by the Tinker Creek fault increases to the northeast at a rate similar to that of the Pen Branch fault.

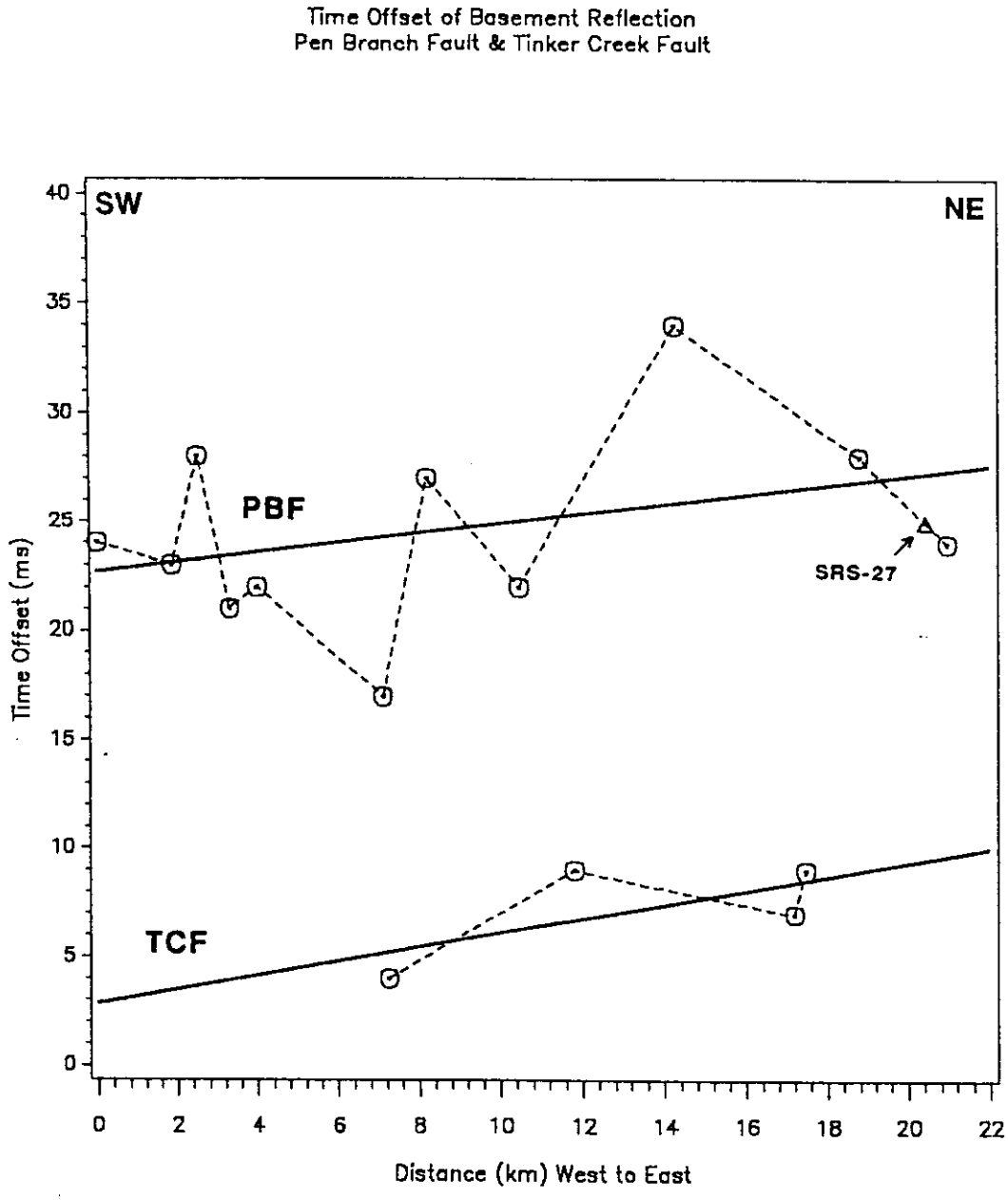

Figure 77. Basement reflection time-offset across PBF and TCF: The time-offset of the Basement reflection across both the Pen Branch fault and the Tinker Creek fault increase to the northeast at similar rates. Note the time-offset across the Tinker Creek fault on seismic line SRS-27 (triangle) does not fit the trend determined for lines SRS-2, SRS-4, SRS-3 and SRS-9.

west of line SRS-2. This conclusion is at variance with an earlier interpretation of these data, based on straight line projection of the fault trace, that the fault became a down-to-the southeast fault on line SRS-7 (Domoracki, 1994a).

Major movement on the Tinker Creek fault is probably post-Cretaceous. Unlike the Pen Branch fault, or the deep Upper Three Runs fault, no appreciable thinning of isochrons over the TCF is noted (Figure 78). This observation implies that fault movement was too slow during the Cretaceous to significantly affect sedimentation. The absence of an isochron anomaly, however, does not preclude the possibility of a significant isopach thin across the fault. Accurate knowledge of the velocity field in the vicinity of the fault is necessary to verify this interpretation. Yet, the time-offset of the basement reflection along SRS-27 is as large as any fault in the Coastal Plain at SRS. If movement on the TCF during the Cretaceous was too slow to significantly affect sedimentation, then the faulting that resulted in the basement offset along SRS-27 must be later. In support of this inference, elevation profiles across the Tinker Creek fault taken from the SRS seismic lines show a probable topographic anomaly associated with the fault (Figure 79). On seismic line SRS-27 a distinct "bump" in the topographic profile is noted at the position of the TCF. In this area recent work with ground penetrating radar has revealed the presence of faulting to within a few meters of the surface (D. Wyatt, WSRC, 1993, personal communication). This evidence suggests that the latest movement along the Tinker Creek fault at SRS-27 is Eocene or younger - inasmuch as Eocene sediments are generally the youngest sediments exposed at SRS.

Large Tertiary age movements along any of the faults at SRS is problematic. Post-Jurassic faulting in this area and in other areas of the Atlantic Coastal Plain is dominantly growth faulting implying steady rates of fault movement since the establishment of the current stress regime 80 Ma (Prowell, 1988; Gardner, 1989). Seismic line SRS-27 is at the northeast edge of the SRS seismic reflection grid and a lack of data precludes speculation of the origin of the apparent large Cenozoic fault movement in this area. Additional data is needed to determine the age and timing of movement along the Tinker Creek fault.

Faults and fault systems in the Atlantic Coastal Plain are typically characterized by *en echelon* fault segments where strain is transferred from fault segment to fault segment such that vertical

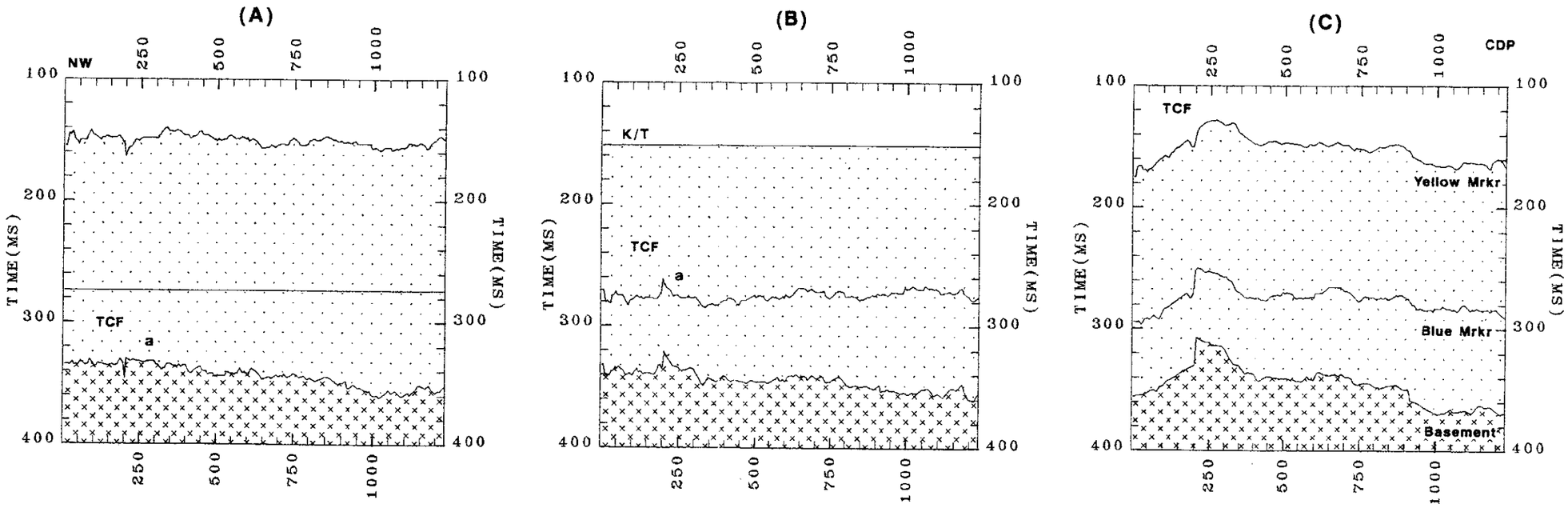

Figure 78. Reflection horizon flattening across TCF: Flattening of digitized horizons across the Tinker Creek fault (TCF) on line SRS-27 shows a barely discernible isochron thin (a) above the hanging wall. The absence of isochron changes across the fault suggests that vertical fault movement during the Cretaceous was too slow to appreciably affect sedimentation and that major movement on the fault is post-Cretaceous. (A) = horizon flattening on the Blue Marker, (B) = horizon flattening on the Yellow Marker, (C) = present-day time-structure. Vertical exaggeration ≈ 24:1.

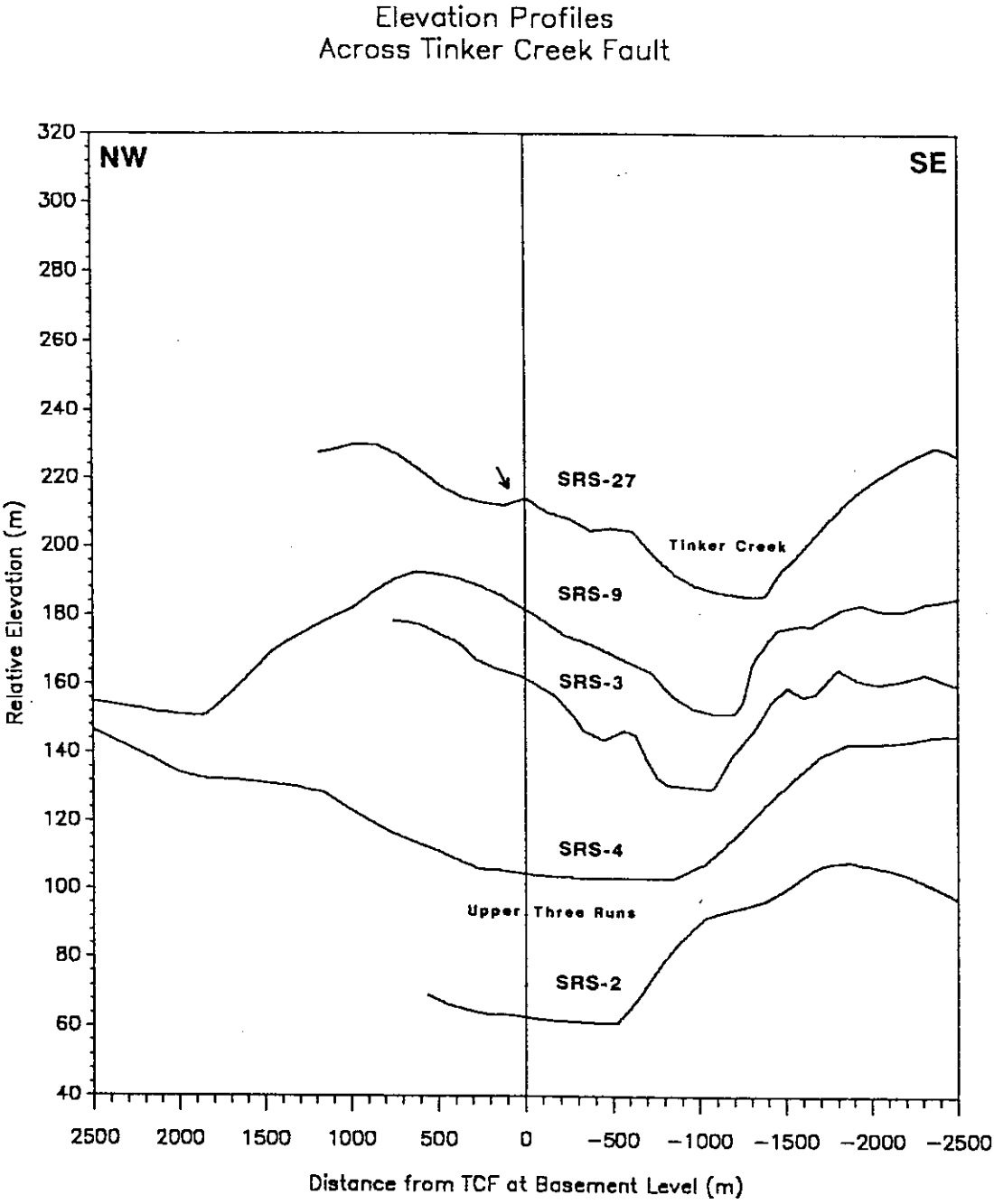

Figure 79. Elevation profiles across the Tinker Creek fault: Elevation profiles from seismic reflection lines crossing the Tinker Creek fault. Profile directions are north to south left to right and west to east bottom to top. The zero distance reference is where the fault offsets the top of basement reflection. Note the marked asymmetry of profiles across Upper Three Runs and Tinker Creek having steep southeast sides and broader northwest sides. The profile along seismic line SRS-27 exhibits what could be a topographic anomaly associated with the fault (indicated by arrow).

displacement occurs along a zone (Prowell, 1988). The Pen Branch fault and the Tinker Creek fault together might represent such a zone where strain is transferred from the Tinker Creek fault to the Pen Branch fault. In this model, only a small part of the fault system occurs within the confines of the Savannah River Site. The length of the fault system, by analogy to the Stafford fault system of northern Virginia (Mixon and Newell, 1977), could be 100 km or more.

Atta fault: As a result of this study the ATTA fault is only interpreted on seismic line SRS-9 (Figure 80). In Figure 42 on page 102 the fault is drawn joining the TCF between seismic lines SRS-9 and SRS-27. Between lines SRS-9 and SRS-27 the TCF slightly changes strike, which could suggest that the Atta fault offsets the trace of the TCF. The Atta fault appears to intersect line SRS-9 at an oblique angle and does not intersect line SRS-25; thus, the fault is interpreted to trend north-south or northwest. The Atta fault might join with the down-to-the-southeast fault that intersects line SRS-9 farther eastward such that the Atta fault would bound a pop-up block similar to the Steel Creek fault or the Meyers Branch fault. The Atta fault, unlike the Upper Three Runs fault or the Tinker Creek fault, does not appear to bound recognizable structures or reflection packages in the crystalline basement; hence, the status of the fault as a reactivation structure is unclear.

In an earlier interpretation of these data the Atta fault was projected through the skip in seismic line SRS-25 to line SRS-10 (Domoracki, 1994a). The data are not conclusive to prove or disprove either interpretation. Further study is necessary to determine the trend of the ATTA fault.

Steel Creek fault: The Steel Creek fault described in this study was originally interpreted by Chapman and DiStefano (1989) as a data processing artifact resulting from near surface velocity variations associated with Pen Branch valley. The Steel Creek fault is a down-to-the-southeast fault within the Pen Branch fault zone and bounds a small uplifted fault block with the Pen Branch fault (Figure 44 on page 104). The thrown of the fault increases to the southwest across SRS. On seismic lines SRS-1 (Figure 44 on page 104) and SRS-8 (stations 540-585, Appendix B) the shallowest resolvable horizons are deformed (in time) by the Steel Creek fault, although no offset

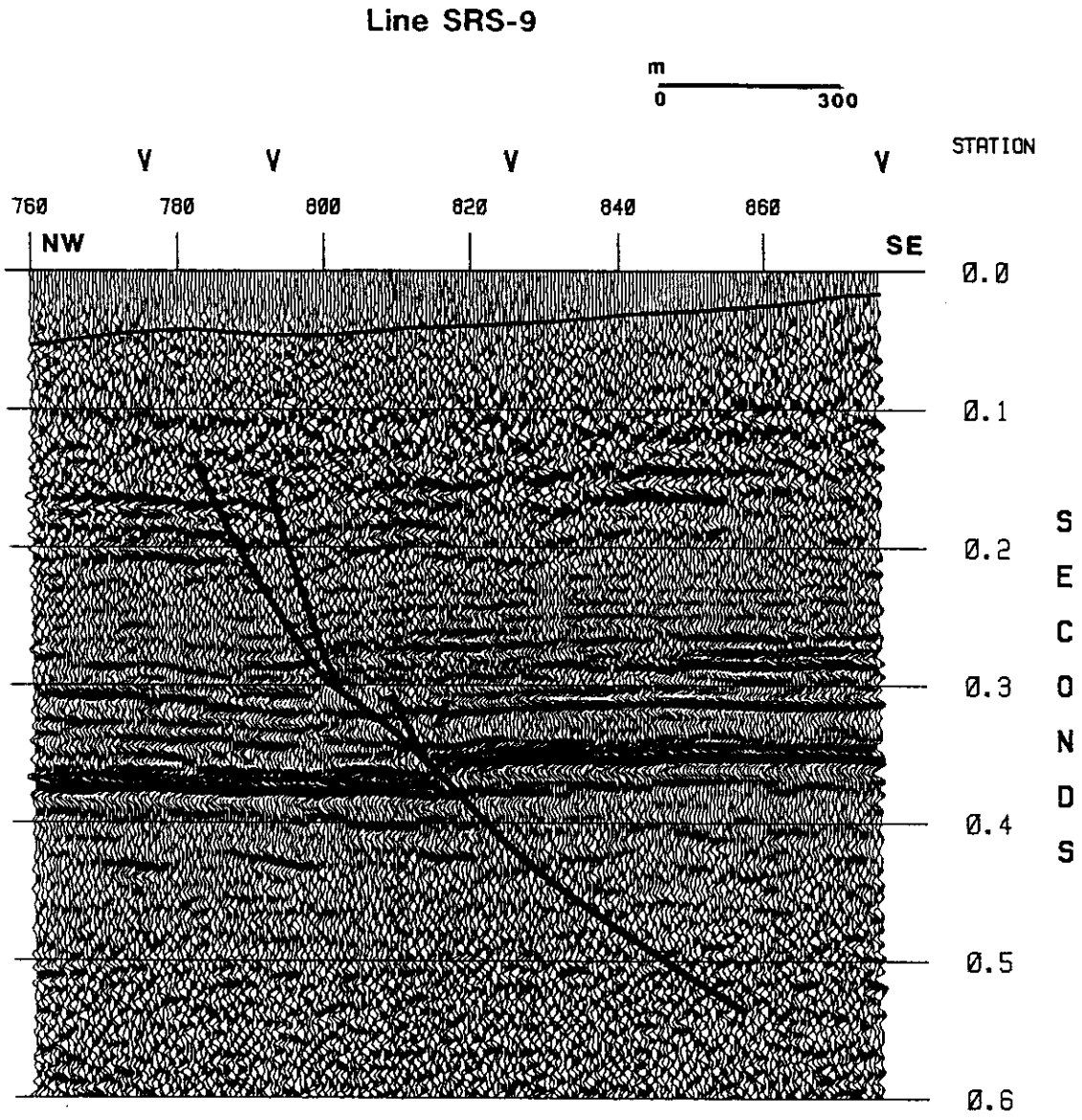

Figure 80. Seismic expression of the Atta fault: The Atta fault is interpreted on line SRS-9.

of the reflections is observed. Eastward, on seismic lines SRS-2 (stations 820-840, Appendix B) and SRS-3 (stations 870-870, Appendix B), the Steel Creek fault is barely discernible. On seismic lines SRS-8 and SRS-1 the projection of the fault to the surface is coincident with Pen Branch Creek (Figure 42 on page 102); that is, the Steel Creek fault appears to control the drainage of Pen Branch Creek.

Below the Coastal Plain the Steel Creek fault is poorly imaged. On those seismic sections where the fault can be traced into the Dunbarton basin it appears to dip to the northwest (e.g. lines SRS-1 and SRS-29, Appendix B). This geometry suggests that Steel Creek fault is not a reactivated Triassic basin fault, but is a post-Jurassic fault dating from onset of reverse movement on the Pen Branch fault, i.e. an antithetic fault.

Crackerneck fault: The Crackerneck fault is a down-to-the-northwest fault (Figure 42 on page 102). On seismic line SRS-1 the time offset of Basement reflection is approximately 22 ms and the Yellow Marker horizon is deformed (Figure 81). The magnitude of the basement offset ranks the Crackerneck fault as one of the major faults in the Coastal Plain at SRS. Isochrons across the fault show slight thinning to the southeast of the fault, which indicates continued movement as reverse fault during the Cretaceous (Figure 52 on page 119 and Figure 54 on page 122). In the deep seismic data, the Crackerneck fault appears to be located at the projection of a reflection boundary within the fan-shaped reflection wedge to the base of the Coastal Plain (line SRS-1 stations 100-200, Appendix B).

Prior to this study the Crackerneck fault was identified only of seismic line SRS-1. The correlation of the Crackerneck fault to a fault interpreted on line SRS-12 is based on the Bouguer gravity data that shows the gravity contours parallel to this trend (Figure 45 on page 107). If the Crackerneck fault is a reactivation structure similar to the Pen Branch fault and the Tinker Creek fault, it would be reasonable that the trend of the fault would parallel the gravity field. The interpreted trend of the Crackerneck fault presented in this report differs from presented earlier by the Author (Domoracki, 1994a) that showed the fault correlated to faults on seismic lines SRS-4 and SRS-7. Additional seismic reflection data are needed to resolve this issue.

Seismic Expression of Crackerneck Fault

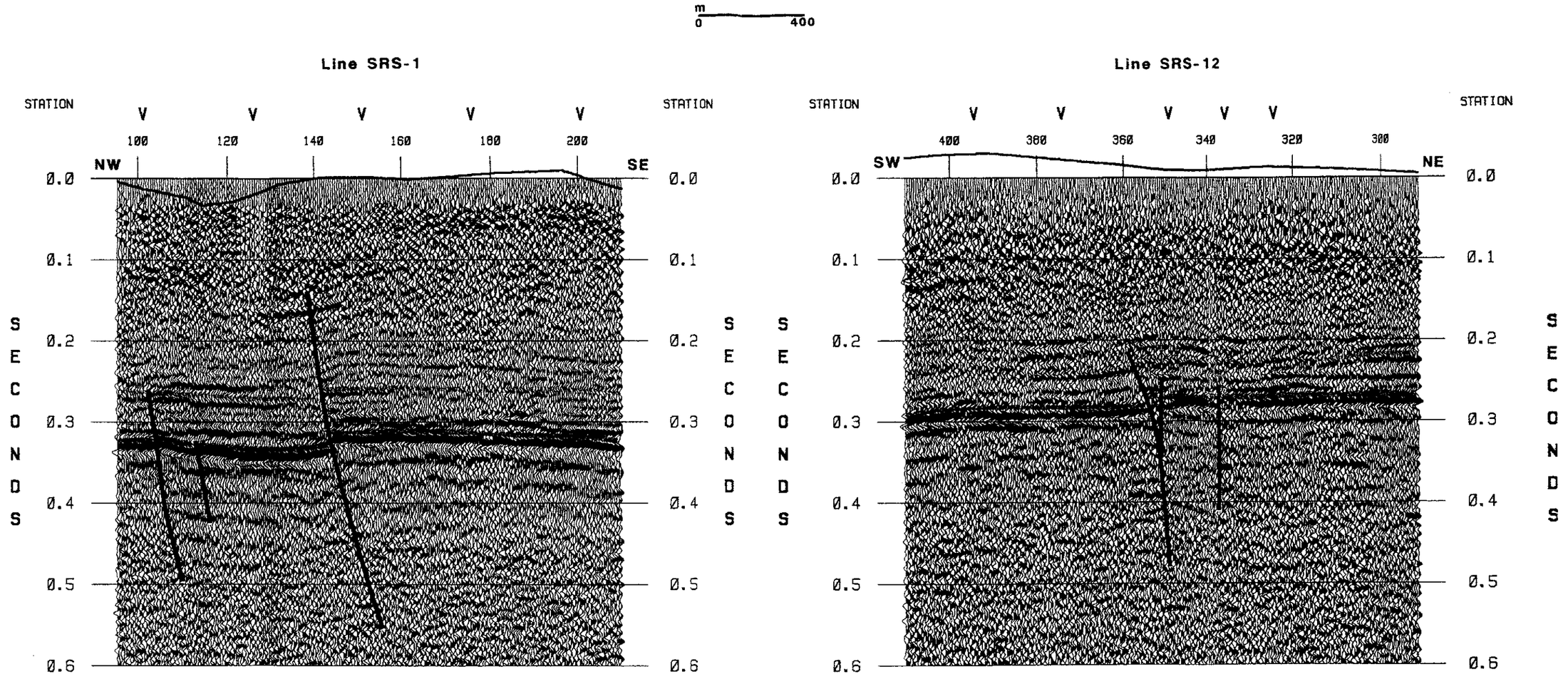

Figure 81. **Seismic expression of the Crackerneck fault:** The Crackerneck fault is interpreted on line SRS-1 (left) and line SRS-12 (right). The identification of the Crackerneck fault on line SRS-12 is based on interpretation of the Bouguer gravity data.

Ellenton fault: The Ellenton fault was discovered during the original processing of the Conoco Phase I data. The location of the fault near the epicenter of the 1985 earthquake prompted the acquisition of seismic lines SRS-21 and SRS-18 (Figure 7 on page 26). Chapman and DiStefano (1989) interpreted the Ellenton fault as a north-south transform fault formed contemporaneously with Dunbarton basin and subsequently reactivated during the Cretaceous (Figure 43 on page 103).

The reprocessed SRS seismic data reveal the Ellenton fault to be a relatively minor down-to-the-southeast fault that is imaged only on seismic lines SRS-7 and SRS-6 (Figure 82). In the deep seismic data the Ellenton fault occurs on the crest of the antiform that is bounded by the Tinker Creek fault (Figure 27 on page 69).

In a previous interpretation of these data the Ellenton fault was interpreted to trend northwest-southeast (Domoracki, 1994a). Subsequent reexamination of seismic line SRS-7 found a possible location for the fault and the interpretation presented herein of the fault trend is similar to that of Chapman and DiStefano (1989) and Stephenson and Stieve (1992).

Meyers Branch fault: The Meyers Branch fault is a new discovery. The fault is down-to-the-southeast and is interpreted to have an arcuate trace (concave northwest) in the Coastal Plain sediments (Figure 42 on page 102). The Meyers branch fault and the down-to-the-northwest fault on the northwest parallel to it form a branching structure that appears to coalesce into a single northwest dipping fault in the Dunbarton basin (Figure 26 on page 68). The fault in the Dunbarton basin separates zones of differing time-dip of the basin strata which indicates that the Meyers branch fault was formed contemporaneously with the basin as an antithetic fault and was subsequently reactivated to fault the Coastal Plain sediments.

The Meyers Branch fault and the Pen Branch fault bound a large scale uplift (Figure 83). This uplift is larger than, but similar in form to, the uplift block bounded by the Pen Branch fault and the Steel Creek fault (Figure 44 on page 104). In previous interpretations of basement structure at SRS hints of this structure are apparent (Marine and Siple, 1974; Chapman and DiStefano, 1989; Snipes et al., 1993a). In particular, the structural contour map by Chapman and DiStefano

Seismic Expression of Ellenton Fault

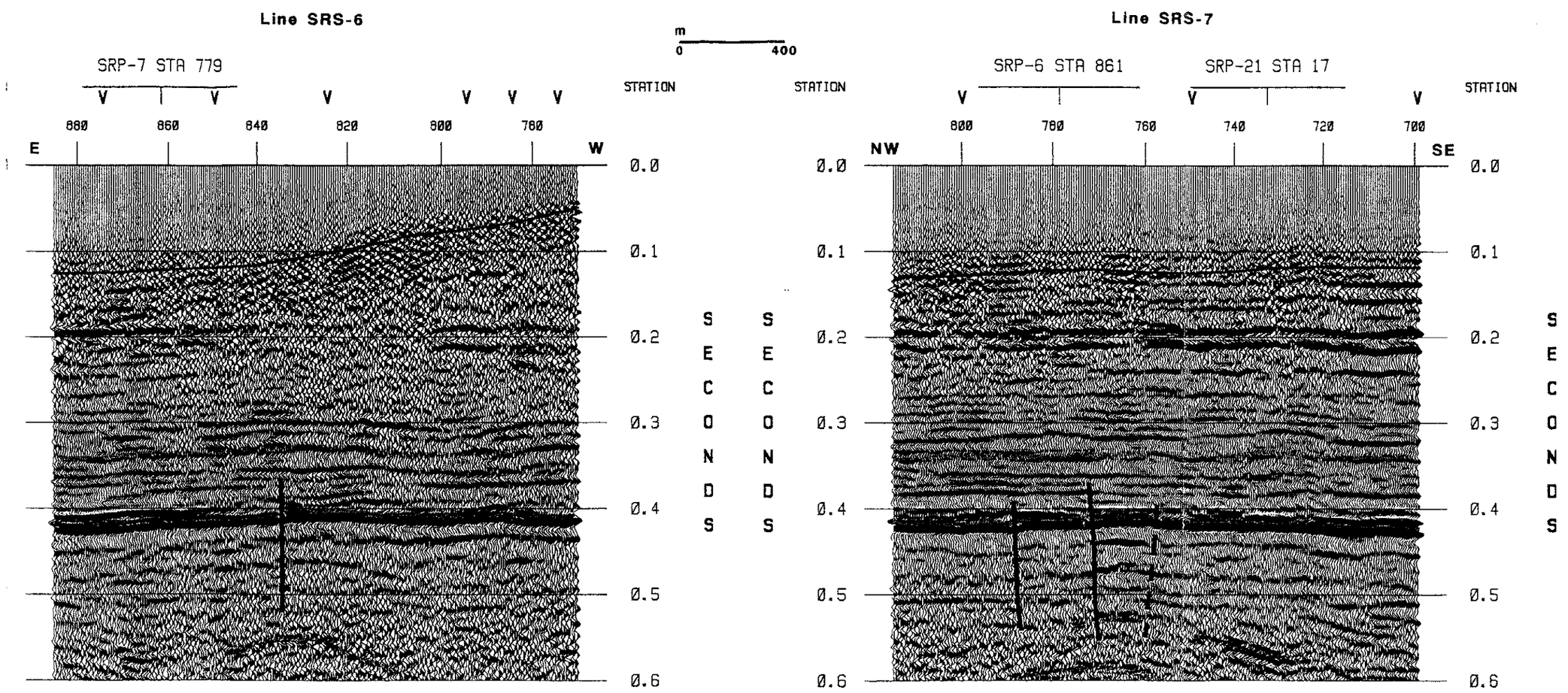

Figure 82. **Seismic expression of the Ellenton fault:** The Ellenton fault is interpreted on line SRS-6 (left) and line SRS-7 (right).

(1989) shows a structurally high area coincident with the uplift (Figure 43 on page 103). Some of the faults mapped in this study that bound the block were apparently detected previously (Marine and Siple, 1974), but not with the orientation interpreted herein. None of these faults was interpreted from the original processed SRS seismic data.

The Coastal Plain sediments on the southern margin of uplift are deformed mostly by folding. On line SRS-11 (stations 100-300, Appendix B), at the southwestern extreme of the uplift, the basement uplift is about 70 ms (≈70 m), but the time-offset of the Meyers Branch fault is only 20 ms in the same area. The isochron maps indicate that movement on this fault block occurred during the Cretaceous to cause time-thinning over the top of the structure (Figure 52 on page 119 and Figure 54 on page 122). Furthermore, this area corresponds to a topographic high that might imply ongoing vertical movement through the Cenozoic (Figure 55 on page 124).

Unlike many of the faults mapped at SRS, the Meyers Branch fault exhibits complex branching patterns in the vertical plane (Figure 84). On lines SRS-1 and SRS-8 the Meyers Branch "fault" is comprised of closely spaced faults at the pre-Cretaceous unconformity. Both these locations are where the fault is interpreted to change direction and would be demonstrative of "horse-tail" structures.

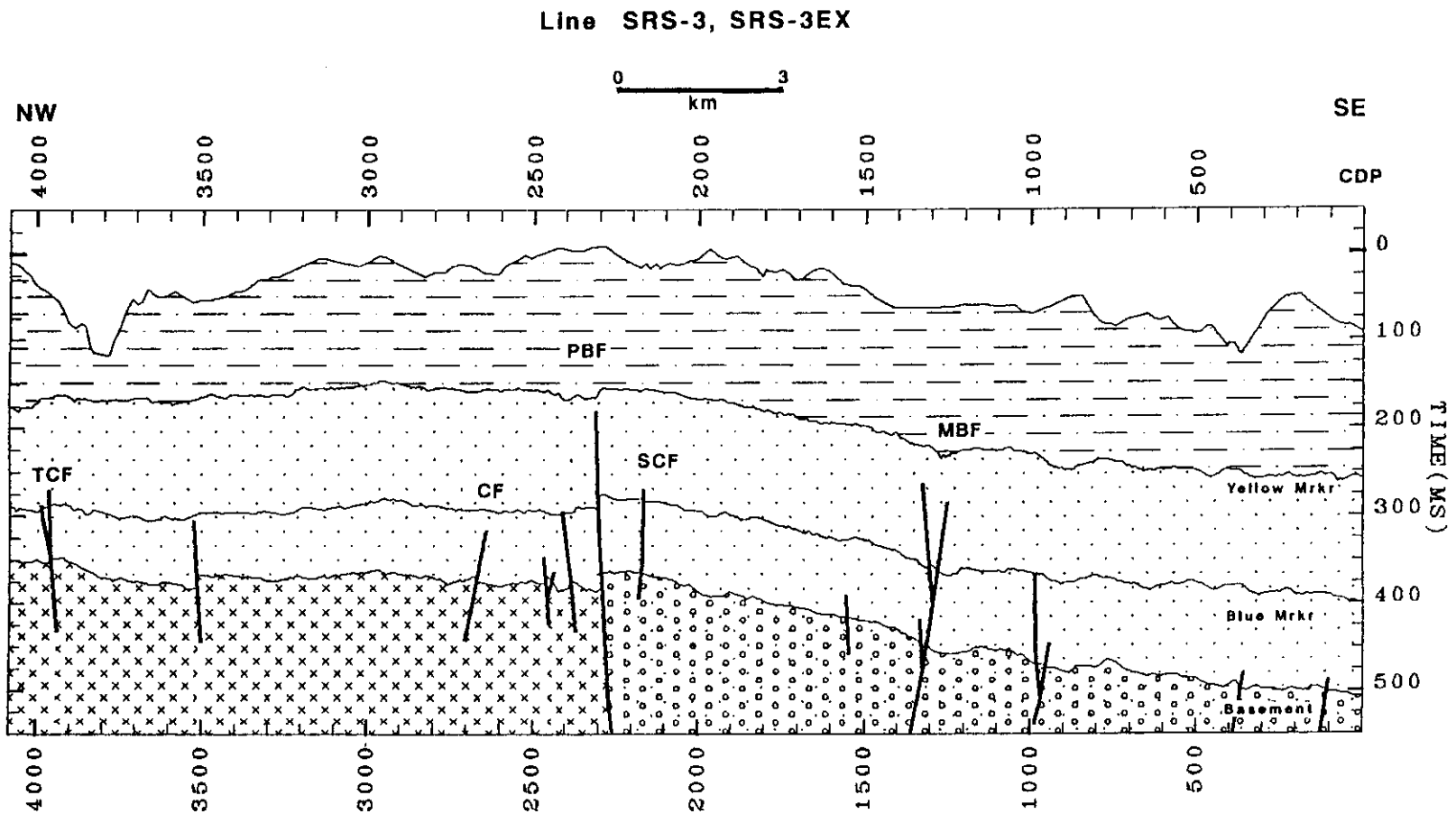

Figure 83. **Pen Branch fault-Meyers Branch fault uplift:** Digitized interpretation of line SRS-3 showing the uplift bounded by the Pen Branch fault and the Meyers Branch fault. TCF = Tinker Creek fault, CF = C line fault, PBF = Pen Branch fault, SCF = Steel Creek fault, MBF = Meyers Branch fault.

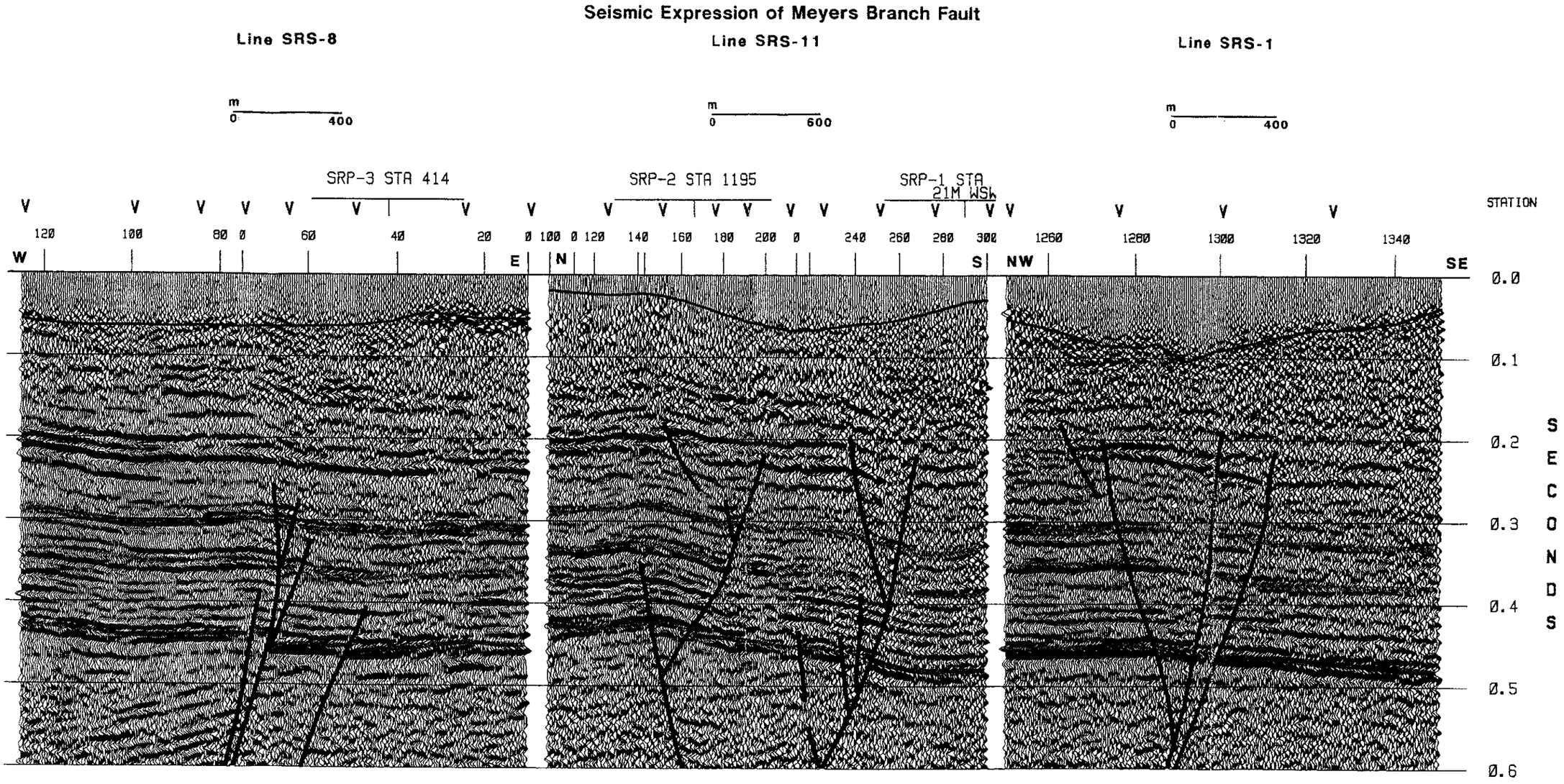

Figure 84. Seismic expression of the Meyers Branch fault: The Meyers Branch fault is interpreted on seismic lines SRS-8 (left), SRS-11 (middle) and SRS-1 (right).

Recommendations for Future Work

Additional Data Acquisition and Geological Investigations: Although the Pen Branch fault has been adequately covered by seismic reflection surveys, the Tinker Creek and Atta faults have not. Seismic time-structure mapping shows that these faults, similar to the Pen Branch fault, increase in throw to the northeast. The analysis of isochrons over the Tinker Creek fault suggests that major movement on that fault is post-Cretaceous. Furthermore, the elevation profile of line SRS-27 across the Tinker Creek fault reveals a topographic anomaly associated with the fault that indicates relatively recent movement. The refraction stack section of line SRS-27 (Çoruh et al., 1994) reveals fault offsets to within a few meters of the surface. Additional seismic data are needed to trace these faults northeast of line SRS-27. For the confirmation of the faults and time-depth correlation of the seismic data, this work should be followed by a drilling program similar to the CFD drillhole series and trenching. Any boreholes drilled should tie directly into a seismic line. If the geophysical logs, including the sonic logs, cannot be utilized from the ground surface to obtain the shallow velocity structure, checkshots or VSPs must be run to enable direct correlation between depth and seismic reflection time.

Of the other faults mapped in this study, the Crackerneck and Meyers Branch faults are also recommended for further research. Both of these faults deform sediments at least as young as Paleocene age and the Meyers Branch fault bounds an area that has possibly undergone Cenozoic uplift. The trend of the Crackerneck fault is speculative. Given that the magnitude of the deformation of the coastal plain sediments associated with the Crackerneck fault is similar to that exhibited in the vicinity of the Pen Branch fault, determination of the trend of this fault in relation to the regional stress field is paramount.

A critical aspect of the evaluation of seismic hazard is determination of fault movement history and age of latest faulting. As a prelude to any contemplated borehole investigations, detailed seis-

mic isochron mapping over identified faults at SRS can be carried out to determine relative ages of fault movement in the Cretaceous and lower Tertiary sections. Refraction/reflection stack sections described by Çoruh (1993) can be used to identify shallow faulting and, thence, sites for shallower investigative techniques.

The topographic profiles across the Pen Branch fault and the comparison between standardized time-structure and topographic maps suggest the possibility that deformation related to the fault affects the present topography. It is clear that the course of Pen Branch is controlled by the Steel Creek fault. Recent work conducted elsewhere on the Atlantic Coastal Plain indicates areas of possible ongoing tectonic uplift (Gardner, 1989; Rhea, 1989; Marple and Talwani, 1993; 1994). At SRS the area between the Pen Branch fault and the Meyers Branch fault bears further investigation. A first step would be analysis of detailed topographic data; the 30 second digital topographic data used in this study is inadequate for the task. To fully address this question might require a field program involving precision topographic surveys.

The extent of the Dunbarton basin off the Savannah River Site is uncertain. Reprocessing of Seisdata Line 4 could establish the northeastern extent of the Dunbarton basin and the Pen Branch Fault and confirm the interpretation from gravity data. Preliminary reprocessing of Seisdata Line 4 indicates that these data can be substantially improved by reprocessing. Reprocessing of Seisdata Line 6 could delineate the southwestern extent of these structures as well as reveal the origin of the magnetic lineament that appears to denote a splay of the Goat Rock fault through the mafic complex south of SRS.

The southern boundary of the Dunbarton basin is undefined. Previous surveys and borehole data south of SRS have been interpreted to show faults offsetting the basal unconformity, e.g. the Millet and Martin faults; therefore, acquisition of seismic data south of SRS and/or reprocessing of older seismic data in this area is suggested. The logical location of a reconnaissance seismic line is to extend line SRS-7 south of SRS along South Carolina Route 125 to the town of Martin in Allendale County.

The reprocessed Conoco data have revealed some of the internal geometry of the Dunbarton basin as well as deep crustal structure under the coastal plain sediments. This data base should be

sufficient to constrain three dimensional potential field modelling of gravity and magnetic anomalies at SRS. Such integrated modelling could be directed toward determining the depth of the Dunbarton basin and the gross geometry of the mafic complex south of SRS. Although Cumbest and others (1992) carried out similar modelling, they acknowledged the limitations of the 2 1/2-D modelling algorithm used. An additional justification for extending seismic line SRS-7 southward would be to provide constraints for modelling the prominent mafic complex.

The evolution of the Mesozoic rift basins of the eastern seaboard is a major question in regional tectonics. It is clear that preexisting fault structures played an important role. Also, most of the rift basins have distinctive associated potential field anomalies. Tectonic models proposed by Bell and others (1988) suggest basin formation by simple shear and upwelling of mantle mafic material into the "accommodation zone". The testing of these models requires high quality seismic reflection data and integrated interpretation with available potential field data. The research presented in this report has demonstrated that high quality deep crustal reflection data can be obtained in the Savannah River Site area. Extension of seismic line SRS-7 north and south of SRS beyond that already proposed, and reprocessing and interpretation of the Seisdata seismic lines could aid in testing these hypotheses.

Seismic Data Processing and Acquisition: This investigation has demonstrated that the Conoco and EMEX seismic reflection data sets collected at SRS can be substantially improved by reprocessing. The recovery of the shallow time-section and enhanced imaging of faults, strata, and basement structure has added new information to the geologic data base at SRS. Other older seismic reflection data sets at SRS and vicinity could also probably be improved by reprocessing.

It is recommended that the main emphasis of future seismic data processing be directed towards solving near-surface statics problems. Variation in near surface velocity can lead to spurious reflection geometries in stacked data that can be misinterpreted as geologic structure or mask true geologic structure. At SRS the results of seismic refraction/ reflection surveys by Conoco and EMEX as well as the CFD drilling program indicate considerable variation in the near surface velocity structure at SRS. The demonstrated correlation between topography and time-structure in-

dicate areas where variable datum correction velocities are required. The use of datum correction velocities determined from seismic refraction surveys along the seismic reflection lines would help to alleviate this problem.

Research by Sen (1991) on a technique to help resolve long wavelength statics problems has shown that reflection continuity of the reprocessed data presented in this report can be further enhanced. Improved datum statics will also lead to better residual statics solutions and stacking velocities. The resulting improvement in seismic reflection data quality will in turn substantially aid geological interpretation.

In the Coastal Plain sediments the low seismic velocities require that extreme care be exercised in picking a velocity function. It was found that constant velocity analysis of both stacked and unstacked data led to good results. Velocity spectra were less useful. Most of the instances of "static busts" encountered were found to be caused by bad stacking velocity determinations. Coupled with the problem of velocity determination is the choice of mute patterns. For most of the seismic lines a mute based on percentage stretch of the waveform was adequate; however, at far offsets the refraction from the top of basement was often not adequately muted and required hand picking a mute function. Likewise, at short offsets picking mutes by hand is advisable.

The EMEX seismic lines required severe surgical muting of shot gathers to eliminate source-generated noise. This surgical muting resulted in more than half the data being lost - a clearly unacceptable result. Frequency-wavenumber filtering cannot be applied to the shot data due to spatial aliasing effects. The stretched automatic amplitude adjustment (SAGC) technique described by Çoruh (1985) and tau-p domain processing by Guo (1994) show some promise in reducing source-generated noise.

Preprocessing of vibroseis seismic data for structural interpretation should include both vibroseis whitening (Çoruh and Costain, 1983) and extended vibroseis correlation (Pratt, 1982; Okaya and Jarchow, 1989). This latter technique allows for the recovery of deep reflections without added field acquisition cost.

The reprocessed seismic data have revealed stratigraphic details in the coastal plain sediments. Sufficient data quality exists for seismic-stratigraphic interpretation. Wavelet processing of the seis-

mic data to preserve amplitude relationships and waveform might enable quantitative analysis of these reflections as well as allow high fidelity ties to geophysical logs.

Preliminary work with migration before stack and poststack Kirchoff migration have shown that these techniques can improve imaging of faults in the Coastal Plain sediments. Further work with this method is warranted.

In any future reprocessing or processing effort the data processor and the interpreter should interact during choice of data processing parameters. Seismic data processing is a form of seismic data interpretation, i.e. "interpretive processing". Care must be taken not to "over process" the data; often a "less is more" approach is advisable. Geological interpretations should be data driven; thus, the quality of seismic data processing has direct bearing on the reliability of any interpretation.

The seismic reflection data reprocessed in this study were acquired using seven different spread geometries. With the exception of line SRS-29, all of the seismic data were acquired to image the Coastal Plain sediments. Of these various acquisition geometries the Conoco experimental lines yielded the best images of the Coastal Plain strata and faults. For additional seismic programs intended to image the Coastal Plain section, acquisition parameters similar to the EXP series lines should be used. Some modifications to this shooting geometry would be to increase the number of recording channels to allow an increased maximum offset and a decreased minimum offset. The increased maximum offset would enable better stacking velocity determinations and would aid in resolution of longer wavelength statics problems. A decreased minimum offset would allow imaging of shallow reflectors and would yield shallow velocity control needed for datum statics computations. Both of these modifications would require increasing the number of recording channels used if the same group intervals and CDP fold per time-depth are to be retained.

For targets deeper than the basal unconformity the maximum recording offset would need to be increased to ensure adequate velocity control. To record and properly migrate reflections from steeply dipping interfaces profile lengths need to be sufficiently long; for deep targets this might necessitate extending profiles off SRS. The recording group intervals could be increased but probably not much beyond 16 m due to spatial aliasing of reflections in the Coastal Plain sediments that are needed for residual statics computations. If an off-end geometry is required the receivers should

be placed up-dip from the source. The results of extended correlation of the EXP lines suggest that a single vibrator source can generate sufficient energy to enable recording of reflections from midcrustal depths.

Conclusions

The reprocessed Savannah River Site seismic reflection data present an extraordinary high resolution window to the deep crustal structure of the Southeast Atlantic Coastal Plain (Figure 85). These data should provide a tie point for future deep seismic reflection profiling in the southeastern United States.

Many of the deep crustal structures interpreted in the Georgia COCORP data are continuous along geologic strike into South Carolina. At the Savannah River Site these structures give rise to well defined, highly reflective, mappable southeast-dipping reflections and reflection packages. Two major crustal reflections at SRS, the Augusta fault and a midcrustal decollement, appear to correspond to events imaged in COCORP lines 60 km to the southwest where the latter event was interpreted to be the Appalachian Master decollement. The continuity of these structures from Georgia to South Carolina supports models for the evolution of the Appalachian orogen that incorporate large scale detachments this far to the southeast beneath the Piedmont and under the Atlantic Coastal Plain.

The strike of the Upper Three Runs fault, Augusta fault and the Pen Branch fault are all nearly identical, which indicates a common structural history for these structures. In contrast, the midcrustal decollement has a more northerly strike, which suggests that the structures beneath the Augusta fault have a different structural history than those above. It is clear from both the Savannah River Site seismic data and the COCORP data that the Augusta fault is a major regional seismic reflection boundary. Distinct magnetic anomalies are associated with many of the fault slices imaged in the upper plate of the Augusta fault and denote the continuation of the Eastern Piedmont fault system under the Atlantic Coastal Plain.

The Dunbarton Triassic basin is revealed to be half-graben bounded on the northwest by the Pen Branch fault. Geometrically, the Dunbarton basin is similar to the nearby Riddleville basin of

which it probably is the northeastern extension. The Pen Branch fault does not sole into the Augusta fault within the confines of SRS, but rather merges into a southeast dipping detachment above the Augusta fault that could be seismogenic. This detachment was a pre-existing Paleozoic structure that was reactivated primarily in dip-slip during Mesozoic extension. The similarity of the strike directions of the Augusta fault, Upper Three Runs fault and the Pen Branch fault and the dissimilar strike direction of the midcrustal decollement suggests that Mesozoic extension was primarily confined to the upper plate of the Augusta fault, i.e., "thin-skinned" extension. Although it is clear that the pre-existing structural fabric was exploited during extension, it was not perfectly along these boundaries; in the southeastern part of SRS the Upper Three Runs fault appears to offset the Augusta fault.

The Dunbarton basin fill dips 10-15° to the northwest. Along the northwest border of the basin, within 2 km of the border fault, the strata undergo dip reversal and dip 15-20° to the southeast. Seismic modelling indicates that the maximum thickness of the basin fill is between 4 to 5 km and that the Pen Branch fault is nearly vertical. Minor intrabasinal faults are imaged as well as bright discontinuous reflections that probably represent sills. The sills occur along the southern margin of the basin and are probably related to the mafic complex south of the Savannah River Site in a manner similar to that proposed by Bell and others (1988) for the Mesozoic rift basins of eastern North America. Refraction stack data and seismic reflection amplitude mapping indicate that no outliers of Triassic strata exist northwest of the Pen Branch fault. The southeast border of the Dunbarton basin was not traversed by seismic data reprocessed in this study; however, the location of the border can be estimated from gravity and borehole data.

Many of basement structures at the Savannah River Site show evidence for reactivation under compression since the development of the passive margin. This deformation history is recorded in the structural geology and stratigraphy of the Coastal Plain strata. Time-structure, isochron, reflection amplitude, and fault maps prepared on reflection markers in the Coastal Plain section indicate that there are three major basement blocks bounded by northeast trending faults that penetrate upward from basement into the Atlantic Coastal Plain strata.

The northernmost fault block is bounded by on the southeast by the Tinker Creek fault, a southeast dipping high-angle reverse fault, which is interpreted to be reactivated splay from the Augusta fault. The Tinker Creek fault offsets the top of basement and shallower reflections and can be traced with certainty for a distance of 15 km across SRS. The throw of the fault, as does its upward penetration into the sedimentary section, increases to the northwest where the shallowest reflections ($\approx$ 20 m) appear to be disturbed. Several hundred meters to the northwest of the Tinker Creek fault is the Upper Three Runs fault, a structure that bounds starkly different reflection packages in the basement and soles into the Augusta fault. The Upper Three Runs fault appears to mark the hinge line of isochron (isopach) thinning in the northwest part of the Savannah River Site during the Late Cretaceous, but the fault does not pierce the Coastal Plain section. The isochron thinning could be caused by hanging wall uplift above a thrust. The leading edge of this hypothetical thrust would occur northwest of the Savannah River Site and the difference in physical properties of the crystalline basement across the Upper Three Runs fault might localize the observed monocline. There is not sufficient data to elaborate on the northwest boundary of this block.

The central block, 9 km wide in a NW-SE direction, is bounded on the northwest by the Tinker Creek fault and on the southeast by the Pen Branch fault, which has been reactivated since rifting as a southeast dipping high-angle reverse fault within the Coastal Plain strata. As a reactivated structure, the Pen Branch fault is the main throughgoing fault in a 3 km wide, 25 km long fault zone. The fault zone is comprised of subparallel fault segments that are commonly down-to-the-northwest north of the Pen Branch fault and down-to-the-southeast south of the Pen Branch fault. The offset of time horizons by the Pen Branch fault increases to the northwest at a rate similar to the Tinker Creek fault and the shallowest resolvable reflection horizons appear to be deformed across its length. The Pen Branch fault and the Tinker Creek fault together might represent a larger fault zone such that strain is transferred from the Tinker Creek fault to the Pen Branch fault. In this model only a small part of the total fault system occurs within the confines of the Savannah River Site. The length of fault system, by analogy to to the Stafford fault system of northern Virginia (Mixon and Newell, 1977), could be 100 km or more.

The third fault block is bounded by the Pen Branch fault on the northwest. In this part of the Savannah River Site the Pen Branch fault bounds smaller pop-up blocks with the Steel Creek fault, an antithetic fault to the Pen Branch fault, and the Meyers Branch fault, a reactivated intrabasin fault. The Steel Creek fault controls the drainage of Pen Branch a tributary stream to the Savannah River. The southeast boundary of this block is unknown, but could be defined by the Martin fault south of the Savannah River Site.

The interpretation of borehole data, isochron maps, and analysis of trend surfaces fitted to reflection time horizons in the Atlantic Coastal Plain section suggest that movement on the Pen Branch fault and related structures was ongoing through the Late Cretaceous. This movement was accompanied by tilting and rotation of the fault blocks as demonstrated by consistent rotation of strike directions through the time section. Fault block movements in the Tertiary are uncertain as shallow time horizons cannot be correlated areally with confidence; however, isochrons and reflection horizons correlated across faults reveal deformation, but not offset, of the shallowest resolvable events. The positive correlation between time-structure and topographic maps suggests the possibility of Cenozoic uplift, unless such a correlation is found to correspond to a near surface velocity variation.

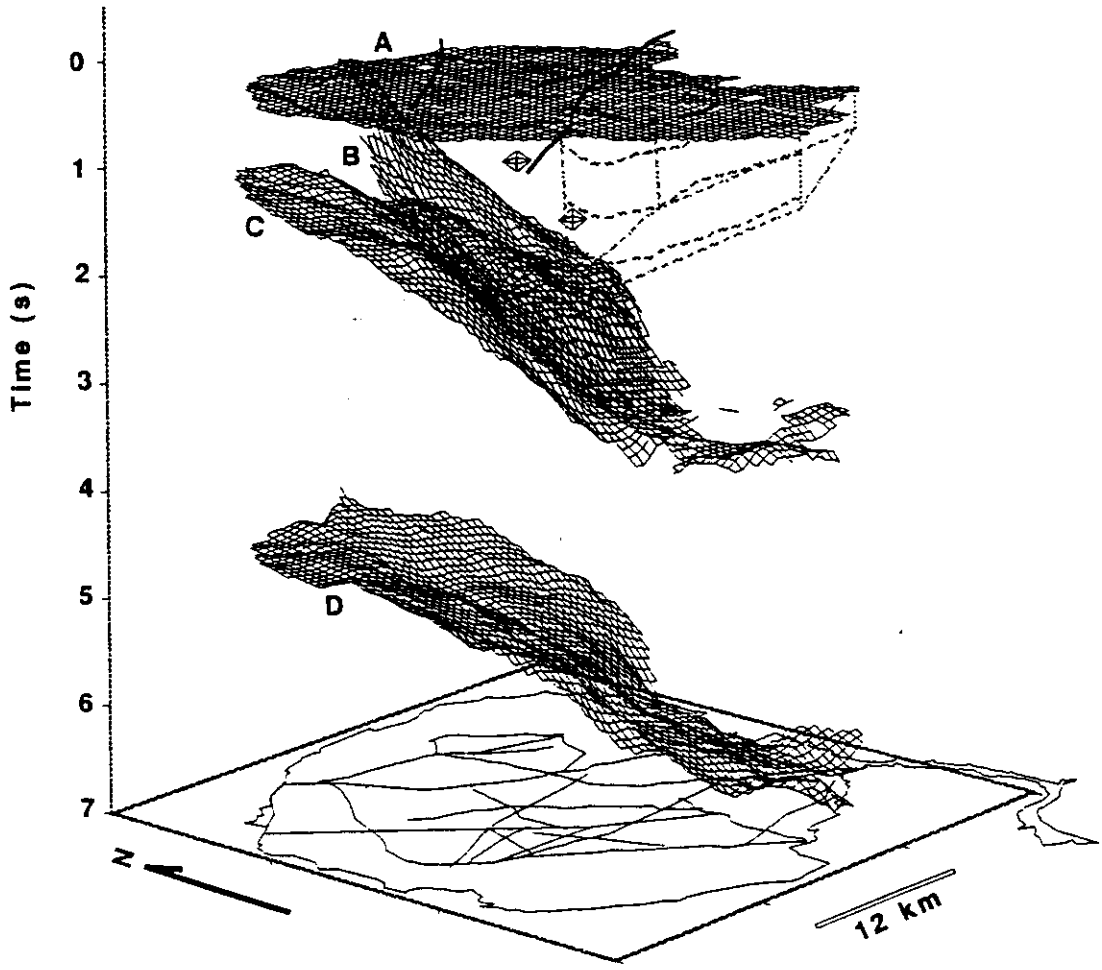

Figure 85. 3-D wire mesh model: The three crustal reflection surfaces mapped at SRS are shown in perspective view. A = Basement reflection, B = Upper Three Runs fault, C = Augusta fault, D = Midcrust reflection. Plotted on the Basement reflection surface are the major basement faults that penetrate the base of the Coastal Plain sediments. The foci of the 1985 and 1988 SRS earthquakes are denoted by octahedra. The attitude of the Pen Branch fault and the thickness of the basin fill are based on the seismic modelling results. Vertical exaggeration approximately 3:1 for a crustal velocity 6.0 km/s.

Selected References

Allmendinger, R.W., Nelson, K.D., Potter, C.J., Barazangi, M., Brown, L.D., and Oliver, J.E., 1987, Deep seismic reflection characteristics of the continental crust: Geology, v. 15, n. 4, p. 304-310.

Anderson, E.E., 1990, The seismotectonics of the Savannah River Site: The results of a detailed gravity survey: M.Sc. thesis, University of South Carolina, Columbia, 246 p.

Anstey, N.A., 1977, Seismic interpretation: The physical aspects: IHRDC, Boston, MA, 625 p.

Baum, G.R., Collins, J.S., Jones, R.M., Madlinger, B.A., and Powell, R.J., 1980, Correlation of the Eocene strata of the Carolinas: South Carolina Geology, v. 24, n. 1, p. 19-17.

Beck, A.E., 1976, The use of thermal resistivity logs in stratigraphic correlation: Geophysics, v. 41, n. 2, p. 300-309.

Behrendt, J.C., 1985, Interpretations from multichannel seismic-reflection profiles of the deep crust crossing South Carolina and Georgia from the Appalachian mountains to the Atlantic coast: U.S. Geological Survey Miscellaneous Field Studies Map MF-1656.

Behrendt, J.C., Hamilton, R.M., Ackermann, H.D., and Henry, V.J., 1981, Cenozoic faulting in the vicinity of the Charleston, South Carolina, 1886 Earthquake: Geology, v. 9, n. 3, p. 117-122.

Bell, R.E., Karner, G.D., and Steckler, M.S., 1988, Early Mesozoic rift basins of eastern North America and their gravity anomalies: The role of detachments during extension: Tectonics, v. 7, n. 3, p. 447-462.

Berkman, E., 1991, High resolution seismic survey Pen Branch fault Savannah River Site, South Carolina: Emerald Exploration Consultants, Inc., Austin, TX, 89 p., 210 fig.

Bobyarchick, A.R., and Glover III, L.G., 1979, Deformation and metamorphism in the Hylas zone and adjacent parts of the eastern Piedmont in Virginia: Geological Society of America Bulletin, v. 90, p. 739-752.

Bollinger, G.A., 1990, Specification of source zones, recurrence rates, focal Depths and maximum magnitudes for earthquakes affecting the Savannah River Site in South Carolina: Seismological Observatory Virginia Polytechnic Inst. & State Univ., Blacksburg, 109 p.

Bollinger, G.A., Chapman, M.C., Sibol, M.S., and Costain, J.K., 1985, An analysis of earthquake focal depths in the southeastern U.S.: Geophysical Research Letters, v. 12., n. 11, p. 785-788.

Bonini and Woollard, 1960, Subsurface geology of North Carolina- South Carolina Coastal Plain from seismic data: American Association of Petroleum Geologists Bulletin, v. 44, n. 3, p. 298-315.

Bramlett, K.W., Secor, D.T., and Prowell, D.C., 1982, The Belair fault: A Cenozoic reactivation structure in the eastern Piedmont: Geological Society of America Bulletin, v. 93, n. 11, p. 1109-1117.

Brown, L.D., 1987, Lower continental crust: Variations mapped by COCORP deep seismic profiling: Annales Geophysicae, v. 5B, n. 4, p. 325-330.

Chapman, M.C., Bollinger, G.A., Sibol, M.S., and Stephenson, D.E., 1990, The influence of the Coastal Plain sedimentary wedge on strong ground motions from the 1886 Charleston, South Carolina, earthquake: Earthquake Spectra, v. 6, n. 4, p. 617-639.

Chapman, M.C., Sibol, M.S., and Bollinger, G.A., 1989, Investigation of anomalous earthquake intensity levels along the Coastal Plain-Piedmont boundary in South Carolina and Georgia: Virginia Tech Seismological Observatory, Blacksburg, Virginia, 70 p.

Chapman, W.L. and DiStefano, M.P., 1989, Savannah River Plant seismic survey, 1987-88: Conoco Inc., Seismic Acquisition Section, research report 1809-005-006-1-89, 110 p.

Claerbout, J.F., 1985, Imaging the Earth's interior: Blackwell Scientific Publications, Oxford, 398 p.

Clark, H.B., Costain, J.K., and Glover III, L.G., 1978, Structural and seismic reflection studies of the Brevard ductile deformation zone near Rosman, North Carolina: American Journal of Science, v. 278, p. 419-441.

Colquhoun, D., 1992, Observations on general allo-stratigraphy and tectonic framework of the southeastern Atlantic coast regional cross section (DNAG E-5 corridor) Georgia and South Carolina as they relate to the Savannah River Site; *in* Fallow, W. and Price, V. eds., Geological investigations of the Central Savannah River Area, South Carolina and Georgia: Carolina Geological Society field trip guidebook, Nov. 13-15, 1992, Augusta, Georgia.

Conaway, J., Temperature logging as an aid to understanding groundwater flow in boreholes: Manuscript, 9 p.

Conaway, J.G. and Beck, A.E., 1977, Fine-scale correlation between temperature gradient logs and lithology: Geophysics, v. 42, n. 7, p. 1401-1410.

Cook, F.A., 1984a, Geophysical anomalies along strike of the southern Appalachian Piedmont: Tectonics, v. 3, n. 1, p. 45-61.

Cook, F.A., 1984b, Comment and Reply on "Reprocessed COCORP southern Appalachian reflection data: Root zone to Coastal Plain": Geology, v. 12, n. 4., p. 249-251.

Cook, F.A., Albaugh, D.S., Brown, L.D., Kaufman, S., Oliver, J.E., and Hatcher, R.D., Jr., 1979, Thin-skinned tectonics in the crystalline southern Appalachians; COCORP seismic reflection profiling of the Blue Ridge and Piedmont: Geology, v. 7, n. 12, p. 563-567.

Cook, F.A., Brown, L.D., Kaufman, S., and Oliver, J.E., 1983, The COCORP Seismic reflection traverse across the southern Appalachians: AAPG studies in geology No. 14, American Association of Petroleum Geologists, Tulsa, OK, 61 p.

Cook, F.A., Brown, L.D., Kaufman, S., Oliver, J.E., and Petersen, T.A., 1981, COCORP seismic profiling of the Appalachian orogen beneath the Coastal Plain of Georgia: Geological Society of America Bulletin, v. 92, n. 10, p. 738-748.

Çoruh, C., 1985, Stretched automatic amplitude adjustment of seismic data (Short note): Geophysics, v. 50, n. 2., p. 252-256.

Çoruh, C., Bollinger, G.A., and Costain, J.K., 1988, Seismogenic structures in the Central Virginia Seismic Zone: Geology, v. 16, p. 748-751.

Çoruh, C. and Costain, J.K., 1983, Noise attenuation by vibroseis whitening (VSW) processing: Geophysics, v. 48, n. 5, p. 543-554.

Çoruh, C. and Costain, J.K., 1994, Upward penetration of the Pen Branch fault beneath Savannah River Site, South Carolina: A search for the shallowest flat lying layer by reprocessing of PBF high resolution seismic reflection data: Department of Geological Sciences, Virginia Polytechnic Inst. and State Univ., Blacksburg, report prepared for Westinghouse Savannah River Company, Aiken, S.C., 24 p.

Çoruh, C., Costain, J.K., Hatcher, R.D., Jr., Pratt, T.L., Williams, R.T., and Phinney, R.A., 1987, Results from regional vibroseis profiling: Appalachian Ultra-deep Core Hole site study: Geophys. Journal Royal Astronomical Society, v. 89, p. 147-156.

Çoruh, C., Costain, J.K., Stephenson, D.E., 1993, Composite Refraction-reflection stack sections: Tracing faults in the Atlantic Coastal Plain sediments (Abstract): Extended abstracts with biographies, Society of Exploration Geophysicists 63rd Annual International Meeting and Exhibition Sept. 26-30, 1993, Washington, DC, p. 1157-1160.

Costain, J.K., 1976, Insulating properties of Coastal Plain sediments (South Carolina and North Carolina); *in* Costain, J.K., Glover III, L., and Sinha, A.K. principal investigators, Evaluation and targeting of geothermal energy resources in the Southeastern United States (Progress report): Energy Research and Development Administration Report VPI&SU-5103-2, Virginia Polytechnic Institute and State University, Blacksburg, Virginia, 170 p.

Costain, J.K., Bollinger, G.A., and Speer, J.A., 1987, Hydroseismicity - A hypothesis for the role of water in the generation of intraplate seismicity: Geology, v. 15, p. 618-621.

Costain, J.K., and Çoruh C., 1989, Tectonic settings of Triassic half-grabens in the Appalachians: Seismic data acquisition, processing, and results; *in* Tankard, A.J. and Balkwill, H.R., eds., Extensional tectonics and stratigraphy of the North Atlantic margins: American Association of Petroleum Geologists Memoir 46, American Association of Petroleum Geologists, Canadian Geological Foundation, p. 155-174.

Costain, J.K., Çoruh, C., Pratt, T.L., Hatcher, R.D., Glover III, L., Phinney, R., Diebold, J., Williams, R., and Zoback, M., 1986, Seismic signatures of tectonic lithofacies from regional lines, Appalachian Ultradeep Core Hole (ADCOH) site area: Society of Exploration Geophysicists expanded abstracts with biographies, 56th Annual International Meeting and Exposition Nov. 2-6, 1986, Houston, Texas, p. 136-139.

Costain, J.K., and Decker, E.R., 1987, Heat flow at the proposed Appalachian Ultradeep Core Hole (ADCOH) Site: Tectonic implications: Geophysical Research Letters, v. 14, n. 3, p. 252-255.

Costain, J.K., and Glover III, L.G., 1979, Heat flow in granites - Implications for crustal structure in the Appalachians; *in* The Caledonides in the U.S.A.: I.G.C.P. 1979, Blacksburg, Virginia, p. 215-220.

Costain, J.K., Hatcher, R.D., Jr., Çoruh, C., Pratt, T.L., Taylor, S.R., Litehiser, J.J, and Zietz, I., 1989, Geophysical characteristics of the Appalachian crust; *in* Hatcher, R.D., Jr., Thomas,

W.A., and Viele, G.W., eds., The geology of North America, Volume F-2, The Appalachian-Ouachita orogen in the United States: Geological Society of America, p. 385-416.

Costain, J.K., Speer, J.A., Glover III, L.G., Dashevsky, and McKinney, M., 1986, Heat Flow in the Piedmont and Atlantic Coastal Plain of the Southeastern United States: Journal of Geophysical Research, v. 91, n. B2, p. 2123-2135.

Cumbest, R.J., and Price, V., 1989a, Continued extension of the Dunbarton basin: An explanation for faulting in the Coastal Plain of South Carolina: USDOE Report WSRC-RP-89-1263, Westinghouse Savannah River Company, Savannah River Site, Aiken, South Carolina.

Cumbest, R.J., and Price, V., 1989b, Extension of the Eastern Piedmont tectonic system beneath the Coastal Plain of South Carolina: USDOE Report WSRC-RP-89-1299, Westinghouse Savannah River Company, Savannah River Site, Aiken, South Carolina.

Cumbest, R.J., Price, V., and Anderson, E.E., 1992, Gravity and magnetic Modeling of the Dunbarton Triassic basin, South Carolina: Southeastern Geology, v. 33, n. 1, p. 37-51.

Daniels, D.L., 1974, Geologic interpretation of geophysical maps, Central Savannah River Area, South Carolina and Georgia: U.S. Geological Survey Geophysical Investigations Map GP-893.

Daniels, D.L., and Leo, G.W., 1985, Geologic interpretation of basement rocks of the Atlantic Coastal Plain: U.S.G.S. Open File Report 85-655, 45 p.

Daniels, D.L., Zietz, I, and Popenoe, P., 1983, Distribution of subsurface Lower Mesozoic rocks in the Southeastern United States, as interpreted from regional aeromagnetic and gravity Maps; *in* Studies related to the Charleston, South Carolina earthquake of 1886 - Tectonics and Seismicity: U.S. Geological Survey Prof. paper 1313-K, p. 1-24.

Davis, J.C., 1973, Statistics and data analysis in geology: John Wiley & Sons, New York, 550p.

Demirbag, M.E., 1990, Estimation of seismic parameters from multifold reflection seismic data by generalized linear inversion of Zoeppritz equations: Ph.D. dissertation, Virginia Polytechnic Inst. & State Univ., Blacksburg, 122 p.

Diment, D.L., Marine, I.W., Neiheisel, J., and Siple, G.E., 1965, Subsurface temperature, thermal conductivity, and heat flow near Aiken, South Carolina: Journal of Geophysical Research, v. 70, n. 22, p. 5635-5644

Domoracki, W.J., 1994a, A geophysical investigation of geologic structure and regional tectonic setting at the Savannah River Site, South Carolina: Department of Geological Sciences, Virginia Polytechnic Inst. and State Univ., Blacksburg, report prepared for Westinghouse Savannah River Company, Aiken, S.C., 173 p.

Domoracki, W.J., Çoruh, C., Costain, J.K., and Stephenson, D.E., 1994b, Faulting in Atlantic Coastal Plain sediments at the Savannah River Site, SC: Interpretations from seismic reflection time Maps (Abstract): Abstracts with Programs, Annual Meeting of the Southeast Section Geological Society of America, Blacksburg, Virginia.

Fallaw, W.C., and Price, V., 1992, Outline of stratigraphy at the Savannah River Site; *in* Fallow, W. and Price, V. eds., Geological investigations of the Central Savannah River Area, South Carolina and Georgia: Carolina Geological Society field trip guidebook, Nov. 13-15, 1992, Augusta, Georgia.

Fallaw, W.C., Snipes, D.S., Hodges, R.A., and Price, S.W., and Temples, T.J., 1994, Outcrop evidence of Post-Early Late Eocene deformation in the north-central Part of the Savannah River

Site, Coastal Plain of South Carolina (Abstract): Abstracts with Programs, Geological Society of America Annual Meeting October, 1994, Seattle, WA.

Faye, R.E. and Prowell, D.C., 1982, Effects of Late Cretaceous and Cenozoic faulting on the geology and hydrology of the Coastal Plain near the Savannah River, Georgia and South Carolina:

Freeman, B., Yielding, G., and Badley, M., 1990, Fault correlation during seismic interpretation: First Break, v. 8, n. 3, p. 87-95.

Fountain, D.M., Hurich, C.A., and Smithson, S.B., 1984, Seismic reflectivity of mylonitic zones in the crust: Geology, v. 12, n. 4, p.195-198.

Garihan, J.M., Ranson, W.A., Orlando, K.A., and Preddy, M.S., 1990, Kinematic history of Mesozoic faults in northwestern South Carolina and adjacent North Carolina: South Carolina Geology, v. 33, n. 1, p. 19-32.

Gardner, G.H.F, Gardner, L.W., and Gregory, A.R., 1974, Formation velocity and density-the diagnostic basics for stratigraphic traps: Geophysics, v. 39, n. 6, p. 770-780.

Gardner, T.W., 1989, Neotectonism along the Atlantic passive continental margin: A review: Geomorphology, v. 2, p. 71-97.

Garland, G.D., 1979, Introduction to geophysics: W.B. Saunders Company, Philadelphia, 494 p.

Geomatrix Consultants, 1993, Preliminary Quaternary and Neotectonic studies Savannah River Site, South Carolina: Lawrence Livermore National Laboratory for Westinghouse Savannah River Company, Aiken, SC, 59 p.

Gibson, B.S., and Levander, A.R., 1990, Apparent layering in common-midpoint stacked images of two-dimensionally heterogeneous targets: Geophysics, v. 55, n. 11, p. 1466-1477.

Glover III, L., Çoruh, C., Costain, J.K., and Bollinger, G.A., 1992, Piedmont seismic reflection study: A program integrated with tectonics to probe the cause of eastern seismicity: NUREG/CR-5731, U.S. Nuclear Regulatory Commission, Washington, D.C., 146 p.

Goetz, J.F., Dupal, L., and Bowler, J., 1979, An Investigation into discrepancies between sonic log and seismic check shot velocities (Manuscript): Schlumberger Technical Services Inc., 11 p.

Gohn, G.S., 1992, Revised nomenclature, definitions, and correlations for the Cretaceous formations in USGS-Clubhouse Crossroads #1, Dorchester county, South Carolina: U.S. Geological Survey Professional Paper 1518, 39 p.

Goodwin, E.B., and Thompson, G.A., 1988, The seismically reflective crust beneath highly extended terranes: Evidence for its origin in extension: Geological Society of America Bulletin, v. 100, n. 10, p. 1616-1626.

Goodwin, E.B., and Thompson, G.A., 1989, Seismic identification of basement reflectors: The Bagdad reflection sequence in the Basin and Range province - Colorado Plateau transition zone, Arizona: Tectonics, v. 8., n. 4, p. 821-831.

Grauch, V.J.S., 1993, Limitations on digital filtering on the DNAG magnetic data set for the conterminous U.S.: Geophysics, v. 58, n. 9, p. 1281-1296.

Guo, M., 1994, Amplitude balancing in τ-p domain: M.Sc. thesis, Virginia Polytechnic Inst. & State Univ., Blacksburg, 71 p.

Hanson, K.L., Bullard, T.L., and DeWitt, M.W., 1994, Applications of Quaternary stratigraphic, soil-geomorphic, and quantitative geomorphic analyses to the evaluation of tectonic activity, Upper Coastal Plain, South Carolina (Abstract): Program and Abstract, Annual Meeting of the Eastern Section Seismological Society of America, Columbia, South Carolina.

Harding, T.P., 1990, Identification of wrench faults using subsurface structural data: criteria and pitfalls: American Association of Petroleum Geologists Bulletin, v. 74, n. 10, p. 1590-1609.

Harris, L.D., and Bayer, K.C., 1979, Sequential development of the Appalachian orogen above a master decollement - A hypothesis: Geology, v. 7, p. 568-572.

Hatcher, R.D., Jr., 1971, Stratigraphic, petrologic, and structural evidence favoring a thrust solution to the Brevard problem: American Journal of Science, v. 270, p. 177-202.

Hatcher, R.D., Jr., 1991, Interactive property of large thrust sheets with footwall rocks - the sub-thrust interactive duplex hypothesis: a mechanism of dome formation in thrust sheets: Tectonophysics, v. 191, p. 237-242.

Hatcher, R.D., Jr., Howell, D.E., and Talwani, P., 1977, Eastern Piedmont fault system: Speculations on its extent: Geology, v. 5. p. 636-640.

Hatcher, R.D., Jr., Odom, A.L., Engelder, T., Dunn, D.E., Wise, D.U., Geiser, P.A., Schamel, S., and Kish, S.A., 1988, Characterization of Appalachian faults: Geology, v. 16, n. 2, p. 178-181.

Hatcher, R.D., Jr., and Zietz, I., 1979, Tectonic implications of regional aeromagnetic and gravity Data from the southern Appalachians; *in* The Caledonides in the U.S.A.: I.G.C.P. 1979, Blacksburg, Virginia, p. 235-244.

Hatherly, P.J., Urosevic, M., Lambourne, A., and Evans, B.J., 1994, A simple approach to calculating refraction statics corrections (Short note): Geophysics, v. 59, n. 1, p. 156-160.

Hattner, J.G., and Wise Jr., S.W., 1980, Upper Cretaceous calcareous nannofossil biostratigraphy of South Carolina: South Carolina Geology, v. 24, n. 2, p. 41-117.

Heck, F.R., 1989, Mesozoic extension in the southern Appalachians: Geology, v. 17, n. 8, p. 711-714.

Hittelman, A.M., Kinsfather, J.O.; and Meyers, H., 1989, Geophysics of North America CD-ROM: National Oceanic and Atmospheric Administration, Boulder, CO.

Hoffschwelle, J.W., 1987, Laying out seismic program: The Leading Edge, v. 6, n. 4, p. 28-31.

Holbrook, W.S., Catchings, R.D., and Jarchow, C.M., 1991, Origin of deep crustal reflections: Implications of coincident seismic refraction and reflection data in Nevada: Geology, v. 19, n. 2., p. 175-179.

Honeyman, W., 1983, Near-surface faulting effects on seismic reflection times (Short note): Geophysics, v. 48, n. 8, p. 1140-1142.

Horton, J.W., Jr., Drake, A.A., Jr., Rankin, D.W., and Dallmeyer, R.D., 1991, Preliminary tectonostratigraphic terrane map of the central and southern Appalachians: U.S. Geological Survey Miscellaneous Investigations Map I-2163.

Hubbard, S.S., 1990, Paleozoic and Grenvillian structures in the southern Appalachians: Extended interpretation from seismic reflection data: M.Sc. thesis, Virginia Polytechnic Inst. & State Univ., Blacksburg, 112 p.

Hutchinson, D.R., Grow, J.A., Klitgord, K.D., and Swift, B.A., 1983, Crustal structure beneath the southern Appalachians: Nonuniqueness of gravity modelling: Geology, v. 11, p. 611-615.

Iverson, W.P., and Smithson, S.B., 1982, Master decollement root zone beneath the southern Appalachians and crustal balance: Geology, v. 10, n. 5, p. 241-245.

Iverson, W.P., and Smithson, S.B., 1983a, Reprocessed COCORP southern Appalachian reflection data: root zone to Coastal Plain: Geology, v. 11, n. 7, p. 422-425.

Iverson, W.P., and Smithson, S.B., 1983b, Reprocessing and reinterpretation of COCORP southern Appalachian profiles: Earth and Planetary Science Letters, v. 62, p. 75-90.

Jacobeen, F.H., Jr., 1972, Seismic evidence for high-angle reverse faulting in the Coastal Plain of Prince Georges and Charles counties, Maryland: Maryland Geological Survey Information Circular 13, 21 p.

Kean, A.E., and Long, L.T., 1980, A seismic refraction line along the axis of the southern Piedmont and crustal thicknesses in the Southeastern United States: Earthquake Notes, v. 51, n. 4, p. 3-13.

Keating, P., 1993, The fractal dimension of gravity data sets and its implication for gridding: Geophysical Prospecting, v. 41, p. 983-993.

Knapp, R.W., 1985, Using half-integer source offset with split spread CDP seismic data: The Leading Edge, v. 4, n. 10, p. 66-69,108.

Knapp, R.W. and Steeples, D.W., 1986, High-resolution common-depth-point reflection profiling: field acquisition parameter design: Geophysics, v. 51, n. 2., p. 283-294.

Kish, S.A., 1992, An initial geochemical and isotopic study of granite from core C-10, Savannah River Site, S.C.; *in* Fallow, W. and Price, V. eds., Geological investigations of the Central Savannah River Area, South Carolina and Georgia: Carolina Geological Society Field Trip Guidebook, Nov. 13-15, 1992, Augusta, Georgia.

Krajewski, S.A., and Gibbs, B.L., 1994, Computer contouring generates artifacts: Geotimes, v. 39, n. 4., p. 15-19.

Kusznir, N.J., and Egan, S.S., 1989, Simple-shear and pure-shear models of extensional sedimentary basin formation: Application to the Jeanne d'Arc basin, Grand Banks of Newfoundland; *in* Tankard, A.J. and Balkwill, H.R., eds., Extensional tectonics and stratigraphy of the North Atlantic margins: American Association of Petroleum Geologists Memoir 46, American Association of Petroleum Geologists, Canadian Geological Foundation, p. 305-322.

Lewis, S.R., 1974, Significance of the vertical and lateral changes in the clay mineralogy of the Dunbarton Triassic basin, South Carolina: M.Sc. thesis, University of North Carolina, Chapel Hill, 34 p.

Lindholm, R.C., 1978, Triassic-Jurassic faulting in eastern North America - A model based on pre-Triassic structures: Geology, v. 6, p. 365-368.

Litak, R.K., and Brown, L.D., 1989, A modern perspective on the Conrad discontinuity: EOS, v. 70, n. 29, p. 1-7.

Litak, R.K., and Hauser, E.C., 1992, The Bagdad reflection sequence as tabular mafic intrusions: Evidence from seismic modeling of mapped exposures: Geological Society of America Bulletin, v. 104, n. 10, p. 1315-1325.

Long, L.T., Talwani, P., and Bridges, S.R., 1975, Simple Bouguer gravity map of South Carolina: South Carolina State Development Board, Division of Geology.

Luetgert, J.H., Benz, H.M., and Madabhushi, S., 1994, Crustal structure beneath the Atlantic Coastal Plain of South Carolina: Seismological Research Letters, v. 65, n. 2, p. 180-191.

Lynn , H.B., and Deregowski, 1981, Dip limitations on migrated sections as a function of line length and recording time: Geophysics, v. 46, n. 10, p. 1392-1397.

Maher, H.D., 1978, Stratigraphy and structure of the Belair and Kiokee belts, near Augusta, Georgia; *in* Snoke, A.W. ed., Geological investigations of the eastern Piedmont, southern Appalachians (With a field trip guide on the bedrock geology of central South Carolina): Carolina Geological Society Field Trip Guidebook, Oct. 7-8, 1978, West Columbia, South Carolina.

Maher, H.D., 1987, Kinematic history of mylonitic rocks from the Augusta fault zone, South Carolina and Georgia: American Journal of Science, v. 287, p. 795-816.

Maher, H.D., Jr., Dallmeyer, R.D., Secor, D.T., Jr., and Sacks, P.E., 1994, $^{40}Ar/^{39}Ar$ Constraints on chronology of Augusta fault zone movement and Late Alleghanian extension, southern Appalachian Piedmont, South Carolina and Georgia: American Journal of Science, v. 294, p. 428-448.

Manspeizer, W., and Cousminer, H.L., 1988, Late Triassic-Early Jurassic synrift basins of the U.S. Atlantic margin; *in* Sheridan, R.E. and Grow, J.A., eds., The Geology of North America, Volume I-2, The Atlantic Continental Margin, U.S.: Geological Society of America, p. 197-216.

Marple, R.T. and Talwani, P., 1993, Evidence of Possible Tectonic Upwarping along the South Carolina Coastal Plain from an Examination of River Morphology and Elevation Data: Geology, v. 21, n. 7, p. 651-654.

Marple, R.T. and Talwani, P., 1994, Evidence for a Major, Tectonically active structure beneath the Coastal Plain of North and South Carolina (Abstract): Abstracts with Programs, Annual Meeting of the Southeast Section Geological Society of America, Blacksburg, Virginia.

Marine, I.W., 1974, Geohydrology of a buried Triassic basin at Savannah River Plant, South Carolina: American Association of Petroleum Geologists Bulletin v. 58, n. 9, p. 1825-1837.

Marine, I.W., 1976, Geochemistry of ground water at the Savannah River Plant: U.S. Energy Research and Development Administration Report DP-1356, E.I. du Pont de Nemours & Co., Savannah River Laboratory, Aiken, South Carolina, 102 p.

Marine, I.W. and Siple, G.E, 1974, Buried Triassic basin in the Central Savannah River Area, South Carolina and Georgia: Geological Society of America Bulletin, v. 85, n. 2, p. 311-320.

McBride, J.H., Lindsey, G.A., Hobbs, R.W., Snyder, D.B., and Totterdell, I.J., 1993, Some problems in velocity analysis for marine deep seismic profiles: First Break, v. 11, n. 8, p. 345-356.

McBride, J.H., and Nelson, K.D., 1988, Integration of COCORP deep reflection and magnetic anomaly analysis in the Southeastern United States: Implications for origin of the Brunswick and East Coast Magnetic Anomalies: Geological Society of America Bulletin, v. 100, n. 3, p. 436-445.

McBride, J.H., and Nelson, K.D., 1991, Deep seismic reflection constraints on Paleozoic crustal structure and definition of the Moho in the buried southern Appalachian orogen; *in* Meissner,

R., Brown., L., Durbaum, H-J, Franke, W., Fuchs, K., and Seifert, F., eds., Continental Lithosphere: Deep seismic reflections: American Geophysical Union, Geodynamics series v. 22, p. 9-20.

McBride, J.H., Nelson, K.D., and Brown, L.D., 1989, Evidence and implications of an extensive early Mesozoic Rift basin and basalt/diabase sequence beneath the southeast Coastal Plain: Geological Society of America Bulletin, v. 101, n. 4, p. 512-520.

McCarthy, J., and Thompson, G.A., 1988, Seismic imaging of extended crust with emphasis on the Western United States: Geological Society of America Bulletin, v. 100, n. 9, p. 1361-1374.

Meissner, R., Rupture, Creep, Lamellae and crocodiles: happenings in the continental crust: Terra Review, v. 1, p. 17-28.

Miller, H.G., 1983, Selected course notes: Memorial University of Newfoundland, St. Johns, Newfoundland.

Mixon, R.B., and Newell, W.L., 1977, Stafford fault system: Structures documenting Cretaceous and Tertiary deformation along the Fall Line in northeastern Virginia: Geology, v. 5, n. 7, p. 437-440.

Mondary, J.F., Pratt, T.L., and Brown, L.D., 1991, A 3-D look at the midcrustal Surrency bright spot beneath southeastern Georgia (Abstract): Extended Abstracts with Biographies Society of Exploration Geophysicists 61st Annual International Meeting and Exhibition Nov. 10-14, 1991, Houston, TX, p. 279-282.

Mooney, W.D., and Braile, L.W., 1989, The seismic structure of the continental crust and upper mantle of North America; *in* Bally, A.W., and Palmer, A.R., eds., The Geology of North America - An overview: Geological Society of America, Boulder, Colorado, p. 39-52.

Mooney, W.D. and Meissner, R., 1992, Multi-genetic origin of crustal reflectivity: A review of seismic reflection profiling of the continental lower crust and Moho; *in* Fountain, D.M., Arculus, R., and Kay, R.W., eds., Continental lower crust: Elsevier, Amsterdam, p. 45-79.

Musgrove, F.W., 1994, Time-variant statics corrections during interpretation: Geophysics, v. 59, n. 3, p. 474-483.

Nelson, K.D., Arnow, J.A., McBride, J.H., Willemin, J.H., Huang, J., Zheng, L., Oliver, J.E., Brown, L.D., and Kaufman, S., 1985, New COCORP profiling in the Southeastern United States. Part I: Late Paleozoic suture and Mesozoic rift basin: Geology, v. 13, n. 10, p. 714-718.

Nelson, K.D., 1991, A unified view of craton evolution motivated by recent deep seismic reflection and refraction results: Geophys. J. Int., v. 105, p. 25-35.

Nelson, K.D., 1992, Are crustal thickness variations in old mountain belts like the Appalachians a consequence of lithospheric delamination?: Geology, v. 20, n. 6, p. 498-502.

Nelson, K.D., McBride, J.H., Arnow, J.A. Wille, D.M., Brown, L.D., Oliver, J.E., and Kaufman, S., 1987, Results of recent COCORP profiling in the southeastern United States: Geophys. Journal Royal Astronomical Society, v. 89, p. 141-146.

Okaya, D.A., and Jarchow, C.M., 1989, Extraction of deep crustal reflections from shallow vibroseis data using extended correlation: Geophysics, v. 54, n. 5, p. 555-562.

Pappano, P.A., 1992, Structure and regional tectonic setting across the Atlantic Coastal Plain of northeastern Virginia as interpreted from reflection seismic data: M.Sc. thesis, Virginia Polytechnic Institute and State University, Blacksburg, 57p.

Parsons, Brinckerhoff, Quade & Douglas, Inc., 1973, Triassic basin fault probing program report: U.S. Atomic Energy Commission, E.I. du Pont de Nemours & Co., Wilmington, Delaware, 33p.

Parsons, T., and Thompson, G.A., 1991, The role of magma overpressure in suppressing earthquakes and topography: Worldwide examples: Science, v. 253, p. 1399-1402.

Peddy, C., and Keen, C., 1987, Deep seismic reflection profiling: How far have we come?: The Leading Edge, v. 6., n. 6, p. 22-24,49.

Petersen, T.A., Brown, L.D., Cook, F.A., Kaufman, S., and Oliver, J.E., 1984, Structure of the Riddleville basin from COCORP seismic data and implications for reactivation tectonics: Journal of Geology, v. 92, p. 261-271.

Phinney, R.A., and Roy-Chowdhury, K., 1989, Reflection seismic studies of crustal structure in the eastern United States; *in* Pakiser, L.C. and Mooney, W.D., eds., Geophysical framework of the continental United States: Geological Society of America Mem. 172, p. 613-653.

Pickard, J.E., 1992, Velocity modeling of a long-period static anomaly, West Cameron Block 225, a Gulf of Mexico case history: Geophysics, v. 57, n. 3, p. 420-430.

Pirkle, W.A., 1982, Geological framework of the Winterseat quadrangle in the southwestern portion of the Carolina Slate belt, South Carolina: South Carolina Geology, v. 26, n. 2., p. 69-79.

Pohn, H.A., and Coleman, Jr., J.L., 1991, Fold patterns, lateral ramps and seismicity in central Pennsylvania: Tectonophysics, v. 186, p. 133-149.

Pratt, T.L., 1982, A geophysical investigation of a concealed granitoid beneath Lumberton, North Carolina: M.Sc. thesis, Virginia Polytechnic Institute and State University, Blacksburg, 55 p.

Pratt, T.L., 1986, A geophysical study of the Earth's crust in central Virginia with implications for lower crustal reflections and Appalachian crustal structure: Ph.D. dissertation, Virginia Polytechnic Inst. & State Univ., Blacksburg, 69 p.

Pratt, T.L., Çoruh, C., and Costain, J.K., 1987, Lower crustal reflections in central Virginia, USA: Geophys. Journal Royal Astronomical Society, v. 89, p. 163-170.

Pratt, T.L., Costain, J.K., Çoruh, C., Glover III, L., and Robinson, E.S., 1985, Geophysical evidence for an allochthonous Alleghanian (?) granitoid beneath the basement surface of the Coastal Plain near Lumberton, North Carolina: Geological Society of America Bulletin, v. 96, n. 8, p. 1070-1076.

Price, V., Maciolek, J.B., Fritz, H., Cumbest, R.J., Hild, J., Hoekstra, P., and Nopper, R.J., 1989, Preliminary results of transient electromagnetic (TEM) surveys of the Savannah River Site: USDOE Report WSRC-RP-89-811, Westinghouse Savannah River Company, Savannah River Site, Aiken, South Carolina, 18 p.

Pritchett, W.C., 1990, Acquiring better seismic data: Chapman and Hall, New York, New York, 427 p.

Prowell, D.C., 1983, Index of faults of Cretaceous and Cenozoic age in the eastern United States: U.S.G.S. Miscellaneous Field Studies Map MF-1269.

Prowell, D.C., 1988, Cretaceous and Cenozoic tectonism on the Atlantic coastal margin; *in* Sheridan, R.E., and Grow, J.A., eds., The Geology of North America, Volume I-2, The Atlantic continental margin, U.S.: Geological Society of America, p. 557-564.

Prowell, D.C., and O'Connor, B.J., 1978, Belair fault zone: Evidence of Tertiary fault displacement in eastern Georgia: Geology, v. 6, p. 681-684.

Quinlan, G., Beaumont, C., and Hall, J., 1993, Tectonic model for crustal seismic reflectivity patterns in compressional orogens: Geology, v. 21, n. 7, p. 663-666.

Randazzo, A.F., Swe, W., and Wheeler, W.H., 1970, A study of tectonic influence on Triassic sedimentation - The Wadesboro basin, central Piedmont: J. Sed. Pet., v 40., n. 3., p. 998-1006.

Ratcliffe, N.M., Burton, W.C., 1985, Fault reactivation models for origin of the Newark basin and studies related to eastern U.S. seismicity; *in* Robinson, G.R., Jr., and Froelich, A.J., eds., Proceedings of the second U.S. Geological Survey workshop on the early Mesozoic basins of the Eastern United States: U.S. Geological Survey Circular 946, p. 36-44.

Ratcliffe, N.M., Burton, W.C., D'Angelo, R.M., and Costain, J.K., 1986a, Seismic reflection geometry of the Newark basin margin in eastern Pennsylvania: NUREG/CR-4676, U.S. Nuclear Regulatory Commission, Washington, D.C., 21 p.

Ratcliffe, N.M., Burton, W.C., D'Angelo, R.M., and Costain, J.K., 1986b, Low-angle extensional faulting, reactivated mylonites, and seismic reflection geometry of the Newark basin margin in eastern Pennsylvania: Geology, v. 14, n. 9, p. 766-770.

Raynaud, B., 1988a, Statistical modelling of lower-crustal reflections: Geophysical Journal, v. 93, p. 111-121.

Raynaud, B., 1988b, Diffraction modelling of 3-D lower-crustal reflectors: Geophysical Journal, v. 93, p. 149-161.

Raynaud, B., 1988c, A 2-D, Ray-based, depth migration method for deep seismic reflections: Geophysical Journal, v. 93, p. 163-171.

Raynaud, B., 1988d, The quantitative interpretation of deep seismic reflection data: First Break, v. 6, n. 7, p. 223-231.

Reinhardt, J., Prowell, D.C., and Christopher, R.A., 1984, Evidence for Cenozoic tectonism in the southwest Georgia Piedmont: Geological Society of America Bulletin, v. 95, n. 10, p. 1176-1187.

Rhea, S., 1989, Evidence of uplift near Charleston, South Carolina: Geology, v. 17, n. 4, p. 311-315.

Robinson, E.S., 1971, The use of Poisson's relation for the extraction of pseudototal magnetic field intensity from gravity observations: Geophysics, v. 36, n. 3, p. 605-608.

Sampson, R.J., 1988, Surface III (user's manual): Interactive Concepts Incorporated, Lawrence, KS, 277 p.

Schlische, R.W., 1992, Structural and stratigraphic development of the Newark extensional basin, eastern North America: Evidence for the growth of the basin and its bounding structures: Geological Society of America Bulletin, v. 104, n. 10, p. 1246-1263.

Schneider, W.A., 1978, Integral formulation for migration in two and three dimensions: Geophysics, v. 43, p. 49-76.

Schneider, W.A., 1983, The reflection seismic prospecting system (course notes for Geophysics 452 *Introduction to seismic prospecting*): Colorado School of Mines, Golden, 86 p. 110 figs.

Secor, D.T., Jr., Snoke, A.W., Bramlett, K.W., Costello, O.P., and Kimbrell, O.P., 1986a, Character of the Alleghanian orogeny in the southern Appalachians: Part I. Alleghanian deformation in the eastern Piedmont of South Carolina: Geological Society of America Bulletin, v. 97, n. 11, p. 1319-1328.

Secor, D.T., Jr., Snoke, A.W., and Dallmeyer, R.D., 1986b, Character of the Alleghanian orogeny in the southern Appalachians: Part III. regional tectonic relations: Geological Society of America Bulletin, v. 97, n. 11, p. 1345-1353.

Sen, A.K., 1991, Removing near-surface effects in seismic data: Application for determination of faults in the Coastal Plain sediments: M.Sc. thesis, Virginia Polytechnic Inst. & State Univ., Blacksburg, 98 p.

Sengbush, R.L., Lawrence, P.L., and McDonal, F.J., 1961, Interpretation of synthetic seismograms: Geophysics, v. 26, n. 2., p. 138-157.

Sexton, G.B., and Pirkle, R.J., 1993, Final report: ground penetrating radar investigations at Atta fault Area Savannah River Site: Microseeps, University of Pittsburgh Applied Research Center, 5 p.

Sheridan, R.E., Musser, D.L., Glover III, L., Talwani, M., Ewing, J.I., Holbrook, W.S., Purdy, G.M., Hawman, R., and Smithson, S., 1993, Deep seismic reflection data of EDGE U.S. Mid-Atlantic continental- margin experiment: Implications for Appalachian sutures and Mesozoic rifting and magmatic underplating: Geology, v. 21, n. 6, p. 563-567.

Sheridan, R.E., Olsson, R.K., and Miller, J.J., 1991, Seismic reflection and gravity study of proposed Taconic suture under the New Jersey Atlantic Coastal Plain: Implications for continental growth: GSA Bulletin, v. 103, n. 3, p. 402-414.

Sheriff, R.E., 1977, Limitations on resolution of seismic reflections and geologic detail derivable from them; *in* Payton, C.E., ed., Seismic stratigraphy-applications to hydrocarbon exploration: American Association of Petroleum Geologists Mem. 26, p. 3-14.

Sheriff, R.E., 1980, Nomogram for Fresnel-zone calculation (Short note): Geophysics, v. 45, n. 5., p. 968-972.

Sherwood, J.W.C., Schultz, P.S., and Judson, D.R., 1978, Some recent developments in migration before stack: Digicon, Inc., Houston, Texas.

Sinha, A.K., Hund, E.A., and Hogan, J.P., 1989, Paleozoic accretionary history of the North American plate margin (central and southern Appalachians): Constraints from the age, origin, and distribution of granitic Rocks; *in* Hillhouse, J.W. ed., Deep structure and past kinematics of accreted terranes: American Geophysical Union, Geophysical Monograph 50, IUGG v. 5, p. 219-238.

Siple, G.E., 1967, Geology and ground water of the Savannah River Plant and vicinity South Carolina: U.S. Geological Survey Water Supply Paper 1841, 113 p.

Snipes, D.S., Fallaw, W.C., Price, V., and Cumbest, R.J., 1993a, The Pen Branch fault: Documentation of Late Cretaceous-Tertiary faulting in the Coastal Plain of South Carolina: Southeastern Geology, v. 33, n. 4, p. 195-218.

Snipes, D.S., Hodges, R.A., Warner, R.D., Fallaw, W.C., Price, V. Jr, Cumbest, R.J., Logan, W.R., 1993b, The Martin fault: southeastern boundary of the early Mesozoic Dunbarton basin (Abstract): Abstracts with Programs, Geological Society of America Annual Meeting October 25-28, 1993, Boston, MA.

Snoke, A.W., and Secor, D.T., Jr., 1982, The Eastern Piedmont fault system and its relationship to Alleghanian tectonics in the southern Appalachians: A discussion: Journal of Geology, v. 90, p. 209-211.

Speer, J.A., 1982, Descriptions of the granitoid rocks associated with two gravity minima in Aiken and Barnwell counties, South Carolina: South Carolina Geology, v. 26, n. 1, p. 15-24.

Stearns, D.W., 1978, Faulting and forced folding in the Rocky Mountain foreland; *in* Matthews, V., III, ed., Laramide folding associated with basement block faulting in the western United States: Geological Society of America Mem. 151, p. 1-37.

Steele, K.B., and Colquhoun, D.J., 1985, Subsurface evidence of the Triassic Newark supergroup in the South Carolina Coastal Plain: South Carolina Geology, v. 28, n. 2, p. 11-22.

Stephenson, D., Talwani, P., and Rawlins, J., 1985, Savannah River Plant earthquake of June 1985: USDOE Report DPST-85-583, E.I. du Pont de Nemours & Co., Savannah River Laboratory, Aiken, South Carolina, 31 p.

Stephenson, D., 1988, August 1988 Savannah River Plant earthquake: USDOE Report DPST-88-841, E.I. du Pont de Nemours & Co., Savannah River Laboratory, Aiken, South Carolina, 12 p.

Stephenson, D. and Stieve, A., 1992, Structural model of the basement in the Central Savannah River Area, South Carolina and Georgia: USDOE Report WSRC-TR-92-120, Westinghouse Savannah River Company, Savannah River Site, Aiken, South Carolina, 18 p.

Stieve, A.L., Çoruh, C., and Costain, J.K., 1993, Confirmatory drilling project interim report: USDOE Report WSRC-RP-93-0334, Westinghouse Savannah River Company, Savannah River Site, Aiken, South Carolina, 12 p.

Stieve, A.L., Stephenson, D.E., and Aadland, R.K., 1991, Pen Branch fault program: Consolidated report on the seismic reflection surveys and the shallow drilling: USDOE Report WSRC-TR-91-87, Westinghouse Savannah River Company, Savannah River Site, Aiken, South Carolina, 26 p.

Swanson, M.T., 1986, Preexisting fault control for Mesozoic basin formation in eastern North America: Geology, v. 14, n. 5, p. 419-422.

Sylvester, A.G., 1988, Strike-slip faults: Geological Society of America Bulletin, v. 100, n. 11, p. 1666-1703.

Tarr, A.C., Talwani, P., Rhea, S., Carver, D., and Amick, D., 1981, Results of recent South Carolina seismological studies: Bulletin Seismological Society of America, v. 71, p. 1883-1902.

Talwani, P., 1986, Current thoughts on the cause of the Charleston, South Carolina earthquakes: South Carolina Geology, v. 29., n. 2, p. 19-38.

Talwani, P., and Rajendran, K., 1991, Some seismological and geometric features of intraplate earthquakes: Tectonophysics, v. 186, p. 19-41.

Talwani, P. and Rawlins, J., 1985, The Savannah River Plant, South Carolina earthquake of June 9, 1985 and its tectonic setting: Earthquake Notes, v. 56, n. 4, p. 101-106.

Wentworth, C.M., and Mergner-Keefer, M., 1983, Regenerate faults of small Cenozoic offset-probable earthquake sources in the southeastern United States; *in* Studies related to the Charleston, South Carolina earthquake of 1886 - Tectonics and seismicity: U.S. Geological Survey Prof. paper 1313-S, p. 1-20.

Withjack, M.O., Islam, Q.T., and La Pointe, P.R., 1995, Normal faults and their hanging-wall deformation: An experimental study: American Association of Petroleum Geologists Bulletin v. 79, n. 1, p. 1-18.

Yantis, B.R., Costain, J.K., and Ackermann, H.D., 1983, A reflection seismic study near Charleston, South Carolina; *in* Studies related to the Charleston, South Carolina earthquake of 1886 - Tectonics and seismicity: U.S. Geological Survey Prof. paper 1313-G, p. 1-20.

Yilmaz, O., 1987, Seismic data processing: Society of Exploration Geophysicists Investigations in Geophysics, v. 2, 526 p.

York, J.E., and Oliver, J.E., 1976, Cretaceous and Cenozoic faulting in eastern North America: Geological Society of America Bulletin, v. 87, n. 8, p. 1105-1114.

Zoback, M.L., Zoback, M.B., and Schiltz, M.E., 1984, Index of stress data for the North American and parts of the Pacific Plate: U.S.G.S. Open File Report 84-157, 62 p.

Appendix A. Seismic Data Processing

In this appendix the details of seismic data reprocessing for the SRS vibroseis data set and the PBF shotgun high resolution data set are presented. All seismic data processing was done at the Regional Geophysics Laboratory (RGL) of Virginia Polytechnic Institute and State University using a VAX 11/780 (later a 11/785) mainframe computer and a Sun Sparc 10 workstation equipped with the CogniSeis DISCO software package and software developed by RGL personnel.

SRS Vibroseis Data Set

The generalized reprocessing sequence for the SRS vibroseis seismic reflection data was previously shown in Figure 9 on page 31. The data reprocessing proceeded from multiplexed field tapes through final migrated and automatic line drawing displays. The critical data processing steps are described below under the appropriate subheadings. Additional data processing information can be found on the individual seismic section side labels in Appendix B.

The entire SRS vibroseis seismic reflection data set with the exception of lines SRS-2, SRS-6 and SRS-8 were reprocessed by the Author. Seismic lines SRS-2, SRS-6 and SRS-8 were reprocessed to 1000 ms by Ashok K. Sen (1991) using the processing scheme developed in this study. Modifications to the stacking velocity functions of lines SRS-2 and SRS-8 required restacking those lines, otherwise these stacks are unchanged from that of Sen.

Preprocessing

Extended Vibroseis Correlation: One of the objectives in the reprocessing of the SRS vibroseis data was to recover any deep crustal reflections that could aid in the interpretation of regional tectonics. To this end extended vibroseis correlation (Pratt, 1982; Okaya and Jarchow, 1989) was performed. The extended vibroseis correlation technique is derived from the fact that as a consequence of the time duration of the sweep the first frequencies in the sweep have been reflected and recorded from deeper levels than the later frequencies. The recovery of these deep reflections can be accomplished in one of two ways, either as a fixed bandwidth extended crosscorrelation, which involves using only part of the original sweep to crosscorrelate the data, or by using the original sweep past the full correlation time, i.e. a self-truncating form of crosscorrelation (Okaya and Jarchow, 1989). In the former case the bandwidth of the output correlated trace contains all frequencies of the truncated sweep, but not of course, those frequencies that have been eliminated through truncation. The self-truncation extended crosscorrelation preserves all the frequencies of the sweep to the full correlation time and past the full correlation time the bandwidth of the data progressively decreases as the length of the sweep that correlates with the field trace becomes less and less.

At RGL extended vibroseis correlation is performed by padding the uncorrelated shot record with zeroes to a user determined length and performing vibroseis crosscorrelation to the new record length, that is, to cross-correlate past the original record length. In essence, this is the self-truncating mode of extended vibroseis correlation. The output record is longer in time than the full correlation time as per the length of zeroes padded and past the full correlation time the bandwidth of the data progressively decreases as per the frequency sweep rate.

The Phase I and Phase II data, with the exception of line SRS-29, were recorded with 10 s duration 20-120 Hz linear upsweeps and 14 s record length to yield 4 s of crosscorrelated data. The 4 s crosscorrelated record length represents the full correlation time, i.e. every frequency in the sweep band is included in the crosscorrelation to 4 s. The lower frequencies in the sweep, as noted above, have been reflected and recorded from deeper levels than 4 s. For these data 9 s of zeroes

were padded to the field records to yield 13 s of data after crosscorrelation which was sufficient to detect reflections from the Moho. Although at 13 s the bandwidth of the data is only 20-30 Hz, at mid-crustal levels, for example at 8 s, the frequency band is 20-80 Hz - a full one and a half octaves, which should allow for good resolution of reflections at those depths.

The EXP lines and line SRS-29 were extend vibroseis correlated to preserve about one octave bandwidth at the extend correlated record length. Line SRS-29 was extend vibroseis correlated to 14 s (29.2 Hz at 14 s) and the EXP lines were extend vibroseis correlated to 8 s (60 Hz at 8 s).

Vibroseis Whitening: For all seismic lines vibroseis whitening (Çoruh and Costain, 1983) was applied to the uncorrelated shot records by applying 1000 ms AGC to the data before extended vibroseis correlation. This process partially compensates for the effects of geometric spreading and anelastic attenuation.

A set of extended vibroseis correlated tapes without vibroseis whitening was also produced for line SRS-1 so that the relative amplitude of crustal seismic reflections could be investigated in future studies.

Shallow Data Set

The large number of seismic lines and the extended record length required for reasons of data management the creation of a 1000 ms subset of the data after CDP sort termed the "shallow" data set. This subset was processed as a separate data package from the "deep" data set, or the entire record length. After processing of the shallow data set was completed, the datum statics, residual statics and stacking velocities determined for the shallow data set were applied to the deep data set.

Datum Statics: All the seismic lines were processed to an 80 m datum using a correction velocity of 900 m/s. A bulk shift of 50 ms was applied to all traces during static application so that data

recorded above datum were not truncated. Therefore, the 50 ms timing line on all the sections represents the 80 m datum.

The 80 m datum was chosen to represent an average elevation for SRS so that there would be roughly equal amounts of cut and fill by the datum correction velocity. The datum correction velocity was chosen empirically after attempts to use subweathering velocities picked from refracted arrivals on shot records led to false geologic structure in brute stack sections. An experiment conducted jointly with A.K. Sen to model the weathered layer using refraction information was tried and abandoned as impractical given the difficulty of determining refraction velocities from vibrator records and the large amount of data present. The results from that experiment were not encouraging, but given the known variation in the near subsurface velocity at SRS, refraction based statics solutions bear further investigation.

The datum correction velocity was determined by repeatedly stacking a part of line SRS-1 (CDPs 2350-2718) recorded over a valley with datum correction velocities from 700-1050 m/s at 50 m/s intervals until the topographic effect of the valley was removed. From these tests 900 m/s was chosen for the datum correction velocity and was subsequently used throughout the data set.

Along some of the seismic lines the use of a single datum correction velocity is clearly inadequate. Notably, the seismic lines recorded over Upper Three Runs valley exhibit velocity push-down under the valley. During the processing of line SRS-4 tests using variable datum correction velocities were made to eliminate the push-down (stations 500-570); however, these tests proved unsuccessful and 900 m/s datum correction velocity was used for all of line SRS-4 to maintain conformity with the other lines. In other areas compressed scale sections show correspondence between topography and time-structure, that suggests either an incorrect datum static resulting from poor velocity control or, possibly, Cenozoic uplift. Undoubtedly, the former situation is most prevalent, although evidence for the latter situation is compelling in some areas, particularly in the hanging wall of the Pen Branch fault along line SRS-3 (Figure 83 on page 170).

The resolution of near surface velocity anomalies that cause false time-structure in these data was the subject of a study by Sen (1991). In that study a method was developed to handle long wavelength statics effects by determining the surface consistent statics necessary to flatten the

shallowest resolvable reflection horizon in a given seismic section. The assumption is that anomalous velocity variations above that horizon give rise to observed false time-structure throughout the data. This static correction, applied in a surface consistent manner to shots and receivers before stack, requires the target horizon to be, indeed, flat. If the target horizon is not flat, then application of the method degrades the quality of the stacked section.

Sen applied his slow-varying statics (SVS) method to parts of lines SRS-1, SRS-2, SRS-2EXP, SRS-3, SRS-4, SRS-6, SRS-7, SRS-8, SRS-23, SRS-27, SRS-28 and PBF-6. The input to the SVS method were the seismic data after two passes of surface consistent residual statics had been run by this Author (except lines SRS-2, SRS-6, and SRS-8). Following application of SVS, stacking velocities were redetermined and a third pass of residual statics run. In many areas application of the SVS method improved reflection continuity. In Figure 86 a part of line SRS-28 processed in this study is compared to that processed using the SVS method. Of particular note is the improvement in reflection continuity between stations 175-225 and increased resolution of sub coastal plain events and the Pen Branch fault with the SVS method. The improvement in overall stack quality obtained by Sen illustrates the need for further work to resolve near surface velocity problems at SRS.

Deconvolution: The Phase I and Phase II data were deconvolved before stack using standard predictive (gapped) deconvolution with a 70 ms operator and 10 ms prediction time (gap). The design window was chosen to span the data and the application gate was 0-1000 ms. Deconvolution of the EXP seismic lines utilized the same parameters with the exception that a 8 ms gap was used.

Velocity Analysis: Stacking velocities were determined through constant velocity stack analysis (CVA). This method was supplemented by use of constant velocity analysis on unstacked gathers in areas where stacking velocities were difficult to determine. Some attempts to use velocity spectra were made, but the method was abandoned early on as the results were difficult to interpret. Generally, stacking velocity functions were picked every 100 CDPs for the Phase I and Phase II lines with infill functions picked in critical or problem areas. Stacking velocity functions for some

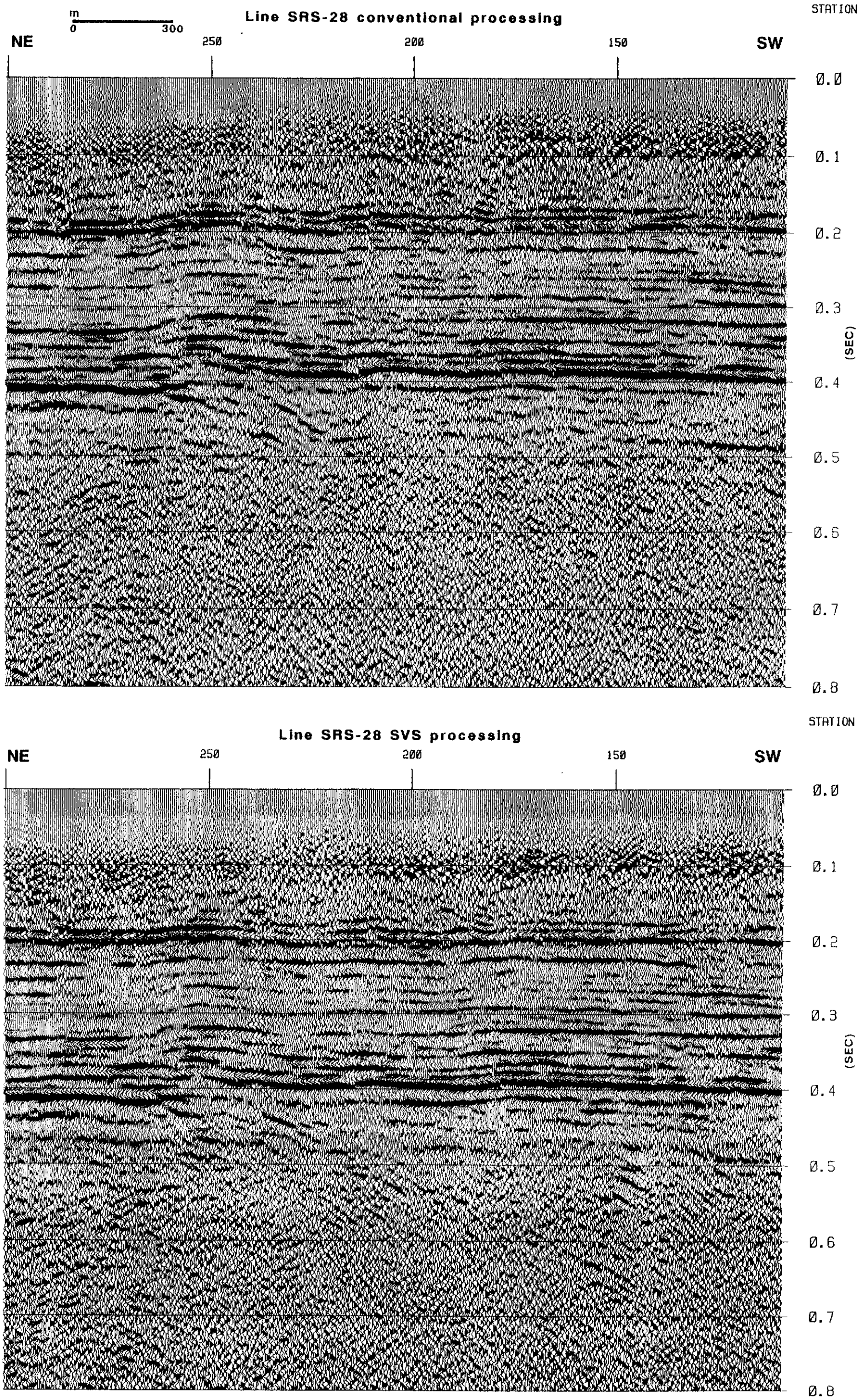

Figure 86. **Line SRS-28 with and without application of SVS:** Conventional data processing (top) versus data processing including the slow-varying statics (SVS) technique by Sen (1991, Fig. 53)(bottom).

of the first seismic lines processed were picked every 50 CDPs, but this density was later found to be unnecessary. Stacking velocities for the EXP lines and line SRS-29 were picked every 50 CDPs with infill functions as appropriate.

To sufficiently cover the range of velocities needed to stack the data, stacking velocity analysis was done separately for reflections from the coastal plain sediments and reflections from basement. For the coastal plain reflections CVA stack panels of 21 CDPs each were generated using constant velocities from 700 to 2200 m/s at increments of 50 m/s to 700 ms. Stack panels for basement reflections were generated using constant velocities from 2200 to 5200 m/s at 100 m/s increments to 1000 ms.

Velocity analysis was closely allied with the residual statics computations. After each of the first two passes of residual statics the stacking velocity functions were updated. All of the seismic lines had stacking velocities computed three times and seismic lines SRS-1, SRS-11, SRS-12, SRS-27, and SRS-28 had stacking velocities computed four times.

The lack of continuity of reflections originating from the Dunbarton basin in the reprocessed lines SRS-2 and SRS-8 processed by Sen (1991) required repicking the final stacking velocities for the basin reflections. With this exception, the prestack processing of lines SRS-2 and SRS-8 was unchanged from that of Sen.

One of the striking differences between the original processed SRS data and the reprocessed data in this study is the recovery of reflections from the Dunbarton basin sediments. In general, the original processed data show little evidence for the Dunbarton basin, other than a decrease in the amplitude of the multiple reflections from the top of basement. Some suppression of multiples occurs through use of deconvolution, but much multiple suppression results from the horizontal stacking process as consequence of the differential NMO between primary and multiples events that arrive at about the same time. The constant velocity analyses and velocity spectra indicated that the multiple energy was quite strong and required that stacking velocities be picked carefully to enhance primary events. In most cases, the reflections from the Triassic sediments are low amplitude, lower amplitude than the multiples on the stack panels, and have high stacking velocity (2600-3500 m/s). The synthetic seismogram from borehole DRB-10 (Appendix C) clearly indicates the lack of

acoustic impedance contrast within the basin fill. Only on lines SRS-4 and SRS-13 could stacking velocities for the Triassic sediments be picked unambiguously. For these two lines, especially along line SRS-13, the greater reflectivity of the basin sediments might result from sill injection and contact metamorphism.

Mute Patterns: Mute patterns were picked automatically using the criterion to mute the data where the seismic wavelet was stretched greater than 40 percent by the stacking velocity function. The mutes picked by this technique compared favorably to mute patterns picked manually using conventional methods; however, for line SRS-29 the automatic mutes did not adequately eliminate the refraction from the top of basement, perhaps as a consequence of the longer spread length (1584 m) compared to the other lines (600-800 m); hence for this line mute patterns were picked manually. Also, mute patterns for line 2EXP were picked manually in an attempt to recover the shallowest reflections possible. In that case, the difference in the stacked section between the mute types was minimal. Inasmuch as the mutes automatically change as the stacking velocity changes, the mutes were fixed after the second velocity function was picked.

In addition to the mute patterns described above, seismic line SRS-12EXP required application of surgical mutes to eliminate source generated noise.

Residual Statics: For all seismic lines at least three passes of surface consistent residual statics with four iterations per pass were computed and applied to the data. After the first and second passes of residual statics stacking velocities were redetermined. In general, stabilization of the statics solution was achieved after the second pass of statics; the third pass was mostly cosmetic.

To reduce computation time, which was exceeding 24 hours per pass for the longer lines, the first two static passes for the Phase I and Phase II lines (except SRS-29) were computed using only every other CDP gather. Elimination of every second gather in computing residual statics can be justified from consideration that each shot and receiver location is used for more than one gather, the spatial lag between CDPs is relatively small, and the Atlantic Coastal Plain sediments are devoid of large geologic structure. Tests comparing stacks made with residual statics computed using every

CDP as opposed to every other CDP showed only slight degradation in stack quality if residual statics computed using every other CDP were used. In Figure 87 plots of the residual statics computed with every CDP and every other CDP for a part of line SRS-7 are shown. The plots are similar; only minor differences exist in the values of the short wavelength statics.

The first and second residual statics passes for the Phase I and Phase II lines were computed using 15 stacked CDPs to form the pilot trace. The third residual statics pass used 30 stacked CDPs to form the pilot trace in order to maintain the same spatial lag as the first two passes. For seismic lines SRS-29 and SRS-2EXP 15 CDPs were used to form the pilot trace and for seismic lines SRS-9EXP and SRS-12EXP 30 CDPs were used to form the pilot trace.

For the first two iterations in any residual statics pass the traces in the gathers were replaced by the envelopes of the traces to ensure that the pilot trace was a coherent stack of CDPs for each update. The envelope of a seismic trace is defined by:

$$E(t) = \sqrt{f(t)^2 + H(f(t))^2}$$

where f(t) is the seismic trace and H(f(t)) is the Hilbert transform of the seismic trace. The envelope of a seismic trace has very low frequency content which would help ensure a coherent stack of CDPs to form the pilot trace while avoiding cycle skips in the crosscorrelation process in the residual static computation.

For computation of residual statics the reflection time-structure was flattened on the top of basement reflection. The static window typically included 200-300 ms of the basement time section and as much as possible of the Coastal Plain time section with care exercised to avoid the mute patterns. The maximum allowable static was 10 ms for all passes, although some experiments indicated that maximum statics of 4-6 ms could be used. Indeed, a maximum allowable static of 3 ms was used for the PBF high resolution lines.

The computation of residual statics was perhaps the most vexing aspect of reprocessing the shallow Conoco data set. Often static busts would be encountered in the stacked data that would require the source of the problem be found (bad velocity function, poor flattening of input data, interference from mutes etc.) and residual statics recomputed for the entire line. What was a

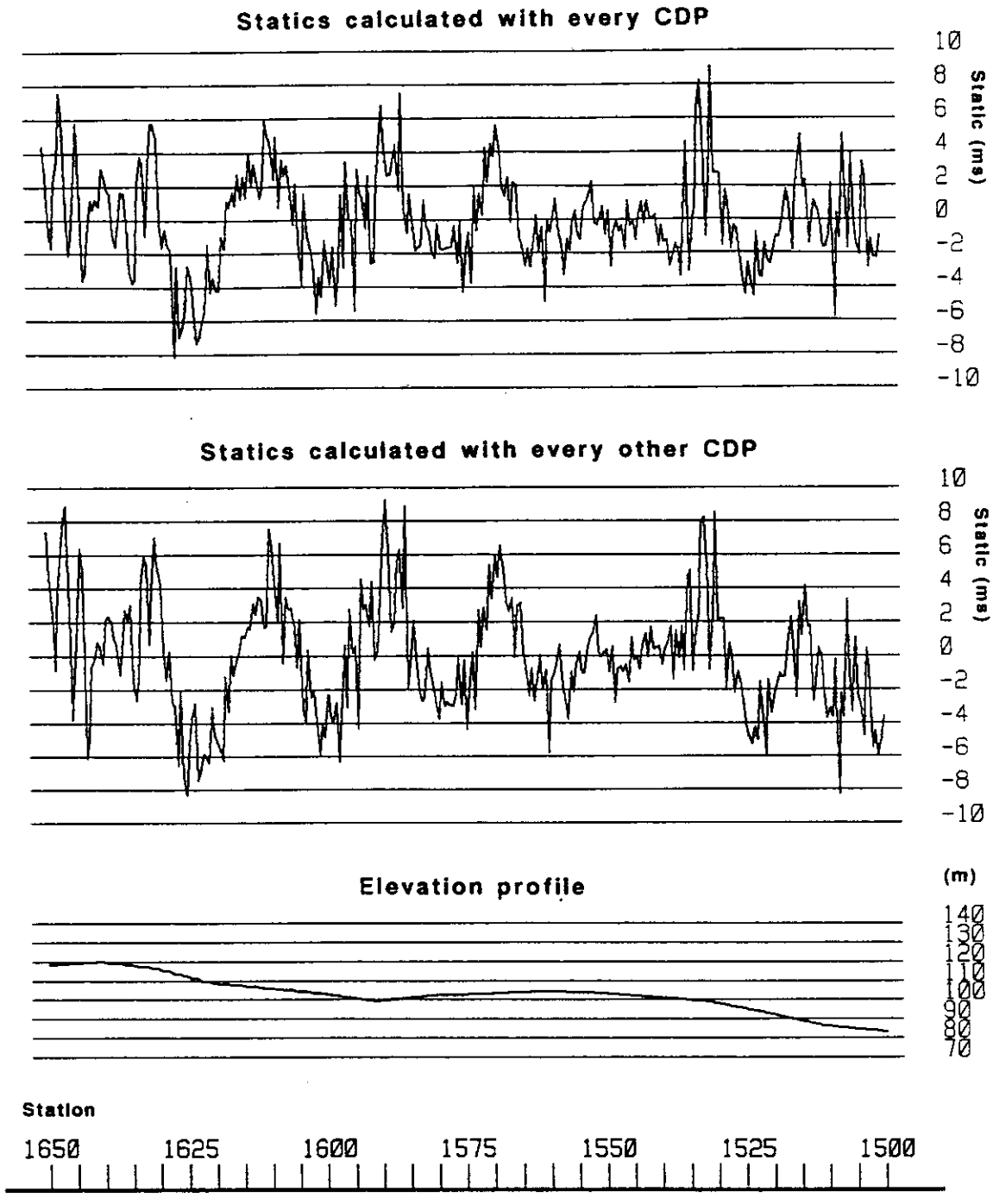

Figure 87. **Plot of residual statics:** Line SRS-7. Total residual statics (sum of shot and receiver statics) calculated using every CDP and every other CDP in the residual statics computations. First pass of residual statics using four iterations, 15 trace pilot, and a maximum static shift of 10 ms.

"correct" stack was guided by brute stacks, comparisons with the previous Conoco processed stacks and the Author's experience in processing land seismic data. For certain problem lines residual statics were recomputed several times for a given pass until a suitable seismic section was obtained. Seismic lines with particularly severe statics problems included: SRS-7 (at the line bend), SRS-12, SRS-28, SRS-29, SRS-12EXP, and SRS-9EXP.

Along line SRS-7 the residual statics were well behaved except in the vicinity of station 850 where Upper Three Runs crosses the line and the line direction changes. There the stacked data showed an offset that could be: (1) a near vertical down-to-the-north fault, or (2) a static bust caused by either near surface velocity variation or improperly stacked data at the line bend. The Conoco stack in the same area also showed an offset, but the brute stack of SRS-7 did not. Furthermore, the brute stack section showed reflections from the Coastal Plain sediments continuous across this area.

To resolve this issue a subset of the line spanning several spread lengths on either side of station 850 was processed separately until the offset was eliminated by judicious choice of stacking velocities and residual statics parameters. Afterwards this subset was spliced back into line SRS-7. To eliminate the offset did not require unrealistic stacking velocities or residual statics parameters. In fact, the data reprocessed in this study as a whole were found to be sensitive to subtle changes in the stacking velocity functions. Although the coastal plain reflections are continuous across station 850, and the basement reflection is not offset in this area, it is still not clear to the Author whether or not there exists a fault. What does appear to be certain is that if a fault offsets the basement reflection, it probably does not penetrate far into the sedimentary cover.

The statics problems along line SRS-9EXP were so severe that the final stacked section required the splicing together of three subsets of data. The cause of the instability in the residual statics solutions for this line is unknown, neither line SRS-9 or the brute stack of SRS-9EXP indicated any problems. An explanation for the unstable residual statics solutions could be that because reflections from the coastal plain sediments are completely muted at the far offsets as result of time-thinning of the sedimentary section across Upper Three Runs, insufficient statistics exist to achieve a stable statics solution. A similar situation occurs along line SRS-12 because of the

thinning of the coastal plain section updip and could explain the difficulties experienced with that line and line SRS-12EXP; however, as previously stated no residual statics problems were encountered with line SRS-9, which tends to weaken the above supposition. In any case, no reasonable combination of stacking velocities or adjustment in residual statics parameters (maximum static, window, center event, pilot sum etc.) was able to yield a problem-free stack for all CDPs.

A severe static bust in line SRS-8 occurs at station 560 at the location of the Steel Creek fault. Although the magnitude of the bust is but a single cycle skipped, it is sufficient to change the apparent sense of fault movement. This example illustrates the critical need for good residual statics determinations as most of the faults detected in the Coastal Plain section at SRS are represented by reflection displacements of one cycle or less. The shallow data set version of line SRS-8 was not reprocessed in this study other than the velocity repicking for the basin reflections and line restacking discussed earlier. The residual statics for this line should be recomputed with extreme care taken to avoid statics problems in the vicinity of known faults.

Postprocessing

Zero-Phase Deconvolution: Zero-phase deconvolution was applied after CDP stack to whiten the amplitude spectrum of the traces and thereby increase seismic resolution. The increased seismic resolution should allow for better ties to borehole data and better definition of sedimentologic structures in the Atlantic Coastal Plain sediments.

The DISCO zero-phase deconvolution operator is a simple frequency domain inverse filter designed to shape the amplitude spectrum of an input trace. The operator, O(f), is defined:

$$O(f) = \frac{D(f)}{A(f)}$$

where D(f) is the desired output amplitude spectrum and A(f) is the amplitude spectrum of the design gate.

For the data in this study the amplitude spectra were shaped to the vibrator sweep band for each seismic line. The design gate included only the Coastal Plain section and the application gate was 0-1000 ms.

Signal Enhancement: Following application of zero-phase deconvolution a signal enhancement process called Digistack (CogniSeis DISCO module) was performed on the stacked data. Digistack is the weighted sum of the data trace with a "signal" trace derived from coherency estimations of the data along time dips in a user defined space-time window. The overall effect is to enhance reflection continuity and strength while still preserving the more subtle amplitude characteristics of the data. Seismic sections processed with Digistack are typically far more realistic appearing than sections processed with other common poststack signal enhancement routines such as F-K filtering and F-X deconvolution.

The Digistack seismic sections represent an equal weight between the data trace and the signal trace. For the Phase I and Phase II data the window for coherency estimation was 15 traces by 164 ms and incremented every 5 traces and 80 ms. The maximum dip range was $\pm$ 30 ms and incremented every 5 ms. The window for coherency estimation for the EXP lines was 7 traces by 80 ms and incremented every 3 traces and 40 ms; the dip range and dip increment was the same as for the Phase I & II lines.

Imaging

All of the seismic lines were migrated to 1000 ms using conventional finite difference time migration as developed by Claerbout (1985). Selected seismic lines were also migrated using Kirchhoff migration (Schneider, 1978). In addition, partial prestack time migration (DEVILISH; Sherwood, Schultz and Judson, 1976) and finite difference prestack time migration were performed on line SRS-2EXP.

Finite Difference Migration: The small CDP intervals for most of lines required spatial decimation of the data to ensure an adequate migration aperture. The decimation factor was chosen to achieve a balance between undermigration and spatial aliasing of steeply dipping reflections. The decimation factors were 2:1 for the 8.4 m CDP spacing data and 3:1 for the 6.1 m CDP spacing data. Line SRS-29 was migrated undecimated. To maintain conformity with the other seismic lines the EXP lines were migrated after 6:1 trace decimation. Seismic line SRS-2EXP was migrated both decimated and undecimated because of spatial aliasing concerns related to imaging the Pen Branch fault.

For finite difference migration the unaltered stacking velocities were used to migrate the data and the downward continuation time-step in all cases was 20 ms. As a whole, the data was relatively insensitive to migration velocity function changes as migrations performed with varying percentages of the stacking velocities were similar.

Seismic lines SRS-3, SRS-3EX and SRS-7, SRS-7EX were composited and migrated as single lines. The compositing process entailed reordering the CDP numbers for each line and sorting the stacked traces in ascending CDP order. The station numbers of these lines are unchanged.

Kirchhoff Space-Time Migration: Seismic lines SRS-3, SRS-4 (CDPs 1800-2458), SRS-27, SRS-28 and SRS-2EXP were also migrated using Kirchhoff time-space migration to investigate whether faults would be better imaged using this method than with the finite difference method. Advantages of Kirchhoff migration over finite difference migration are derived from the fact that the method is an exact solution to the scalar wave equation; hence no approximations are used and structural dips up to 90° and beyond can be migrated. Furthermore, the DISCO module for Kirchhoff migration uses a time and space variant migration aperture and thus, the data need not be decimated to ensure an adequate migration aperture. However, the operator is prone to aliasing, lateral velocity variations are difficult to handle, and computation times are much longer compared to other methods (Yilmaz, 1987).

The data input to the Kirchhoff migration module were interpolated to 1 ms and migrated using the stacking velocities. In general, the data migrated with this technique had slightly higher

signal-to-noise ratio and better definition of shallow time horizons than the finite difference migrated data. Reflection events within the Coastal Plain section appear slightly undermigrated and subcoastal plain reflections are overmigrated. The optimum migration velocity would need to be empirically determined.

Partial Prestack Migration and Prestack Migration: The partial prestack migration, or dip moveout (DMO), method DEVILISH (Sherwood, Schultz and Judson, 1976) and finite difference prestack time migration was applied to line SRS2EXP to image the Pen Branch fault. Inasmuch as prestack migration techniques require the generation of common offset sections, line SRS-2EXP was resorted using a straight line geometry. The line was recorded with consistent shot to receiver offsets and source moveups so that the modified geometry is justified.

The data processing sequence adopted for partial prestack migration was similar to that described by Yilmaz (1987). In brief, DEVILISH was applied to CDP gathers after the NMO correction, NMO was removed and a new stacking velocity was determined, followed by stacking and data processing as per Figure 9 on page 31. The output seismic section was migrated with finite difference migration using the parameters previously mentioned. The final poststack time migrated data should be equivalent to the result from a full prestack time migration.

The finite difference prestack time migration option in DISCO was applied to the straight line sort CDP gathers after the NMO correction followed by stacking and poststack processing as described above.

Comparison Among Imaging Techniques: Comparisons among finite difference migration, Kirchhoff migration, partial prestack migration, and prestack migration applied to image the Pen Branch fault are shown in Figure 88 for line SRS-2EXP.

Between the prestack migration sections, the section produced with DEVILISH shows better definition of the shallow time section above 200 ms; in particular the reflection at 140 ms between stations 750-760 is well imaged. This result might also be caused by stacking velocity repicking given the sensitivity of these data to velocity variations and not necessarily the DEVILISH tech-

nique. The prestack migrated section appears slightly undermigrated, especially the lower coastal plain time section. No comparison can be made for the deeper events as the stacking velocities for the DEVILISH section were not determined for reflections below the basal unconformity.

Only subtle differences exist among the sections produced by the various imaging techniques - probably insufficient to alter an interpretation. Among the various imaging methods investigated the partial prestack migration section resulted in slightly better definition of the Coastal Plain section than the other methods. For general use finite difference migration, by far the least time intensive of the techniques investigated, is likely to be adequate to image geologic structures that exist in the Atlantic Coastal Plain section at SRS. The more exotic and time intensive (costly) methods might be reserved for special applications.

Refraction Stack

In addition to the conventional reflection data processing described above, a refraction stack section of line SRS-1 was produced. The stacking of the refractions rather than the reflections was motivated by two ideas: (1) whether it was possible to recover information on the upward penetration of faults shallower than the reflection stacks would allow, and (2) detection of possible outliers of Triassic basin fill northwest of the Pen Branch fault. Sen (1991) in his work produced refraction stacks of parts of lines SRS-1, SRS-2, SRS-7, SRS-23, SRS-27 and SRS-28 to investigate shallow deformation associated with the Pen Branch and ATTA (Upper Three Runs) faults.

The construction of the refraction stack section is based on the concept that each reflection CDP also corresponds to a refraction midpoint so that application of linear moveout (LMO) to the refracted arrivals and performing horizontal stacking produces a trace that represents the refraction delay time for the center of the CDP. Stacking CDPs in this manner produces a delay time refraction stack section. The refraction stack produced in this study is predicated on the assumptions that within the offset range of a CDP geologic dip is small; therefore, stacking unreversed raypaths is permissible. Also, the averaging of the refractor topography during the stack is weighted towards

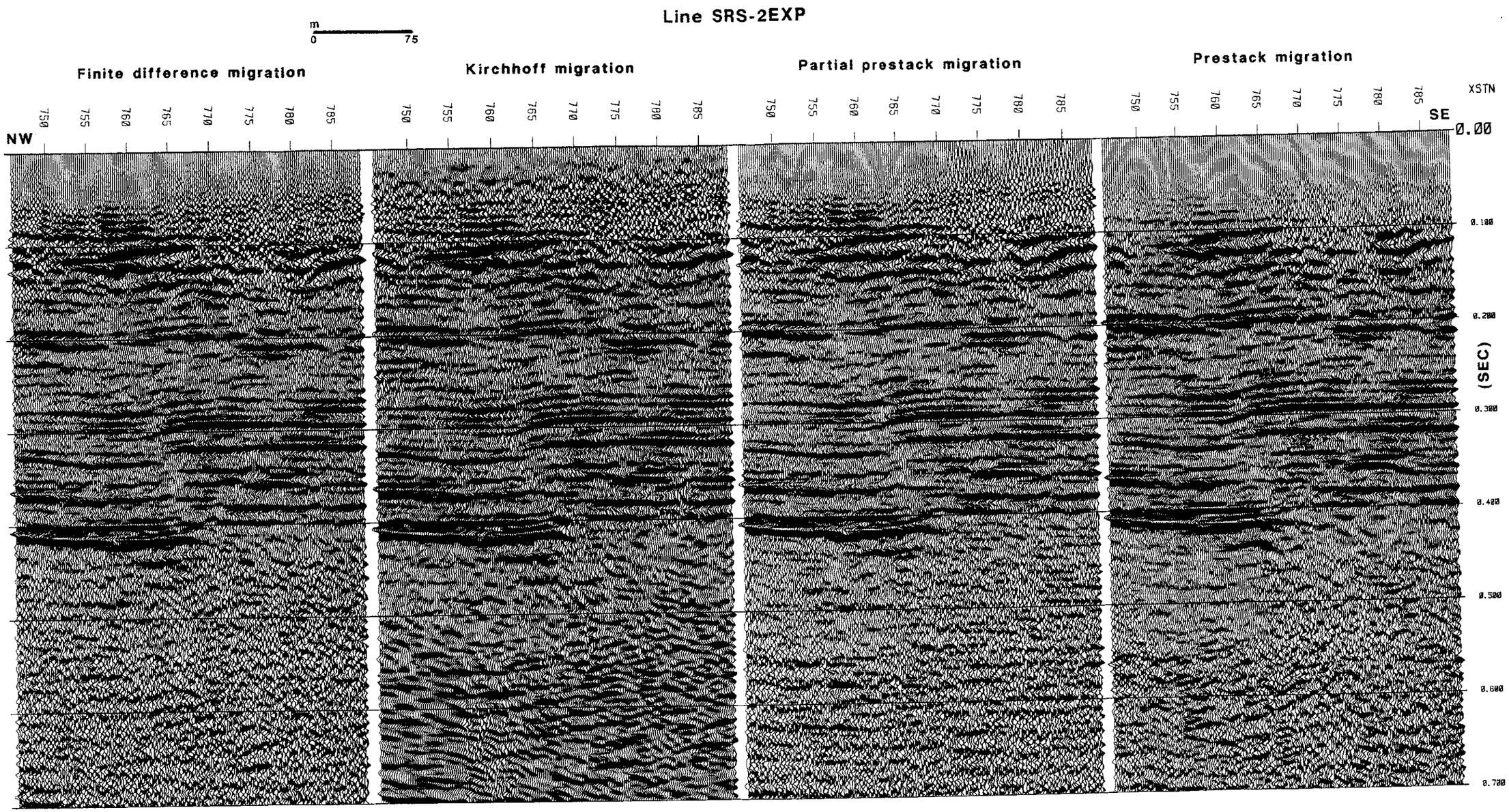

Figure 88. Comparisons among migration methods: Line SRS-2EXP. Comparisons among finite difference migration, Kirchhoff migration, partial prestack migration and prestack migration applied to image the Pen Branch fault.

the midpoint of the gather so that faults and other abrupt geologic features can be resolved. The latter assumption can be improved upon if the range of offsets is restricted to optimize the stack.

The use of the refraction stack to retrieve shallow geologic information is derived from the circumstance that because reflections from shallow layers are muted during processing to eliminate NMO stretch and postcritical angle reflections, the CDP fold at early times in the section is typically far less than the nominal value and the corresponding signal-to-noise ratio is low. If, however, shallow refractions can be stacked the nominal fold of the stacked refractions might be much greater than the shallow reflections and produce a sufficiently high quality section to allow interpretation of shallow geologic structure that otherwise could not be reliably interpreted.

The data used to produce the refraction stack consisted of the CDP gathers processed as per Figure 9 on page 31 to the point before application of the NMO correction. At this stage the LMO correction was applied using velocities previously determined from constant velocity LMO stacks. The data were then stacked, filtered, and displayed.

The critical step in producing the refraction stack is determination of the refraction stacking velocities. The choice of velocity changes the delay time of the stacked refraction and the apparent structure portrayed by the refraction stack. Therefore, refraction velocities must be picked with care. The best refraction stack section in terms of continuity of the stacked event were obtained by using either constant velocities or slowing varying velocities for a refractor. For the three refractions that could be stacked on line SRS-1 the range of stacking velocities was 1650-1850 m/s for the shallowest event, 2300-3200 m/s for the middle event, and 4700-6000 m/s for the basement refraction. To detect the present or absence of Triassic basin fill a constant velocity stack at 5500 m/s was sufficient to discriminate between refractions from crystalline basement and Triassic basement.

Display

The display filter for the Phase I and Phase II seismic lines (except SRS-29) is 30-35-110-120 Hz; for the EXP lines 30-40-150-160 Hz and for SRS-29 25-30-100-110 Hz. The

display gain for all lines is 250 ms AGC. Conventional wiggle trace, variable area paper seismic section copies are produced at 40 traces per inch and 10 inches per second.

Deep Data Set

Following completion of the reprocessing of the shallow data set the bulk shift, datum statics, and residual statics determined for each line were applied to the CDP gathers of the corresponding deep data set. Afterward, the data, except for the EXP lines and line SRS-29, were resampled to 4.0 ms. The resampling of the data was necessary to reduce processing time, which was in the excess of 24 hours, to produce stacks of the longer lines. Consideration of the frequency content of the data, the existence of the shallow data set, and the insensitivity of the stacking velocity function to velocity changes below 1000 ms further justified the coarser sample interval.

Deconvolution: All the seismic lines were deconvolved before stack using standard predictive deconvolution operators determined from three design gates in the data from 10-900 ms, 1200-2800 ms, and 4500-6500 ms and applied to the data from 0-900 ms, 1200-3500 ms, and 4500-13000 ms (4500-8000 ms for EXP lines, 4500-14000 ms for line SRS-29) with linear interpolation of the operators between application gates. The gaps and filter lengths were unchanged from that used for the shallow data.

Velocity Analysis: Except for those portions of the Phase I and Phase II seismic lines that crossed the Dunbarton basin, no additional velocity analyses were performed. The stacking velocity function used for times greater than 1000 ms was a type function developed from stacking velocities determined from line SRS-29 and other lines. Examination of plots of normal moveout versus zero-offset time for various velocities and fixed offset (Figure 89) demonstrates that at 1000 ms for RMS velocities of 3-5 km/s the normal moveout at the farthest offsets is only 6-19 ms - barely resolvable given the sample interval of data. For times greater than 2000 ms Figure 89 can be in-

terpreted that almost any stacking velocity can be used to stack the data because of the flattening of the reflection hyperbola with increasing time. Despite the lack of NMO for deep reflections, the deep data appear to be relatively free of multiples. Possibly, most of the multiples are eliminated through use of predictive deconvolution.

Velocity analysis for the lines that crossed the Dunbarton basin was carried out to 3000 ms using the same parameters as for the shallow data. As demonstrated by Figure 89 the amount of normal moveout expected from reflections from the basin fill is only negligibly greater than that from the crystalline basement; hence detailed velocity analysis is probably unnecessary beyond 1500 ms for these data.

Postprocessing: After CDP stack, predictive deconvolution was performed using the same parameters as for the prestack deconvolution and prior to display a time-variant bandpass filter was was applied. The time-variant bandpass filters used for the Phase I and Phase II lines, EXP lines, and line SRS-29 appear in Table 5.

Migration

All of the seismic lines were migrated to 6 s using finite difference migration and the unaltered stacking velocities. The migration layer thickness was increased to 40 ms for the basement events and to maintain conformity with the shallow data set the same section decimation values were used. In general, a visually acceptable migration for the Phase I and Phase II data can be obtained to 3 s.

The relatively short line lengths of the Conoco data set preclude obtaining a good image of reflectors beneath the coastal plain sediments to all but 2-3 s migrated time. The problem arises because reflections from steeply dipping reflectors could not be recorded with the line lengths present; thus, the migrated data are effectively dip-filtered.

Following an analysis developed by Lynn and Deregowski (1981) for zero-offset data and straight raypaths, Figure 90 was produced to show the maximum recordable dip for a typical seis-

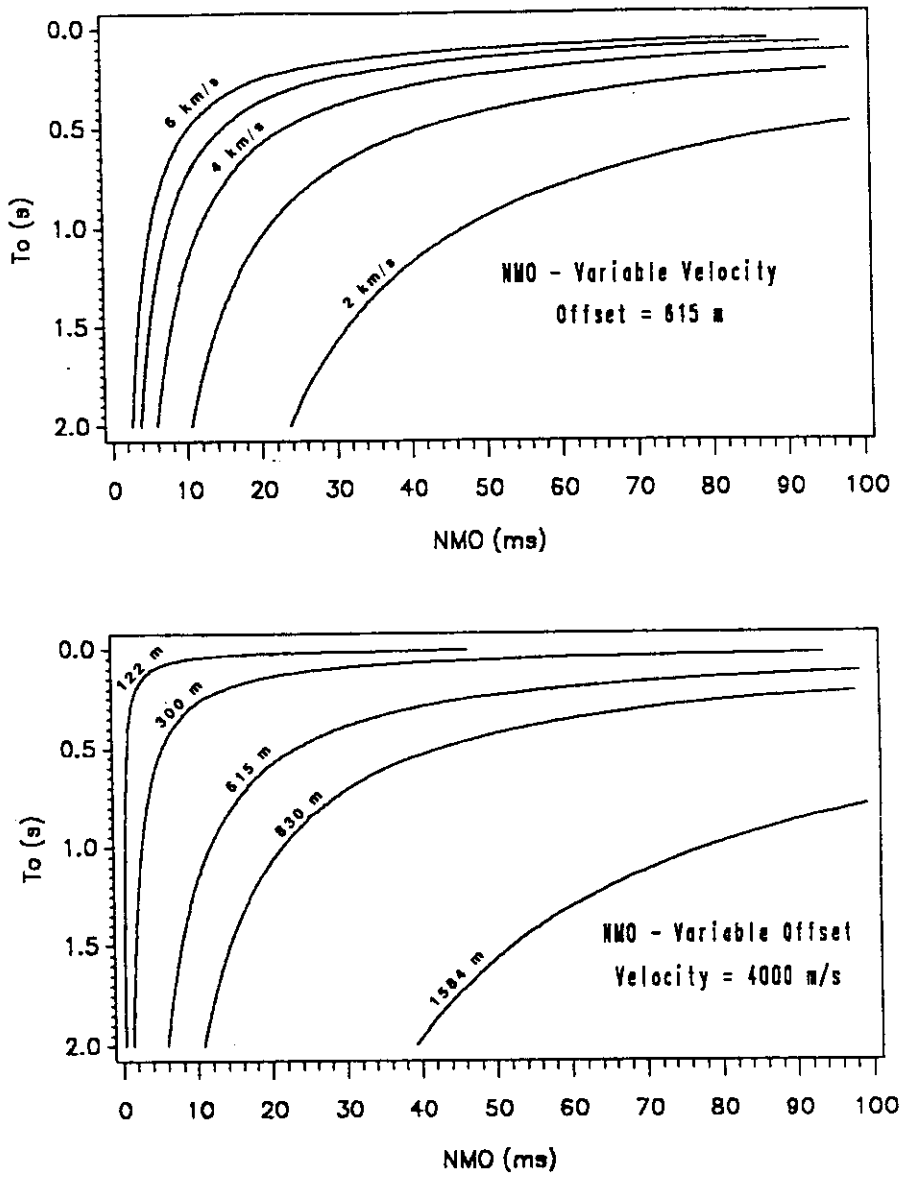

Figure 89. NMO curves: (A) NMO versus zero-offset time for 615 m offset and RMS velocities 2-6 km/s. (B) NMO versus zero-offset time for velocity 4 km/s and the range of maximum offsets of the seismic data reprocessed in this study. The above curves are calculated from the approximation $NMO \simeq X^2/[2V_{RMS}^2 t_o]$ (e.g. Yilmaz, 1987) which holds for flat reflectors and small spreads. In the presence of the structural dip stacking velocity increases and correspondingly the normal moveout decreases resulting in even less resolvability of the stacking velocity function.

Table 5. SRS deep data time-variant filters.

Phase I & Phase II

Time ms	Passband Hz
0 - 550	30-35-110-120
2000 -	25-30- 95-105
4000 -	15-20- 70- 75
5500 -	15-20- 65- 70
7000 -	15-20- 45- 50
- 13000	15-20- 40- 45

Line SRS-29

0 - 1000	25-30-100-120
1600 -	20-25- 95-100
4000 -	15-20- 85- 90
7000 -	8-15- 80- 85
11000 -	8-15- 60- 65
- 14000	8-15- 30- 35

Experimental

0 - 700	35-40-150-160
1200 -	30-35-140-150
2800 -	25-30- 85- 90
6000 -	25-30- 75- 80
7000 -	25-30- 70- 75
- 8000	25-30- 60- 65

mic line in the Conoco data set (20 km by 13 s; V = 6 km/s). For example, at 3 s on a migrated section a 30° dipping reflection is imaged 5 km from its position on the unmigrated section. That is, a 5 km stepin is needed to image a 30° dip at 3 s. If a 50° dip is imaged, which is similar to known dips of foliations in the crystalline basement at SRS, the lateral displacement of that event is nearly 11 km if imaged at 3 s. Therefore, most of the Phase II data and many of the Phase I seismic lines probably represent highly dip-filtered data at migrated times below 3 s. The unrecordable dip problem discussed above is ameliorated somewhat if the true migration velocities, curved raypaths, and refraction through the Coastal Plain sediments are considered; however,

counteracting those effects are the geophone array response and the limitations inherent in the the migration algorithm used.

Another illustration of the limitations of the migrated deep data is shown in Figure 91, which is essentially a display of the impulse response of the finite difference migration operator used. Note that at 8 s the breadth of the migration operator is greater than the seismic line length. This result is consistent with the dip limitations shown in Figure 90.

Although determination of an accurate deep velocity function is not necessary to either attenuate multiple reflections or even to stack these data, it is of critical importance in order to perform a good migration. To this end, refraction data and wide angle reflection data have been used in other areas to develop velocity functions necessary to migrate short spread-length deep seismic reflection data (McBride et al., 1993). In lieu of better velocity information, constant velocity migration stacks can be used to image selectively specific features of interest. In any case, even with better velocity information, the migration accuracy is limited by the profile length as discussed above.

Automatic Line Drawing

Conventional wiggle trace, variable area displays of crustal seismic reflection data are usually inadequate to portray the geometry of the reflection packages. Often these data are presented in some sort of subjective line drawing form. The automatic line drawing (ALD) display (Çoruh et al., 1988) developed at RGL is designed to be an objective display of crustal seismic reflection data based on the coherency of reflection events within a user-defined moving time-space window. The ALD process preserves the original waveform and relative reflectivity of the original seismic data and enhances those reflections that are weak or otherwise obscured by noise. The method is similar to the signal trace extraction previously described for the Digistack process with the addition that in the ALD process the values of signal traces are raised to a power by a user defined exponent to further discriminate among coherent events.

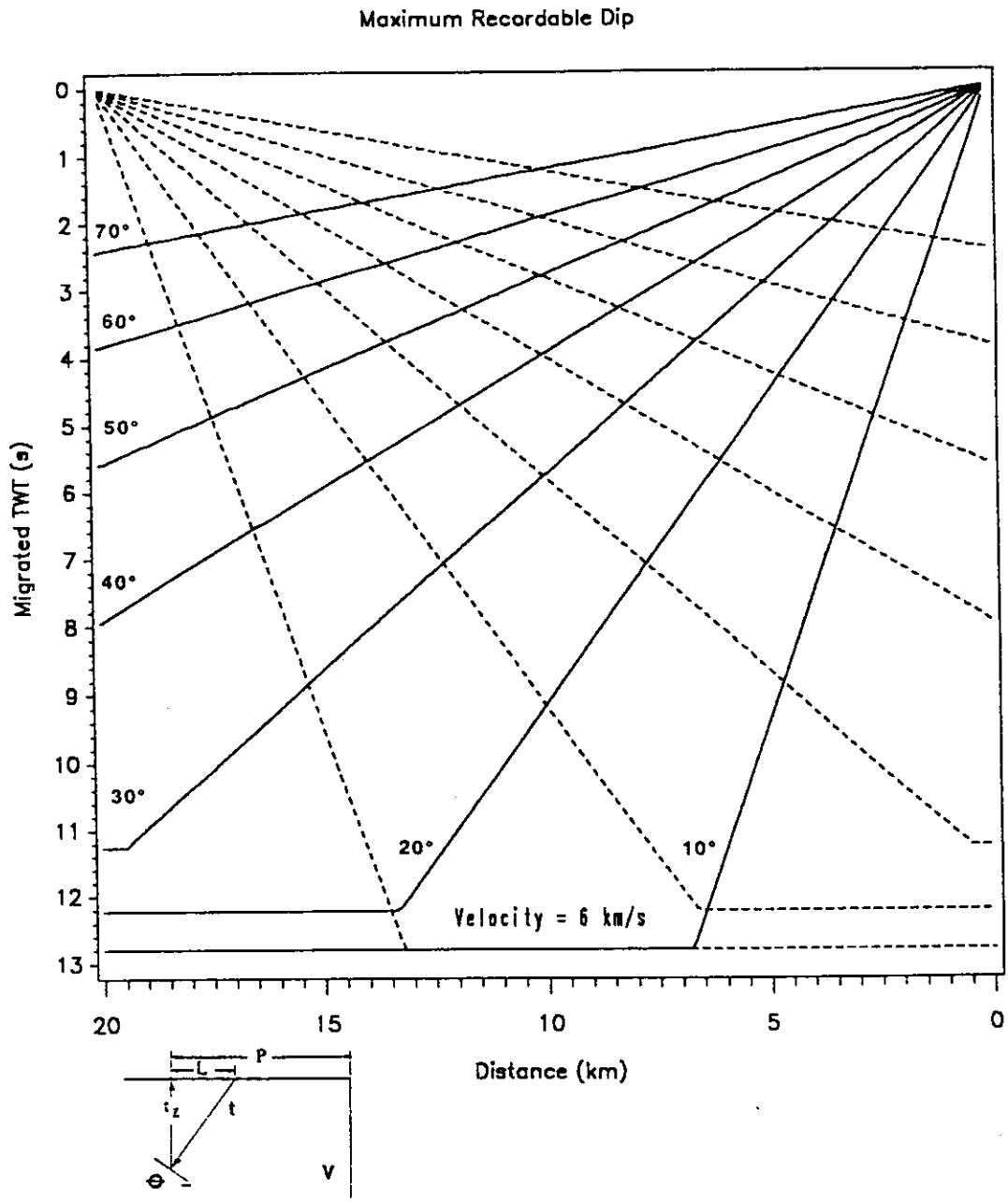

Figure 90. **Maximum recordable dip:** Contours of maximum recordable dip, or lateral displacement of reflection events, for a migrated seismic line (20 km by 13 s). Crustal velocity of 6 km/s is assumed. Dips to the right are solid lines, dips to the left are dotted lines. Horizontal contours represent dip limitation resulting from insufficient recording time. The inset figure shows the geometry used to develop the contour plot where θ is dip, t_z is the migrated two-way time, t is the recorded unmigrated time, L is the lateral displacement of the event and P is distance of the event from the downdip edge of the seismic line, i.e. the instep of the event. As long as the instep P, is greater than or equal to the lateral displacement L the event is recorded and can be migrated. From this geometry the lateral displacement of a reflection event is $L = [Vt_z/2] \tan \theta$.

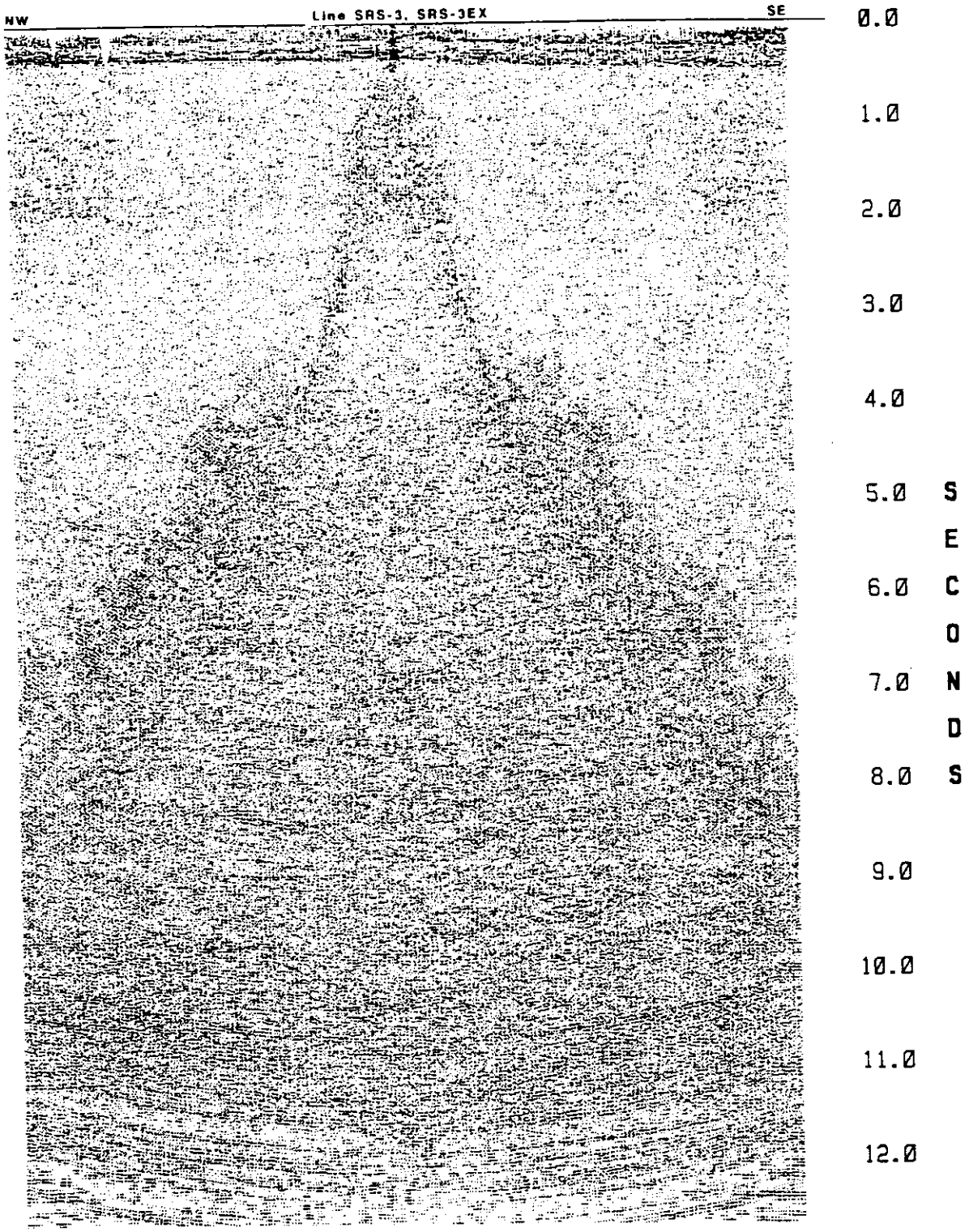

Figure 91. Migration cone: Line SRS-3. The maximum migratable dip decreases with increasing time. Figure was produced by gaining a single trace by 100 db and performing migration as would be done conventionally. The resulting migration cone defines the impulse response of the migration operator. Display is 1:1 for velocity 6 km/s. AGC 5000 ms.

Automatic line drawings were produced for all the migrated and unmigrated deep seismic lines. Prior to the ALD process the basement reflections were gained (20 db for the unmigrated sections, 30 db for the migrated sections) to suppress the AGC shadow caused by the strength of the top of basement reflection. The window for coherency estimation for all seismic lines was 21 traces by 200 ms and incremented every trace and every 100 ms. The maximum dip range across the window was $\pm$ 15 ms for the 3.1 m CDP data, $\pm$ 43 ms for the 6.1 m CDP data, $\pm$ 55 ms for the 8.4 m CDP data, and $\pm$ 100 ms for line SRS-29. For all seismic lines the dip increment was 5 ms.

The available displays of the Conoco seismic reflection data set are tabulated in Table 6. Note that not all displays tabulated in Table 6 are collected in Appendix B.

PBF Shotgun High Resolution Data Set

The generalized reprocessing sequence for the PBF high resolution seismic reflection data was previously shown in Figure 14 on page 38. Described below under the appropriate subheadings are the critical processing steps. In general, the data reprocessing scheme for these data closely followed that of the SRS shallow data set to maintain conformity with the latter. Additional data processing information can be found in the individual seismic section side labels in Appendix B.

Preprocessing: Spectral analysis of shot records indicated that most of the usable reflection signal in the data existed below 250 Hz (Figure 92); therefore, to speed computation times the data were resampled to 1.0 ms. Also at this stage debiasing was performed and the record length was padded to 500 ms. The latter was done so that the 50 ms bulk shift could be accommodated without loss of data beyond the recorded record length. The debiasing was found necessary for the shot data of line PBF-18 and was applied to the shot data of line PBF-6 as a matter of course.

Table 6. Available displays of Conoco SRS seismic reflection data.

Stacked seismic sections

Phase I

Line No.	Stack	FD Mig.	Kirch. Mig.	Stack Deep	ALD	FD Mig. Deep	ALD FD Mig.
1	x	x		x	x	x	x
2	x	x		x	x	x	x
*3	x	x	x	x	x	x	x
3EX	x			x	x		
4	x	x	x	x	x	x	x
5	x	x		x	x	x	x
6	x	x		x	x	x	x
*7	x	x		x	x	x	x
7EX	x			x	x		
8	x	x		x	x	x	x
9	x	x		x	x	x	x
10	x	x		x	x	x	x
11	x	x		x	x	x	x
12	x	x		x	x	x	x
13	x	x		x	x	x	x

Phase II

18	x	x		x	x	x	x
21	x	x		x	x	x	x
23	x	x		x	x	x	x
25	x	x		x	x	x	x
26	x	x		x	x	x	x
27	x	x	x	x	x	x	x
28	x	x	x	x	x	x	x
29	x	x		x	x	x	x

Experimental

2EXP	x	x	x	x	x	x	x
9EXP	x	x		x	x	x	x
12EXP	x	x		x	x	x	x

* Seismic lines SRS-3, SRS-3EX and SRS-7, SRS-7EX were composited and migrated as single profiles. Deep stacks for the Phase I and Phase II data are to 13 s, for line SRS-29 to 14 s and for the EXP lines to 8 s. All of the deep stacks were migrated to 6 s. Not listed above is the refraction stack of line SRS-1 and the partial prestack migration and prestack migration sections of line SRS-2EXP.

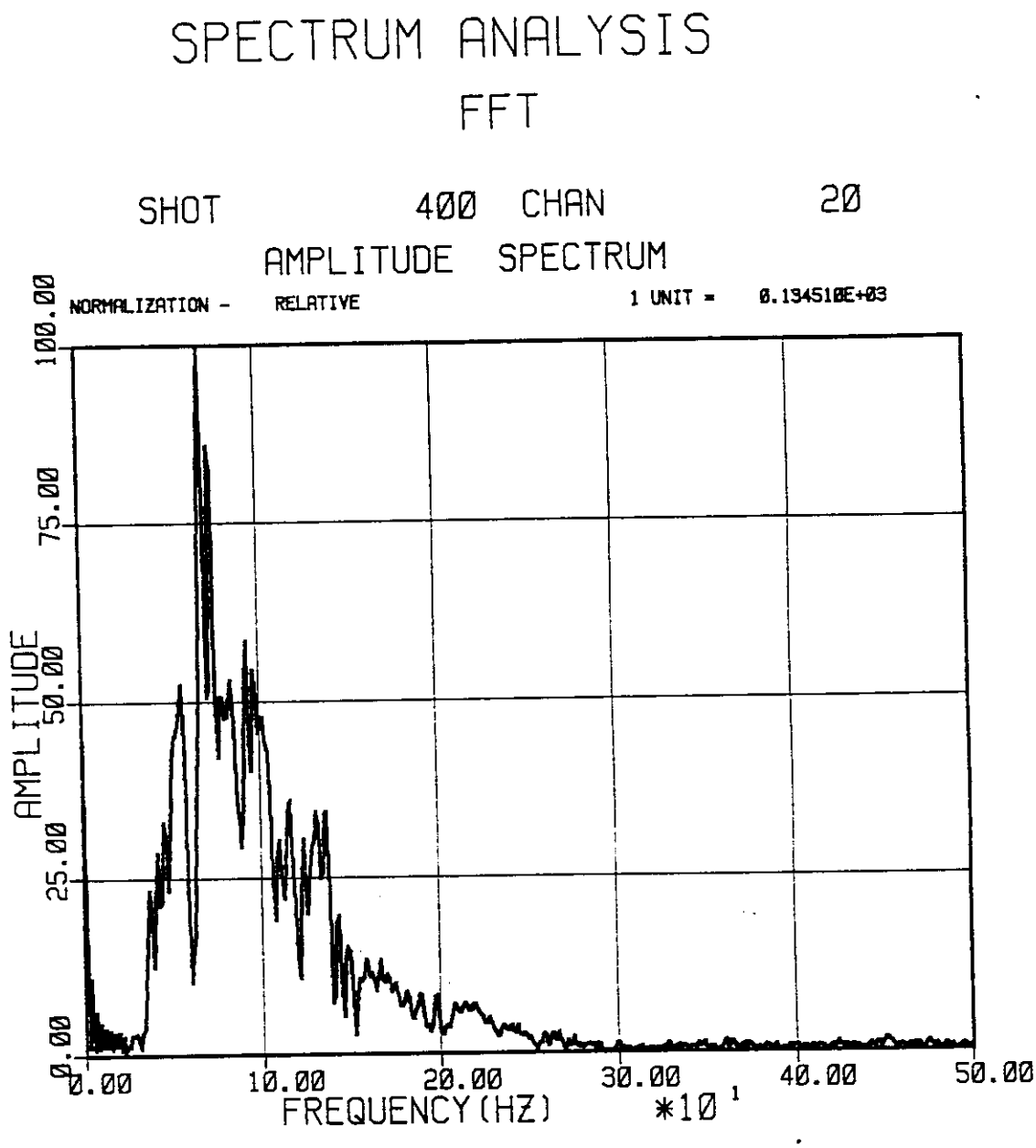

Figure 92. **Amplitude spectrum - PBF shot data:** Line PBF-18. Most of the usable reflection signal exists below 250 Hz; therefore the data can be resampled to 1 ms without loss of temporal resolution. Recording band in the field was 70-1000 Hz.

Displays of shot records revealed that considerable problems existed with source generated noise and overall low signal-to-noise ratio that would seriously compromise the reprocessing effort. Simple bandpass filtering was found to effect some noise reduction, but not without greatly restricting the bandwidth of the filtered data. Application of F-K filters to suppress source generated noise led to unsatisfactory results because of spatial aliasing in the data. Some encouraging results were obtained using stretched automatic gain control (SAGC)(Çoruh, 1985), but the method is computationally intensive and was abandoned.

A partial solution to the noise problem was achieved by combining the traces of adjacent CDP gathers to form nominal 24-fold gathers, i.e. the traces from shots taken at half station intervals were combined with those taken at full station intervals. One benefit of increased CDP fold is that the signal-to-noise ratio of the horizontal stack is correspondingly increased by the square root of the summing fold. Furthermore, because adjacent CDPs have different source-receiver offset ranges combining the CDPs should aid in stacking velocity analysis. Inasmuch as CDPs are combined and not shots, the stacking velocities and residual statics calculated for the 24-fold data can be readily applied to the original 12-fold gathers if greater spatial resolution is required.

A further justification for combining adjacent CDPs in the data processing follows from consideration of the size of the Fresnel zone, or the area of the reflecting surface sampled, i.e. the size of the reflection point. A general rule of seismic data acquisition is that to prevent spatial aliasing of reflections at least four traces per Fresnel zone are required (Knapp and Steeples, 1986). In Figure 93 plots of the radius of the Fresnel zone versus zero-offset time show that this sampling criterion is adequately met for the new 3 m CDP interval, although in the upper 70 ms of the data some spatial aliasing of the highest frequency components might occur for velocities under 1000 m/s. Thus, combining adjacent CDPs should not result in undersampling of important reflections.

Despite the improvement in stack quality obtained by combining adjacent CDPs, ultimately it was necessary to resort to use of surgical mutes to eliminate source generated noise. As illustrated in Figure 94 the muting results in elimination of nearly half the data; consequently, the effective CDP fold is halved to 12. Another important consequence is that the stacking fold versus time is

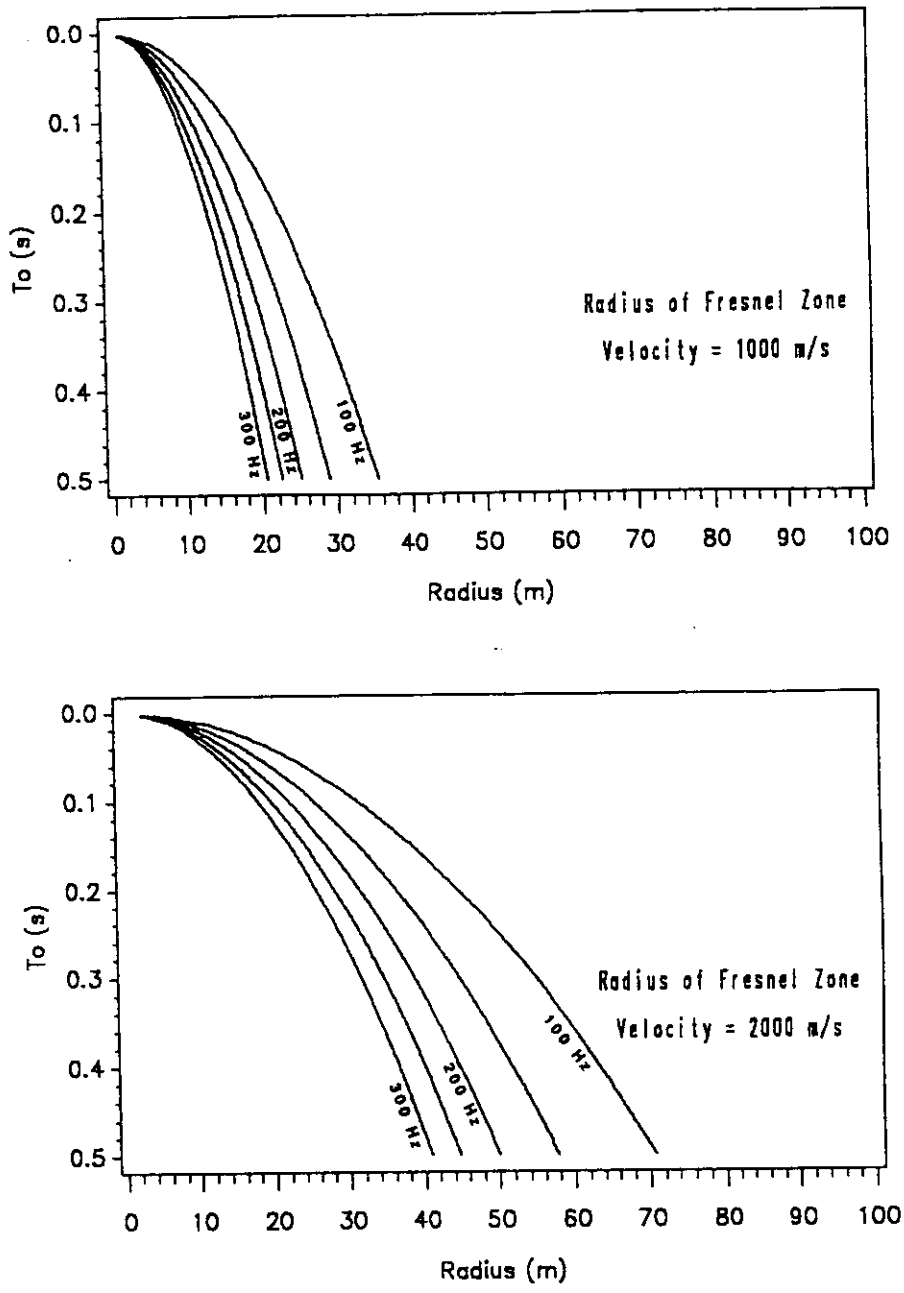

Figure 93. **Fresnel zone curves:** Radius of first Fresnel zone for frequencies and average velocities present in the EMEX data. The calculation of Fresnel zone radius is for spherical waves and straight raypaths as follows:

$$R \simeq 0.5V\sqrt{t_o/f}$$

where V is average velocity, t_o is two-way zero-offset time and f is frequency (Sheriff, 1980). Consideration of plane waves and curved raypaths results in a slightly smaller Fresnel zone radius.

greatest in the upper to middle part of the stacked section; thus, the residual statics computation gates and center event must be picked accordingly.

Seismic line PBF-18 was recorded with a larger minimum offset than line PBF-6 and was processed with a much less severe surgical mute.

Datum Statics: Although displays of shot records indicated some problems existed with inconsistent shot time-breaks, the magnitude of the timing problems was small, and given consideration of the relatively shallow shot hole depths, it was decided to process the PBF seismic lines as if the shots were at the surface. Consequently, any time delays that exist would be incorporated into the residual statics computations. It is possible that some of the problems later encountered with static busts might be traceable to inconsistent shot time-breaks.

To maintain conformity with the Conoco shallow seismic reflection data set both seismic lines were processed to an 80 m datum using a correction velocity of 900 m/s. A bulk shift of 50 ms was applied; hence, the 50 ms timing line on all sections represents 80 m.

Deconvolution: The data were deconvolved before stack using predictive deconvolution with a 10 ms operator and 4 ms prediction time.

Velocity Analysis: Stacking velocities were determined primarily through use of constant velocity stacks with occasional use made of constant velocity analysis of unstacked gathers to verify velocity functions. Stacking velocities were nominally picked every 100 CDPs with infill velocity functions determined as necessary. CVA stack panels of 21 CDPs each were generated using constant velocities 700-2200 m/s at increments of 50 m/s. The velocity increments were reduced to 20 m/s in areas where strong reflectors appeared to occur at shallow depths

Stacking velocity analysis was iterative with residual statics computations. After each of the first two passes of residual statics the stacking velocity functions were updated. As with the Conoco data set, the residual statics and the quality of the CDP stack was found to be sensitive to minor changes in the stacking velocity function. Often changing a velocity pick up or down a few tens of

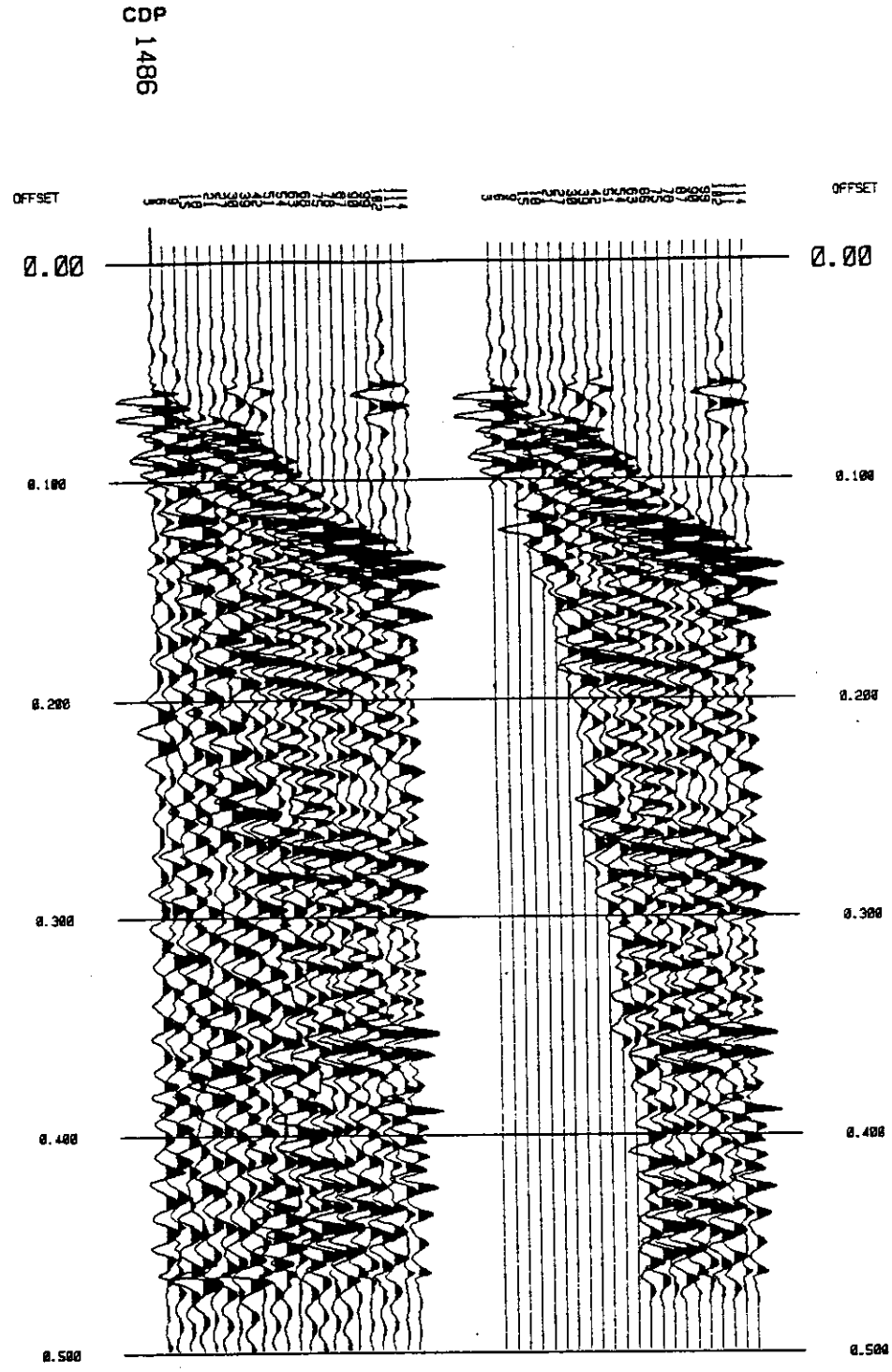

Figure 94. PBF-6 surgical mute: CDP without and with surgical mute applied. The mute at later times eliminates most of the traces in the gather. This CDP is in an area of very good signal-to-noise. Display: 125 ms AGC, 60-70-250-300 Hz bandpass filter.

milliseconds would induce a statics bust or a degradation in the quality of the stacked data. In particular, because of stretching effects of time and space variant velocity functions, it was found that the shallowest reflections could only be adequately stacked by use of slowly varying velocity functions or total section constant velocity stacks

Mute Patterns: Mute patterns were picked automatically using the criterion to mute the data where the seismic wavelet was stretched greater than 40 percent by the stacking velocity function. Because the mutes defined in this manner change as the stacking velocity function changes, the mutes were fixed after the second stacking velocity function was determined.

Residual Statics: Three passes of surface consistent residual statics with four iterations per pass were computed and applied to the data. After the first and second passes of residual statics the stacking velocities were redetermined. As with the Conoco shallow data, stabilization of the statics solution was achieved after the second pass of statics.

For both seismic lines the pilot trace was a 15 CDP sum and the envelope of the seismic traces was used in the first two iterations of any one static pass. The maximum allowable static was only 3 ms. Subsequent to the processing of these lines experiments were conducted that suggested a maximum static of only 1-2 ms is appropriate for these data.

The residual statics were generally poorly behaved requiring adjustment of stacking velocity functions, event flattening etc. followed by recomputation of the statics to eliminate busts in the stacked data. It was found that event flattening and selection of the static window were critical. For both lines the statics windows were from approximately 130-390 ms and the flattened event needed to be closely followed with 8 or more control points along the line. Nevertheless, minor static busts are still present in both lines.

Postprocessing: Zero-phase deconvolution was applied after CDP stack to shape the amplitude spectrum of the traces to a 60-70-250-300 Hz trapezoidal bandpass.

The signal enhancement process Digistack, previously described under the processing the shallow Conoco data, was performed on the stacked seismic sections. The window for coherency estimation for the signal traces was 7 traces by 80 ms and incremented every 3 traces and 40 ms. The maximum dip range was $\pm$ 30 ms and incremented every 5 ms. The output seismic sections represent a 50-50 mix of the original stacked seismic data with the signal trace section.

Migration: Finite difference migration was performed on both seismic lines using the unaltered stacking velocities and a migration layer thickness of 20 ms. Because of the relatively small trace spacings of these data, it was necessary to decimate the sections 4:1 to ensure an adequate migration aperture.

Display: For display the data were filtered with a 60-70-250-300 Hz trapezoidal bandpass filter and 250 ms AGC was applied. The available displays of the EMEX seismic reflection data set are tabulated in Table 7. Note that not all displays tabulated in Table 7 are collected in Appendix B.

Table 7. Available displays of EMEX PBF seismic reflection data.

	Stacked seismic sections		
Line No.	Stack 24 fold	Stack 12 fold	Migration 24 fold
PBF-6	x	x	x
PBF-18	x	x	x

Appendix B. Seismic Sections

Shallow Seismic Sections

Migrated Seismic Data

Deep Seismic Sections

Unmigrated Seismic Data

Vita

William J. Domoracki was born May 24, 1959 in Garfield Heights, Ohio the second of three children of Joseph F. and Amelia Ann Domoracki. At the age of three his family moved from Cleveland, Ohio to Glenwillow Village, Ohio where he attended elementary and middle school in nearby Solon. In 1972 his family moved to Cicero, New York. After graduating from high school in 1977 he enrolled as a geology major at State University of New York, College at Potsdam and graduated with a Bachelor of Arts degree, *Summa Cum Laude*, in May, 1981. While at Potsdam State he cross-enrolled in courses in civil engineering at Clarkson College of Technology and completed courses at Indiana University and Onondaga Community College. In August 1981 he enrolled in graduate school at the University of Arizona to study geophysics and later transferred to the Colorado School of Mines where he received a Master of Science degree in Geophysics in 1986. During this period he held internships with Amoco Production Company (1982) and Getty Oil Company (1983) and helped teach and co-ordinate Mines' world renowned geophysics field school (1984-6). After graduation, at the height of the Oil Bust, he found temporary employment with the Colorado School of Mines as a seismic data processor. In fall 1987 he entered the doctorate program in geophysics at Virginia Polytechnic Institute and State University.

William J. Domoracki is a member of Early American Coppers Club, National Geographic Society, Geological Society of America, American Association of Petroleum Geologists, and the Society of Exploration Geophysicists. His research interests include early Bust coinage, antebellum America, military and world history.

Following completion of his degree at Virginia Polytechnic Institute and State University he will seek gainful employment.

Appendix C. Synthetic Seismograms

Vita

William J. Domoracki was born May 24, 1959 in Garfield Heights, Ohio the second of three children of Joseph F. and Amelia Ann Domoracki. At the age of three his family moved from Cleveland, Ohio to Glenwillow Village, Ohio where he attended elementary and middle school in nearby Solon. In 1972 his family moved to Cicero, New York. After graduating from high school in 1977 he enrolled as a geology major at State University of New York, College at Potsdam and graduated with a Bachelor of Arts degree, *Summa Cum Laude*, in May, 1981. While at Potsdam State he cross-enrolled in courses in civil engineering at Clarkson College of Technology and completed courses at Indiana University and Onondaga Community College. In August 1981 he enrolled in graduate school at the University of Arizona to study geophysics and later transferred to the Colorado School of Mines where he received a Master of Science degree in Geophysics in 1986. During this period he held internships with Amoco Production Company (1982) and Getty Oil Company (1983) and helped teach and co-ordinate Mines' world renowned geophysics field school (1984-6). After graduation, at the height of the Oil Bust, he found temporary employment with the Colorado School of Mines as a seismic data processor. In fall 1987 he entered the doctorate program in geophysics at Virginia Polytechnic Institute and State University.

William J. Domoracki is a member of Early American Coppers Club, National Geographic Society, Geological Society of America, American Association of Petroleum Geologists, and the Society of Exploration Geophysicists. His research interests include early Bust coinage, antebellum America, military and world history.

Following completion of his degree at Virginia Polytechnic Institute and State University he will seek gainful employment.